Neural Plasticity

Acupuncture Therapies and Neuroplasticity

Guest Editors: Cun-Zhi Liu, Jian Kong, and Ke-Lun Wang

Acupuncture Therapies and Neuroplasticity

Neural Plasticity

Acupuncture Therapies and Neuroplasticity

Guest Editors: Cun-Zhi Liu, Jian Kong, and Ke-Lun Wang

Copyright © 2017 Hindawi Publishing Corporation. All rights reserved.

This is a special issue published in "Neural Plasticity." All articles are open access articles distributed under the Creative Commons Attribution License, which permits unrestricted use, distribution, and reproduction in any medium, provided the original work is properly cited.

Editorial Board

Shimon Amir, Canada
Michel Baudry, USA
M. S. Beattie, USA
Clive R. Bramham, Norway
Anna K. Braun, Germany
S. Chattarji, India
Rajnish Chaturvedi, India
Vincenzo De Paola, UK
Michele Fornaro, USA
Zygmunt Galdzicki, USA
Preston E. Garraghty, USA
Anthony J. Hannan, Australia
George W. Huntley, USA
Alexandre H. Kihara, Brazil
Jeansok J. Kim, USA
Eric Klann, USA
Malgorzata Kossut, Poland
Stuart C. Mangel, USA
A. R. Møller, USA
Diane K. O'Dowd, USA
Martin Oudega, USA
Maurizio Popoli, Italy
Bruno Poucet, France
Menahem Segal, Israel
P. Smirniotis, USA
Naweed I. Syed, Canada
Christian Wozny, UK
Chun-Fang Wu, USA
Long-Jun Wu, USA
J. Michael Wyss, USA
Lin Xu, China

Contents

Hindawi
Neural Plasticity
Volume 2017, Article ID 6178505, 2 pages
https://doi.org/10.1155/2017/6178505

Editorial

Acupuncture Therapies and Neuroplasticity

Cun-Zhi Liu,[1,2] Jian Kong,[3] and KeLun Wang[4]

[1]*Acupuncture and Moxibustion Department, Beijing Hospital of Traditional Chinese Medicine Affiliated to Capital Medical University, 23 Meishuguanhou Street, Dongcheng District, Beijing 100010, China*
[2]*Beijing Key Laboratory of Acupuncture Neuromodulation, Beijing Hospital of Traditional Chinese Medicine Affiliated to Capital Medical University, 23 Meishuguanhou Street, Dongcheng District, Beijing 100010, China*
[3]*Department of Psychiatry, Massachusetts General Hospital (MGH), Harvard Medical School, Charlestown, MA 02129, USA*
[4]*SMI, Department of Health Science and Technology, Faculty of Medicine, Aalborg University, Aalborg, Denmark*

Correspondence should be addressed to Cun-Zhi Liu; lcz623780@126.com

Received 21 February 2017; Accepted 21 February 2017; Published 27 April 2017

Copyright © 2017 Cun-Zhi Liu et al. This is an open access article distributed under the Creative Commons Attribution License, which permits unrestricted use, distribution, and reproduction in any medium, provided the original work is properly cited.

Neuroplasticity, including dendritic remodeling, synapse turnover, long-term potentiation (LTP), and neurogenesis, is a feature of the brain's response to the environment. This physiological process is engaged in development of brain, skill learning, formation and extinction of memory, and self-repair of neural injuries. Acupuncture has been demonstrated to be effective in many disorders such as stroke, Alzheimer's disease, and pain, the pathologies of which are related to neural plasticity. As a form of peripheral stimulation, acupuncture may relieve the symptoms of patients via mediating on neural plasticity.

This special issue contains 11 manuscripts, of which 3 manuscripts study the mechanism of acupuncture in various pain diseases using animal models. Among these, G.-H. Tian et al. found that electroacupuncture (EA) treatment exerts abirritative effects by inhibiting brain neuronal apoptosis and aberrant astrocyte activation. J.-Y. Wang et al. suggested that EA reduced the effects of the noxious stimulus on pain-related neurons in chronic constrictive injury rats. X.-M. Shao et al. demonstrated that EA can alleviate retrieval of pain memory due to the partial inhibition of cAMP/PKA/CREB signaling pathway. And not only that, but also H. Jiang et al. found that acupuncture could ameliorate depressive-like behaviors by regulating the PKA/CREB signaling pathway in the hippocampus.

In the special issue, there are 4 manuscripts about the neuroprotection of acupuncture on neurologic disease. One manuscript found that musical electroacupuncture therapy performed better than EA treatment in decreasing amyloid-beta levels in the frontal lobe of SAMP8 mice with Alzheimer's disease. The other three explored the molecular mechanisms of acupuncture. Y. Mo et al. suggested EA can greatly promote neuronal function recovery after spinal cord injuries in rats, which may result from upregulating the expression of neurotrophin-3. W. Liu et al. detected that miR-134-mediated LIMK 1 function was involved in EA-induced the hippocampal synaptic plasticity, which served as a contributor to improving spatial reference learning and memory during the recovery stage of ischemic stroke. And H.-Q. Li et al. suggested that EA can improve neurological deficit scores and reduce blood-brain barrier permeability after intracerebral haemorrhage, and the mechanism possibly targets caveolin-1/matrix metalloproteinase/blood-brain barrier permeability pathway.

In addition, there are 2 manuscripts using functional magnetic resonance imaging to explore the mechanism underlying acupuncture treatment. One manuscript investigated how causal influences between brain regions during the rubber hand illusion are modulated by tactile and visual stimuli. The other one investigated neuroplasticity changes induced by a single session of acupuncture therapy in healthy adults, regarding the excitability change on bilateral primary motor cortex and interhemispheric inhibition. Furthermore, J. W. Yang et al. investigated the effect and underlying

mechanism of acupuncture on renal sympathetic activity in spontaneously hypertensive rats.

In summary, this issue provides varies evidences presented by diverse authors covering several topics related to advances in acupuncture for mediating neural plasticity. Neural plasticity could be a bridge between acupuncture and various neurological diseases. More in-depth researches are required to reveal the underlying mechanism of acupuncture.

Cun-Zhi Liu
Jian Kong
KeLun Wang

Hindawi
Neural Plasticity
Volume 2017, Article ID 4135164, 11 pages
https://doi.org/10.1155/2017/4135164

Research Article

Mechanisms Underlying the Antidepressant Response of Acupuncture via PKA/CREB Signaling Pathway

Huili Jiang,[1] Xuhui Zhang,[1] Yu Wang,[1] Huimin Zhang,[2] Jing Li,[1] Xinjing Yang,[1] Bingcong Zhao,[1] Chuntao Zhang,[3] Miao Yu,[1] Mingmin Xu,[1] Qiuyun Yu,[1] Xingchen Liang,[1] Xiang Li,[1] Peng Shi,[1] and Tuya Bao[1]

[1]*School of Acupuncture-Moxibustion and Tuina, Beijing University of Chinese Medicine, Beijing 100029, China*
[2]*Department of Traditional Chinese Medicine, Beijing United Family Rehabilitation Hospital, Beijing 100016, China*
[3]*School of Acupuncture-Moxibustion and Tuina, Shaanxi University of Chinese Medicine, Xianyang 712046, China*

Correspondence should be addressed to Tuya Bao; tuyab@263.net

Received 5 August 2016; Accepted 28 November 2016; Published 16 April 2017

Academic Editor: Ke-Lun Wang

Copyright © 2017 Huili Jiang et al. This is an open access article distributed under the Creative Commons Attribution License, which permits unrestricted use, distribution, and reproduction in any medium, provided the original work is properly cited.

Protein kinase A (PKA)/cAMP response element-binding (CREB) protein signaling pathway, contributing to impaired neurogenesis parallel to depressive-like behaviors, has been identified as the crucial factor involved in the antidepressant response of acupuncture. However, the molecular mechanisms associated with antidepressant response of acupuncture, neurogenesis, and depressive-like behaviors ameliorating remain unexplored. The objective was to identify the mechanisms underlying the antidepressant response of acupuncture through PKA signaling pathway in depression rats by employing the PKA signaling pathway inhibitor H89 in in vivo experiments. Our results indicated that the expression of hippocampal PKA-α and p-CREB was significantly downregulated by chronic unpredicted mild stress (CUMS) procedures. Importantly, acupuncture reversed the downregulation of PKA-α and p-CREB. The expression of PKA-α was upregulated by fluoxetine, but not p-CREB. No significant difference was found between Acu and FLX groups on the expression of PKA-α and p-CREB. Interestingly, H89 inhibited the effects of acupuncture or fluoxetine on upregulating the expression of p-CREB, but not PKA-α. There was no significant difference in expression of CREB among the groups. Conclusively, our findings further support the hypothesis that acupuncture could ameliorate depressive-like behaviors by regulating PKA/CREB signaling pathway, which might be mainly mediated by regulating the phosphorylation level of CREB.

1. Introduction

Depressive disorder is a common mental disorder which has been affecting millions of people worldwide [1]. The main symptoms of depressive disorder are characterized by mood disturbances, anhedonia, cognitive dysfunction, or heightened vulnerability to relapse [2]. It has been investigated that stressful factors are the most prevalently precipitating factors for the development, maintenance, or exacerbation of depressive disorder. There is sufficient evidence that stressful factors are closely associated with impaired neurogenesis and structural plasticity in the hippocampus [3, 4]. Furthermore, additional studies have indicated that morphological changes, impaired neurogenesis, damaged structural plasticity, or even apoptosis in the hippocampus were detected in depressive disorder [5–9].

Presently, antidepressant drugs (e.g., paroxetine, fluoxetine) are the major treatment for depression and have been widely used for the treatment of depression in the clinic. Fluoxetine, one of the antidepressant drugs characterized by a selective serotonin (5-hydroxytryptamine (5-HT)) reuptake inhibitor (SSRI), has been approved by the Food and Drug Administration (FDA) to treat stress-related disorders (including depression and anxiety) in patients [10]. Antidepressant drugs are indeed available nowadays. However, it has been evidenced that approximately one third of all

patients with depressive disorder fail to respond to conventional antidepressant therapies [11]. Meanwhile, data from clinical investigations and laboratory animals have provided compelling evidence that some antidepressant drugs have anxiogenic effects during the acute phase of treatment or even aggravate suicidal thinking and behavior [10, 12, 13]. Accordingly, there is an urgent need for investigating new conceptual frameworks for understanding the pathogenesis of depression and exploring better treatments for depression.

The precise contributing factors and mechanisms of depression are still unknown. The precise pathogenesis and etiology of depression has been a challenging issue recently. Nowadays, the involvement of alterations concerning immune response and inflammatory response in the pathophysiology of depression and stress has been evidenced by various studies [14–16]. Numerous studies have reported that cAMP-dependent protein kinase- (PKA-) CREB signaling is involved in the pathogenesis of depression. cAMP response element-binding (CREB) protein has been evidenced to be one of the best-studied transcription factors implicated in depression and antidepressant-like process. Data from humans and laboratory experiments have provided compelling evidence that the PKA/CREB signal pathway is involved in the effect on regulating synaptic plasticity and learning memory [17–22]. The systemic perturbations of the PKA/CREB signal pathway could induce cascade reactions of neuropathology in depression, including abnormalities in regional brain activity, alterations in synaptic function, and impaired neurogenesis. Downregulated expression of CREB level has been investigated in the postmortem hippocampus of patients who suffered from depression [23]. CREB signaling has been considered to be a crucial factor implicated in promoting synaptic and neural plasticity by regulating the genes that increase synaptic and neural plasticity, including BDNF [24]. PKA, the upstream activator of CREB, has been evidenced to exhibit antidepressive effect by upregulating CREB or p-CREB [25, 26].

During our previous studies, we have been focusing on investigating the clinical effects and mechanisms of acupuncture on depression. We found distinct abnormalities in regional brain activity [27, 28]. Moreover, data from laboratory animals supporting the involvement of PKA/CREB in the pathogenesis of depression are compelling and include findings that verify the antidepressant response of acupuncture by regulating PKA/CREB [29, 30]. However, the mechanisms underlying the antidepressant response of acupuncture via PKA/CREB have not been investigated in depth.

Here, we established a rat model of depression induced by CUMS and assessed the difference in antidepressant effect between acupuncture and fluoxetine. Importantly, H89, a moderately specific inhibitor for PKA [31, 32], was employed in the present study to investigate the role of CREB or p-CREB, activated by PKA. The expressions of PKA-α, CREB, and p-CREB were assessed. We aimed to elucidate the molecular mechanisms underlying the antidepressant response of acupuncture and shed new light on conceptual frameworks of prospects for new therapies in the treatment of depression.

2. Materials and Methods

2.1. Experimental Animals and Grouping. Adult 6-week-old male Sprague-Dawley (SD) rats, weighing 220 ± 20 g, were obtained from Weitong Lihua Experimental Animal Center of Beijing, China. Rats were housed in a quiet room with a controlled environment of 23°C–26°C and $50\% \pm 10\%$ humidity. The rats subjected to CUMS were housed separately in different cages for social isolation, and 5 animals per cage were housed for rats in the control group. All experimental procedures were in full observance of the Bioethical Committee of the Institute of Animal Care Committee, Beijing University of Chinese Medicine, Beijing, China (permit no. Kj-dw-32-20150612).

The body weight (BW), sucrose preference test (SPT), and open-field test (OFT) were investigated to guarantee the consistency of baseline characteristics before the experimental procedure was conducted. Five rats were excluded due to the inconsistent baseline characteristics. Then, a total of 60 rats under the circumstance of similar baseline characteristics of BW, SPT, and OFT were assigned into control, model, model + acupuncture (Acu), model + fluoxetine (FLX), model + acupuncture + H89 (Acu + H89), and model + fluoxetine + H89 (FLX + H89) groups at random, with 10 rats in each group. All rats were exposed to social isolation and CUMS for 21 days excluding rats in the control group. Thirty minutes before CUMS procedure, the rats in the Acu group were acupunctured at Baihui (GV 20) and Yintang (EX-HN 3); the rats in the FLX group were administered with fluoxetine (0.18 mg/ml) by gavage (1 ml/100 g). Intracerebroventricular injections of the PKA signaling pathway inhibitor H89 (10 μM, 5 μl) were administered in Acu + H89 and FLX + H89 groups 60 minutes before the CUMS procedure, once every other day, and then, acupuncture stimulation and intragastric administration of fluoxetine were conducted, respectively (Figure 1).

2.2. Chronic Unpredictable Mild Stress (CUMS). A depressive disorder model induced by CUMS in rats was established in this study as described previously [29, 33]. Furthermore, some adjustments were made to add the unpredictability. The rats were exposed to CUMS for 21 days, including restricted access to food deprivation for 24 h, water deprivation for 24 h, housing in a wet cage for 24 h (containing 100 g of sawdust in 200 ml water), continuous overnight illumination for 12 h, restricted access to chronic restraint stress for 2 h (restraining in a cylinder-shaped wire net, 20 cm in length and 5 cm in diameter), shaking once per second for 30 min, and clip tail for 3 min (1 cm apart from the tail). Rats were subjected to one of these 7 stimuli at random per day, and the same stressor was not employed on consecutive days to avoid the rat's prediction. Each stressor was used 3 times randomly (Table 1). Rats in the control group were normally fed for 21 days with food and water ad libitum without any stimulus.

2.3. Surgical Procedures for Intracerebroventricular (ICV) Catheterization. Rats in the Acu + H89 and FLX + H89 groups were subjected to surgical procedures for intracerebroventricular (ICV) cannulae implanted 7 days before

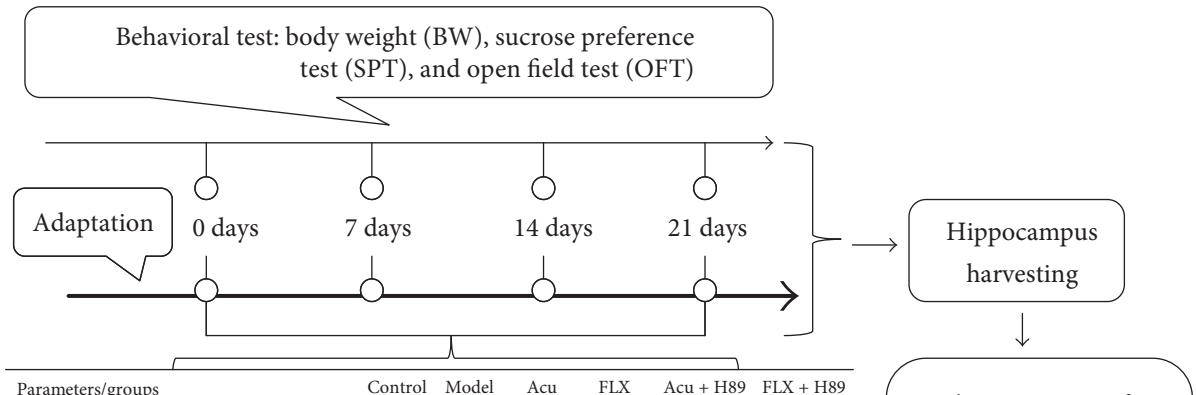

Parameters/groups	Control	Model	Acu	FLX	Acu + H89	FLX + H89
Social isolation for 21 days.	−	+	+	+	+	+
Induction of CUMS for 21 days.	−	+	+	+	+	+
Acupunctured at GV 20 and EX-HN 3, 30 min before CUMS.	−	−	+	−	+	−
Administered with fluoxetine by gavage, 30 min before CUMS.	−	−	−	+	−	+
Intracerebroventricular cannulae catheterization, 7 days before experiment.	−	−	−	−	+	+
Intracerebroventricular injection of H89, 60 min before CUMS.	−	−	−	−	+	+

Figure 1: Experimental procedures. Acu: acupuncture group; FLX: fluoxetine group; Acu + H89: Acupuncture + H89 group; FLX + H89: Fluoxetine + H89 group; PKA-α: protein kinase A-α; CREB: cyclic adenosine monophosphate response element-binding protein; p-CREB: Phosphor-CREB.

Table 1: The CUMS procedure of applied stressors during 1 week.

Days	Duration	Stressor
Day 1	30 minutes	Shaking once per second
Day 2	2 hours	Chronic restraint stress
Day 3	3 minutes	Clip tail
Day 4	24 hours	Housing in a wet cage
Day 5	12 hours	Continuous overnight illumination
Day 6	24 hours	Water deprivation
Day 7	24 hours	Food deprivation

the experimental design as described by previous studies [34, 35]. Rats were anesthetized with 10% chloral hydrate (0.35 ml/100 g, i.p.) and then placed on a stereotaxic apparatus (catalogue no. 68001, RuiWoDe Life Science Co., Ltd., Shenzhen, China). The fixed positions were (coordinates: −0.8 mm from the bregma, ±1.5 mm lateral from sagittal suture, and −1.9 mm deep from the dura) referred to the atlas of the previous study [36, 37]. ICV cannulae (OD 0.56 × ID 0.38 mm/M 3.5, RuiWoDe Life Science Co., Ltd., Shenzhen, China) were inserted bilaterally into the ventricle. Upon screening and confirming outflow of cerebrospinal fluid from the ICV cannulae, the guide cannula was secured with screws and dental cement and closed with a dummy cannula. Then, all rats were sent to a relatively warm room for better recovery for 7 days from surgery, so as to become accustomed to the procedures of further experimentation.

2.4. Intracerebroventricular Injection of PKA Inhibitor H89. In the microinfusion experiments, the ICV cannulae were strictly disinfected with 75% alcohol. Microinfusion probes were gently inserted through the guide cannulae. The solution of PKA inhibitor H89 (dissolved with 0.9% sodium chloride solution, 10 μM), 5 μl, was infused bilaterally into the encephalocele at a rate of 0.25 μl/min for 2 min, once every two days. Then, the infusion probes were left in place for an additional 2 min to allow solutions to diffuse away from the probe tips. After redisinfection with 75% alcohol, the ICV cannulae were closed with a dummy cannula.

2.5. Acupuncture Stimulation. For the animals that received acupuncture stimulation, acupuncture commenced 30 minutes before CUMS procedure, 10 minutes per session, and 1 session daily for 21 days. After disinfection of the acupoint sites with 75% alcohol, the acupuncture needles (0.3 mm in diameter and 25 mm long; Suzhou Acupuncture & Moxibustion Appliance Co., Ltd., Jiangsu, China) were inserted transversely (keeping the angle between the needle and the skin surface at 15°) into Baihui (GV 20) and Yintang (EX-HN 3) (acupoint coordinates [38]: GV 20, located at the bregma or on the junction of coronal suture and sagittal suture; EX-HN 3: midway between the medial ends of the two eyebrows) to a depth of 5 mm as described by our

previous study [29]. When acupuncture procedure was conducted, rats were placed in separated room and under the conditions of free activities.

2.6. ICV Catheterization Assessment. To verify the effectiveness and validity of ICV injection of H89 in rats in the Acu + H89 and FLX + H89 groups, another 6 rats were subjected to ICV catheterization and ICV injection of 1% Evans blue. Briefly, rats that received posttraining infusions of 0.9% sodium chloride solution after successful ICV catheterization were returned to the holding cage for better recovery for 7 days from surgery. Then, 0.1% Evans blue (dissolved with deionized water, 5 μl) was injected into the lateral ventricle. After being exposed to free activity for 4 h, rats were deeply anesthetized with 10% chloral hydrate (0.35 ml/100 g, i.p.) and then perfused intracardially with 100 ml of 0.9% sodium chloride solution followed by 200 ml of 4% paraformaldehyde in 0.1 M phosphate-buffered saline (PBS). Then, rats were decapitated, and the brains were removed and placed into 4% paraformaldehyde in 0.1 M PBS for 72 h at 4°C. The brains were transferred to 20% and 30% sucrose solutions for dehydration at 4°C. The morphology of lateral ventricle was detected and visualized under a laser confocal scanning microscope (FV1000, Olympus, Japan) through frozen sections (8 μm) (CM-1950, Leica, German).

2.7. Observation of Rat Behavior. All behavioral tests were conducted under relatively quiet and dark circumstances. Body weight (BW), sucrose preference test (SPT), and open-field test (OFT) were investigated at least 12 hours after the stress stimulation at the end of experimental period. Mood states, quality of feces, and appetite of rats were observed.

2.7.1. Body Weight (BW). The changes in body weight gain in comparison to the baseline were calculated to evaluate the states of food preference and nutrition status. Body weight was detected on day 0 and day 21 for each rat throughout the experimental procedures.

2.7.2. Open-Field Test (OFT). Locomotor activity of each rat was detected through open-field test (OFT) as illuminated by previous studies [29, 39]. The open-field apparatus consisted of a 80 cm × 80 cm × 40 cm square arena with black wall and black base, of which the base was divided into 16 × 16 cm equal squares with legible white lines. Each rat was gently placed in the center of the open-field floor and then allowed to enjoy independent movement and explore freely for 5 minutes. Crawling square numbers (numbers of crossing the horizontal sectors including three paws in the same square) and standing times (numbers of erection including rearing) were monitored and recorded as an index of locomotion activity and exploratory behavior. After each trial, 75% ethyl alcohol was used to refresh the open-field apparatus, which could get rid of the interference of odor signals. OFT was conducted on day 0 and day 21.

2.7.3. Sucrose Preference Test (SPT). Referring to investigations of recent studies [29, 33], sucrose preference test (SPT) was employed to evaluate the condition of anhedonic-like behaviors of rats. Rats were trained to adapt to 1% sucrose solution (Amresco, USA) during the adaptation cycles. After the adaptation, all rats were deprived of food and water for 23 hours. Then, they were all housed in individual cages and had free access to two preweighed bottles containing 150 ml sucrose solution (1% w/v) and 150 ml pure water for 1 hour. At the end of the test, the bottles of 1% sucrose solution and pure water were reweighted and recorded. SPT was conducted on day 0 and day 21. Anhedonia was expressed by reduced sucrose consumption.

2.8. Western Blot. Following the last experimental procedure, the rats were sacrificed and decapitated. The brains were removed quickly, and the hippocampus was isolated and stored at −80°C for the next process. The samples were homogenized with RIPA lysis buffer, containing 50 mM Tris (pH 7.4), 150 mM NaCl, 1% NP-40, and 0.5% Na deoxycholate and protease inhibitor cocktail (or phosphatase inhibitor cocktail for phosphorylated protein) for protein extraction. And then, the supernatant was collected following centrifugation at 13,000 rpm at 4°C for 20 minutes. The total protein content was determined by using bicinchoninic acid (BCA) assay. Following the quantitative determination of the total protein content, the proteins of each sample were denatured at 100°C for 5 min and fractionated through 10% SDS polyacrylamide gel electrophoresis (PAGE). The proteins of samples were electrotransferred onto polyvinylidene difluoride membranes with voltage at 80 V for 60 min. The membranes were blocked with 5% bull serum albumin-(BSA-) TBST for 1 h at room temperature. Protein expression was subsequently detected by incubation with rabbit polyclonal primary antibodies against PKA-α (1 : 2000; 5842s, Cell Signaling Technology, USA), p-CREB (1 : 500; ser133-9198S, Cell Signaling Technology, USA), CREB (1 : 500; ser133-4820S, Cell Signaling Technology, USA), and GAPDH (1 : 1000; 2118s, Cell Signaling Technology, USA) at 4°C overnight. Following incubation with the primary antibody, the membranes were incubated with goat anti-rabbit HRP-conjugated IgG (1 : 2000; ZDR-5118, Zhongshan Jinqiao Biotechnology Co., Ltd, Beijing, China) at room temperature for 60 min. The bound antibodies were visualized using an enhanced chemiluminescence reagent by ECL kit (RPN2232; GE Healthcare Life Sciences, UK) and quantified densitometrically using Gel-image analyzing system (Gene Gnome, Syngene, USA). The experiments were performed in triplicates with triplicate samples. The mean optical density value of each protein band relative to that of the glyceraldehyde-3-phosphate dehydrogenase (GAPDH) band from the same sample was calculated.

2.9. Statistical Analysis. All data were statistically analyzed by SPSS 22.0 software (IBM, Armonk, NY, USA) and expressed as the mean ± standard deviation ($\overline{x} \pm s$). The total sucrose consumption, body weight gain, and expression of PKA-α, CREB, and p-CRE were analyzed by a one-way analysis of variance (ANOVA) test. Differences between individual means were tested for significance using Fisher's least significant difference (LSD) or Tamhane's T2 procedure. The horizontal and vertical motion scores were analyzed by the

Table 2: Differences showing the effects of stress/antidepressant treatments on depressive-like behaviors in depression rats induced by CUMS.

(a) Differences in body weight following stress/antidepressant treatments

Group	n	0 days	21 days
Control	10	277.01 ± 11.10	363.83 ± 38.06
Model	10	275.24 ± 12.75	$319.61 \pm 17.95^{\star\star}$
Acu	10	281.42 ± 17.26	$348.04 \pm 31.05^{\blacktriangle}$
FLX	10	271.93 ± 20.34	$350.99 \pm 30.49^{\blacktriangle}$
Acu + H89	10	$256.58 \pm 15.01^{\star\star,\blacktriangle\blacktriangle,\blacklozenge\blacklozenge}$	$257.86 \pm 28.48^{\star\star,\blacktriangle\blacktriangle,\blacklozenge\blacklozenge}$
FLX + H89	10	$250.37 \pm 11.57^{\star\star,\blacktriangle\blacktriangle,\blacksquare\blacksquare}$	$252.73 \pm 31.61^{\star\star,\blacktriangle\blacktriangle,\blacksquare\blacksquare}$

(b) Differences in sucrose intake levels following stress/antidepressant treatments

Group	n	0 days	21 days
Control	10	22.96 ± 2.52	36.71 ± 8.04
Model	10	24.57 ± 2.98	$22.52 \pm 5.92^{\star\star}$
Acu	10	24.80 ± 3.50	$29.29 \pm 7.99^{\star,\blacktriangle}$
FLX	10	25.97 ± 4.64	$33.51 \pm 5.17^{\blacktriangle\blacktriangle}$
Acu + H89	10	25.19 ± 2.59	$20.52 \pm 4.57^{\star\star,\blacklozenge\blacklozenge}$
FLX + H89	10	25.12 ± 1.98	$13.39 \pm 6.92^{\star\star,\blacktriangle\blacktriangle,\blacksquare\blacksquare,*}$

(c) Differences in horizontal and vertical motion scores following stress/antidepressant treatments

Group	0 days		21 days	
	Horizontal	Vertical	Horizontal	Vertical
Control	65.10 ± 13.01	12.10 ± 4.04	50.70 ± 13.84	18.40 ± 8.76
Model	66.60 ± 14.04	10.00 ± 3.53	$9.50 \pm 4.97^{\star\star}$	$2.10 \pm 1.29^{\star\star}$
Acu	65.80 ± 14.40	10.80 ± 2.90	$18.10 \pm 7.37^{\star\star,\blacktriangle}$	$5.80 \pm 1.81^{\star\star,\blacktriangle\blacktriangle}$
FLX	65.20 ± 13.74	10.30 ± 4.01	$16.90 \pm 5.30^{\star\star,\blacktriangle}$	$6.10 \pm 2.23^{\star\star,\blacktriangle\blacktriangle}$
Acu + H89	58.20 ± 13.66	9.20 ± 3.12	$10.20 \pm 8.20^{\star\star,\blacklozenge}$	$1.20 \pm 1.03^{\star\star,\blacklozenge\blacklozenge}$
FLX + H89	58.70 ± 12.69	9.50 ± 2.76	$5.30 \pm 3.80^{\star\star,\blacktriangle,\blacksquare\blacksquare}$	$1.50 \pm 1.27^{\star\star,\blacksquare\blacksquare}$

Acu: acupuncture group; FLX: fluoxetine group; Acu + H89: Acupuncture + H89 group; FLX + H89: Fluoxetine + H89 group. Results are presented as $\bar{x} \pm s$ for 10 rats in each group. Differences are shown as follows: $^{\star}P < 0.05$ versus control group; $^{\star\star}P < 0.01$ versus control group; $^{\blacktriangle}P < 0.05$ versus model group; $^{\blacktriangle\blacktriangle}P < 0.05$ versus model group; $^{\blacklozenge}P < 0.05$ versus acupuncture group; $^{\blacklozenge\blacklozenge}P < 0.01$ versus acupuncture group; $^{\blacksquare\blacksquare}P < 0.01$ versus fluoxetine group; $^{*}P < 0.05$ versus Acu + H89.

Kruskal-Wallis H test. Probability values less than 0.05 were considered greatly significant.

3. Results

3.1. Acupuncture Alleviates Depressive-Like Behaviors in Depression Rats Induced by CUMS. To investigate the effects of acupuncture on the depressive-like behaviors in the rat model of depression induced by CUMS, the BW, SPT, and OFT of pre-experiment versus postexperiment were observed. The results showed that, compared with the control group, the gain in body weight was significantly prolonged and less, and the sucrose intake and the times of horizontal and vertical motion scores were notably reduced in the model group, all with statistical significance ($P < 0.01$, $P < 0.01$, $P < 0.01$, and $P < 0.01$) (Tables 2(a), 2(b), and 2(c); Figures 2(a), 2(b), 2(c), and 2(d)). However, the gain in body weight was evidently increased, and the sucrose intake and the times of horizontal and vertical motion scores were notably elevated when the Acu and FLX groups versus those of the model group following treatment with acupuncture and fluoxetine (Acu versus model with statistical significance: $P < 0.05$, $P < 0.05$, $P < 0.05$, and $P < 0.01$) (FLX versus model with statistical significance: $P < 0.05$, $P < 0.01$, $P < 0.05$, and $P < 0.01$) (Tables 2(a), 2(b), and 2(c); Figures 2(a), 2(b), 2(c), and 2(d)). Both acupuncture and fluoxetine could well alleviate the depressive-like behaviors induced by CUMS.

Furthermore, to identify the effects underlying the antidepressant response of acupuncture through PKA pathway in rats exposed to CUMS by employing the PKA signaling pathway, the inhibitor H89 was performed as intracerebroventricular injection to specifically inhibit the PKA signaling pathway. As the results indicated, compared with the control group, the gain in body weight was significantly reduced in the Acu + H89 and FLX + H89 groups' pre-experiment ($P < 0.01$; $P < 0.01$), which might be due to the anesthetization during ICV catheterization surgery disturbing the regular diet order. After 7 days of recovery from surgery, the baseline characteristic of behaviors of rats in the Acu + H89

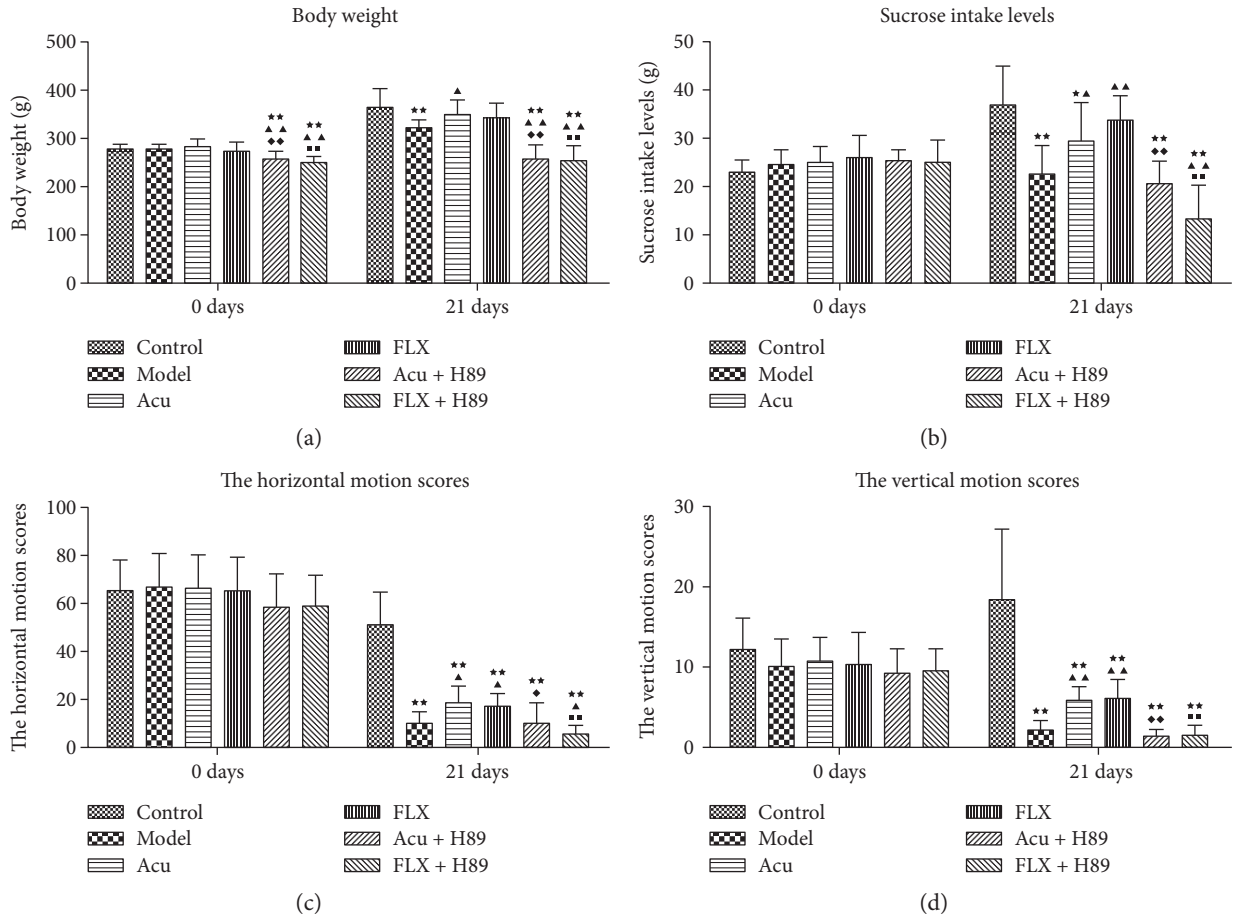

Figure 2: Differences showing the effects of stress/ antidepressant treatments on depressive-like behaviors in depression rats induced by CUMS. (a) The effects of stress/antidepressant treatments on the body weight in depression rats induced by CUMS. (b) The effects of stress/antidepressant treatments on the sucrose intake levels in depression rats induced by CUMS. (c) The effects of stress/antidepressant treatments on the horizontal motion scores in depression rats induced by CUMS. (d) The effects of stress/antidepressant treatments on the vertical motion scores in depression rats induced by CUMS. Differences are shown as follows: $^{\star}P < 0.05$ versus control group; $^{\star\star}P < 0.01$ versus control group; $^{\blacktriangle}P < 0.05$ versus model group; $^{\blacktriangle\blacktriangle}P < 0.05$ versus model group; $^{\blacklozenge}P < 0.05$ versus acupuncture group; $^{\blacklozenge\blacklozenge}P < 0.01$ versus acupuncture group; $^{\blacksquare\blacksquare}P < 0.01$ versus fluoxetine group. Values are given as $\bar{x} \pm s$ for 10 rats in each group. Acu: acupuncture group; FLX: fuoxetine group; Acu + H89: Acupuncture + H89 group; FLX + H89: Fluoxetine + H89 group.

and FLX + H89 groups kept pace with the others. Then, the BW, SPT, and OFT of pre-experiment versus postexperiment were observed. The results showed that, compared with the Acu group, the gain in body weight and the sucrose intake were significantly reduced ($P < 0.01$; $P < 0.01$), and the times of horizontal and vertical motion scores were notably reduced in the Acu + H89 group, all with statistical significance ($P < 0.05$ and $P < 0.01$) (Tables 2(a), 2(b), and 2(c); Figures 2(a), 2(b), 2(c), and 2(d)). Interestingly, the difference between FLX and FLX + H89 was inconsistent with the results of Acu versus Acu + H89. The antidepressive effects of acupuncture and fluoxetine were both inhibited by PKA inhibitor H89.

3.2. ICV Catheterization Assessment. Rats were subjected to ICV catheterization (Figures 3(a) and 3(b)) as described by previous studies [35, 37]. ICV injection of 1% Evans blue into the bilateral paracele was performed to verify and guarantee the effectiveness and validity of ICV injection of H89 in rats in the Acu + H89 and FLX + H89 groups. The results showed that the bilateral paracele were suffused with blue substance after ICV injection of 1% Evans blue when detected with the naked eye (Figure 3(c)). Meanwhile, the structure and morphology of bilateral paracele were investigated by frozen sections and screened under the fluorescence microscope. We found that the wall of the whole bilateral paracele, including frontal, occipital, temporal, and inferior horn, was suffused with Evans blue exhibiting red fluorescence (Figure 3(d)). Accordingly, the effectiveness and validity of ICV catheterization and ICV injection have been notably evidenced by our present study.

3.3. The Analysis of Antidepressive Effects of Acupuncture on the PKA/CREB Signaling Pathway. PKA signaling pathway has been evidenced to be associated with the pathogenesis of mental disorders, including depression. In the present study, the expression levels of PKA-α, CREB, and p-CREB were

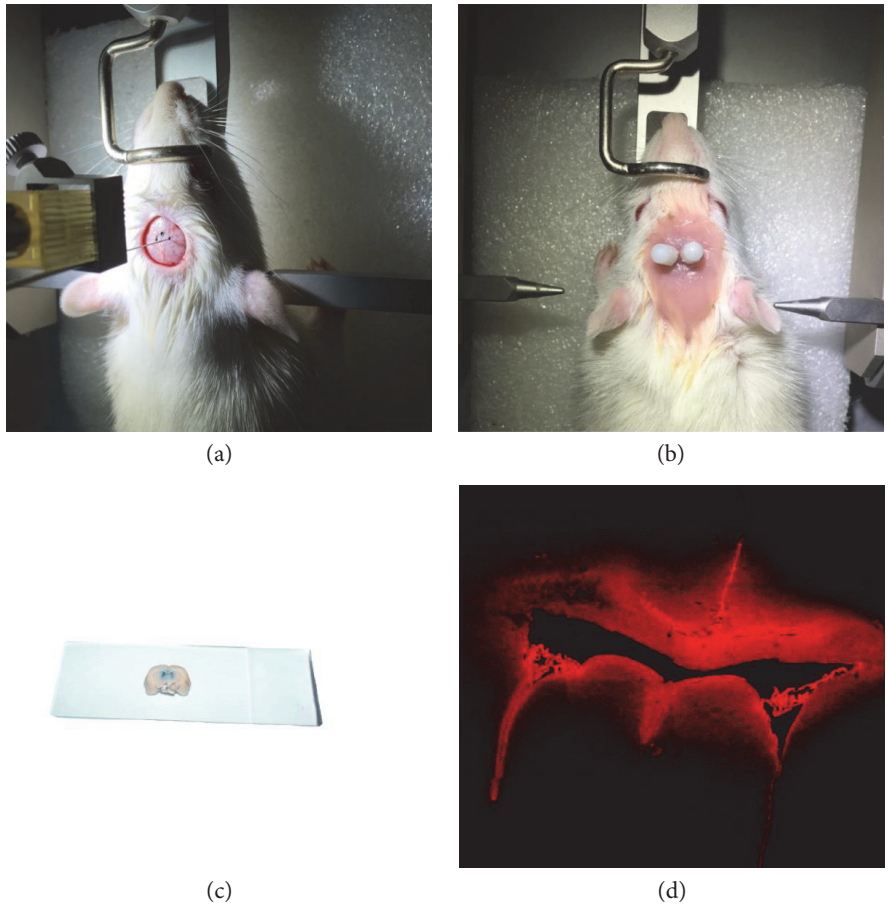

(a) (b) (c) (d)

Figure 3: The effectiveness and validity of ICV catheterization. (a) The fixed position of ICV catheterization. (b) The rat subjected to effective ICV catheterization. (c) The structure and morphology of bilateral paracele detected with the naked eye. The bilateral paracele was suffused with blue substance after ICV injection of 1% Evans blue, suggesting the validity of ICV injection and ICV catheterization. (d) The structure and morphology of bilateral paracele screened under the fluorescence microscope. The wall of the whole bilateral paracele, including frontal, occipital, temporal and inferior horn, was suffused with Evans blue exhibiting red fluorescence.

detected by western blot analysis to investigate the mechanisms through which acupuncture ameliorates depressive-like behaviors in rats exposed to CUMS. H89, the inhibitor of PKA, was used to explore whether PKA signaling pathway was involved in the antidepressive effects of acupuncture, which in turn investigate the mechanisms underlying the antidepressant response of acupuncture via PKA signaling pathway.

3.3.1. Expression Level of PKA-α in the Hippocampus. The results showed that, compared with control group, the expression of hippocampal PKA-α in the model group was significantly downregulated ($P < 0.01$) (Table 3 and Figure 4). Following the treatment of acupuncture and fluoxetine, the expression of hippocampal PKA-α in the acupuncture group and fluoxetine group was significantly upregulated compared with that in the model group ($P < 0.01$; $P < 0.05$) (Table 3 and Figure 4). Both acupuncture and fluoxetine could reverse the downregulation of hippocampal PKA-α induced by CUMS. No significant difference was found between acupuncture and fluoxetine groups ($P > 0.05$). Similarly, no significant differences were found between the Acu group versus Acu + H89 group and the FLX group versus FLX + H89 group ($P > 0.05$; $P > 0.05$).

3.3.2. Expression Level of CREB and p-CREB in the Hippocampus. Furthermore, expressions of hippocampal CREB and p-CREB were assessed. The results showed that there were no significant differences among the control group, model group, Acu group, FLX group, Acu + H89 group, and FLX + H89 group. However, the p-CREB expression level in the model group was notably decreased compared with that in the control group ($P < 0.01$) (Table 3 and Figure 4). Similarly, the expression of p-CREB was notably downregulated between Acu + H89 versus control group and FLX + H89 versus control group ($P < 0.01$; $P < 0.01$) (Table 3 and Figure 4). By contrast, the p-CREB expression level in the acupuncture group was significantly upregulated compared with that in the model group ($P < 0.01$). While the expression of p-CREB in the fluoxetine group presented a trend of escalation in comparison with the model group ($P > 0.05$). No significant difference was found between the acupuncture and fluoxetine groups. The expression of p-CREB was notably downregulated between the Acu

Table 3: Differences showing the effects of stress/antidepressant treatments on the expression levels of hippocampal PKA-α, CREB, and p-CREB in depression rats induced by CUMS.

Group	n	PKA-α/GAPDH	CREB/GAPDH	p-CREB/GAPDH
Control	10	3.277 ± 0.964	1.673 ± 0.226	1.268 ± 0.405
Model	10	$2.089 \pm 0.614^{\star\star}$	1.665 ± 0.107	$0.733 \pm 0.197^{\star\star}$
Acu	10	$3.185 \pm 0.579^{\blacktriangle\blacktriangle}$	1.666 ± 0.124	$1.117 \pm 0.211^{\blacktriangle}$
FLX	10	$3.048 \pm 0.425^{\blacktriangle}$	1.612 ± 0.366	1.037 ± 0.164
Acu + H89	10	$3.057 \pm 0.473^{\blacktriangle}$	1.478 ± 0.463	$0.671 \pm 0.295^{\star\star,\blacklozenge\blacklozenge}$
FLX + H89	10	$3.067 \pm 0.595^{\blacktriangle}$	1.572 ± 0.382	$0.619 \pm 0.204^{\star\star,\blacksquare\blacksquare}$

Acu: acupuncture group; FLX: fluoxetine group; Acu + H89: Acupuncture + H89 group; FLX + H89: Fluoxetine + H89 group; PKA-α: protein kinase A-α; CREB: cyclic adenosine monophosphate response element-binding protein; p-CREB: Phosphor-CREB; GAPDH: glyceraldehyde-3-phosphate dehydrogenase. Differences are shown as follows: $^{\star\star}P < 0.01$ versus control group; $^{\blacktriangle}P < 0.05$ versus model group; $^{\blacktriangle\blacktriangle}P < 0.01$ versus model group; $^{\blacklozenge\blacklozenge}P < 0.01$ versus acupuncture group; $^{\blacksquare\blacksquare}P < 0.01$ versus fluoxetine group. Results are presented as $\overline{x} \pm s$ for 10 rats in each group.

group versus Acu + H89 group and the FLX group versus FLX + H89 group (Table 3 and Figure 4).

4. Discussion

The present study aimed to identify molecular and neurobiological mechanisms responsible for antidepressant response following the treatment of acupuncture. A rat model of depressive disorder induced by CUMS was established. Open-field test (OFT), sucrose consumption, and body weight were employed to evaluate the depression-relevant behaviors, including the ability to adapt to new environments, the sensitivity to reward stimulation and pleasure, or mainly the state of anhedonia. Our findings indicated that the rats subjected to CUMS were observed to exhibit obviously poor appetite and significantly slow increase in body weight, the adaptive regression to new environments, the stagnancy to reward stimulation and pleasure, or altered mood switching from irascibility to low spirits throughout the CUMS procedure. The result of the present study is consistent with the current study illustrated that CUMS could induce depressive-like behaviors, effectively imitating the symptoms of depression in the patients [40, 41].

Acupuncture showed compelling antidepressant effects on ameliorating depression-related behaviors. Importantly, PKA, the CREB upstream regulator, and the phosphorylation of CREB on Ser133 by PKA, p-CREB, also showed a strain-dependent expression pattern. Although PKA and p-CREB expression levels were upregulated following the treatment of acupuncture and fluoxetine, inhibition of PKA-CREB signaling by H89 reversed the upregulation of p-CREB expression level (but not PKA and CREB) and the antidepressant effects on ameliorating depression-related behaviors of acupuncture and fluoxetine, suggesting that both acupuncture and fluoxetine could achieve the antidepressant effects by promoting the phosphorylation of CREB on Ser133 by PKA-CREB signaling. Other studies concerning the CREB signaling have shed light on the potentially promoting effects on neurogenesis implicated in cognitive behaviors or synaptic plasticity function involved in antidepression [42–44]. In the present study, we found that the downregulated expression levels of hippocampal PKA-α and p-CREB, induced by CUMS, were reversed by acupuncture. What is more, the upregulated expression level of p-CREB, but not PKA and CREB, was inhibited by H89, indicating that the increased p-CREB expression (phosphorylation of CREB) might be partly attributable to the increased activation of PKA. Although no significant difference was found in acupuncture versus fluoxetine, concerning inhibiting the phosphorylation of CREB (expression of p-CREB) by the PKA inhibitor H89, it is notable that the antidepressive effects of acupuncture on alleviating sucrose intake level and the horizontal motion scores were more compelling than fluoxetine following the administration of H89. All these results might indicate that the antidepressive response of acupuncture is not just dependent on PKA/CREB signaling, which is identical with our previous studies [45].

Acupuncture, one of the conventional therapies in traditional Chinese medicine (TCM), contributes to therapeutic effects by regulating the nervous, endocrine, and immune systems [45] and plays an important role in maintaining normal physiologic state of the organism. Based on the basic theory of TCM, acupoint compatibility plays an important role in the acupuncture prescription, which in turn is directly involved in the therapeutic effect clinically. During our previous studies, the underlying effects and mechanisms of acupuncture on depression have been investigated [46, 47]. Baihui (GV 20) and Yintang (GV 29) are considered to be the optimized acupoint modules in the treatment of depression [46, 47]. According to the basic theory of TCM, Baihui (GV 20) and Yintang (GV 29) are acupoints pertaining to the governor meridian, which has a direct contact with the brain through channels and collaterals [48, 49]. Accordingly, acupuncture at these acupoint modules can dredge channels and regulate the flow of Qi and the blood of the governor meridian, which in turn regulates mentality and alleviates depression [48–50]. Data from clinical investigations and laboratory animals have provided evidence that acupuncture exhibited antidepressant-like efficacy on depression [47, 51, 52]. Our previous studies have investigated that acupunctured at Baihui (GV 20) and Yintang (EX-HN 3) could well alleviate depression by increasing the expression of excitatory neurotransmitter in the hippocampus, attenuating impaired neurogenesis and inhibiting the apoptosis of hippocampal neurons [46, 47].

The present study has been evidenced that the activation of phosphorylation of CREB through the strain-dependent PKA/CREB signaling exhibits compelling antidepressant

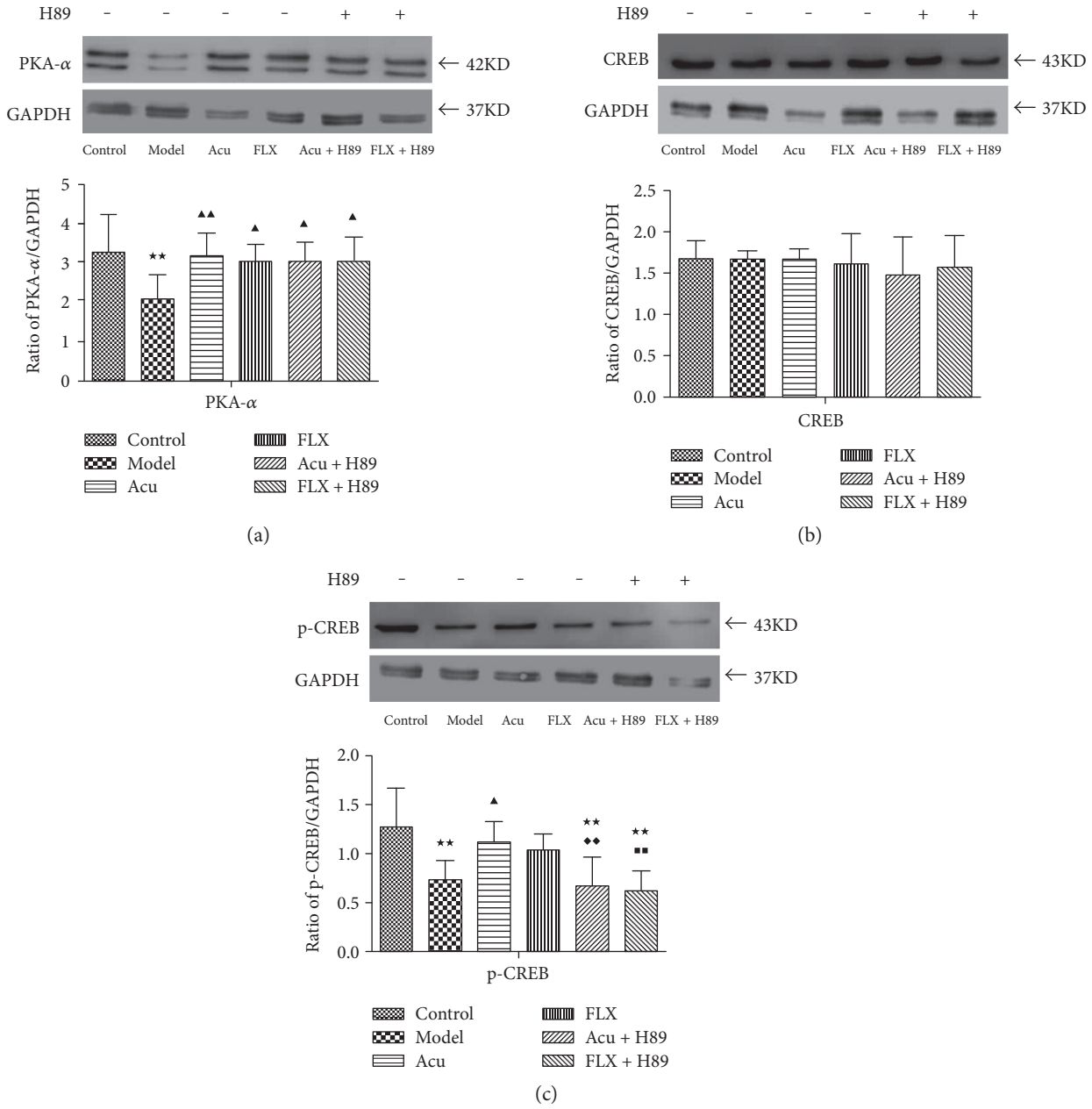

Figure 4: Differences showing the effects of stress/antidepressant treatments on the expression levels of hippocampal PKA-α, CREB, and p-CREB in depression rats induced by CUMS. (a) The effects of stress/antidepressant treatments on the expression level of hippocampal PKA-α in depression rats induced by CUMS. (b) The effects of stress/antidepressant treatments on the expression level of hippocampal CREB in depression rats induced by CUMS. (c) The effects of stress/antidepressant treatments on the expression level of hippocampal p-CREB in depression rats induced by CUMS. Differences are shown as follows: $^{\star\star}P < 0.01$ versus control group; $^{\blacktriangle}P < 0.05$ versus model group; $^{\blacktriangle\blacktriangle}P < 0.01$ versus model group; $^{\blacklozenge\blacklozenge}P < 0.01$ versus acupuncture group; $^{\blacksquare\blacksquare}P < 0.01$ versus fluoxetine group. Results are presented as $\bar{x} \pm s$ for 10 rats in each group. Acu: acupuncture group; FLX: fluoxetine group; Acu + H89: Acupuncture + H89 group; FLX + H89: Fluoxetine + H89 group; PKA-α: protein kinase A-α; CREB: cyclic adenosine monophosphate response element-binding protein; p-CREB: Phosphor-CREB; GAPDH: glyceraldehyde-3-phosphate dehydrogenase.

responses to acupuncture. Further studies will focus on the expression of BDNF and the downstream effector of PKA/CREB signaling and other signaling commonly responsible for individual differences in antidepressant responses between antidepressants and acupuncture, which in turn will elucidate the underlying mechanisms concerning the antidepressant response of acupuncture and explore new prospects of integrated medicine in the treatment of depression.

Conflicts of Interest

The authors declare that they have no competing interests.

Authors' Contributions

Huili Jiang and Xuhui Zhang contributed equally to this work. Huili Jiang and Xuhui Zhang had full access to all of the data in the study and take responsibility for the integrity of the data and the accuracy of the data analysis.

Acknowledgments

The authors' work reported here was supported by the National Natural Science Foundation of China (no. 81173334; no. 81373729).

References

[1] S. M. Thompson, A. J. Kallarackal, M. D. Kvarta, A. M. Van Dyke, T. A. LeGates, and X. Cai, "An excitatory synapse hypothesis of depression," *Trends in Neurosciences*, vol. 38, no. 5, pp. 279–294, 2015.

[2] R. C. Kessler, P. Berglund, O. Demler et al., "The epidemiology of major depressive disorder: results from the National Comorbidity Survey Replication (NCS-R)," *Journal of the American Medical Association*, vol. 289, no. 23, pp. 3095–3105, 2003.

[3] S. Hayley and D. Litteljohn, "Neuroplasticity and the next wave of antidepressant strategies," *Frontiers in Cellular Neuroscience*, vol. 7, p. 218, 2013.

[4] N. Vitureira and Y. Goda, "Cell biology in neuroscience: the interplay between Hebbian and homeostatic synaptic plasticity," *The Journal of Cell Biology*, vol. 203, no. 2, pp. 175–186, 2013.

[5] N. Maggio and M. Segal, "Differential modulation of long-term depression by acute stress in the rat dorsal and ventral hippocampus," *The Journal of Neuroscience*, vol. 29, no. 27, pp. 8633–8638, 2009.

[6] Y. Iwakura, H. Nawa, I. Sora, and M. V. Chao, "Dopamine D1 receptor-induced signaling through TrkB receptors in striatal neurons," *The Journal of Biological Chemistry*, vol. 283, no. 23, pp. 15799–15806, 2008.

[7] S. L. Oliveira, M. M. Pillat, A. Cheffer, C. Lameu, T. T. Schwindt, and H. Ulrich, "Functions of neurotrophins and growth factors in neurogenesis and brain repair," *Cytometry. Part a*, vol. 83, no. 1, pp. 76–89, 2013.

[8] L. M. Holsen, K. Lancaster, A. Klibanski et al., "HPA-axis hormone modulation of stress response circuitry activity in women with remitted major depression," *Neuroscience*, vol. 250, pp. 733–742, 2013.

[9] E. T. Rolls, "The mechanisms for pattern completion and pattern separation in the hippocampus," *Frontiers in Systems Neuroscience*, vol. 7, p. 74, 2013.

[10] G. J. Emslie, N. D. Ryan, and K. D. Wagner, "Major depressive disorder in children and adolescents: clinical trial design and antidepressant efficacy," *The Journal of Clinical Psychiatry*, vol. 66, Supplement 7, pp. 14–20, 2005.

[11] A. J. Rush, M. H. Trivedi, S. R. Wisniewski et al., "Acute and longer-term outcomes in depressed outpatients requiring one or several treatment steps: a STAR*D report," *The American Journal of Psychiatry*, vol. 163, no. 11, pp. 1905–1917, 2006.

[12] J. A. Bridge, S. Iyengar, C. B. Salary et al., "Clinical response and risk for reported suicidal ideation and suicide attempts in pediatric antidepressant treatment: a meta-analysis of randomized controlled trials," *Journal of the American Medical Association*, vol. 297, no. 15, pp. 1683–1696, 2007.

[13] F. Gomez, C. Venero, M. P. Viveros, and L. García-García, "Short-term fluoxetine treatment induces neuroendocrine and behavioral anxiogenic-like responses in adolescent male rats," *Experimental Brain Research*, vol. 233, no. 3, pp. 983–995, 2015.

[14] C. L. Raison, L. Capuron, and A. H. Miller, "Cytokines sing the blues: inflammation and the pathogenesis of depression," *Trends in Immunology*, vol. 27, no. 1, pp. 24–31, 2006.

[15] T. Traks, K. Koido, T. Eller et al., "Polymorphisms in the interleukin-10 gene cluster are possibly involved in the increased risk for major depressive disorder," *BMC Medical Genetics*, vol. 9, no. 1, pp. 111–118, 2008.

[16] S. Chourbaji, A. Urani, I. Inta et al., "IL-6 knockout mice exhibit resistance to stress-induced development of depression-like behaviors," *Neurobiology of Disease*, vol. 23, no. 3, pp. 587–594, 2006.

[17] P. V. Nguyen and N. H. Woo, "Regulation of hippocampal synaptic plasticity by cyclic AMP-dependent protein kinases," *Progress in Neurobiology*, vol. 71, no. 6, pp. 401–437, 2003.

[18] D. J. Titus, C. Furones, Y. Kang, and C. M. Atkins, "Age-dependent alterations in cAMP signaling contribute to synaptic plasticity deficits following traumatic brain injury," *Neuroscience*, vol. 231, pp. 182–194, 2013.

[19] G. Lonart, S. Schoch, P. S. Kaeser, C. J. Larkin, T. C. Südhof, and D. J. Linden, "Phosphorylation of RIM1alpha by PKA triggers presynaptic long-term potentiation at cerebellar parallel fiber synapses," *Cell*, vol. 115, no. 1, pp. 49–60, 2003.

[20] O. V. Vitolo, A. Sant'Angelo, V. Costanzo, F. Battaglia, O. Arancio, and M. Shelanski, "Amyloid beta-peptide inhibition of the PKA/CREB pathway and long-term potentiation: reversibility by drugs that enhance cAMP signaling," *Proceedings of the National Academy of Sciences of the United States of America*, vol. 99, no. 20, pp. 13217–13221, 2002.

[21] C. M. Powell, "Gene targeting of presynaptic proteins in synaptic plasticity and memory: across the great divide," *Neurobiology of Learning and Memory*, vol. 85, no. 1, pp. 2–15, 2006.

[22] J. A. Esteban, S. H. Shi, C. Wilson, M. Nuriya, R. L. Huganir, and R. Malinow, "PKA phosphorylation of AMPA receptor subunits controls synaptic trafficking underlying plasticity," *Nature Neuroscience*, vol. 6, no. 2, pp. 136–143, 2003.

[23] V. Duric, M. Banasr, P. Licznerski et al., "A negative regulator of MAP kinase causes depressive behavior," *Nature Medicine*, vol. 16, no. 11, pp. 1328–1332, 2010.

[24] S. Finkbeiner, S. F. Tavazoie, A. Maloratsky, K. M. Jacobs, K. M. Harris, and M. E. Greenberg, "CREB: a major mediator of neuronal neurotrophin responses," *Neuron*, vol. 19, no. 5, pp. 1031–1047, 1997.

[25] A. J. Shaywitz and M. E. Greenberg, "CREB: a stimulus-induced transcription factor activated by a diverse array of extracellular signals," *Annual Review of Biochemistry*, vol. 68, pp. 821–861, 1999.

[26] Y. Hu, D. L. Wu, C. X. Luo et al., "Hippocampal nitric oxide contributes to sex difference in affective behaviors [J]," *Proceedings of the National Academy of Sciences of the United States of America*, vol. 109, no. 35, pp. 14224–14229, 2012.

[27] J. W. Hwang, S. C. Xin, Y. M. Ou et al., "Enhanced default mode network connectivity with ventral striatum in subthreshold depression individuals," *Journal of Psychiatric Research*, vol. 76, pp. 111–120, 2016.

[28] J. W. Hwang, N. Egorova, X. Q. Yang et al., "Subthreshold depression is associated with impaired resting-state functional connectivity of the cognitive control network," *Translational Psychiatry*, vol. 5, article e683, 2015.

[29] J. Lu, J. Liang, J. R. Wang, L. Hu, Y. Tu, and J. Y. Guo, "Acupuncture activates ERK-CREB pathway in rats exposed to chronic unpredictable mild stress," *Evidence-Based Complementary and Alternative Medicine*, vol. 2013, Article ID 469765, p. 7, 2013.

[30] J. Liang, J. Lu, S. F. Cui, J. R. Wang, and Y. Tu, "Effect of acupuncture on expression of brain-derived neurotrophic factor gene and protein in cortex and hippocampus of depression in rats," *Journal Acupuncture Research*, vol. 37, no. 1, pp. 20–24, 2012, [Chinese].

[31] T. Chijiwa, A. Mishima, M. Hagiwara et al., "Inhibition of forskolin-induced neurite outgrowth and protein phosphorylation by a newly synthesized selective inhibitor of cyclic AMP-dependent protein kinase, N-[2-(p-bromocinnamylamino)ethyl]-5-isoquinolinesulfonamide (H-89), of PC12D pheochromocytoma cells," *The Journal of Biological Chemistry*, vol. 265, no. 9, pp. 5267–5272, 1990.

[32] A. Lochner and J. A. Moolman, "The many faces of H89: a review," *Cardiovascular Drug Reviews*, vol. 24, no. 3-4, pp. 261–274, 2006.

[33] P. Willner, A. Towell, D. Sampson, S. Sophokleous, and R. Muscat, "Reduction of sucrose preference by chronic unpredictable mild stress, and its restoration by a tricyclic antidepressant," *Psychopharmacology*, vol. 93, no. 3, pp. 358–364, 1987.

[34] B. H. Herman, S. Berger, and S. G. Holtzman, "Comparison of electrical resistance, bubble withdrawal, and stereotaxic method for cannulation of cerebral ventricles," *Journal of Pharmacological Methods*, vol. 10, no. 2, pp. 143–155, 1983.

[35] Y. Xia and T. L. Krukoff, "Differential neuronal activation in the hypothalamic paraventricular nucleus and autonomic/neuroendocrine responses to I.C.V. endotoxin," *Neuroscience*, vol. 121, no. 1, pp. 219–231, 2003.

[36] G. Paxinos and C. Watson, *The Rat Brain in Stereotaxic Coordinates*, Elsevier Academic Press, Burlington, MA, USA, fifth edition, 2003.

[37] K. A. Morris and P. E. Gold, "Epinephrine and glucose modulate training-related CREB phosphorylation in old rats: relationships to age-related memory impairments," *Experimental Gerontology*, vol. 48, no. 2, pp. 115–127, 2013.

[38] S. G. Yu and Y. Guo, *Experimental Acupuncture Science*, Shanghai Science and Technology Press, Shanghai, 2009.

[39] R. J. Katz, K. A. Roth, and B. J. Carroll, "Acute and chronic stress effects on open field activity in the rat: implications for a model of depression," *Neuroscience and Biobehavioral Reviews*, vol. 5, no. 2, pp. 247–251, 1981.

[40] Y. W. Luo, Y. Xu, W. Y. Cao et al., "Insulin-like growth factor 2 mitigates depressive behavior in a rat model of chronic stress," *Neuropharmacology*, vol. 89, pp. 318–324, 2015.

[41] A. B. Hains, Y. Yabe, and A. F. Arnsten, "Chronic stimulation of alpha-2A-Adrenoceptors with guanfacine protects rodent prefrontal cortex dendritic spines and cognition from the effects of chronic stress," *Neurobiology of Stress*, vol. 2, pp. 1–9, 2015.

[42] A. E. Freitas, D. G. Machado, J. Budni et al., "Fluoxetine modulates hippocampal cell signaling pathways implicated in neuroplasticity in olfactory bulbectomized mice," *Behavioural Brain Research*, vol. 237, pp. 176–184, 2013.

[43] S. S. Patil, F. Schlick, H. Höger, and G. Lubec, "Involvement of individual hippocampal signaling protein levels in spatial memory formation is strain-dependent," *Amino Acids*, vol. 39, no. 1, pp. 75–87, 2010.

[44] R. S. Duman, J. Malberg, S. Nakagawa, and C. D'Sa, "Neuronal plasticity and survival in mood disorders," *Biological Psychiatry*, vol. 48, no. 8, pp. 732–739, 2000.

[45] Z. Guo, Y. Tu, T. W. Guo et al., "Electroacupuncture pretreatment exhibits anti-depressive effects by regulating hippocampal proteomics in rats with chronic restraint stress," *Neural Regeneration Research*, vol. 10, no. 8, pp. 1298–1304, 2015.

[46] D. Duan, X. Yang, T. Ya, and L. Chen, "Hippocampal gene expression in a rat model of depression after electroacupuncture at the Baihui and Yintang acupoints," *Neural Regeneration Research*, vol. 9, no. 1, pp. 76–83, 2014.

[47] D. M. Duan, Y. Tu, L. P. Chen, and Z. J. Wu, "Efficacy evaluation for depression with somatic symptoms treated by electroacupuncture combined with fluoxetine [J]," *Journal of Traditional Chinese Medicine*, vol. 29, no. 3, pp. 167–173, 2009.

[48] T. Guo, Z. Guo, X. Yang et al., "The alterations of IL-1beta, IL-6, and TGF-beta levels in hippocampal CA3 region of chronic restraint stress rats after electroacupuncture (EA) pretreatment," *Evidence-Based Complementary and Alternative Medicine*, vol. 2014, Article ID 369158, p. 7, 2014.

[49] X. Zhang, Y. Song, T. Bao et al., "Antidepressant-like effects of acupuncture involved the ERK signaling pathway in rats," *BMC Complementary and Alternative Medicine*, vol. 16, no. 1, p. 380, 2016.

[50] Y. Mo, H. Yao, H. Song et al., "Alteration of behavioral changes and hippocampus galanin expression in chronic unpredictable mild stress-induced depression rats and effect of electroacupuncture treatment," *Evidence-Based Complementary and Alternative Medicine*, vol. 2014, Article ID 179796, p. 8, 2014.

[51] Y. Feng, J. Johansson, R. Shao, L. Mannerås-Holm, H. Billig, and E. Stener-Victorin, "Electrical and manual acupuncture stimulation affect oestrous cyclicity and neuroendocrine function in an 5α-dihydrotestosterone-induced rat polycystic ovary syndrome model," *Experimental Physiology*, vol. 97, no. 5, pp. 651–662, 2012.

[52] W. M. Jung, I. S. Lee, C. Wallraven, Y. H. Ryu, H. J. Park, and Y. Chae, "Cortical activation patterns of bodily attention triggered by acupuncture stimulation," *Scientific Reports*, vol. 5, p. 12455, 2015.

Hindawi
Neural Plasticity
Volume 2017, Article ID 4716792, 8 pages
https://doi.org/10.1155/2017/4716792

Clinical Study

Neuroplasticity Changes on Human Motor Cortex Induced by Acupuncture Therapy: A Preliminary Study

Yi Yang,[1,2] Ines Eisner,[1] Siqi Chen,[3] Shaosong Wang,[1] Fan Zhang,[1] and Linpeng Wang[1]

[1]*Acupuncture and Moxibustion Department, Beijing Hospital of Traditional Chinese Medicine, Capital Medical University, Meishuguanhoujie No. 23, Dongcheng District, Beijing 100010, China*
[2]*Department of Chinese Medicine, Capital Medical University, Youanmenwai Xitoutiao No. 10, Fengtai District, Beijing 100069, China*
[3]*Acupuncture Department, Beijing University of Chinese Medicine, Beisanhuan Donglu No. 11, Chaoyang District, Beijing 100029, China*

Correspondence should be addressed to Linpeng Wang; wlp5558@sina.com

Received 23 August 2016; Revised 3 January 2017; Accepted 19 January 2017; Published 15 February 2017

Academic Editor: Ke-Lun Wang

Copyright © 2017 Yi Yang et al. This is an open access article distributed under the Creative Commons Attribution License, which permits unrestricted use, distribution, and reproduction in any medium, provided the original work is properly cited.

While neuroplasticity changes measured by transcranial magnetic stimulation have been proved to be highly correlated to motor recovery and have been tested in various forms of interventions, it has not been applied to investigate the neurophysiologic mechanism of acupuncture therapy. The aim of this study is to investigate neuroplasticity changes induced by a single session of acupuncture therapy in healthy adults, regarding the excitability change on bilateral primary motor cortex and interhemispheric inhibition. Ten subjects took a 30-minute acupuncture therapy and the same length relaxing phase in separate days. Transcranial magnetic stimulation measures, including resting motor threshold, amplitudes of motor-evoked potential, and interhemispheric inhibition, were assessed before and 10 minutes after intervention. Acupuncture treatment showed significant changes on potential amplitude from both ipsilateral and contralateral hemispheres to acupuncture compared to baseline. Also, interhemispheric inhibition from the contralateral motor cortex to the opposite showed a significant decline. The results indicated that corticomotoneuronal excitability and interhemispheric competition could be modulated by acupuncture therapy on healthy subjects. The following question about whether these changes will be observed in the same way on stroke patients and whether they correlate with the therapeutic effect on movement need to be answered by following studies. This trial is registered with ISRCTN13074245.

1. Introduction

Motor functional recovery after stroke depends on a number of neuroplastic underpinnings. By using transcranial magnetic stimulation (TMS), studies targeting cortical and corticospinal physiology of both the affected and the spared hemisphere have provided us insight into these underlying mechanisms of motor deficits and beneficial effects of therapeutic interventions. One fundamental finding is that patients after stroke exhibit overactive in their contralesional primary motor cortex (M1) and therefore show high level of neural excitability, while the ipsilesional M1 exhibit low excitatory level [1]. The downregulating excitability in the contralesional M1 as well as the upregulating excitability in the ipsilesional M1 are correlated with better motor outcome in stroke patients [2–5]. Another important finding is that the rebalance of interhemispheric competition could play an important role in the process of motor recovery. It is suggested that suppressing the excitability of the unaffected hemisphere could enhance motor recovery by reducing abnormal interhemispheric inhibition (IHI) of the hemisphere affect by stroke [6–8]. Although TMS measures have been used to dissect the mechanism of various forms of treatments [9, 10], it has not been applied to investigate the neurophysiologic mechanism of acupuncture therapy.

Acupuncture is a promising adjuvant intervention that was introduced for the rehabilitation of patients with hemiparesis for decades. It has been applied to stroke patients with

motor deficits and led to a remarkable motor recovery [11, 12]. This phenomenon led to studies demonstrating and characterizing physiological mechanisms associated with acupuncture. Previous data on physiological effects of acupuncture assessed by TMS generally suggested an inhibitory effect of specific single acupoint on motor cortex excitability [13–16]. However, it is not yet known that in what way could the clinical acupuncture regimen, comprising multiple acupoints as in the real-world settings, modulate plastic changes in the human primary motor cortex. Moreover, the TMS measure to interhemispheric inhibition (IHI) has not been reported in any previous acupuncture studies. To address these issues, this present exploratory study was conducted. We used TMS to investigate how bilateral M1 excitability and IHI could be modulated by one single session of acupuncture therapy on healthy subject.

2. Method

2.1. Subjects. Ten healthy volunteers (five males, five females; 24–40 years old, 28.3 ± 5.5 years, mean ± SD) participated in the study. None of the participants had neurological, psychiatric, or other medical problems or reported any contraindication to TMS [17]. All subjects were right-handed according to the Oldfield handedness inventory[18]. The protocol for this study was approved by the Research Ethical Committee of Beijing Traditional Chinese Medicine Hospital (China) and was conducted according to the Declaration of Helsinki. All subjects gave written informed consent before their participation.

2.2. Intervention. All subjects underwent both needling intervention (a 30-min period of acupuncture treatment) and control period (a 30-min idle time, with no stimulation) in different days in a randomized order, with an interval of 7 days.

An experienced acupuncturist performed the acupuncture needling with disposable acupuncture needles (Huatuo brand, Suzhou Medical Appliance Factory, Suzhou, China; 0.25 mm diameter, 30 mm length). The acupoints used in this study were based on the acupuncture prescription for the treatment of poststroke motor dysfunction, named "Wang's Extremities' Acupoints Recipe" (*Wang Shi Shou Zu Shi Er Zhen*). The ten acupoints (*Quchi* (LI-11), *Shousanli* (LI-10), *Waiguan* (TB-5), *Hegu* (LI-4), *Zusanli* (ST-36), *Yanglingquan* (GB-34), *Sanyinjiao* (SP-6), and the last three points of *Baxie* (EX-UE9)) used were located on the left forearm, hand and lower leg. The needling methods of "lifting and thrusting" (120 times per minute) and "rotating" (180 degrees, 120 circle per minute) were conducted on each point until the sensation of *Deqi* (a characteristic sensation of aching and tingling) was reported by the subjects. Then, the needles were kept in situ without further stimulation. The control condition was conducted because attentional and cognitive factors vary during the course of the experiment and that could influence cortical excitability [19]. Subjects sat comfortably on an armchair and were instructed to keep relaxed but alert during both the control period and acupuncture intervention.

2.3. Transcranial Magnetic Stimulation Measures. Transcranial magnetic stimulation was used to evaluate the corticomotor excitability in each hemisphere as well as interhemispheric inhibition (IHI), before and at 10 min after the experimental intervention (needling/control). The TMS procedure was performed with the subject seated comfortably in a quiet, semidarkened room. The upper limbs were kept supported with muscles in resting condition. Surface electromyogram (EMG) was recorded from the left and right first dorsal interosseous (FDI) muscles with 9 mm diameter Ag/AgCl surface electrodes on a belly tendon montage. Responses were input to an amplifier through filters set at 100 Hz and 3 kHz. They were then digitized at 10 kHz and stored in a computer for later offline analyses (Cambridge Electronics Design, Cambridge, UK).

TMS was delivered to the hand area of the motor cortex on the left ($M1_L$) and right hemisphere ($M1_R$) using the Magstim 200 stimulator (Magstim Co. Ltd., Whitland, Dyfed, UK), via a figure-of-eight coil (wing diameter 9 cm) oriented to induce current flow in a posterior to anterior direction in the underlying tissues. The coil was positioned over scalp at the "hot spot" for the FDI muscle.

2.3.1. Measures of Corticomotoneuronal Excitability. The resting motor threshold (rMT) and MEP amplitudes were determined, respectively, for each side of FDIs, to elucidate the basic properties of acupuncture-induced plasticity. The rMT was defined as the lowest stimulation intensity that generated motor-evoked potentials (MEPs) ≥ 50 μV amplitude (peak to peak) in the relaxed FDI in at least 5 of 10 consecutive stimuli [20]. Mean MEP amplitudes were obtained in response to 15 TMS stimuli delivered at each of five stimulus intensities: 90, 100, 110, 130 and 150% of the rMT in randomized order at 5 s interstimulus interval. Based on these data, the recruitment curve was constructed to relate the amplitude of the response to the TMS stimulation intensity. Cortical stimulation was consistently performed first on the left hemisphere followed by the right hemisphere.

2.3.2. Interhemispheric Inhibition. Interhemispheric inhibition effect from the right hemisphere to the left hemisphere was evaluated by delivering paired-pulse stimuli bilaterally (Bistim module, Magstim Co. Ltd.) to the previously determined M1 hotspot for FDIs while participants maintained the muscles in a full relaxed position. The testing stimulus (TS) was set at intensity of +30% rMT in the right FDI muscle. The conditioning stimulus (CS) intensities were randomized at intensities +0%, +10%, +30%, and +50% rMT of the left FDI. Recording blocks consisted of 15 MEPs, the interstimulus interval between CS and TS was set as 10 ms, and the interval between each paired stimuli was 5 s. The amplitude of the conditioned response from IHI was expressed as a percentage of the size of mean MEP amplitude of test stimuli alone.

2.4. F-Wave. Supramaximal electrical stimulation was performed in five subjects in a separate session, to measure the F-wave from the left FDI. This measure was chosen to test the effect of acupuncture therapy at the spinal level and therefore

to differentiate excitability changes at cortical or subcortical sites [21]. F-waves were recorded and averaged before and 10 min after acupuncture intervention.

3. Statistical Analysis

SPSS software (version 23.0, SPSS Inc., Chicago, IL) was used for statistical analysis. Two-way repeated-measures ANOVA was used to compare rMTs over treatments on the same side of FDI before and after the intervention (factors: TIME and TREATMENT). Differences of intervention-induced changes on MEP amplitudes from the recruitment curve were compared with three-way repeated-measures ANOVA model with factors "TIME" (pre- and postintervention), "TREATMENT" (acupuncture and control), and "INTENSITY" (five levels). Bonferroni's post hoc test was used for further analyses. Changes of IHI were compared with three-way repeated-measures ANOVA model with factors "TIME" (pre- and postintervention), "TREATMENT" (acupuncture and control), and "INTENSITY" (four levels). The significance level was set at $P < 0.05$. Unless otherwise stated, values are reported as mean ± standard deviation. All ANOVA results are given with the F value and P value.

4. Results

Based on the acupuncture prescription for poststroke motor dysfunctional treatment, acupuncture needling for this experiment was performed on the left arm and leg. All TMS assessments were performed on both hemispheres, monitoring EMG on left and right FDI muscles. All thresholds are expressed as a percentage of maximum stimulator output (%MSO).

4.1. Effects of Acupuncture on rMT. Neither the acupuncture intervention nor the relaxing period altered rMT (Table 1). Mean rMTs for the left FDI were 51.50±6.364 preintervention and 49.90 ± 5.109 postintervention for the acupuncture treatment, and 51.30±7.17 preintervention and 50.80±7.361, postintervention for the control condition. Mean rMT for the right FDI were 52.50±5.986 preintervention and 51.50±4.720 postintervention for the acupuncture treatment and 49.10 ± 2.923 preintervention and 48.90 ± 3.695 postintervention for the control. Two-way repeated-measures ANOVA showed no significant effects of intervention nor time or on either left FDIs (TREATMENT, $F = 0.016$, $P = 0.902$; TIME, $F = 2.702$, $P = 0.135$; TREATMENT × TIME interaction, $F = 0.595$, $P = 0.460$) or right FDIs (TREATMENT, $F = 2.201$, $P = 0.172$; TIME, $F = 0.764$, $P = 0.405$; TREATMENT × TIME interaction, $F = 0.310$, $P = 0.591$) (Figures 1(a) and 1(d)).

4.2. Effects of Acupuncture on MEP Amplitude. According to the three-way ANOVA, the pattern of MEP amplitudes differed significantly between the acupuncture and control intervention across time for both sides of FDIs, respectively (Table 1). For the left FDI, significant effects were shown on TREATMENT ($F = 6.202$, $P = 0.034$), TIME × TREATMENT interaction ($F = 19.431$, $P = 0.002$) and TIME × TREATMENT × INTENSITY interaction ($F = 6.049$, $P = 0.027$). This indicates that the two interventions modulated MEP in significantly different ways across time. Similarly, for the right FDI, it also showed significant effects of TREATMENT ($F = 7.151$, $P = 0.025$), TIME × TREATMENT interactions ($F = 25.475$, $P = 0.001$), and TIME × TREATMENT × INTENSITY interactions ($F = 4.558$, $P = 0.049$).

Post hoc analysis using Bonferroni's adjustment revealed that the MEP amplitudes were modulated only by acupuncture, on both left and right FDI, but not the control period. There were significantly smaller MEPs on the left FDI elicited at all the four intensities above 90% RMT after acupuncture than baseline (Figure 1(b) and Table 2). Meanwhile, the right FDI showed significantly larger MEPs elicited at intensities 100%, 110% and 130% rMT after acupuncture than baseline (Figure 1(c) and Table 2). On the contrary, the control intervention induced no significant changes on neither sides of FDI across time ($P > 0.05$ for both sides at all intensity levels, Figures 1(e) and 1(f)).

4.3. Effects of Acupuncture on IHI. The three-way ANOVA analysis showed that the percentage of the size of MEP amplitudes from TS performed differently between the two interventions across time points (TIME × TREATMENT interaction, $F = 11.976$, $P = 0.007$) (Table 1). Post hoc analysis with Bonferroni's adjustment showed significant increment after the acupuncture treatment on the percentage of MEP amplitudes from TS at CS intensity 100%, 130% and 150%, which indicated a declined inhibition from the right M1 (contralateral to acupuncture side) to the left M1 (ipsilateral to acupuncture side) (Figure 2(a) and Table 2). In contrast, no significant difference was shown after the control condition (Figure 2(b)).

4.4. Site of Changes in Motor Excitability (F-Wave). The mean F-wave amplitudes in the left FDI before and after acupuncture intervention were not significantly different at 198.00 ± 25.48 μV and 218.20 ± 36.27 μV, respectively ($t = 1.822$, $P = 0.143$).

5. Discussion

This is the first study that investigated the neuroplastic mechanism of acupuncture therapy on cortical excitability and interhemispheric inhibition. The acupuncture therapy was found to induce a significant modulation of MEP amplitudes of the motor pathways that depart from the contralateral primary motor cortex. Changes in MEP amplitude also occur on the ipsilateral corticospinal excitability following acupuncture. No significant changes of peripheral excitability (F-wave) were observed before and after acupuncture. The results indicate that changes in corticomotoneuronal excitability could be elicited by acupuncture intervention. Also, the interhemispheric inhibition from the contralateral M1 to the ipsilateral M1 showed a significant decline, which might explain the change on ipsilateral M1.

The recruitment curve of MEP amplitudes is a convincible parameter for cortical excitement level [10]. The decrease of

Table 1: General comparisons by two-way/three-way repeated-measures ANOVA on TMS measures of cortical excitability from both hemisphere and IHI.

	df	*F* value	*P* value
RMT			
Left FDI			
TIME	1,9	2.702	0.135
TREATMENT	1,9	0.016	0.902
TIME ∗ TREATMENT	1,9	0.595	0.460
Right FDI			
TIME	1,9	0.764	0.405
TREATMENT	1,9	2.201	0.172
TIME ∗ TREATMENT	1,9	0.310	0.591
MEP amplitudes			
Left FDI ($n = 10$)			
TIME	1,9	29.474	<0.001*
TREATMENT	1,9	6.202	0.034*
INTENSITY	4,6	44.853	<0.001*
TIME ∗ TREATMENT	1,9	19.431	0.002*
TIME ∗ INTENSITY	4,6	1.930	0.225
TREATMENT ∗ INTENSITY	4,6	2.418	0.160
TIME ∗ TREATMENT ∗ INTENSITY	4,6	6.049	0.027*
Right FDI ($n = 10$)			
TIME	1,9	48.285	<0.001*
TREATMENT	1,9	7.151	0.025*
INTENSITY	4,6	27.591	0.001*
TIME ∗ TREATMENT	1,9	25.475	0.001*
TIME ∗ INTENSITY	4,6	4,722	0.046*
TREATMENT ∗ INTENSITY	4,6	8.096	0.013*
TIME ∗ TREATMENT ∗ INTENSITY	4,6	4.558	0.049*
IHI			
TIME	1,9	2,739	0.132
TREATMENT	1,9	3.480	0.095
INTENSITY	3,7	16.012	0.002*
TIME ∗ TREATMENT	1,9	11.976	0.007*
TIME ∗ INTENSITY	3,7	1.425	0.314
TREATMENT ∗ INTENSITY	3,7	0.879	0.496
TIME ∗ TREATMENT ∗ INTENSITY	3,7	1.128	0.401

RMT: resting motor threshold; MEP: motor-evoked potential; IHI: interhemispheric inhibition; FDI: first dorsal interosseous; df: degrees of freedom. *$P < 0.05$.

the recruitment curve on the hemisphere contralateral to acupuncture suggested a reduction in the excitability level of the contralateral M1. The results of F-wave further ruled out the possibility of excitability change of the motoneuronal pool in the spinal cord, which has been previously addressed in other studies and gave evidence to the supraspinal mechanism for this acupuncture-induced plasticity change [13, 14].

The rMT and MEP amplitudes were chosen in this study as measures of neuroplasticity change. While there were noticeable changes on MEP amplitudes, few modulations

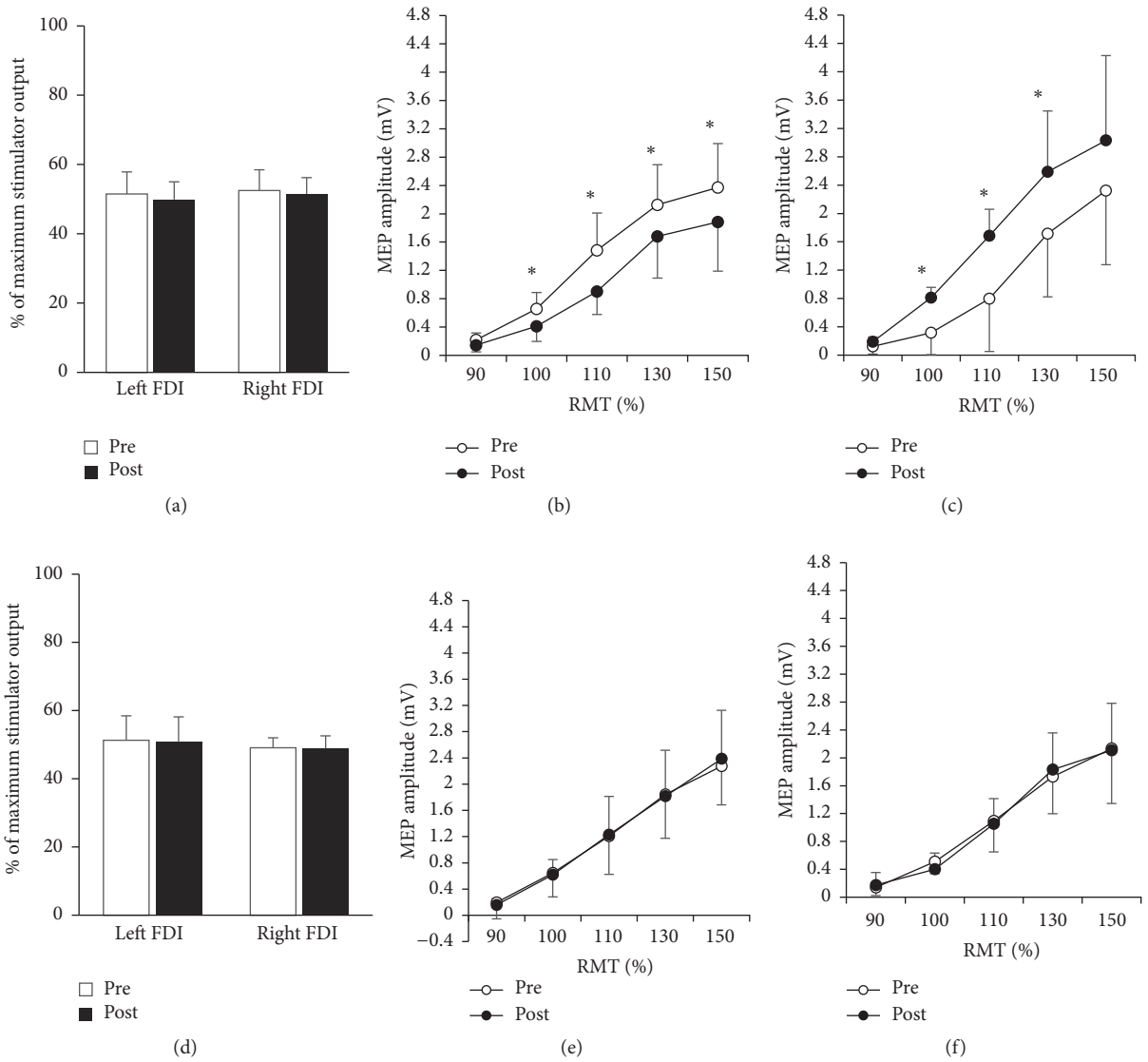

Figure 1: TMS properties of intervention-induced plasticity. (a–c) Effects of acupuncture on TMS variables. (a) Motor thresholds (mean ± SD). Acupuncture affected the RMT of neither the contralateral nor ipsilateral FDI of acupuncture ($P > 0.5$). Preintervention (open bars); postintervention (filled bars). (b) The recruitment curve (mean ± SEM) from the left FDI (ipsilateral FDI of acupuncture). The ordinate gives the MEP size in mV; the abscissa shows the stimulus intensity relative to RMT. Preintervention (○); postintervention (●). Significantly smaller MEPs were elicited at intensities greater than 90% RMT after acupuncture. (c) The recruitment curve (mean ± SEM) from the right FDI (contralateral FDI of acupuncture). Significantly larger MEPs were elicited at intensities 100%, 110%, and 130% RMT after acupuncture. (d–f) Variables by the control intervention. (d) Motor thresholds (mean ± SD). RMT in neither the left FDI nor the right FDI was altered by the control period. (e) The recruitment curve (mean ± SEM) from the left FDI. No significant changes of MEP amplitude were elicited by the control period. (f) The recruitment curve (mean ± SEM) from the right FDI. No significant changes of MEP amplitude were elicited by the control period. $^{*}P < 0.01$ (Bonferroni's post hoc adjustment).

were altered on rMT after acupuncture. Although both rMT and MEP amplitude are measures of cortical excitability, rMT is mainly affected by mechanisms of neuronal membrane excitability involving sodium and calcium channels [22, 23]. In contrast, MEP amplitudes are predominantly influenced by changes in synaptic excitability, which was evidenced by alterations in presence of pharmacological modifiers for synaptic transmission [24]. Our results imply that acupuncture might modulate the cortical excitability by influencing the activity of neural synapsis, instead of the neuronal membrane.

Our results show that acupuncture also influenced the excitability of the ipsilateral hemisphere. The increasement of the MEP amplitudes on the hemisphere ipsilateral to acupuncture indicate an increase of excitability of the ipsilateral M1. A reasonable explanation of this excitability increment is the transcallosal pathway model. As mentioned above, the acupuncture intervention reduced the excitability level of the

Table 2: Post hoc comparison by paired t-test on MEP amplitudes and IHI before and after acupuncture.

	Time 1	Time 2	t value	P value
MEP amplitudes (mV)				
Left FDI				
90% RMT	0.218 ± 0.099	0.137 ± 0.091	2.616	0.028
100% RMT	0.658 ± 0.229	0.405 ± 0.221	3.333	0.009*
110% RMT	1.485 ± 0.526	0.837 ± 0.359	4.407	0.002*
130% RMT	2.129 ± 0.565	1.509 ± 0.494	4.159	0.002*
150% RMT	2.372 ± 0.620	1.732 ± 0.666	4.738	0.001*
Right FDI				
90% RMT	0.124 ± 0.069	0.189 ± 0.108	−1.648	0.134
100% RMT	0.317 ± 0.145	0.812 ± 0.309	−4.169	0.002*
110% RMT	0.796 ± 0.376	1.683 ± 0.744	−3.781	0.004*
130% RMT	1.714 ± 0.859	2.587 ± 0.892	−3.769	0.004*
150% RMT	2.323 ± 1.198	3.031 ± 1.046	−2.859	0.019
IHI (%)				
100% RMT	88.281 ± 15.831	106.079 ± 11.508	−3.556	0.006*
110% RMT	88.497 ± 15.868	102.046 ± 19.423	−1.945	0.084
130% RMT	69.545 ± 20.314	92.743 ± 17.763	−3.826	0.004*
150% RMT	55.937 ± 20.865	77.705 ± 19.524	−4.410	0.002*

MEP: motor-evoked potential; IHI: interhemispheric inhibition; FDI: first dorsal interosseous.
Time 1. Before acupuncture intervention.
Time 2. 10 min after the removal of all needles.
* $P < 0.01$ for MEP analysis and $P < 0.0125$ for IHI, as Bonferroni's post hoc adjusted significant level.

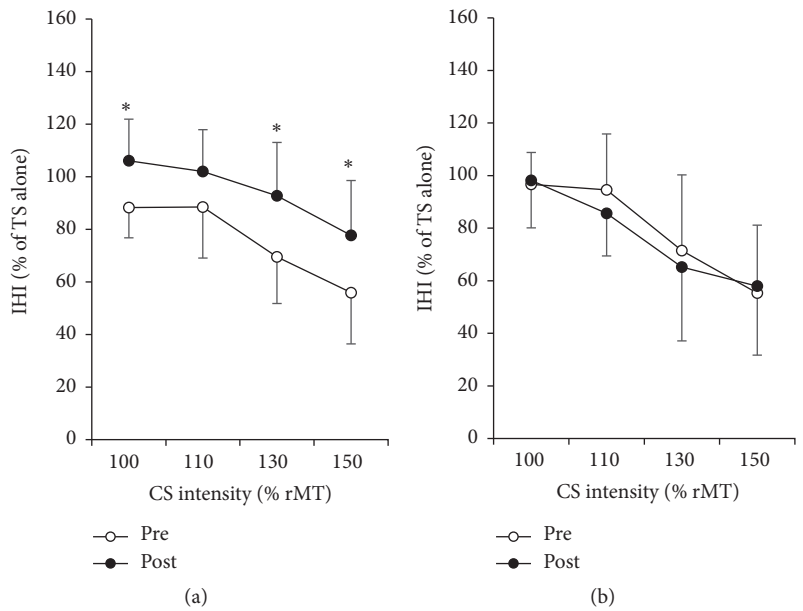

Figure 2: Interhemispheric inhibition (IHI) curves. IHI curves ($N = 10$) show inhibition effect from the M1 in the right hemisphere (where the conditioning stimulus (CS) was delivered) to the M1 in the left hemisphere (where the testing stimulus (TS) was delivered). The abscissa indicates the CS intensities expressed as a fraction of rMT. The ordinate indicates the amplitude of conditioned MEP from the left M1 expressed as a percentage of the MEPs from TS alone. Higher values represent lower inhibition from the right M1 to the left M1. Preintervention (○); postintervention (●). After the intervention, significantly lower inhibitions from CS to TS were observed from the treatment of acupuncture (a) but not the control (b). * $P < 0.0125$ (Bonferroni's post hoc adjustment).

contralateral M1. As a result, its inhibitive influence toward the opposite site–the ipsilateral M1, might also be declined. This assumption was supported by the change of IHI curves, which showed that the inhibitory effect from the right M1 (contralateral to acupuncture side) to the left M1 (ipsilateral to acupuncture side) declined significantly after acupuncture intervention. Since the ipsilateral M1 received less inhibition, its excitability increased. It might be the explanation of how acupuncture modulates the excitability of the ipsilateral M1. Besides, since acupuncture could modulate the interhemispheric activity, which has been proved to be an important mechanism underlying motor recovery, this model could be one possible explanation of the effect of acupuncture treatment for poststroke dysfunctions.

According to Chinese medical theory, acupuncture therapy functions through the regulation of *Qi* (the energy). There are twelve main channels and meridians (called *Jing Luo*) that located all over the body and connected in circles with certain orders. The *Qi* keeps running through the twelve channels and meridians and this takes it 28 minutes to finish one whole round. Therefore, the therapeutic effect of stimuli on acupoints could travel to everywhere around the body through the channels and meridians, carried by the circular movement of *Qi*. The needling in the left extremities could then modulate not only the body function nearby the acupoints but also the function of the distant organs, including the ipsilateral and contralateral hemisphere.

In this study, the acupuncture intervention with acupoint formula for the treatment of motor recovery after stroke is demonstrated being capable of modulating the excitability of primary motor cortex as well as the interhemispheric competition, which have been proposed as essential mechanisms for motor recovery on stroke patients. However, results from this study could not answer the question how this therapy could affect the neuroplasticity on poststroke brain. After a stroke attack, the human brain shows various changes based on the location and range of the lesion. Therefore, future studies should be conducted using acupuncture treatment on patients sorted with lesion location (cortical, subcortical, etc.) to figure out the effect of acupuncture therapy on poststroke neuroplasticity.

There are other sorts of technique that can modulate cortical excitability and have been explored as a possible adjuvant of poststroke neurorehabilitative treatment. For example, previous studies have suggested that noninvasive brain stimulation (NIBS), including repetitive transcranial magnetic stimulation (rTMS) and direct current stimulation (tDCS), may be beneficial to motor recovery after neurological injury, by modulating cortical motor excitability from both the ipsilesional and contralesional hemispheres [3, 25–27]. Meanwhile, it has been proven that the plasticity of primary sensorimotor cortex is also responsive to peripheral sensory stimulations. Besides acupuncture, peripheral electrical nerve stimulation, as a form of simple, painless somatosensory input, has been demonstrated to modulate corticomotoneuronal excitability [28]. The mechanisms underlying this sensorimotor cortical plasticity are still not well understood. One possible mechanism involves the thalamic nucleus, which receives somatosensory input while links to the primary motor cortex by direct projections. Another hypothesis is that the site of this sensory-motor interaction located at the motor cortex itself [29]. It is also possible that other motor cortical areas which receive somatotopically organized somatosensory information are involved in this sensorimotor interaction [28]. As a unique kind of peripheral sensory stimulation, acupuncture may share some of these mechanisms with regard to its effectiveness on cortical plasticity. However, since it has quite different characteristics from peripheral electrical stimulation (e.g., acupuncture induces pain during treatment), its mechanism requests further research.

The main limitation of this study is the small sample size. Also, as for the method of control, no sham acupuncture was applied in the present study. According to the Standards for Reporting Interventions in Clinical Trials of Acupuncture (STRICTA), sham acupuncture is a proper control method for acupuncture studies. There are commonly recommended methods as sham acupuncture intervention, such as needling unrelated or sham acupoints and superficial needling. However, as a preliminary study, the aim of this research is to demonstrate the effect of acupuncture treatment on cortical activity, instead of comparing the effect of different acupoints or needling techniques. Hence, idle period, as a classic design for control in cortical excitability research, rather than sham acupuncture, was identified as the optimal method for the control design in this study.

6. Conclusion

Our finding indicated that acupuncture could modulate the excitability of M1 as well as the interhemispheric inhibition on healthy subjects. The following question about whether these changes will be observed in the same way on stroke patients and if it is correlated with the beneficial effect on behavioural improvement need to be answered by following studies.

Competing Interests

The authors declare that there is no conflict of interests regarding the publication of this paper.

Acknowledgments

This study is funded by Beijing Municipal Administration of Hospitals Clinical Medicine Development of Special Funding Support (code: ZYLX201412).

References

[1] J. Liepert, F. Hamzei, and C. Weiller, "Motor cortex disinhibition of the unaffected hemisphere after acute stroke," *Muscle and Nerve*, vol. 23, no. 11, pp. 1761–1763, 2000.

[2] N. Takeuchi, T. Chuma, Y. Matsuo, I. Watanabe, and K. Ikoma, "Repetitive transcranial magnetic stimulation of contralesional primary motor cortex improves hand function after stroke," *Stroke*, vol. 36, no. 12, pp. 2681–2686, 2005.

[3] N. Takeuchi, T. Tada, M. Toshima, T. Chuma, Y. Matsuo, and K. Ikoma, "Inhibition of the unaffected motor cortex by 1 Hz

repetitive transcranical magnetic stimulation enhances motor performance and training effect of the paretic hand in patients with chronic stroke," *Journal of Rehabilitation Medicine*, vol. 40, no. 4, pp. 298–303, 2008.

[4] N. Yozbatiran, M. Alonso-Alonso, J. See et al., "Safety and behavioral effects of high-frequency repetitive transcranial magnetic stimulation in stroke," *Stroke*, vol. 40, no. 1, pp. 309–312, 2009.

[5] P. S. Boggio, A. Nunes, S. P. Rigonatti, M. A. Nitsche, A. Pascual-Leone, and F. Fregni, "Repeated sessions of noninvasive brain DC stimulation is associated with motor function improvement in stroke patients," *Restorative Neurology and Neuroscience*, vol. 25, no. 2, pp. 123–129, 2007.

[6] F. Fregni, P. S. Boggio, C. G. Mansur et al., "Transcranial direct current stimulation of the unaffected hemisphere in stroke patients," *NeuroReport*, vol. 16, no. 14, pp. 1551–1555, 2005.

[7] B. W. Vines, D. G. Nair, and G. Schlaug, "Contralateral and ipsilateral motor effects after transcranial direct current stimulation," *NeuroReport*, vol. 17, no. 6, pp. 671–674, 2006.

[8] M. Zimerman, K. F. Heise, J. Hoppe, L. G. Cohen, C. Gerloff, and F. C. Hummel, "Modulation of training by single-session transcranial direct current stimulation to the intact motor cortex enhances motor skill acquisition of the paretic hand," *Stroke*, vol. 43, no. 8, pp. 2185–2191, 2012.

[9] C.-L. Yen, R.-Y. Wang, K.-K. Liao, C.-C. Huang, and Y.-R. Yang, "Gait training—induced change in corticomotor excitability in patients with chronic stroke," *Neurorehabilitation and Neural Repair*, vol. 22, no. 1, pp. 22–30, 2008.

[10] M. A. Dimyan and L. G. Cohen, "Contribution of transcranial magnetic stimulation to the understanding of functional recovery mechanisms after stroke," *Neurorehabilitation and Neural Repair*, vol. 24, no. 2, pp. 125–135, 2010.

[11] K. Johansson, I. Lindgren, H. Widner, I. Wiklund, and B. B. Johansson, "Can sensory stimulation improve the functional outcome in stroke patients?" *Neurology*, vol. 43, no. 11, pp. 2189–2192, 1993.

[12] P. Wu, E. Mills, D. Moher, and D. Seely, "Acupuncture in post-stroke rehabilitation: a systematic review and meta-analysis of randomized trials," *Stroke*, vol. 41, no. 4, pp. e171–e179, 2010.

[13] Y. L. Lo and S. L. Cui, "Acupuncture and the modulation of cortical excitability," *NeuroReport*, vol. 14, no. 9, pp. 1229–1231, 2003.

[14] Y. L. Lo, S. L. Cui, and S. Fook-Chong, "The effect of acupuncture on motor cortex excitability and plasticity," *Neuroscience Letters*, vol. 384, no. 1-2, pp. 145–149, 2005.

[15] C. Maioli, L. Falciati, M. Marangon, S. Perini, and A. Losio, "Short- and long-term modulation of upper limb motor-evoked potentials induced by acupuncture," *European Journal of Neuroscience*, vol. 23, no. 7, pp. 1931–1938, 2006.

[16] M. Zunhammer, P. Eichhammer, J. Franz, G. Hajak, and V. Busch, "Effects of acupuncture needle penetration on motor system excitability," *Neurophysiologie Clinique*, vol. 42, no. 4, pp. 225–230, 2012.

[17] E. M. Wassermann, "Risk and safety of repetitive transcranial magnetic stimulation: report and suggested guidelines from the International Workshop on the Safety of Repetitive Transcranial Magnetic Stimulation, June 5–7, 1996," *Electroencephalography and Clinical Neurophysiology*, vol. 108, no. 1, pp. 1–16, 1998.

[18] R. C. Oldfield, "The assessment and analysis of handedness: the Edinburgh inventory," *Neuropsychologia*, vol. 9, no. 1, pp. 97–113, 1971.

[19] P. M. Rossini, S. Rossi, P. Pasqualetti, and F. Tecchio, "Corticospinal excitability modulation to hand muscles during movement imagery," *Cerebral Cortex*, vol. 9, no. 2, pp. 161–167, 1999.

[20] P. M. Rossini, A. T. Barker, A. Berardelli et al., "Non-invasive electrical and magnetic stimulation of the brain, spinal cord and roots: basic principles and procedures for routine clinical application. Report of an IFCN committee," *Electroencephalography and Clinical Neurophysiology*, vol. 91, no. 2, pp. 79–92, 1994.

[21] B. Mercuri, E. M. Wassermann, P. Manganotti, K. Ikoma, A. Samii, and M. Hallett, "Cortical modulation of spinal excitability: An F-wave Study," *Electroencephalography and Clinical Neurophysiology—Electromyography and Motor Control*, vol. 101, no. 1, pp. 16–24, 1996.

[22] U. Ziemann, "TMS and drugs," *Clinical Neurophysiology*, vol. 115, no. 8, pp. 1717–1729, 2004.

[23] R. Chen, A. Samii, M. Caños, E. M. Wassermann, and M. Hallett, "Effects of phenytoin on cortical excitability in humans," *Neurology*, vol. 49, no. 3, pp. 881–883, 1997.

[24] B. Boroojerdi, F. Battaglia, W. Muellbacher, and L. G. Cohen, "Mechanisms influencing stimulus-response properties of the human corticospinal system," *Clinical Neurophysiology*, vol. 112, no. 5, pp. 931–937, 2001.

[25] Y.-H. Kim, S. H. You, M.-H. Ko et al., "Repetitive transcranial magnetic stimulation-induced corticomotor excitability and associated motor skill acquisition in chronic stroke," *Stroke*, vol. 37, no. 6, pp. 1471–1476, 2006.

[26] M. C. Pellicciari, D. Brignani, and C. Miniussi, "Excitability modulation of the motor system induced by transcranial direct current stimulation: a multimodal approach," *NeuroImage*, vol. 83, pp. 569–580, 2013.

[27] D. J. Kidgell, A. M. Goodwill, A. K. Frazer, and R. M. Daly, "Induction of cortical plasticity and improved motor performance following unilateral and bilateral transcranial direct current stimulation of the primary motor cortex," *BMC Neuroscience*, vol. 14, article 64, 2013.

[28] A. Kaelin-Lang, A. R. Luft, L. Sawaki, A. H. Burstein, Y. H. Sohn, and L. G. Cohen, "Modulation of human corticomotor excitability by somatosensory input," *Journal of Physiology*, vol. 540, no. 2, pp. 623–633, 2002.

[29] Y. Terao, Y. Ugawa, R. Hanajima et al., "Air-puff-induced facilitation of motor cortical excitability studied in patients with discrete brain lesions," *Brain*, vol. 122, no. 12, pp. 2259–2277, 1999.

Hindawi
Neural Plasticity
Volume 2017, Article ID 8696402, 9 pages
https://doi.org/10.1155/2017/8696402

Research Article

Acupuncture Attenuates Renal Sympathetic Activity and Blood Pressure via Beta-Adrenergic Receptors in Spontaneously Hypertensive Rats

Jing-Wen Yang,[1] Yang Ye,[2] Xue-Rui Wang,[1] Fang Li,[1] Ling-Yong Xiao,[2] Guang-Xia Shi,[1] and Cun-Zhi Liu[1]

[1]*Acupuncture and Moxibustion Department, Beijing Hospital of Traditional Chinese Medicine Affiliated to Capital Medical University, 23 Meishuguanhou Street, Dongcheng District, Beijing 100010, China*
[2]*Beijing University of Chinese Medicine, 11 Beisanhuan East Road, Chaoyang District, Beijing 100029, China*

Correspondence should be addressed to Cun-Zhi Liu; lcz623780@126.com

Received 8 August 2016; Accepted 11 January 2017; Published 8 February 2017

Academic Editor: Preston E. Garraghty

Copyright © 2017 Jing-Wen Yang et al. This is an open access article distributed under the Creative Commons Attribution License, which permits unrestricted use, distribution, and reproduction in any medium, provided the original work is properly cited.

The sympathetic nervous system, via epinephrine and norepinephrine, regulates β-adrenergic receptor (β-AR) expression, and renal sympathetic activation causes sustained increases in blood pressure by enhanced renin release. In this study, we aim to investigate the effect and underlying mechanism of acupuncture at Taichong (LR3) on renal sympathetic activity in spontaneously hypertensive rats. Unanesthetized rats were subject to daily acupuncture for 2 weeks. Mean blood pressure (MBP) and heart rate variability (HRV) were monitored at days 0, 7, and 14 by radiotelemetry. After euthanasia on the 14th day, blood and the kidneys were collected and subject to the following analyses. Epinephrine and norepinephrine were detected by ELISA. The expression of β-ARs was studied by western blotting and PCR. The renin content was analyzed by radioimmunoassay. 14-day acupuncture significantly attenuates the increase of MBP. The HRV indices, the standard deviation of all normal NN intervals (SDNN), and the ratio of the low-frequency component to the high-frequency component (LF/HF) were improved following acupuncture. Renal sympathetic activation induced upregulation of epinephrine, norepinephrine, and renin content were attenuated by acupuncture. In addition, acupuncture decreased β1-AR expression and improved β2-AR expression. These results indicated that acupuncture relieves the increased MBP via the regulation of renal sympathetic activity and β-ARs.

1. Introduction

Enhanced sympathetic nervous system activity is linked to the development and maintenance of hypertension [1–3]. The extensive sympathetic innervation of the kidney occupies a special place in the development of hypertension. Calaresu and Ciriello [4, 5] showed that renal afferent nerves project directly into a number of areas in the central nervous system, such as the lateral tegmental fields, the paramedial reticular nucleus, the dorsal vagal complex of the medulla, and the lateral hypothalamic area, contributing to arterial blood pressure regulation. Renal efferent sympathetic activity participates in renin release, sodium retention, and reduced renal blood flow, which contribute to the development of hypertension [6–8]. In animal models, Kumagai and his colleagues [9] found that stimulation of afferent sympathetic nerve increased systemic sympathetic nerves activity and caused vasoconstriction. Moreover, the attenuation of either the efferent or afferent renal nerves theoretically contributes to lowering blood pressure (BP) [8]. The renal sympathetic nervous system regulates BP mainly through catecholamines (epinephrine and norepinephrine) binding to β-adrenergic receptors (β-ARs). Moreover, β1-ARs in the kidney may activate renin release [10] and, consequently, result in the renin-angiotensin-aldosterone system (RAAS) activation and angiotensin II formation followed by vasoconstriction [11]. Therefore, the renal sympathetic nervous system and β-ARs are critical for regulating peripheral

resistance and play important roles in the development of hypertension.

Acupuncture has been recommended as a complementary therapy for hypertension. In 1996, 64 acupuncture indications were declared by World Health Organization in Milan conference including hypertension [12]. Numerous animal and clinical studies have reported the efficacy of acupuncture in treating hypertension [13–15]. Although there is some disagreement among the reports, the majority of them indicate that acupuncture causes a significant decrease in BP [13]. However, the underlying mechanism through which acupuncture lowers BP remains to be elucidated. Acupuncture could affect the sympathetic nervous system. Knardahl et al. found that acupuncture produces moderate hypoalgesia in humans paralleled by a regulation of muscle sympathetic nerve activity [16]. Song et al. suggested that acupuncture pretreatment improved the survival rate in rats with lethal endotoxemia, which involves the activation of the autonomic nervous system [17]. Research has shown that electroacupuncture modulates the renal sympathetic nerve activity in chronic kidney disease rats [18]. Although the relationship between acupuncture and the sympathetic nervous system has been demonstrated in a variety of models, the antihypertensive effect of acupuncture on spontaneously hypertensive rats (SHRs) via sympathetic nervous system and β-ARs remains unclear.

The present study was conducted to examine the hypothesis that the activation of the renal sympathetic nervous system in SHRs is mediated by acupuncture. Furthermore, we assessed if this renal nerve-mediated effect contributes to the downregulation of β1-AR and upregulation of β2-AR, leading to the decreased BP in SHRs.

2. Materials and Methods

2.1. Experimental Animal. Male SHR and WKY rats (12 weeks), weighing 260–300 g, were purchased from Vital River Laboratory Animal Technology Co. Ltd (Beijing China). The animals were housed in cages at 22 ± 2°C and humidity of 40 ± 5% under a 12-hour light/dark cycle and received standard diet and water ad libitum. The experimental procedures were in accordance with the Guidelines for the Institutional Animal Care and Use Committee of China Academy of Chinese Medical Sciences (Beijing, China).

2.2. Animal Grouping and Acupuncture Stimulation. The rats were randomly divided into 4 groups, the control group (WKY), the model group (SHR), the acupuncture stimulation group at LR3 (located between the first and second metatarsal bones on the dorsum of the foot) (Acu), and nonacupoint acupuncture stimulation (Non-Acu), with 10 rats in each group. Sterilized disposable stainless steel needles (0.3 mm × 40 mm, Hwato, China) were inserted 5 mm deep at LR3. For the Non-Acu group, the rats received similar treatment as Acu group but the acupuncture site was at a sham acupoint (on the bilateral hypochondrium, 10 mm above iliac crest) to replace LR3. The rats in the WKY and SHR groups were given the same time and same level catching-grasping stimulus without acupuncture stimulation. Acupuncture proceeded for 30 seconds each time, once daily for a period of 2 weeks (1 day rest after 6 days of treatment).

2.3. Radiotelemetry. We measured BP and HRV by radiotelemetry combined with fast Fourier transform analysis of BP and HRV. DSCF-FS01 HRV devices or DSCF-FS02 BP devices (Softron, USA) were implanted in rats to follow BP and HRV changes continuously over time. The telemetric techniques and the techniques employed to analyze the autonomic nervous system are described in detail elsewhere [19]. Briefly, we anesthetized the rats with intraperitoneal injection of pentobarbital sodium (Sigma, USA). Then, The telemeter was placed in the abdominal cavity, the blood pressure catheter tip was inserted into the descending abdominal aorta, and the electrode leads approximated the Lead II orientation as previously described [20]. The rats recovered for 7 days before baseline BP and HRV values were recorded. By this time, the rats had regained their circadian BP and HRV rhythm; and surgery and anesthesia-induced changes had abated.

Data were sampled every 5 min for 10 sec continuously day and night and stored on a hard disk. BP and HRV were recorded using the SP 2006 Lan software. Continuous beat-by-beat values of BP and HRV were recorded during morning hours. Measurements to analyze the autonomic control of BP and HR were performed between 8:00 and 10:00 AM.

2.4. ELISA. NE and E contents in the plasma and kidney were measured by enzyme-linked immunosorbent assay (ELISA) kit (R&D Systems, USA) according to the manufacturer's instruction. Absorbance in each well was measured using microplate reader (Thermo Fisher, USA) at 450 nm. Concentrations of NE and E in the plasma and renal were determined by interpolation from the standard curve.

2.5. Real-Time Quantitation PCR. Total RNA was extracted from the kidney using Trizol Reagent (Invitrogen) according to the manufacturer's instructions. Quantification of the relative amounts of mRNA was performed using the Rotor-Gene6000 1.7 version software (Corbett research). In brief, 2 μL of the cDNA was mixed with primers, 100 nM of probe, and 1x TaqMan Universal Master Mix in each reaction. Predeveloped assay reagents were used and were purchased from Applied Biosystems. Sequence for the primers and TaqMan probes for the rat β1-AR, β2-AR, and renin are shown in Table 1. Samples were tested in triplicate, and differences of threshold cycles between target genes and house-keeping gene (18s rRNA) were calculated. The relative mRNA abundance in the treatment groups was calculated using $2^{-\Delta\Delta CT}$ method using the control group as the calibrator according to the manufacturer's user manual. The value of relative mRNA quantity for control group is 1 with arbitrary units.

2.6. Western Blot Analysis. Total protein in each sample was measured by the BCA assay (Bio-Rad, USA) using bovine serum albumin as the standard protein. A fixed amount of protein (20 μg) from each sample was fractionated by 10% SDS-polyacrylamide gel electrophoresis (SDS-PAGE) and transferred to a polyvinylidene difluoride (PVDF) membrane

Table 1: Sequence for the primers and TaqMan probes for the rat β1-AR, β2-AR, and renin.

	Forward primer	Reverse primer
β1-AR	GCCGATCTGGTCATGGGAC	GGCGATGACACACAGGGTC
β2-AR	CATCCTCATGTCGGTTATC	ATGACTAGATCAGCACACG
Renin	GAGGCCTTCCTTGACCAATC	TGTGAATCCCACAAGCAAGG

(Pall, USA). Membranes were incubated in 5% milk in TBS for 1 h in room temperature. For identification of β-ARs, membranes were exposed to primary antibodies (anti-β1-AR, 1 : 250 dilution, or anti-β2-AR, 1 : 500 dilution, abcam, USA). After washing, the membranes were incubated with secondary antibodies (HRP-conjugated anti-rabbit antibody, 1 : 5000 dilution, KBL, USA). The bound antibodies were detected using the enhanced chemiluminescent reagent (GE Health Care, USA). Data are presented as the β-ARs to actin ratio and then expressed as fold-change compared to WKY group.

2.7. Radioimmunoassay. For determination of PRC, 50 μL of blood was collected into EDTA-containing 75-μL microhematocrit tubes from conscious rats by tail vein puncture. For determination of renal renin content, samples of kidney cortex were dissected under the microscopy, frozen in liquid nitrogen, and stored at −80°C until assay. For renin analysis, tissue was weighed, homogenized with two 30-second pulses in a 100-fold excess of homogenization buffer (5% [vol/vol] glycerol, 0.1 mmol/L of PMSF, 10 mmol/L of EDTA, and 0.1 mmol/L of 4-[2-aminomethyl]benzenesulfonyl fluoride) using a Polytron homogenizer (Kinematica), and centrifuged at 4°C at 140,000*g* for 5 minutes. Supernatants were incubated with saturating concentrations of rat renin substrate, and angiotensin I generation was assayed by radioimmunoassay (DiaSorin).

2.8. Statistical Analysis. Data analysis was performed with SPSS software version 16.0. All values were expressed as the mean ± standard error (SEM). Comparison between the treatment group and the control group was performed by one-way ANOVA test followed by a post hoc least significant difference multiple comparison test. A P value < 0.05 was considered statistically significant.

3. Results

3.1. Effect of Acupuncture on BP in SHRs. To confirm the efficacy of acupuncture, BP levels were measured in all groups by the telemetry method after two weeks of acupuncture treatment (Figure 1(a)). Before acupuncture, the mean blood pressure (MBP) of SHR, Acu, and Non-Acu group were insignificantly different ($P > 0.05$), but significantly higher than in the WKY rats. After 7 days of acupuncture, the MBP was significantly decreased compared with SHR group and Non-Acu group ($P < 0.01$), and this decrease was sustained throughout the treatment period (days 7–14). Although the MBP of Acu group was significantly decreased, it was still higher than the WKY group ($P < 0.01$) over the experimental period. These results suggested that acupuncture could lower BP but is unable to reduce it to normal levels.

3.2. Effect of Acupuncture on the Balance of Autonomic Nervous in SHRs. To investigate whether the attenuation of BP in SHRs by the treatment with acupuncture is associated with beneficial effects of the automatic nervous system, we used radiotelemetry method to examine the heart rate variability (HRV) in all groups at days 0, 7, and 14 (Figures 1(b)–1(d)). The values of standard deviation of all normal NN intervals (SDNN) and root mean square of differences between adjacent NN intervals (rMSDD) show acupuncture effects on HRV by mean variation of the short-term period. Before acupuncture, the SDNN of the WKY group was higher than the other groups, and SDNN was slightly improved in the Acu group after 7 days of treatment without significance ($P > 0.05$). In the 14 days of acupuncture, the SDNN was significantly increased compared with the SHR group and Non-Acu group ($P < 0.01$). However, there was no significant change in RMSSD among the four groups ($P > 0.05$).

The ratio of the low-frequency component to the high-frequency component (LF/HF) shows acupuncture effects on autonomic regulation. LF/HF of the SHR group, Acu group, and Non-Acu group were significantly higher than that of the WKY group at days 0 and 7 ($P > 0.05$). On the 14th day, acupuncture significantly reduced the ratio of LF/HF compared with the SHR group and Non-Acu group ($P < 0.01$).

3.3. Effect of Acupuncture on the Contents of Catecholamine in SHRs. The catecholamines, including norepinephrine (NE) and epinephrine (E), acting as neurotransmitters, play important roles in the sympathetic control of arterial BP. Therefore, we tested the contents of NE and E in plasma and renal tissues by ELISA (Figure 2). At the end of the study, NE and E levels induced by sympathetic nervous system activation were significantly higher in plasma and renal tissues from SHR than in those from WKY rats. Acupuncture at LR3 but not the nonacupoint significantly decreased NE and E concentrations in SHR group, and there was no significant difference between WKY group and Acu group.

3.4. Effect of Acupuncture on β-Adrenergic Receptor in SHRs. Both NE and E act at G protein-coupled receptors of the adrenergic receptor family to mediate sympathetic effects. Within this main classification, there are several subtypes α1A, α1B, α1D, α2A, α2B, α2C, β1, β2, and β3. In this study we focused on two of these receptors, β1 and β2. Both of these receptor subtypes have been strongly implicated in cardiovascular control. To determine whether the antihypertensive

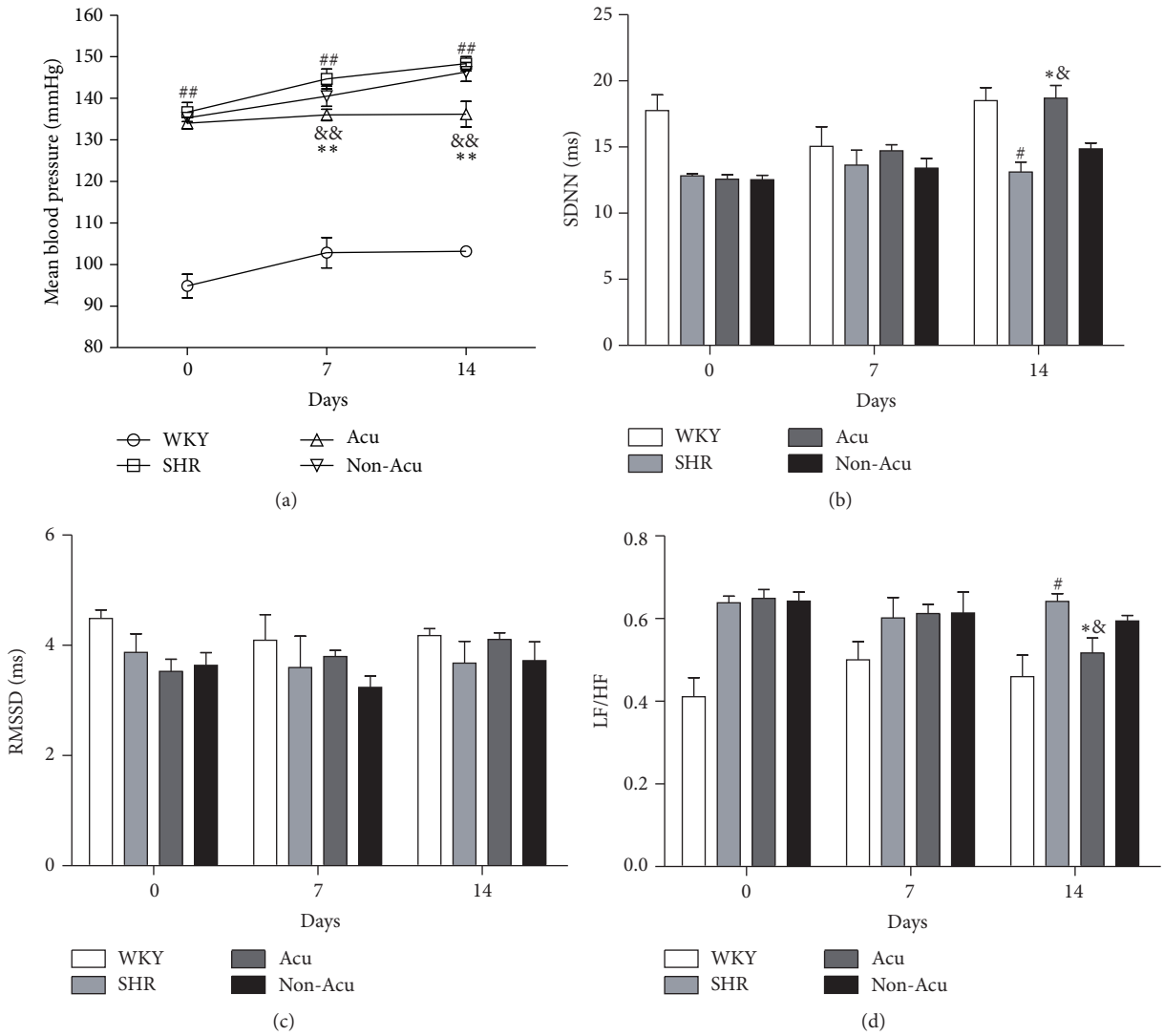

Figure 1: Effects of acupuncture on mean blood pressure (a) and heart rate variability (b–d) as measured by radiotelemetry in all groups. Data are presented as mean ± SEM ($n = 10$ rats). # and ## indicate $P < 0.05$ and $P < 0.01$, respectively, compared with the WKY group; * and ** indicate $P < 0.05$ and $P < 0.01$, respectively, compared with SHR group; & and && indicate $P < 0.05$ and $P < 0.01$, respectively, compared with Non-Acu group.

effect of acupuncture is associated with beneficial outcome in β-ARs, we detected the mRNA and protein levels of β-ARs after acupuncture treatment by PCR and Western blot, respectively (Figure 3). Compared to WKY rats, SHR rats had significantly increased β1-AR protein levels and decreased β2-AR protein levels. After acupuncture, β1-AR protein levels were significantly decreased compared to SHR group. The signal ratio of β1-AR protein to actin was reduced by about 16.5% (1.01 versus 1.21). In contrast, β1-AR protein levels were similar between SHR group and Non-Acu group. The trends of the β-ARs mRNA levels were consistent with its protein levels.

3.5. Effect of Acupuncture on Plasma Renin Concentration, Renal Renin Content, and Renin mRNA Expression in SHRs. The juxtaglomerular (JG) cells in the media of renal afferent arterioles are the major sites of synthesis of the aspartic protease renin, the rate-limiting enzyme in the formation of angiotensin II. The JG cells are in contact with sympathetic nerve varicosities and express postjunctional β-ARs. Activation of β-ARs directly increases renin secretion. To address the role of acupuncture in the regulation of renin, we used radioimmunoassay to detect the concentration of renin. As shown in Figure 4, plasma renin concentration (PRC) increased significantly in SHR group and Non-Acu group and decreased significantly after acupuncture at LR3. Renal renin content was significantly higher in SHR rats compared with WKY rats. There was a significant reduction in renin content in the Acu group, whereas the decrease in renin content in Non-Acu group did not reach significance. Renal renin mRNA was markedly higher in SHR rats compared with WKY rats. Renin mRNA was significantly altered by

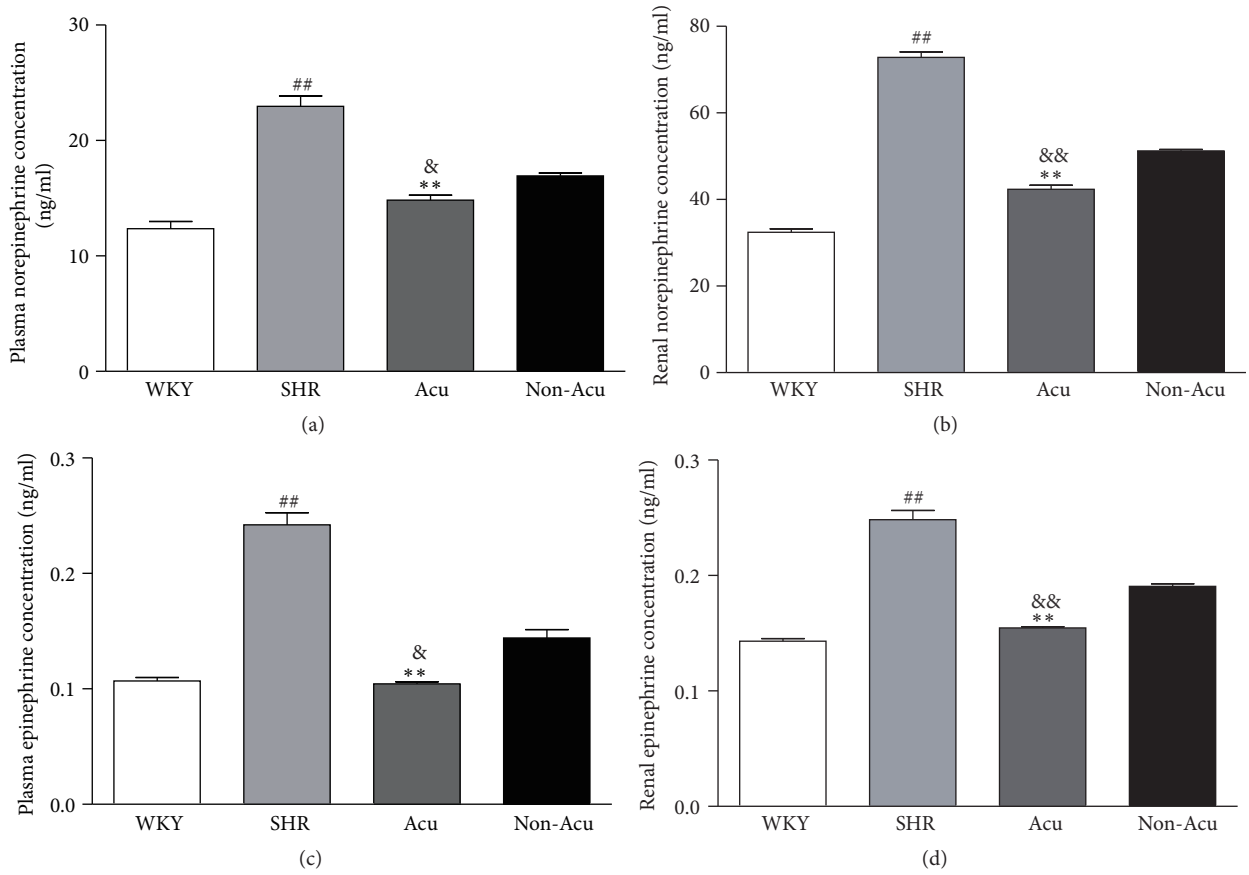

Figure 2: Effects of acupuncture on the contents of norepinephrine (a and b) and epinephrine (c and d) in plasma and renal tissues as measured by ELISA in all groups. Data are presented as mean ± SEM ($n = 10$ rats). ## indicate $P < 0.01$, compared with the WKY group; ** indicate $P < 0.01$, compared with SHR group; & and && indicate $P < 0.05$ and $P < 0.01$, respectively, compared with Non-Acu group.

acupuncture at LR3, whereas acupuncture at nonacupoint caused nonsignificant reductions of renin mRNA.

4. Discussion

In the present study, we show that acupuncture at LR3 reduced MBP and regulated HRV in SHR. And the therapeutic effects were associated with renal sympathetic nervous system, which can be manifested by the significant reductions in the levels of E and NE (an indirect marker of sympathetic activity) and the content of renin (indicative of increased renal sympathetic activity) in the plasma and renal by acupuncture. In addition, acupuncture decreased β1-AR expression and increased β2-AR expression, which means acupuncture has bidirectional regulation effects on β-ARs.

Autonomic imbalance with increased sympathetic activity has been strongly implicated in the pathophysiology of hypertension. Among the different available noninvasive techniques for assessing the autonomic status, HRV has emerged as a simple, noninvasive method to evaluate the sympathovagal balance. In this experiment, we focus on three HRV indexes. SDNN is associated with overall autonomic tone. Therefore, our findings of depressed SDNN in SHR rats suggested a homeostatic disruption in sympathovagal balance. However, because rMSSD is generally associated with vagal pathways, our results with unchanged rMSSD suggest an increase in sympathetic tone in SHR rats. This result is consistent with Schroeder's finding that individuals with low SDNN at baseline were at an increased risk of developing hypertension over 9 years of follow-up [21]. An analysis of LF/HF ratios rather than single components is considered by many investigators to better reflect the activity of the sympathovagal balance. Neto et al. showed a significant correlation between reduction BP levels and lower LF/HF ratio [22]. In our study, the higher LF/HF ratio demonstrated that SHRs have excessive sympathetic activation and autonomic imbalance. After acupuncture treatment, SDNN increased and LF/HF ratio decreased, but the rMSDD did not change. These results indicated that acupuncture could regulate the balance of the autonomic nervous system mainly through reducing the sympathetic activity.

Evidence collected throughout the years has shown that alterations in sympathetic cardiovascular control participate in the development, maintenance, and progression of hypertension. Renal sympathetic nerves induce high BP via E and NE regulates β-ARs expression. Of the two main β-AR subtypes (β1 and β2), β1-AR signaling has been linked to cardiotoxicity. In contrast, β2-AR activates signaling pathways

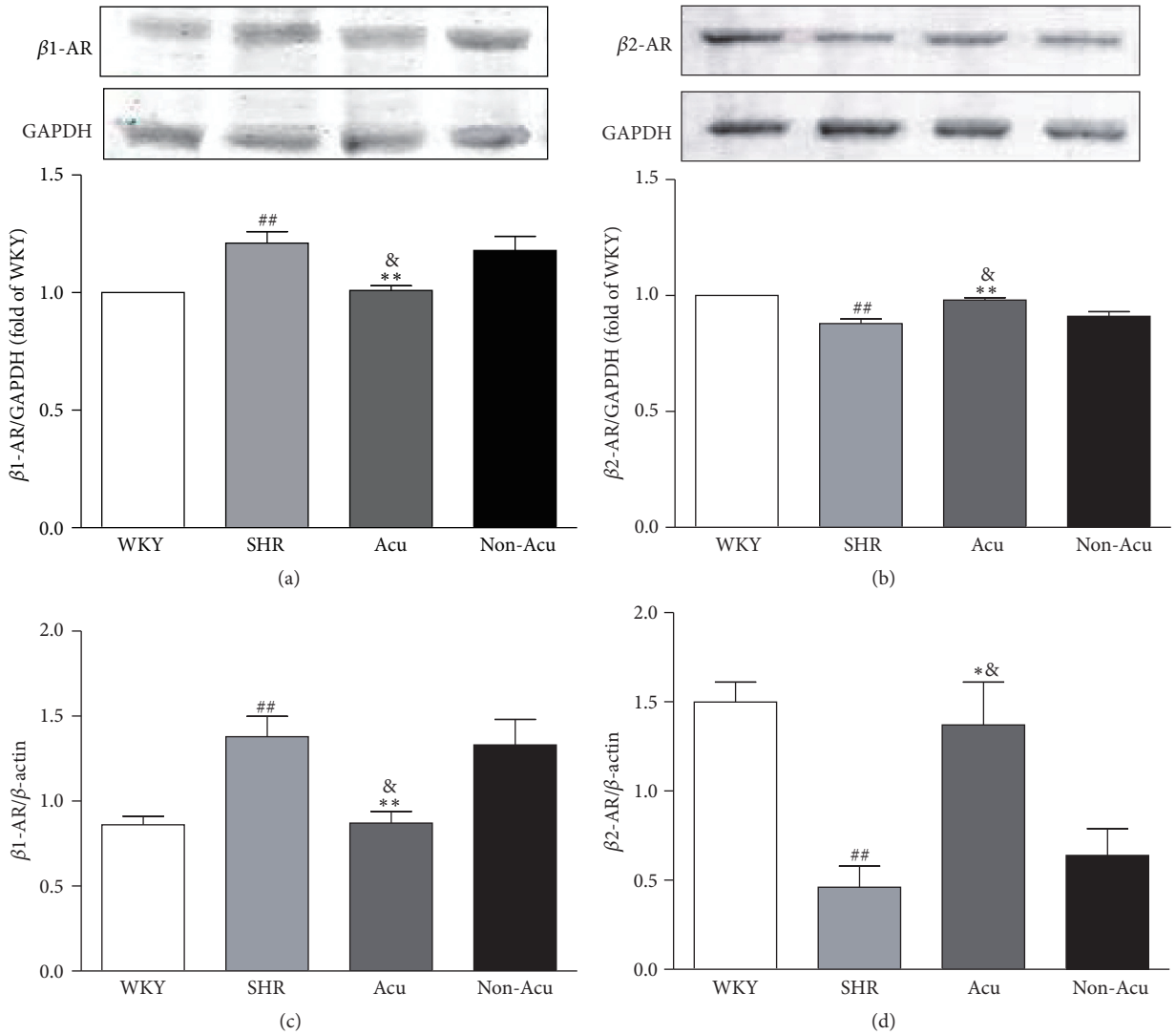

Figure 3: Effects of acupuncture on renal protein expression of β1-AR (a), β2-AR (b) and mRNA expression of β1-AR (c), β2-AR (d) in all groups. Data are presented as mean ± SEM (n = 10 rats). ## indicate $P < 0.01$, compared with the WKY group; $*$ and $**$ indicate $P < 0.05$ and $P < 0.01$, respectively, compared with SHR group; & indicate $P < 0.05$, compared with Non-Acu group.

involved in cardioprotection. Gui et al. found that β2-AR has a vasodilatation effect, and Raf kinase inhibitory protein could correct impaired β2-AR to treat hypertension [23]. Thus, some have proposed that the β1-AR is the "cardiotoxic subtype" whereas the β2-AR is the "cardioprotective subtype." The two receptors regulate the peripheral resistance which reflects the balance between vasoconstrictor and vasodilator mechanisms. Based on this, we examined the effect of acupuncture on E, NE, and β-ARs. Here we observed that the contents of E and NE of SHR rats were significantly higher compared with the WKY rats. This gives direct evidence that the sympathetic nervous system is hyperreactive in the SHR and is in general agreement with previous studies [24, 25]. Then acupuncture at LR3, not nonacupoint, could decrease the contents of E and NE. In addition, acupuncture significantly decreased the expression of β1-AR and increased β2-AR expression in SHR. Therefore, the antihypertensive effect of acupuncture in SHR might be associated with the balance of β1/β2-AR. β-blockers therapy plays a major role in the treatment of cardiovascular diseases. To date, 14 β-blockers have received Federal Drug Administration approval for oral use in patients having systemic hypertension [26]. By receptor selective classification, β-blockers can be divided into three categories, namely, nonselective b-blocker, selective b1- receptor blocker, and b1-receptor blocker with additional α1-receptor blocking activity. Among them, the nonselective b-blocker is used most widely. In general, β-blockers are well tolerated, but serious side effects may occur, which are usually associated with the β2-AR antagonistic activity (e.g., increase in peripheral vascular resistance, worsening of asthma symptoms) [27]. Wong et al. suggested that β1 selective blockers lowered BP by a greater magnitude compared to dual receptor beta-blockers [28]. Acupuncture is reported to have potential for treating hypertension with

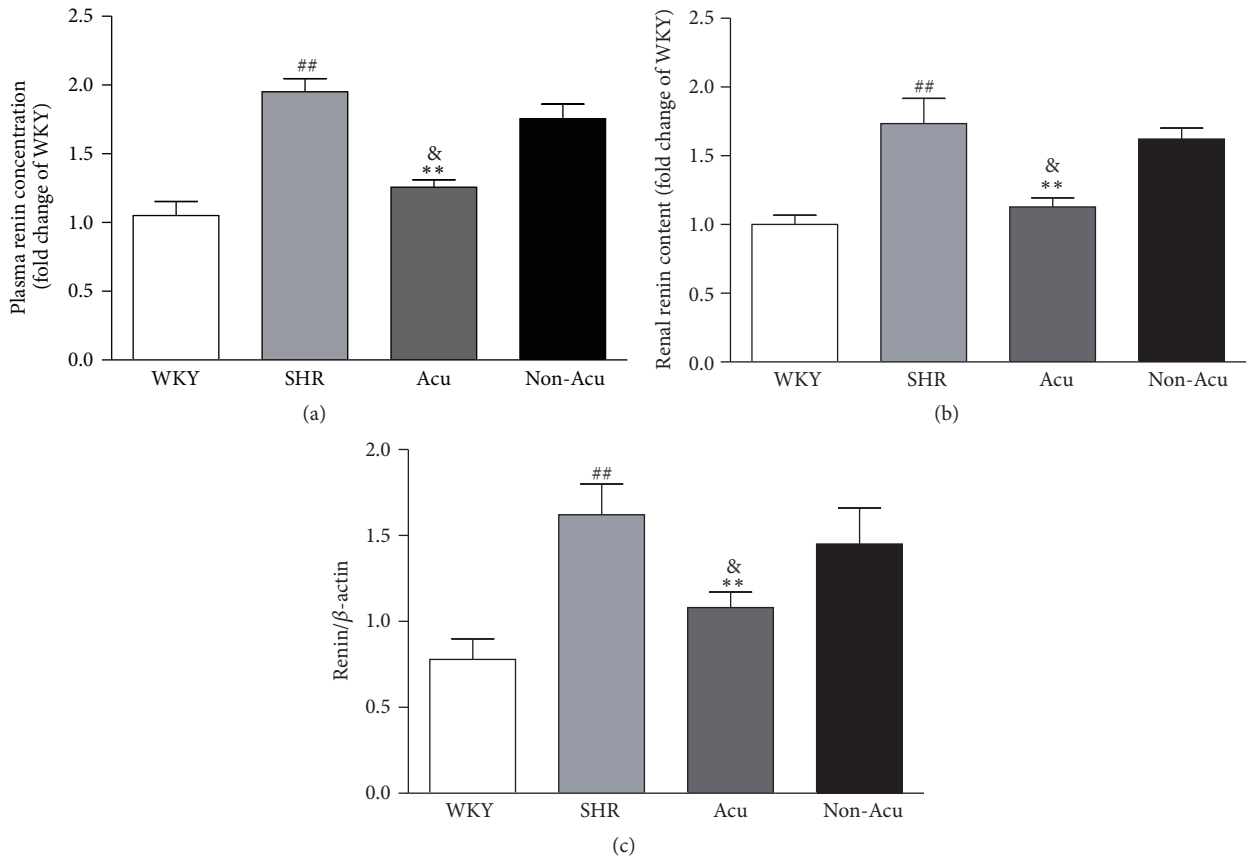

Figure 4: Effects of acupuncture on renin content (a and b) and renin mRNA expression (c). Data are presented as mean ± SEM ($n = 10$ rats). ## indicate $P < 0.01$, compared with the WKY group; ∗∗ indicate $P < 0.01$, compared with SHR group; & indicate $P < 0.05$, compared with Non-Acu group.

fewer side effects [29]. Moreover, Zhang et al. reported that acupuncture may serve as an alternative for hypertensive patients, especially for those who cannot tolerate the side effects of antihypertensive drugs [30]. Combined with our experimental results, where acupuncture could decrease β1-AR expression and increase β2-AR expression, we consider that the low side effects of acupuncture may be related to the increased expression of β2 receptors, which needs to be further investigated.

The RAAS is an important mechanism in regulating BP. For that reason, an alteration in any molecule that composes the RAAS contributes to developing hypertension [31]. Classically, the sympathetic nervous system rapidly activates the RAAS through β1-AR mediated release of renin [32]. Therefore, inhibition of renin may exert complete inhibition of the RAAS, leading to a decrease of BP. Hisa et al. found that a β-AR blocker could reduce renal nerve stimulation-induced renin release. In our experiment, we found a significant reduction of renin content after acupuncture. Consistent with our results, Lohmeier et al. demonstrated that renal denervation decreased plasma renin content and abolished the hypertension [33]. However, the effect of acupuncture on RAAS in SHRs needs further study.

The renal sympathetic nervous system plays an active role in the modulation of BP, and its overactivation can lead to hypertension [34]. The Symplicity HTN-1 and HTN-2 studies proposed renal denervation as an effective and safe approach to treat patients with hypertension and were followed by substantial enthusiasm [35, 36]. In contrast with Symplicity HTN-1 and HTN-2, the announcement that Symplicity HTN-3 failed to meet its primary efficacy endpoint and put an abrupt stop to these overoptimistic expectations shows that renal denervation is not ready for clinical dissemination [37]. However, some researchers considered that the execution of the study was hampered by operational weaknesses and drug adherence [38, 39]. Despite the disappointing outcome of Simplicity HTN-3, the renal sympathetic system is still a potential target for treating hypertension, and our results indicate that acupuncture could reduce the renal sympathetic nervous activity and lower BP without related risk.

In conclusion, our results provide evidence that acupuncture at LR3 can significantly relieve the increased MBP through reducing renal sympathetic nervous activity. The effect of acupuncture on renal sympathetic nervous activity is evidenced by the improved HRV and the reduction of NE and E contents. The decreased β1-AR and increased β2-AR

expression we observed may also be involved in the beneficial effect of acupuncture on hypertension.

Competing Interests

The authors declare that they have no conflict of interests with the contents of this article.

Authors' Contributions

Jing-Wen Yang conducted experiments on the role of renin, analyzed the results, and wrote most of the paper. Xue-Rui Wang and Fang Li conducted the radiotelemetry. Yang Ye and Ling-Yong Xiao conducted experiments searching for β-ARs function. Guang-Xia Shi conducted the ELISA of epinephrine and norepinephrine content. Cun-Zhi Liu conceived the idea for the project and wrote the paper with Jing-Wen Yang.

Acknowledgments

This work was supported in whole or partly by National Natural Science Foundation of China (Grant no. 81473501), Beijing Municipal Administration of Hospitals Clinical Medicine Development of Special Funding Support (code: ZYLX201412), and National Basic Research Program of China (Grant no. 2014CB543203).

References

[1] P. A. Smith, L. N. Graham, A. F. Mackintosh, J. B. Stoker, and D. A. S. G. Mary, "Relationship between central sympathetic activity and stages of human hypertension," *American Journal of Hypertension*, vol. 17, no. 3, pp. 217–222, 2004.

[2] S. C. Malpas, "Sympathetic nervous system overactivity and its role in the development of cardiovascular disease," *Physiological Reviews*, vol. 90, no. 2, pp. 513–557, 2010.

[3] A. E. Simms, J. F. R. Paton, A. E. Pickering, and A. M. Allen, "Amplified respiratory-sympathetic coupling in the spontaneously hypertensive rat: does it contribute to hypertension?" *The Journal of Physiology*, vol. 587, no. 3, pp. 597–610, 2009.

[4] F. R. Calaresu and J. Ciriello, "Renal afferent nerves affect discharge rate of medullary and hypothalamic single units in the cat," *Journal of the Autonomic Nervous System*, vol. 3, no. 2–4, pp. 311–320, 1981.

[5] J. Ciriello and F. R. Calaresu, "Central projections of afferent renal fibers in the rat: an anterograde transport study of horseradish peroxidase," *Journal of the Autonomic Nervous System*, vol. 8, no. 3, pp. 273–285, 1983.

[6] H. Krum, P. Sobotka, F. Mahfoud, M. Böhm, M. Esler, and M. Schlaich, "Device-based antihypertensive therapy: therapeutic modulation of the autonomic nervous system," *Circulation*, vol. 123, no. 2, pp. 209–215, 2011.

[7] G. F. DiBona, "Neural control of the kidney: past, present, and future," *Hypertension*, vol. 41, no. 3, pp. 621–624, 2003.

[8] G. F. DiBona, "Physiology in perspective: The Wisdom of the Body. Neural control of the kidney," *American Journal of Physiology—Regulatory Integrative and Comparative Physiology*, vol. 289, no. 3, pp. R633–R641, 2005.

[9] H. Kumagai, N. Oshima, T. Matsuura et al., "Importance of rostral ventrolateral medulla neurons in determining efferent sympathetic nerve activity and blood pressure," *Hypertension Research*, vol. 35, no. 2, pp. 132–141, 2012.

[10] T. K. Keeton and W. B. Campbell, "The pharmacologic alteration of renin release," *Pharmacological Reviews*, vol. 32, pp. 81–227, 1980.

[11] H. Kubista and S. Boehm, "Molecular mechanisms underlying the modulation of exocytotic noradrenaline release via presynaptic receptors," *Pharmacology and Therapeutics*, vol. 112, no. 1, pp. 213–242, 2006.

[12] J.-Y. Wang, H. Li, C.-M. Ma, J.-L. Wang, X.-S. Lai, and S.-F. Zhou, "MicroRNA profiling response to acupuncture therapy in spontaneously hypertensive rats," *Evidence-Based Complementary and Alternative Medicine*, vol. 2015, Article ID 204367, 9 pages, 2015.

[13] C. Yin, B. Seo, H.-J. Park et al., "Acupuncture, a promising adjunctive therapy for essential hypertension: a double-blind, randomized, controlled trial," *Neurological Research*, vol. 29, no. 1, pp. S98–S103, 2007.

[14] J.-M. Park, A.-S. Shin, S.-U. Park, I.-S. Sohn, W.-S. Jung, and S.-K. Moon, "The acute effect of acupuncture on endothelial dysfunction in patients with hypertension: a pilot, randomized, double-blind, placebo-controlled crossover trial," *Journal of Alternative and Complementary Medicine*, vol. 16, no. 8, pp. 883–888, 2010.

[15] L. A. Kalish, B. Buczynski, P. Connell et al., "Stop Hypertension with the Acupuncture Research Program (SHARP): clinical trial design and screening results," *Controlled Clinical Trials*, vol. 25, no. 1, pp. 76–103, 2004.

[16] S. Knardahl, M. Elam, B. Olausson, and B. G. Wallin, "Sympathetic nerve activity after acupuncture in humans," *Pain*, vol. 75, no. 1, pp. 19–25, 1998.

[17] J.-G. Song, H.-H. Li, Y.-F. Cao et al., "Electroacupuncture improves survival in rats with lethal endotoxemia via the autonomic nervous system," *Anesthesiology*, vol. 116, no. 2, pp. 406–414, 2012.

[18] J. C. Paterno, C. T. Bergamaschi, R. R. Campos et al., "Electroacupuncture and moxibustion decrease renal sympathetic nerve activity and retard progression of renal disease in rats," *Kidney and Blood Pressure Research*, vol. 35, no. 5, pp. 355–364, 2012.

[19] V. Gross, J. Tank, M. Obst et al., "Autonomic nervous system and blood pressure regulation in RGS2-deficient mice," *American Journal of Physiology—Regulatory Integrative and Comparative Physiology*, vol. 288, no. 5, pp. R1134–R1142, 2005.

[20] L. B. Wichers, J. P. Nolan, D. W. Winsett et al., "Effects of instilled combustion-derived particles in spontaneously hypertensive rats. Part I: cardiovascular responses," *Inhalation Toxicology*, vol. 16, no. 6-7, pp. 391–405, 2004.

[21] E. B. Schroeder, D. Liao, L. E. Chambless, R. J. Prineas, G. W. Evans, and G. Heiss, "Hypertension, blood pressure, and heart rate variability: the atherosclerosis risk in communities (ARIC) study," *Hypertension*, vol. 42, no. 6, pp. 1106–1111, 2003.

[22] O. B. Neto, D. T. R. S. Abate, M. Marocolo Júnior et al., "Exercise training improves cardiovascular autonomic activity and attenuates renal damage in spontaneously hypertensive rats," *Journal of Sports Science and Medicine*, vol. 12, no. 1, pp. 52–59, 2013.

[23] Y.-J. Gui, C.-X. Liao, Q. Liu, Y. Guo, and D.-Y. Xu, "RKIP corrects impaired beta (2)-adrenergic receptor vasodilatation in hypertension by downregulation of GRK2," *International Journal of Cardiology*, vol. 207, pp. 359–360, 2016.

[24] S. D. Stocker, S. M. Lang, S. S. Simmonds, M. M. Wenner, and W. B. Farquhar, "Cerebrospinal fluid hypernatremia elevates sympathetic nerve activity and blood pressure via the rostral ventrolateral medulla," *Hypertension*, vol. 66, no. 6, pp. 1184–1190, 2015.

[25] N. Marina, R. Ang, A. Machhada et al., "Brainstem hypoxia contributes to the development of hypertension in the spontaneously hypertensive rat," *Hypertension*, vol. 65, no. 4, pp. 775–783, 2015.

[26] W. H. Frishman, "Beta-adrenergic receptor blockers in hypertension: alive and well," *Progress in Cardiovascular Diseases*, vol. 59, no. 3, pp. 247–252, 2016.

[27] J. López-Sendón, K. Swedberg, J. McMurray et al., "Expert consensus document on b-adrenergic receptor blockers," *European Heart Journal*, vol. 25, pp. 1341–1362, 2004.

[28] G. W. Wong, H. N. Boyda, and J. M. Wright, "Blood pressure lowering efficacy of beta-1 selective beta blockers for primary hypertension," *Cochrane Database of Systematic Reviews*, vol. 2016, no. 3, Article ID CD007451, 2016.

[29] F. A. Flachskampf, J. Gallasch, O. Gefeller et al., "Randomized trial of acupuncture to lower blood pressure," *Circulation*, vol. 115, no. 24, pp. 3121–3129, 2007.

[30] L. Zhang, P. Shen, and S. Wang, "Acupuncture treatment for hypertension: a case study," *Acupuncture in Medicine*, vol. 32, no. 1, pp. 73–76, 2014.

[31] L. Te Riet, J. H. M. van Esch, A. J. M. Roks, A. H. van den Meiracker, and A. H. J. Danser, "Hypertension: renin-angiotensin-aldosterone system alterations," *Circulation Research*, vol. 116, no. 6, pp. 960–975, 2015.

[32] G. Z. Kalil and W. G. Haynes, "Sympathetic nervous system in obesity-related hypertension: mechanisms and clinical implications," *Hypertension Research*, vol. 35, no. 1, pp. 4–16, 2012.

[33] T. E. Lohmeier, R. Iliescu, B. Liu, J. R. Henegar, C. Maric-Bilkan, and E. D. Irwin, "Systemic and renal-specific sympathoinhibition in obesity hypertension," *Hypertension*, vol. 59, no. 2, pp. 331–338, 2012.

[34] K. Kario, D. L. Bhatt, S. Brar, S. A. Cohen, M. Fahy, and G. L. Bakris, "Effect of catheter-based renal denervation on morning and nocturnal blood pressure: insights from SYMPLICITY HTN-3 and SYMPLICITY HTN-Japan," *Hypertension*, vol. 66, no. 6, pp. 1130–1137, 2015.

[35] H. T. N. I. Symplicity, "Catheter-based renal sympathetic denervation for resistant hypertension: durability of blood pressure reduction out to 24 months," *Hypertension*, vol. 57, pp. 911–917, 2011.

[36] Symplicity HTN-2 Investigators, M. D. Esler, H. Krum et al., "Renal sympathetic denervation in patients with treatment-resistant hypertension (The Symplicity HTN-2 Trial): a randomised controlled trial," *The Lancet*, vol. 376, no. 9756, pp. 1903–1909, 2010.

[37] D. L. Bhatt, D. E. Kandzari, W. W. O'Neill et al., "A controlled trial of renal denervation for resistant hypertension," *New England Journal of Medicine*, vol. 370, no. 15, pp. 1393–1401, 2014.

[38] R. E. Schmieder, "Renal denervation—a valid treatment option despite SYMPLICITY HTN-3," *Nature Reviews Cardiology*, vol. 11, no. 11, article no. 638, 2014.

[39] R. E. Schmieder, "Hypertension: how should data from SYMPLICITY HTN-3 be interpreted?" *Nature Reviews Cardiology*, vol. 11, no. 7, pp. 375–376, 2014.

Hindawi
Neural Plasticity
Volume 2017, Article ID 9545646, 11 pages
https://doi.org/10.1155/2017/9545646

Research Article

Electroacupuncture Regulates Hippocampal Synaptic Plasticity via miR-134-Mediated LIMK1 Function in Rats with Ischemic Stroke

Weilin Liu,[1] Jie Wu,[2] Jia Huang,[1] Peiyuan Zhuo,[2] Yunjiao Lin,[2] Lulu Wang,[2] Ruhui Lin,[2] Lidian Chen,[1] and Jing Tao[1]

[1]*College of Rehabilitation Medicine, Fujian University of Traditional Chinese Medicine, Fuzhou, Fujian 350122, China*
[2]*Fujian Key Laboratory of Rehabilitation Technology, Fuzhou, Fujian 350122, China*

Correspondence should be addressed to Lidian Chen; cld@fjtcm.edu.cn and Jing Tao; taojing01@163.com

Received 26 August 2016; Accepted 3 November 2016; Published 2 January 2017

Academic Editor: Cun-Zhi Liu

Copyright © 2017 Weilin Liu et al. This is an open access article distributed under the Creative Commons Attribution License, which permits unrestricted use, distribution, and reproduction in any medium, provided the original work is properly cited.

MircoRNAs (miRs) have been implicated in learning and memory, by regulating LIM domain kinase (LIMK1) to induce synaptic-dendritic plasticity. The study aimed to investigate whether miRNAs/LIMK1 signaling was involved in electroacupuncture- (EA-) mediated synaptic-dendritic plasticity in a rat model of middle cerebral artery occlusion induced cognitive deficit (MICD). Compared to untreatment or non-acupoint-EA treatment, EA at DU20 and DU24 acupoints could shorten escape latency and increase the frequency of crossing platform in Morris water maze test. T2-weighted imaging showed that the MICD rat brain lesions were located in cortex, hippocampus, corpus striatum, and thalamus regions and injured volumes were reduced after EA. Furthermore, we found that the density of dendritic spine and the number of synapses in the hippocampal CA1 pyramidal cells were obviously reduced at Day 14 after MICD. However, synaptic-dendritic loss could be rescued after EA. Moreover, the synaptic-dendritic plasticity was associated with increases of the total LIMK1 and phospho-LIMK1 levels in hippocampal CA1 region, wherein EA decreased the expression of miR-134, negatively regulating LIMK1 to enhance synaptic-dendritic plasticity. Therefore, miR-134-mediated LIMK1 was involved in EA-induced hippocampal synaptic plasticity, which served as a contributor to improving learning and memory during the recovery stage of ischemic stroke.

1. Introduction

Ischemic stroke results in a high mortality rate and increased disability rate all over the world [1]. Approximately 64% of stroke patients are often followed with cognitive impairment and 33% of them turn into dementia existing for several months during decubation [2]. Cognitive deficits arise frequently after ischemic stroke, which cause difficulties with analysis, concentration, organization, interpretation, and other abates in cognitive functions that bring about the low quality of life [3, 4]. The dysfunction of learning and memory is the cardinal symptom of cognitive impairment after stroke and is the main culprit of persistent sequelae [5]. A recent study demonstrated that the incidence rate of poststroke mild cognitive impairment was diagnosed in 24.4% of individuals after 3 years, and each year the mean growth rate is approximately 8% [6]. In addition to conventional cognitive training, electroacupuncture (EA) is a stretch therapeutic method of acupuncture, which is traditional acupuncture incorporation with modern electrotherapy. The clinical efficacy of EA on poststroke cognitive impairment has been widely demonstrated [7, 8]. However, the functional mechanism of EA is far from been fully elucidated.

The hippocampus is a pivotal structure of the brain; the area plays an important role in the formation of acquisition, consolidation, and recognition of declarative and spatial memory [9, 10]. The loss of hippocampal synapses and neurons in poststroke induces cognitive deficits including spatial reference learning and memory impairment [11, 12]. In the formation of spatial reference memory is closely related to the

plasticity of dendritic spines and the morphological changes such as expansion and contraction [13]. Dendritic spines alter their shape to make the information spreading more easily and influence the synaptic efficacy (i.e., long-term potentiation and long-term depression) [14, 15], which have been widely considered as a cellular mechanism for learning and memory [16]. LIM domain kinase (LIMK1) is enriched in both axonal and dendritic growth cones of hippocampal pyramidal neurons in rats [17]. LIMK1 encodes a serine/threonine protein kinase that regulates the actin cytoskeleton by phosphorylating and inactivating the actin depolymerization factor (ADF)/cofilin [18]. In addition, LIMK1 is also known as having an important role in synapse and dendritic spine function. It has been reported that the knockout mice lacking LIMK1 are severely impaired in dendritic spine morphology and hippocampal long-term potentiation [19, 20]. Evidence showed that LIMK1 regulated long-term memory (LTM) and long lasting synaptic plasticity through interacting with and activating cyclic AMP response element-binding protein (CREB) [21].

In addition, a potential role for microRNAs (miRNAs or miRs) in synaptic function has been particularly intriguing given the evidence that a brain-specific miRNA contributes to synaptic development, maturation, and/or plasticity [22]. miRNAs are endogenous, noncoding RNAs that mediate the posttranscriptional regulation of gene expression mainly by binding to the 3′-untranslated region of messenger RNAs (mRNAs) [23]. A number of miRNAs have been isolated from nervous system, and a recent study has demonstrated a crucial role for dynamically regulating synaptic plasticity [24, 25]. Moreover, miRNAs have been implicated in hippocampus-dependent function, which have a significant potential in learning and memory formation, regulating LIMK1 expression to induce synaptic-dendritic plasticity [22]. Dendritic mRNAs encode diversified functionalities in hippocampal pyramidal neurons and play an important role in synaptic plasticity, as well as learning and memory [26].

Therefore, miRNA-LIMK1 can be considered as a target for cognitive deficit. Our previous study has shown that EA at Baihui (DU20) and Shenting (DU24) acupoints could improve cognitive impairment through Rho GTPases to enhance dendritic plasticity in rats with ischemic stroke [27]. Interestingly, it has been suggested that the activation of the Rho GTPases signaling is essential for LIMK1 activation by phosphorylation on threonine 508, which is widely known as master regulator of actin dynamics [28, 29]. Thus, the study aimed to elucidate whether EA at the DU20 and DU24 acupoints could improve the cognitive deficits in rats with ischemic stroke via miRNA-LIMK1-mediated synaptic plasticity to enhance spatial reference learning and memory.

2. Materials and Methods

2.1. Animal Ethics Statement. 96 male Sprague-Dawley rats (weight, 250 ± 20 g) were obtained from Shanghai SLAC Laboratory Animal Co., Ltd. (Shanghai, China, SCXK2013-0005), and housed under pathogen-free conditions with a 12 h light/dark cycle. The study was approved by the Committee of Fujian University of Traditional Chinese Medicine (protocol #FUTCM-2015008) and was performed in accordance with the national guidelines for the care and use of laboratory animals. For euthanasia, 3% sodium pentobarbital (40 mg/kg body weight, i.p.) was used. Middle cerebral artery occlusion (MCAO) surgery was carried out under general anesthesia (1.5% isoflurane in 68.5% N_2O and 30% O_2). All efforts were made to minimize suffering.

2.2. Experimental Procedures. The MCAO-induced cognitive deficit (MICD) model was established as previously described [5, 30]. Rats were randomly assigned to four groups according to the random number table ($n = 24$ rats each group) as follows: (1) Sham group, (2) MICD group, (3) MICD+EA group, and (4) MICD+non-EA group. The left middle cerebral artery was occluded by a 4-0 nylon monofilament (0.23 mm in diameter, Jialing-bio, China). Focal cerebral ischemia was monitored using transcranial temporal laser Doppler (BIOPAC Systems, Goleta, CA, USA) and an 80% decrease in blood flow after the occlusion was recorded. After 90 min of occlusion, reperfusion was achieved by pulling out the filament to restore blood flow. Sham-operated rats of the Sham group underwent the same procedure, but arterial occlusion was not performed.

After 24 hours of MCAO surgery, rats of the Sham group and the MICD group received no treatment. Rats of the MICD+EA group were given EA treatment for 30 min per day for 14 consecutive days. The EA needles (diameter, 0.3 mm, needle purchased from Hualun acupuncture of Suzhou Co., Ltd., Suzhou China) were inserted at a depth of 2-3 mm into the Baihui (DU20, located in the median of frontalis) and Shenting (DU24, located in the median of the parietal bone) acupoints [31]. Stimulation was then generated using the EA apparatus [Model G6805, Shanghai Huayi (Group) Company, Ltd., Shanghai, China] and the stimulation parameters were set as follows: dilatational waves of 1~20 Hz (adjusted to the muscle twitch threshold), peak voltage of 6 V, and 0.2 mA intensity [31]. Rats of the MICD+non-EA group were given EA treatment at the bilateral nonacupoints (located in the costal region and 10 mm distal to the iliac crest) for 30 min per day for 14 consecutive days [32]. The EA needles and stimulation parameters of the bilateral nonacupoints were consistent with the EA treatment. Manipulators were experienced and blinded to the rat's group.

2.3. Behavioral Assessment. Behavioral testing was conducted by researchers who were blinded to the rat's group. At 10 days after EA, all the rats were subjected to the Morris water maze test (Shanghai Xinruan Information Technology Co., Ltd, Shanghai, China) to evaluate spatial reference learning and memory (Figure 1). The Morris water maze consisted of a circular pool (diameter 150 cm, height 60 cm) filled with water (depth of 30 cm and temperature of 25 ± 2°C). A circular escape platform (diameter 12 cm, height 29 cm) was submerged 2 cm below the water surface, in the middle of the third quadrant of the pool and the reference objects around the pool were placed. Morris water maze tasks mainly include orientation navigation and space exploration trials. During the first set of trials, each rat was placed in the water at each of the four equidistant locations to the platform. When the

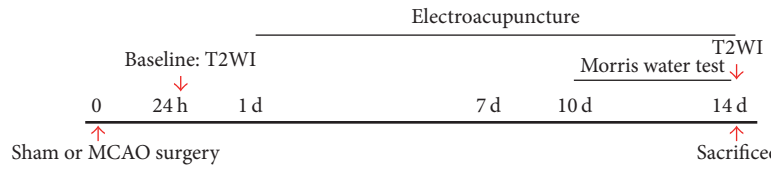

Figure 1: Experimental design used in the study.

rats arrived at the platform within the 90 sec time restriction and remained on it for 3 sec, they were considered to have found the platform and were scored by the time taken/length of the route. When the rats were unable to find the platform within 90 sec, they were placed on the platform for 10 sec and the time score was 90 sec. The time taken and the length of the route by which each rat found the safe platform were recorded by the computer. The average of the time taken and the length of the route for the four quadrants as a result of each rat were assessed every day. The duration of the first set of trials was performed on Days 10 to 13 after EA. The second part of the experiment was performed on Day 14, to examine the time in which rats found the location of the platform within the 90 sec time restriction, which tested their ability to remember the position of the platform. After all trials, the rats were dried thoroughly with a hair drier and returned to their cages (Guangzhou RiboBio Co., Ltd., Guangzhou, China). Morris water maze test was repeated three times.

2.4. Measurement of Brain Lesions. Animal MRI scans were performed on a 7.0 T MRI scanner (70/20 USR BioSpec, Bruker Biospin Gmbls, Germany) using a 38 mm birdcage rat brain quadrature resonator for radiofrequency transmission and reception. Animals were anesthetized with isoflurane/O_2 (with 3% induction for 5 min and 1.2–1.5% maintenance in order to let the rats in the depth of anesthesia state) and kept warm with circuit. After anesthesia, the rat was put in prone position on a custom-made holder to minimize head motion, set the location of head position, and perform real-time monitor of the breathing rate and maintained in 40 breaths/min. Rat's temperature is maintained at 33 ± 2°C in the process of scanning holder to minimize head motion while respiration was maintained.

T2-weighted imaging (T2WI) in three planes with a fast spin echo (FSE) pulse sequence was first acquired to control rat head positioning. T2WI scan was acquired using a Rapid Acquisition with Relaxation Enhancement (RARE) pulse sequence with the following parameters: field of view = 32 mm × 32 mm, matrix size = 256 × 256, repetition time (TR) = 4200 ms, echo time (TE) = 35 ms, slice thickness = 1.0 mm, and slice gap = 0 mm.

Image J analysis and processing system was applied for T2W images, the percentage of the brain lesions = brain lesions volume/whole brain volume ×100%.

2.5. Golgi Staining. Golgi staining of brain was performed using an FD Rapid GolgiStain Kit following the manufacturer's instructions (FD Neurotechnologies, Inc., Columbia, MD, USA). The removed rat brains were placed incubated in a mixture of A and B solutions from the kit and stored in the dark at room temperature, following which they were transferred into solution C from the kit, stored at 4°C for 7 days. Finally, brains were then frozen and coronal sections (150 μm) were made using a cryostat (Leica CM3050S, Leica Microsystems K. K., Tokyo, Japan). The sections incubated in a mixture of D and E solutions from the kit and then dehydrated in alcohol (50, 70, 90, and 100% for 5 min each), cleared in xylene, and were cover-slipped. The images finally were viewed under a microscope (Leica DM6000 B, Leica Microsystems, Wetzlar, Germany). The slides were reviewed by two or three pathologists blind to the study.

2.6. Transmission Electron Microscopy. Four rats in each group were anesthetized and the left ventricle was perfused with 200 mL of saline followed by 400 mL 4% paraformaldehyde (pH 7.4). The tissue was taken from the left ischemic hippocampus, cut into 1 mm^3 size cubes, and fixed in 1% paraformaldehyde with 1% lanthanum nitrate tracer for 24 h followed by fixation with 3% glutaraldehyde for 24 h. Samples were fixed in 1% osmium tetroxide for 2 h and dehydrated in graded ethanol 1% lanthanum nitrate tracer (LNT) solution and embedded in araldite. Ultrathin hippocampal CA1 slices were obtained (90 nm); then they were stained with uranyl acetate and lead citrate and observed under TEM (H-7650; Hitachi, Ltd., Tokyo, Japan). The photos were obtained on hp digital CCD camera (SIS4 million voxel). Images were acquired digitally from a randomly selected pool of 10 to 15 fields under each condition.

2.7. Western Blotting. Isolated left hippocampus tissue was lysed in 100 μL radioimmunoprecipitation assay (RIPA) buffer (Beyotime, Haimen, Jiangsu, China) plus protease inhibitors. Total protein (50 μg) was loaded into 10% SDS-PAGE gels, electrophoresed, and then transblotted onto polyvinylidene difluoride membranes (Immobilon-P; Millipore, Billerica, MA) in a Tris-glycine transfer buffer. After being blocked in 5% milk in PBST for 1 h at room temperature with shaking, membranes were incubated with antibodies overnight at 4°C against the following: anti-LIMK1 antibody (dilution, 1 : 1000; ab81046, Abcam) and anti-LIM kinase 1 antibody (phospho-Thr508) (dilution, 1 : 1000; ab131341, Abcam) and β-actin (dilution, 1 : 1000; ab189073; Abcam). The following day, membranes were incubated in 5% milk (in TBST) with an anti-goat or anti-mouse IgG antibody (dilution, 1 : 5000; PerkinElmer Life Sciences, Waltham, MA) for 1 h at room temperature with shaking. Membranes were washed a minimum of four times (10 min per wash) in PBST

between each antibody treatment. Detected bands were visualized using enhanced chemiluminescence and images were captured using a Bio-Image system (Bio-Rad Laboratories, Inc., Hercules, USA). Western blotting was repeated three times.

2.8. Real Time Quantitative RT-PCR. The expression of miRNAs was determined by real time quantitative reverse transcription polymerase chain reaction (RT-PCR). Total RNA was extracted from hippocampal region of the ipsilateral lesion tissue using the TRIzol Reagent (Life Technologies (AB & Invitrogen), Carlsbad, USA). Then extracted total RNA was reverse transcribed to generate cDNA according to manufacturer instructions of Revert AidTM First-Strand cDNA Synthesis Kit (Thermo Fisher Scientific, Beijing, China). The reverse transcription reaction was amplified using a Bio-Rad CFX96 Detection System (Bio-Rad, Hercules, CA, USA) with the Plexor™ One-Step qRT-PCR System (Promega, Madison, WI, USA). For miRNA amplification, the following primers were used: rno-miR-134 (RmiRQP0168, GeneCopoeia, Guangzhou, China). The fold change in relative mRNA and miRNA expression was determined using the $2^{-\Delta\Delta Ct}$ method as described previously [33] and U6 snRNA (RQP047936, GeneCopoeia) as mRNA and miRNA internal control, respectively.

2.9. Statistical Analysis. Statistical analysis was performed with the SPSS package for Windows statistical analysis software (Version 18.0, SPSS, Inc., Chicago, IL, USA). The data from all groups were determined by one-way analysis of variance (ANOVA) and Student's t-tests. The homogeneity of variance was analyzed using the least significant difference method and missing variance using the Games-Howell method. Intergroup comparisons of the brain lesions volume at different time points were performed with paired-samples t-tests. All data are presented as mean ± standard error, and the significance was regarded as at least $p < 0.05$. All final results were analyzed in a blinded manner.

3. Results

3.1. EA Improved Cognitive Impairment in MICD Rats. To assess the effect of EA on spatial reference learning and memory impairments in MICD rats, the Morris water maze (MWM) test was performed. All groups of rats learned to find the platform, and the latency time to reach the platform was reduced in the four training days. However, learning ability was significantly reduced in MICD rats compared with the Sham group ($p < 0.01$, Figure 2(a)); the MICD rats treated with EA significantly took less time to find the platform compared with the MICD group and the MICD+non-EA group ($p < 0.01$ or $p < 0.05$, Figure 2(a)). There was no significant difference about path length among the four groups ($p > 0.05$, Figure 2(b)). As illustrated in Figures 2(c) and 2(d), tracing images from the MWM test showed that in the space exploration test where the platform was removed the MICD rats passed through the original position of the platform fewer times than the Sham group ($p < 0.01$, Figure 2(d)), whereas in the MICD+EA group the times where the rats crossed the position of the platform were significantly increased compared with the MICD group and the MICD+non-EA group ($p < 0.01$, $p < 0.05$, Figure 2(d)). As illustrated in Figures 2(e) and 2(f), the percentage of time spent in the target quadrant was used for statistical analysis during the probe trial. The date showed that the rats spent more time in the target quadrant compared to other quadrants ($p < 0.01$; Figure 2(e)). The MICD group spent less time in the target quadrant compared with the other groups ($p < 0.01$; Figure 2(e)). The MICD+EA group spent more time in the target quadrant compared with the MICD group and MICD+non-EA group ($p < 0.01$, $p < 0.05$, Figure 2(f)). Therefore, these results suggest that acquisition or retention of spatial reference learning and memory was ameliorated in MICD rats by EA treatment.

3.2. EA Attenuated Left Cortex, Hippocampus, Corpus Striatum, and Thalamus Lesions in MICD Rats. The brain lesions were determined by T2-weighted imaging (T2WI) (Figures 3(a) and 3(c)) before and after EA treatment. The volumes of brain lesions that included left cortex, hippocampus, corpus striatum, and thalamus regions in the all groups had no significant difference before EA treatment ($p > 0.05$, Figures 3(a) and 3(b)). There was mild spontaneous recovery for 14 days in the brain lesions of the MICD group. The volumes of left cortex, hippocampus, corpus striatum, and thalamus lesions showed comprising approximately 23% of the whole brain in the MICD group, whereas the brain lesions sizes were significantly reduced to 15% in the MICD+EA group ($p < 0.01$, Figures 3(c) and 3(d)). The difference of brain lesions between the MICD+EA and the MICD+non-EA group showed significant changes at Day 14 after EA ($p < 0.05$, Figures 3(c) and 3(d)).

3.3. EA Increased the Density of Dendritic Spines in the Hippocampus of MICD Rats. To investigate the function of EA on synaptic plasticity, dendritic spine density in the hippocampal neurons was analyzed by the primary basilar dendrites of Golgi-stained pyramidal neurons at Days 14 after EA. Golgi-Cox staining clearly filled the dendritic shafts and the spines of neurons from pyramidal neurons (Figure 4(a)). Hereby, the representative hippocampus showed that the density of dendritic spines was reduced in different degree by macroscopic examination in the MICD group, the MICD+EA group, and MICD+non-EA group, and the loss of dendritic spines in hippocampal CA1 was obvious in the MICD group. Thus, as illustrated in Figures 4(b) and 4(c), the density of selected dendritic spines that derived from hippocampal CA1 was significantly decreased in the MICD group compared with the Sham group ($p < 0.01$); however, the density of dendritic spines of the hippocampal CA1 in the MICD+EA group was more than that of the MICD group and the MICD+non-EA group ($p < 0.01$). In brief, EA treatment triggered large-scale remodeling of dendrites in the hippocampal area CA1.

3.4. EA Enhanced the Number of Hippocampus CA1 Synapses in MICD Rats. Furthermore, we observed the effect of EA on

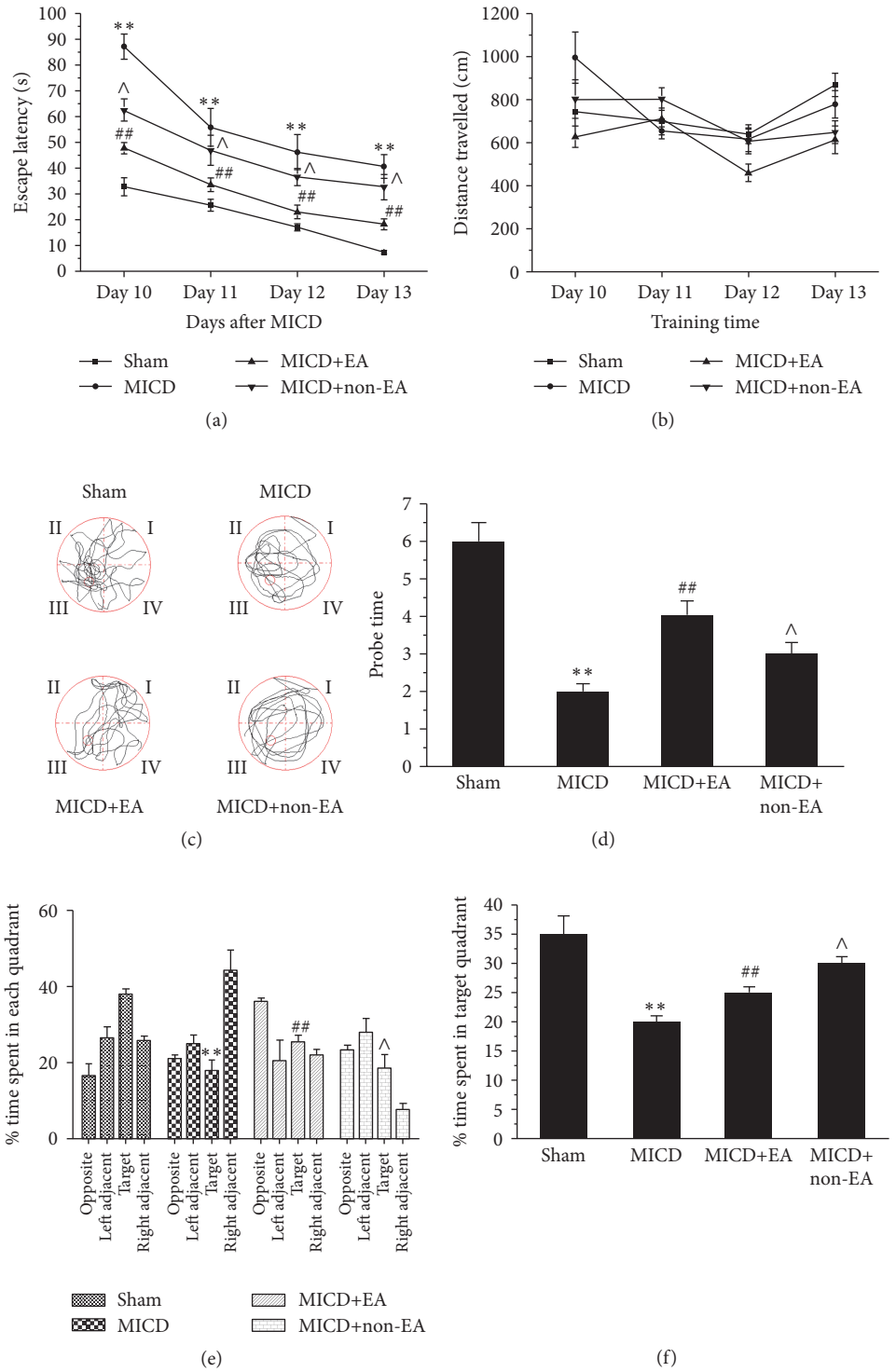

FIGURE 2: Evaluation of spatial reference learning and memory by Morris water maze test at Days 10–14 after EA. (a and b) Mean escape latency time and path length during the orientation navigation test on Days 10–13 after EA treatment. (c and d) Times the rats crossed over previous platform location on Day 14 after EA treatment during the spatial memory test in different groups. (e) The percentage of times spent in each quadrant in all probe trials is shown on Day 14 after EA treatment. (f) The times of passing the hidden platform position on Day 14 after EA treatment (each group; $^{**}p < 0.01$ versus the Sham group; $^{\#\#}p < 0.01$, $^{\#}p < 0.05$ versus the MICD group; $^{\wedge\wedge}p < 0.01$, $^{\wedge}p < 0.05$ versus the MICD+EA group). EA: electroacupuncture. MICD: middle cerebral artery occlusion induced cognitive deficits.

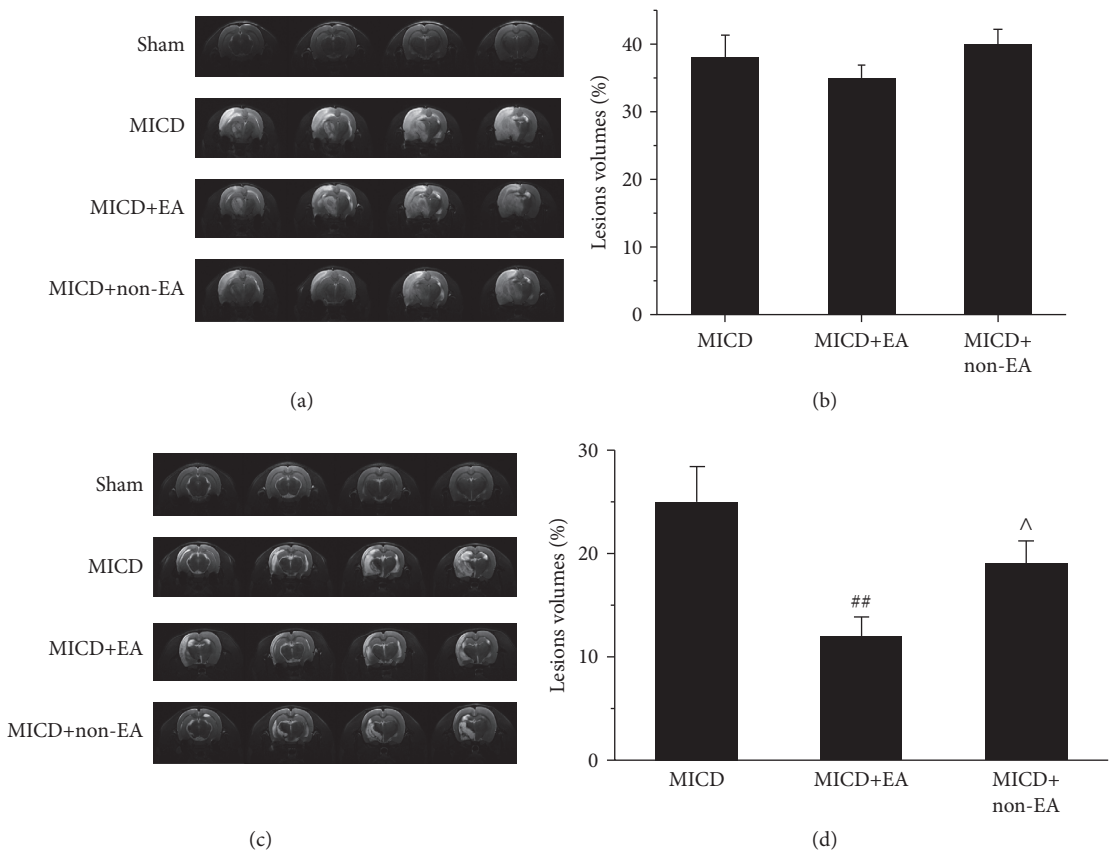

Figure 3: T2WI signal changes before and after EA (a and c). The brain lesions were measured by T2WI (slices from 11 to 13) in the Sham group, the MICD group, the MICD+EA group, and the MICD+non-EA group before (a) and after (c) EA. (b and d) Lesion volume is represented as a percentage of the total brain volume and data are presented as the mean ± standard deviation from 12 individual rats in each group. ($^{**}p < 0.01$ versus the Sham group; $^{\#\#}p < 0.01$, $^{\#}p < 0.05$ versus the MICD group; $^{\wedge\wedge}p < 0.01$, $^{\wedge}p < 0.05$ versus the MICD+EA group). T2WI: T2-weighted magnetic resonance imaging; MICD: middle cerebral artery occlusion induced cognitive deficits.

ultrastructural morphology of hippocampal CA1 pyramidal neurons. Obviously, the density of synapses in the MICD group was decreased compared with the Sham group ($p < 0.01$, Figures 5(a) and 5(b)), whereas there was amplifying in the number of synapses in the MICD+EA group compared with the MICD group and the MICD+non-EA group ($p < 0.05$ or $p < 0.01$, Figures 5(a) and 5(b)).

Taken together, these results suggest that EA could improve synaptic-dendritic plasticity in vivo.

3.5. EA Promoted LIMK1 Expression and Phosphorylation of Hippocampus CA1 in MICD Rats. To explore the underlying molecular mechanism of EA-induced synaptic-dendritic plasticity, the levels of total LIMK1 and phospho-LIMK1 (P-LIMK1, Thr508) in hippocampal CA1 were investigated. As shown in Figures 6(a) and 6(b), the expression of total LIMK1 of hippocampal CA1 was significantly decreased in the MICD group compared with the Sham group ($p < 0.01$). However, the total LIMK1 level in the MICD+EA group was more than that of the MICD group and the MICD+non-EA group ($p < 0.01$, Figures 6(a) and 6(b)). Moreover, the changes of phospho-LIMK1 (Thr508) in groups were similar to the total LIMK1 expression. The level of P-LIMK1 was significantly increased in the MICD+EA group compared with the MICD group and the MICD+non-EA group ($p < 0.01$, Figures 6(a) and 6(c)).

3.6. EA Regulated miR-134 Expression in Hippocampal CA1 in MICD Rats. To identify the role of synaptic-dendrite-related miR-134 in hippocampus CA1, the levels were detected. As shown in Figure 7, the expression of miR-134 was significantly increased in the MICD group compared with the Sham group ($p < 0.01$). However, repeated EA treatment significantly decreased the expression of miR-134 compared with the MICD group and the MICD+non-EA group ($p < 0.05$).

4. Discussion

Ischemic stroke leads to a high incidence of long-term cognitive impairment, which is strongly associated with loss of hippocampal neurons and synapses [34]. While reviewing ancient Chinese documents regarding acupuncture and cognitive impairment-related terms, we discovered that the DU20 and DU24 acupoints were the most frequently selected acupoints for cognitive impairment-related rehabilitation in China. A number of studies have shown that EA can improve

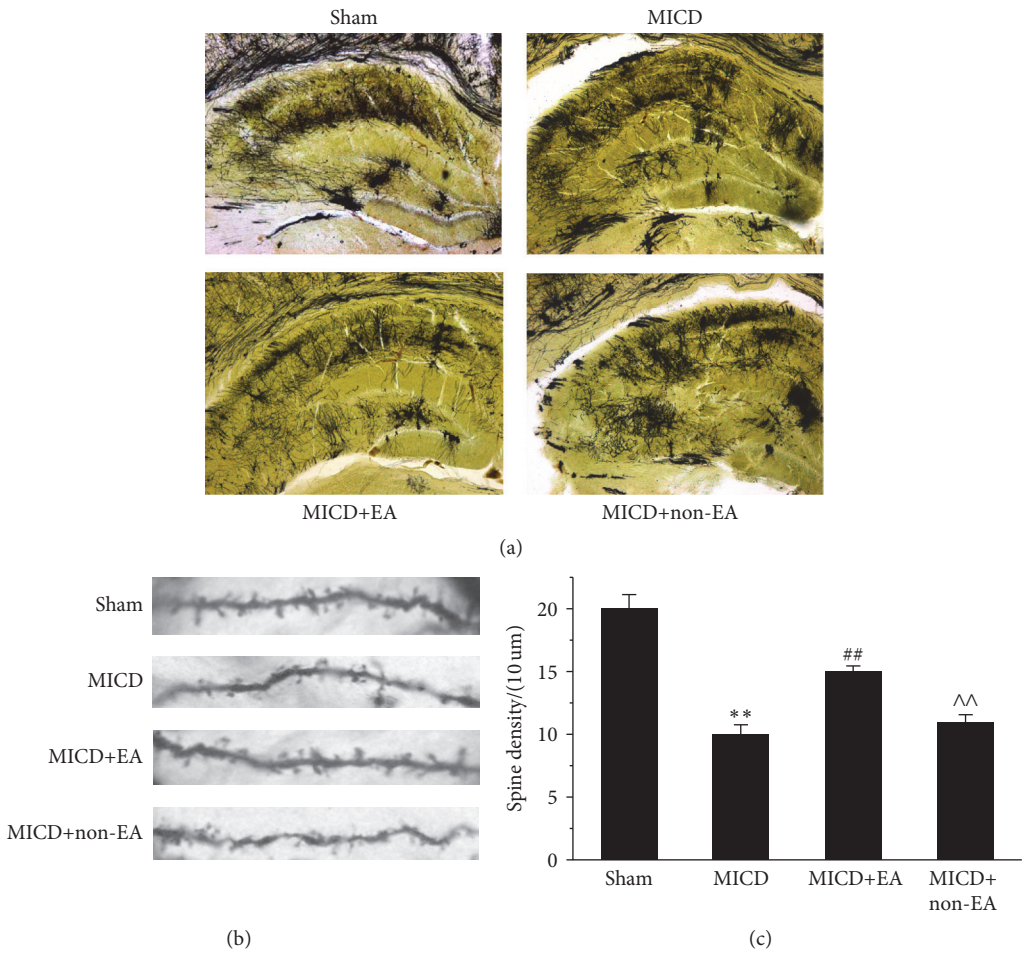

Figure 4: The structures and densities of dendritic spine in the hippocampus of rats. (a) Representative images of dendritic spine in the hippocampus of each group (Golgi staining, ×50). (b) Representative images of dendritic spine density and morphology from the pyramidal cell layer of hippocampal CA1 area in each group (Golgi staining, ×1000). (c) The density of dendritic spine was analyzed in hippocampal CA1 pyramidal cells in each group ($n = 6$/group; $^{**}p < 0.01$ versus the Sham group; $^{\#\#}p < 0.01$, $^{\#}p < 0.05$ versus the MICD group; $^{\wedge\wedge}p < 0.01$, $^{\wedge}p < 0.05$ versus the MICD+EA group). All experiments were repeated three times.

learning and memory ability and stimulate consciousness [30, 31, 35]. These results indicated that EA could be a complementary therapy for cognitive impairment after stroke. The present study found that EA at the DU20 and DU24 acupoints shortened time to find the platform and increased the times of crossing the position of the platform compared to untreatment or nonacupoint EA (stimulation control) in Morris water maze test, suggesting that EA could improve spatial reference learning and memory ability in MCAO-induced cognitive deficit (MICD) rats. Moreover, it is worth mentioning that the path length in the Morris water maze in the four groups showed no significant difference, indicating that the time spending of MICD rats to find the object was not affected by the motor function. However, the mechanisms of cognitive treatment involved are far from being fully elucidated.

Firstly, the cognitive deficit-related brain regions were determined by a small animal MRI in rats with ischemic stroke. T2-weighted imaging showed that MICD caused the lesions of left cortex, hippocampus, corpus striatum, and thalamus regions before EA. It had been noticed that the brain lesion exhibited a mild spontaneous recovery performance in MICD rats. However, the lesion regions comprising approximately 23% of the whole brain volume were reduced to 15% by EA treatment, indicating that EA could attenuate cortex and hippocampus, corpus striatum, and thalamus region lesions in the MICD rats. Some of these regions, such as the hippocampus and cortex, are essential for regulating learning and memory behaviors including spatial exploration [36]. Studies have confirmed that the hippocampus regions play a very important role in learning and memory through their specific structure and location which connect with other brain regions together [37]. Furthermore, in order to identify the hippocampus function in cognitive deficit, the hippocampal morphology staining was observed.

Using Golgi staining and electron microscopy, we demonstrated that the density of dendritic spine and the number of synapses in hippocampal CA1 pyramidal cells were obviously reduced at Day 14 after MICD. However, EA can rescue the loss of dendritic spine and synapses in hippocampal CA1 region. Moreover, EA promoted synaptic-dendritic spine

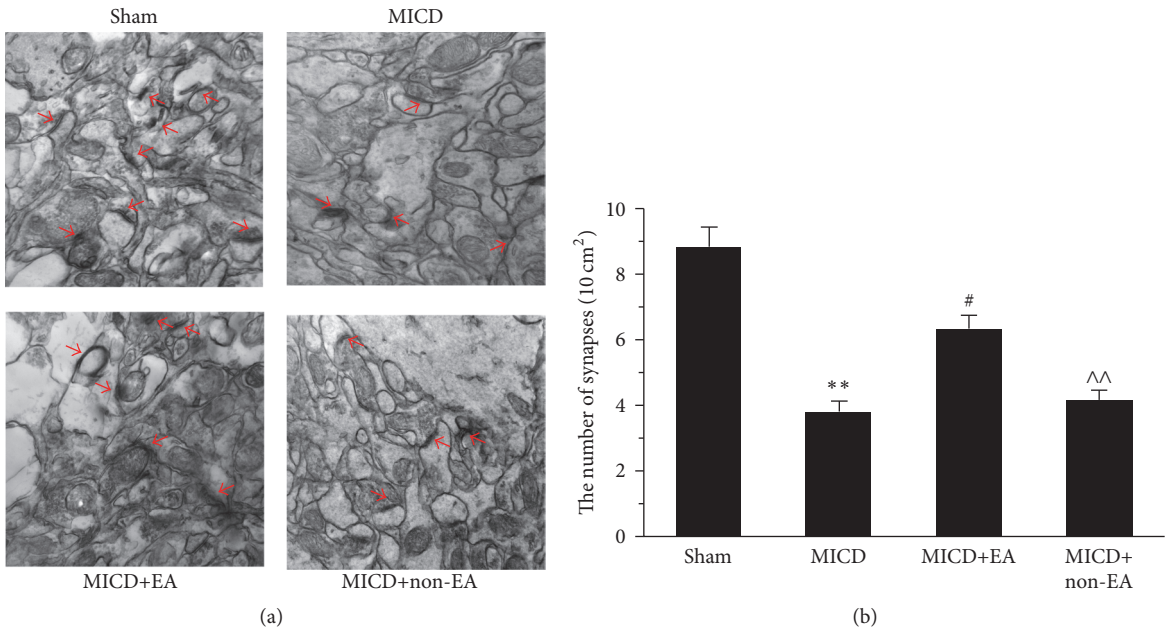

Figure 5: The number of synapses in hippocampal CA1 pyramidal cells. (a) Representative electron micrographic images of synapses (arrows) in the CA1 region of each group (magnification, ×50000). (b) Histogram shows the significant difference in the mean ± SEM of the number of synapses in each group ($n = 5$/group; $^{**}p < 0.01$ versus the Sham group; $^{\#\#}p < 0.01$, $^{\#}p < 0.05$ versus the MICD group; $^{\wedge\wedge}p < 0.01$, $^{\wedge}p < 0.05$ versus the MICD+EA group).

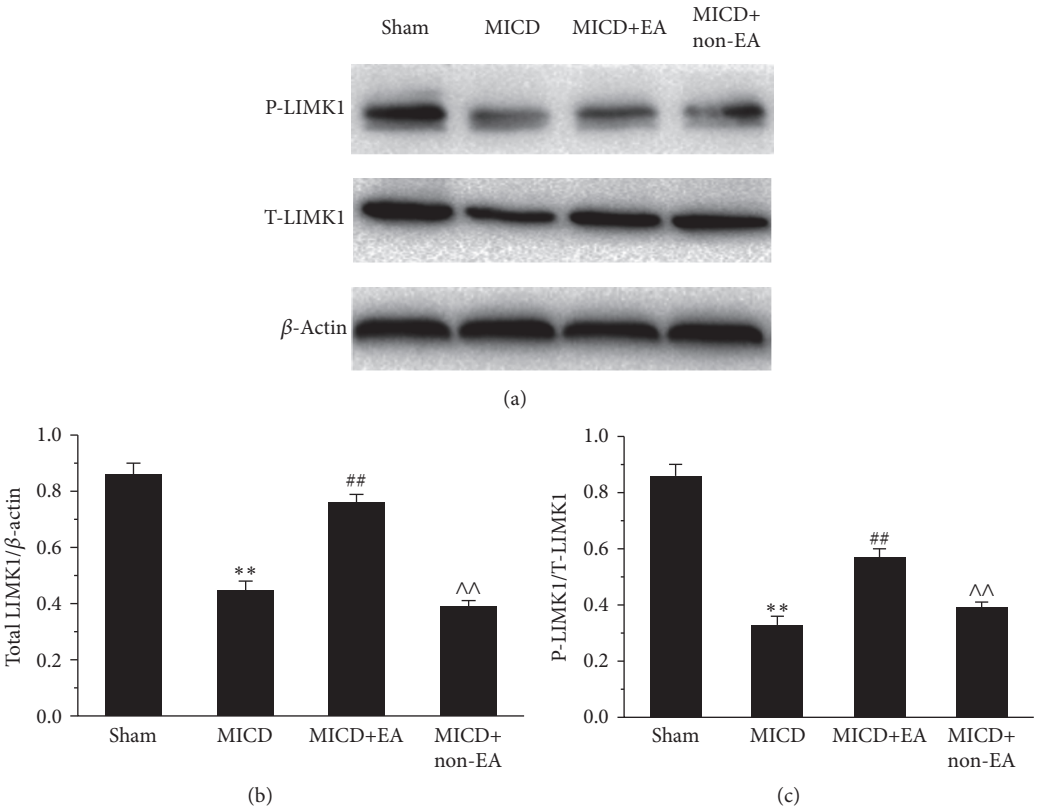

Figure 6: EA amplified the LIMK1 level in the hippocampus CA1 pyramidal cells. (a) The expression of total LIMK1 and phosphorylated LIMK1 was evaluated using western blotting. (b and c) Histogram shows significant difference of the levels of P-LIMK1 and phosphor-LIMLK1 in each group. Data are means ± SEM ($n = 6$/group; $^{**}p < 0.01$ versus the Sham group; $^{\#\#}p < 0.01$, $^{\#}p < 0.05$ versus the MICD group; $^{\wedge\wedge}p < 0.01$, $^{\wedge}p < 0.05$ versus the MICD+EA group).

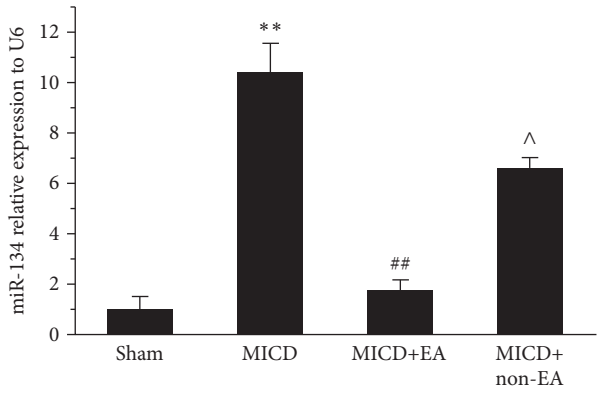

Figure 7: Changes of miR-134 expression in the hippocampus CA1 cells. The changes of miR-134 expression level were measured using quantitative RT-PCR. U6 was used as internal control for quantification of miRNAs. Data are mean ± SEM ($n = 6$/group; $^{**}p < 0.01$ versus the Sham group; $^{\#\#}p < 0.01$, $^{\#}p < 0.05$ versus the MICD group; $^{\wedge\wedge}p < 0.01$, $^{\wedge}p < 0.05$ versus the MICD+EA group).

regeneration. Dendritic spine is the tiny protrusions with multi-dense body and ion channels on the surface of various types of neurons, which serve as cellular substrates of brain connectivity and the major sites of information processing in the brain [38, 39]. Evidence is increasing that synaptic-dendritic plasticity enables the encoding of memory [40]. Indeed, the modification on dendritic spine number, size, and shape is of importance for the plasticity of synapses, accompanied by hippocampus-dependent learning and memory [41, 42]. Studies have well described that dendritic spine remodeling in ischemia surrounding areas may contribute to cognitive functional recovery after stroke [43, 44].

Increasing evidence showed that LIMK1 protein is activated at dendritic spine membranes [45]. LIMK1 positive cells were located in the CA1 region of the hippocampus, which is important in the regulation of the spine morphology and synaptic function in vivo. A prominent form of long lasting synaptic plasticity is thought to be critical to memory formation [26]. The present study found that the expression of total LIMK1 and phospho-LIMK1 in hippocampal CA1 was significantly decreased in the MICD rats; however, EA could enhance the total LIMK1 and phospho-LIMK1 levels to promote synaptic-dendritic plasticity in hippocampal CA1 area.

In addition, we have identified a dendritically localized miRNA that regulated the expression of the synaptic LIMK1 protein, thereby controlling dendritic pine size. miR-134 is the first discovered dendritic microRNA, enriched in the neuronal dendrites of rat hippocampal neurons, and negatively controls the size of dendritic spines [46]. This effect is mediated by miR-134 inhibition of the translation of LIMK1 mRNA [47]. The present study showed that the expression of miR-134 was obviously increased in the MICD rats. However, repeated EA treatment could relieve the upregulation of miR-134 expression in hippocampal CA1 area.

In conclusion, the study indicated that EA at the DU20 and DU24 acupoints could ameliorate cognitive impairment of MICD rats through the regulation of synaptic-dendritic plasticity of the hippocampal CA1 area, and the expression and phosphorylation of synaptic LIMK1 protein were activated to control dendritic spine number, size, and shape. Furthermore, the mechanism of LIMK1 increase induced by EA treatment may be associated with miR-134, which is localized in hippocampal CA1, by negatively regulating LIMK1 to enhance synaptic-dendritic plasticity in the recovery stage of ischemic stroke.

Competing Interests

The authors declare no financial or commercial conflict of interests.

Authors' Contributions

Weilin Liu, Jie Wu, and Jia Huang contributed equally to this work.

Acknowledgments

The present study was supported by the Natural Science Foundation of China (no. 81403450) and the Natural Science Foundation of Fujian Province (no. 2016J01382).

References

[1] V. L. Roger, "Heart disease and stroke statistics—2011 update: a report from the American Heart Association," *Circulation*, vol. 131, no. 4, pp. 29–322, 2014.

[2] T. E. Nichols and A. P. Holmes, "Nonparametric permutation tests for functional neuroimaging: a primer with examples," *Human Brain Mapping*, vol. 15, no. 1, pp. 1–25, 2002.

[3] T. K. Tatemichi, D. W. Desmond, Y. Stern, M. Paik, M. Sano, and E. Bagiella, "Cognitive impairment after stroke: frequency, patterns, and relationship to functional abilities," *Journal of Neurology, Neurosurgery & Psychiatry*, vol. 57, no. 2, pp. 202–207, 1994.

[4] F. Liu, Z.-M. Li, Y.-J. Jiang, and L.-D. Chen, "A meta-analysis of acupuncture use in the treatment of cognitive impairment after stroke," *Journal of Alternative & Complementary Medicine*, vol. 20, no. 7, pp. 535–544, 2014.

[5] W. Li, R. Huang, R. A. Shetty et al., "Transient focal cerebral ischemia induces long-term cognitive function deficit in an experimental ischemic stroke model," *Neurobiology of Disease*, vol. 59, pp. 18–25, 2013.

[6] P. S. Sachdev, X. Chen, H. Brodaty, C. Thompson, A. Altendorf, and W. Wen, "The determinants and longitudinal course of post-stroke mild cognitive impairment," *Journal of the International Neuropsychological Society*, vol. 15, no. 6, pp. 915–923, 2009.

[7] A.-J. Liu, J.-H. Li, H.-Q. Li et al., "Electroacupuncture for acute ischemic stroke: a meta-analysis of randomized controlled trials," *The American Journal of Chinese Medicine*, vol. 43, no. 8, pp. 1541–1566, 2015.

[8] X. Ding, C.-Y. Li, Q.-S. Wang et al., "Patterns in default-mode network connectivity for determining outcomes in cognitive function in acute stroke patients," *Neuroscience*, vol. 277, no. 10, pp. 637–646, 2014.

[9] H. Alipanahzadeh, M. Soleimani, S. Soleimani Asl, B. Pourheydar, A. Nikkhah, and M. Mehdizadeh, "Transforming growth factor-alpha improves memory impairment and neurogenesis following ischemia reperfusion," *Cell Journal*, vol. 16, no. 3, pp. 315–324, 2014.

[10] H. Eichenbaum, "Hippocampus: cognitive processes and neural representations that underlie declarative memory," *Neuron*, vol. 44, no. 1, pp. 109–120, 2004.

[11] T. Kadar, S. Dachir, B. Shukitt-Hale, and A. Levy, "Sub-regional hippocampal vulnerability in various animal models leading to cognitive dysfunction," *Journal of Neural Transmission*, vol. 105, no. 8-9, pp. 987–1004, 1998.

[12] J. B. Pereira, C. Valls-Pedret, E. Ros et al., "Regional vulnerability of hippocampal subfields to aging measured by structural and diffusion MRI," *Hippocampus*, vol. 24, no. 4, pp. 403–414, 2014.

[13] S. Knafo, G. Ariav, E. Barkai, and F. Libersat, "Olfactory learning-induced increase in spine density along the apical dendrites of CA1 hippocampal neurons," *Hippocampus*, vol. 14, no. 7, pp. 819–825, 2004.

[14] S. Schacher and J.-Y. Hu, "The less things change, the more they are different: contributions of long-term synaptic plasticity and homeostasis to memory," *Learning and Memory*, vol. 21, no. 3, pp. 128–134, 2014.

[15] K. Park, H. Heo, M. E. Han et al., "Learning-induced synaptic potentiation in implanted neural precursor cell-derived neurons," *Scientific Reports*, vol. 5, article 17796, 2015.

[16] S. Knafo, F. Libersat, and E. Barkai, "Dynamics of learning-induced spine redistribution along dendrites of pyramidal neurons in rats," *European Journal of Neuroscience*, vol. 21, no. 4, pp. 927–935, 2005.

[17] V. C. Foletta, N. Moussi, P. D. Sarmiere, J. R. Bamburg, and O. Bernard, "LIM kinase 1, a key regulator of actin dynamics, is widely expressed in embryonic and adult tissues," *Experimental Cell Research*, vol. 294, no. 2, pp. 392–405, 2004.

[18] M. Endo, K. Ohashi, Y. Sasaki et al., "Control of growth cone motility and morphology by LIM kinase and slingshot via phosphorylation and dephosphorylation of cofilin," *Journal of Neuroscience*, vol. 23, no. 7, pp. 2527–2537, 2003.

[19] C. Jarrold, A. D. Baddeley, and C. Phillips, "Long-term memory for verbal and visual information in Down syndrome and Williams syndrome: performance on the doors and people test," *Cortex*, vol. 43, no. 2, pp. 233–247, 2007.

[20] Y. Meng, Y. Zhang, V. Tregoubov et al., "Abnormal spine morphology and enhanced LTP in LIMK-1 knockout mice," *Neuron*, vol. 35, no. 1, pp. 121–133, 2002.

[21] Z. Todorovski, S. Asrar, J. Liu et al., "LIMK1 regulates long-term memory and synaptic plasticity via the transcriptional factor CREB," *Molecular and Cellular Biology*, vol. 35, no. 8, pp. 1316–1328, 2015.

[22] G. M. Schratt, F. Tuebing, E. A. Nigh et al., "A brain-specific microRNA regulates dendritic spine development," *Nature*, vol. 439, no. 7074, pp. 283–289, 2006.

[23] F. Capitano, J. Camon, V. Ferretti et al., "microRNAs modulate spatial memory in the hippocampus and in the ventral striatum in a region-specific manner," *Molecular Neurobiology*, vol. 53, no. 7, pp. 4618–4630, 2015.

[24] J. Gao, W.-Y. Wang, Y.-W. Mao et al., "A novel pathway regulates memory and plasticity via SIRT1 and miR-134," *Nature*, vol. 466, no. 7310, pp. 1105–1109, 2010.

[25] J. Remenyi, M. W. M. van den Bosch, O. Palygin et al., "miR-132/212 knockout mice reveal roles for these miRNAs in regulating cortical synaptic transmission and plasticity," *PLoS ONE*, vol. 8, no. 4, Article ID e62509, p. 65, 2013.

[26] L. An, J. Liu, W. W. Li et al., "Distribution of LIM domain kinase 1 in the olfactory bulb, cerebral cortex, hippocampus, and cerebellum of the App/PS$^{+/-}$ mice," *Genetics & Molecular Research*, vol. 14, no. 4, pp. 17244–17251, 2015.

[27] R. Lin, Y. Wu, J. Tao et al., "Electroacupuncture improves cognitive function through Rho GTPases and enhances dendritic spine plasticity in rats with cerebral ischemia-reperfusion," *Molecular Medicine Reports*, vol. 13, no. 3, pp. 2655–2660, 2016.

[28] P. Castañeda, M. Muñoz, G. García-Rojo et al., "Association of N-cadherin levels and downstream effectors of Rho GTPases with dendritic spine loss induced by chronic stress in rat hippocampal neurons," *Journal of Neuroscience Research*, vol. 93, no. 10, pp. 1476–1491, 2015.

[29] A. Romarowski, M. A. Battistone, F. A. La Spina et al., "PKA-dependent phosphorylation of LIMK1 and Cofilin is essential for mouse sperm acrosomal exocytosis," *Developmental Biology*, vol. 405, no. 2, pp. 237–249, 2015.

[30] R. Lin, K. Yu, X. Li et al., "Electroacupuncture ameliorates post-stroke learning and memory through minimizing ultrastructural brain damage and inhibiting the expression of MMP-2 and MMP-9 in cerebral ischemia-reperfusion injured rats," *Molecular Medicine Reports*, vol. 14, no. 1, pp. 225–233, 2016.

[31] X. Feng, S. Yang, J. Liu et al., "Electroacupuncture ameliorates cognitive impairment through inhibition of NF-κB-mediated neuronal cell apoptosis in cerebral ischemia-reperfusion injured rats," *Molecular Medicine Reports*, vol. 7, no. 5, pp. 1516–1522, 2013.

[32] Z. K. Wang, N. I. Guang-Xia, K. Liu et al., "Research on the changes of IL-1 receptor and TNF-α receptor in rats with cerebral ischemia reperfusion and the chronergy of acupuncture intervention," *Zhongguo Zhen Jiu*, vol. 32, no. 11, pp. 1012–1018, 2012.

[33] X. S. Liu, M. Chopp, R. L. Zhang, and Z. G. Zhang, "MicroRNAs in cerebral ischemia-induced neurogenesis," *Journal of Neuropathology & Experimental Neurology*, vol. 72, no. 8, pp. 718–722, 2013.

[34] X. He, T. Yan, R. Chen, and D. Ran, "Acute effects of electroacupuncture (EA) on hippocampal long term potentiation (LTP) of perforant path-dentate gyrus granule cells synapse related to memory," *Acupuncture and Electro-Therapeutics Research*, vol. 37, no. 2-3, pp. 89–101, 2012.

[35] W. Dong, W. Guo, X. Zheng et al., "Electroacupuncture improves cognitive deficits associated with AMPK activation in SAMP8 mice," *Metabolic Brain Disease*, vol. 30, no. 3, pp. 777–784, 2015.

[36] B. Milner and D. Klein, "Loss of recent memory after bilateral hippocampal lesions: memory and memories—looking back and looking forward," *Journal of Neurology, Neurosurgery & Psychiatry*, vol. 87, no. 3, article 230, 2016.

[37] A. Veronica Witte, L. Kerti, D. S. Margulies, and A. Flöel, "Effects of resveratrol on memory performance, hippocampal functional connectivity, and glucose metabolism in healthy older adults," *Journal of Neuroscience*, vol. 34, no. 23, pp. 7862–7870, 2014.

[38] T. Bonhoeffer and R. Yuste, "Spine motility: phenomenology, mechanisms, and function," *Neuron*, vol. 35, no. 6, pp. 1019–1027, 2002.

[39] H. Qiao, M. Li, C. Xu, H. Chen, S. An, and X. Ma, "Dendritic spines in depression: what we learned from animal models," *Neural Plasticity*, vol. 2016, Article ID 8056370, 26 pages, 2016.

[40] S. C. McQuown, R. M. Barrett, D. P. Matheos et al., "HDAC3 is a critical negative regulator of long-term memory formation," *Journal of Neuroscience*, vol. 31, no. 2, pp. 764–774, 2011.

[41] K.-O. Lai and N. Y. Ip, "Structural plasticity of dendritic spines: the underlying mechanisms and its dysregulation in brain disorders," *Biochimica et Biophysica Acta—Molecular Basis of Disease*, vol. 1832, no. 12, pp. 2257–2263, 2013.

[42] C. H. Bailey, E. R. Kandel, and K. M. Harris, "Structural components of synaptic plasticity and memory consolidation," *Cold Spring Harbor Perspectives in Biology*, vol. 7, no. 7, Article ID a021758, 2015.

[43] C. E. Brown, P. Li, J. D. Boyd, K. R. Delaney, and T. H. Murphy, "Extensive turnover of dendritic spines and vascular remodeling in cortical tissues recovering from stroke," *Journal of Neuroscience*, vol. 27, no. 15, pp. 4101–4109, 2007.

[44] R. Mostany, T. G. Chowdhury, D. G. Johnston, S. A. Portonovo, S. T. Carmichael, and C. Portera-Cailliau, "Local hemodynamics dictate long-term dendritic plasticity in peri-infarct cortex," *Journal of Neuroscience*, vol. 30, no. 42, pp. 14116–14126, 2010.

[45] J. George, C. Soares, A. Montersino, J.-C. Beique, and G. M. Thomas, "Palmitoylation of LIM kinase-1 ensures spine-specific actin polymerization and morphological plasticity," *eLife*, vol. 2015, no. 4, Article ID e06327, 2015.

[46] S. Bicker, M. Lackinger, K. Weiß, and G. Schratt, "MicroRNA-132, -134, and -138: a microRNA troika rules in neuronal dendrites," *Cellular and molecular life sciences: CMLS*, vol. 71, no. 20, pp. 3987–4005, 2014.

[47] H.-C. Tai and E. M. Schuman, "MicroRNA: microRNAs reach out into dendrites," *Current Biology*, vol. 16, no. 4, pp. R121–R123, 2006.

Hindawi Publishing Corporation
Neural Plasticity
Volume 2016, Article ID 8307175, 9 pages
http://dx.doi.org/10.1155/2016/8307175

Research Article

Neural Network Underlying Recovery from Disowned Bodily States Induced by the Rubber Hand Illusion

In-Seon Lee[1,2,3,4] and Younbyoung Chae[1]

[1]*Acupuncture & Meridian Science Research Center, College of Korean Medicine, Kyung Hee University, Seoul, Republic of Korea*
[2]*fMEG Center, University of Tübingen, Tübingen, Germany*
[3]*IMPRS for Cognitive and Systems Neuroscience, University of Tübingen, Tübingen, Germany*
[4]*Department of Internal Medicine, Psychosomatic Medicine and Psychotherapy, University of Tübingen, Tübingen, Germany*

Correspondence should be addressed to Younbyoung Chae; ybchae@khu.ac.kr

Received 23 August 2016; Accepted 24 October 2016

Academic Editor: Cun-Zhi Liu

Copyright © 2016 I.-S. Lee and Y. Chae. This is an open access article distributed under the Creative Commons Attribution License, which permits unrestricted use, distribution, and reproduction in any medium, provided the original work is properly cited.

We used functional magnetic resonance imaging to investigate how causal influences between brain regions during the rubber hand illusion (RHI) are modulated by tactile and visual stimuli. We applied needle rotations during the RHI in two different ways: one was with the real hand (reinstantiation by tactile stimuli, R-TS) and the other was with the rubber hand (reinstantiation by visual stimuli, R-VS). We used dynamic causal modeling to investigate interactions among four relevant brain regions: the ventral premotor cortex (PMv), the intraparietal sulcus (IPS), the secondary somatosensory cortex (SII), and the lateral occipitotemporal cortex (LOC). The tactile aspects of needle rotations changed the effective connectivity by directly influencing activity in the SII, whereas visual aspects of needle rotation changed the effective connectivity by influencing both the SII and the LOC. The endogenous connectivity parameters between the IPS and the PMv were reduced significantly in the R-TS condition. The modulatory parameters between the IPS and the PMv were enhanced significantly in the R-TS condition. The connectivity patterns driven by disowned bodily states could be differentially modulated by tactile and visual afferent inputs. Effective connectivity between the parietal and frontal multimodal areas may play important roles in the reinstantiation of body ownership.

1. Introduction

The "rubber hand illusion" (RHI) is an experimental paradigm that can manipulate body ownership via congruent touching on the rubber hand and the subject's real hand [1]. The brain interprets the interaction of the visual, tactile, and proprioceptive systems of the body and leads to the recalibration of touch and the felt position of the hand [1, 2]. Several functional magnetic resonance imaging (fMRI) studies have demonstrated that the illusory body ownership during the RHI was highly associated with the parietal and frontal multimodal areas [2, 3] and the lateral occipitotemporal cortex (LOC) [4]. Recently, Limanowski and Blankenburg used dynamic causal modeling (DCM) and revealed the effective connectivity underlying the illusory self-attribution of the rubber hand among four relevant brain regions: the ventral premotor cortex (PMv), the intraparietal sulcus (IPS), the secondary somatosensory cortex (SII), and the LOC [5].

Illusory body ownership during the RHI is known to induce a disowned bodily state for the subject's own hand. Psychologically disrupting the sense of body ownership decreased the awareness of physical self and the physiological regulation of self [6]. Furthermore, illusory ownership over an artificial body part boosted histamine reactivity in the real arm, a key pathway of the innate immune response [7]. Generally, the change in body representation induced by the RHI is considered a temporary phenomenon rather than convincing recalibration of one's bodily representation [8]. However, there has been little interest in investigating how the brain would recover from the disowned bodily state induced by the RHI. Given that models of bodily self-perception are explained by basic spatiotemporal principles of multisensory

integration as the key mechanism underlying self-attribution of the body [9], we propose two plausible reinstantiation methods from the disowned bodily states: one involves novel tactile information from the real hand and the other involves novel visual information about the artificial hand.

A stimulating acupuncture needle on the body is known to produce unique sensations and common activation in the sensorimotor cortical network in the brain [10]. In a previous study, we found that participants exhibited reduced, but still prominent, peripheral and central responses to acupuncture needle rotation following the RHI [11]. Furthermore, visual manipulation in the acupuncture stimulation was an important factor for autonomic responses, even without somatosensory tactile stimulation [12]. Taken together, acupuncture stimulation on the body could be a useful tool to reinstantiate body ownership after a disowned bodily state. When needle rotations are provided to the real hand as tactile stimuli, the subject could recover from the disowned bodily state with direct tactile information from his/her own body [11]. In contrast, when needle rotations are provided to the rubber hand as visual stimuli, the subject may recover from the disowned bodily state because visual information from the rubber hand does not correspond to tactile input from the real hand [13]. Thus, it is assumed that the brain networks in the disowned bodily states induced by the RHI could recover in different ways based on two different external information sources.

DCM can provide the strength of effective connectivity and its modulation under experimental conditions between brain regions [14]. We used DCM in conjunction with fMRI to investigate how brain networks are modulated during the RHI by two different stimuli: recovery from the RHI with tactile stimuli to the real hand (reinstantiation by tactile stimuli, R-TS) and recovery from the RHI with visual stimuli to the rubber hand (reinstantiation by visual stimuli, R-VS). Using DCM, we conducted a data-driven estimation of the effective connectivity (causal influence of the activities of certain brain regions on the activities of others), including endogenous connectivity (endogenous connectivity strength independent of experimental condition), and its changes (modulatory effects), under experimental conditions (driving input) between brain regions.

2. Methods

2.1. Participants. The present study included 17 healthy, right-handed participants (7 females, aged 20–31 years). The participants had no history of neurological, psychiatric, or visual disorders. Each participant received a detailed explanation of the study, and written informed consent was obtained prior to participation. All procedures were performed with the approval of the institutional review board of Korea University, Seoul, Republic of Korea (IRB number KU-IRB-12-48-A-1).

2.2. Experimental Design. To induce the RHI, a rubber hand (left hand; Korean Prosthetic Limbs Research Institute, Seoul, Korea) was placed 15 cm above the left hand of the participant. To ensure that the locations of the visual stimuli in the eye-centered coordinates remained the same, the participant was asked to look at the rubber hand throughout the entire experiment, while his/her real hand was completely occluded from view. Details of the experimental design are described in our previous reports [11, 13].

The RHI was induced by gentle strokes with soft brushes. We considered different types of mechanical stimulation, with clear tactile and visual stimulus components that could induce recovery from the illusory state. For example, mechanical stimuli delivering a light sensation, a serious emotional response, such as fear or a threat, and visually ambiguous methods (such as a pad-shape stimulator that could deliver electric or thermal stimuli) were all excluded. Ultimately, rotation of an inserted acupuncture needle was chosen because it provides concise tactile and visual sensory information with no threat. Importantly, all participants had previous experience with acupuncture treatment.

Prior to scanning, a needle was inserted at the same location in the real hand and the rubber hand (dorsum of radial to the midpoint of the second metacarpal bone). The two sessions involved an identical degree of mechanical stimulation (needle rotation) in the real hand (tactile stimulus condition) and the rubber hand (visual stimulus condition). All mechanical stimulations were applied by a licensed and experienced doctor of Korean medicine. Each session included four blocks of resting period (60 s), four blocks of stroking brushes (30 s, at a frequency of 1 Hz, synchronously at the same location on the rubber and the real hand) to induce the RHI, and four subsequent blocks of tactile or visual stimuli (30 s, at a frequency of 1 Hz) immediately thereafter. In the R-TS session, the RHI was expected to be modulated by tactile information during needle rotation in the real hand (Figure 1(a)). The participants could not see the stimulation from their real hand. In contrast, the RHI was expected to be modulated by visual information during needle rotation in the rubber hand in the R-VS session (Figure 1(b)).

After fMRI scanning, the participants were asked to assess their perception of the RHI by answering Item 3 on the RHI perception scale: "I felt as if the rubber hand was my hand" [1].

2.3. fMRI Data Acquisition. fMRI scans were acquired with a MAGNETOM Trio 3 T scanner (Siemens, Erlangen, Germany) using echo planar imaging (EPI) with a 64×64 matrix (TE = 30 ms, TR = 2,000 ms) across 37 slices with a thickness of 4 mm. To minimize movement artifacts, the head of each participant was fixed using a head holder. Each scan session contained 240 volumes of the whole brain in the 37-axial-slice acquisition (TR = 2,000 ms, TE = 30 ms, flip angle = 90°, field of view = $240 \times 240\ mm^2$, and voxel size = $3.8 \times 3.8 \times 4.0\ mm^3$). As an anatomical reference, a three-dimensional T1-weighted magnetization-prepared rapid gradient echo (MPRAGE) image data set was acquired using the following parameters: TR = 2,000 ms, TE = 2.37 ms, flip angle = 9°, field of view = $240 \times 240\ mm^2$, voxel size = $0.9 \times 0.9 \times 1.0\ mm^3$, and 192 slices.

2.4. fMRI Data Analysis. Preprocessing of the data was conducted using Statistical Parametric Mapping software

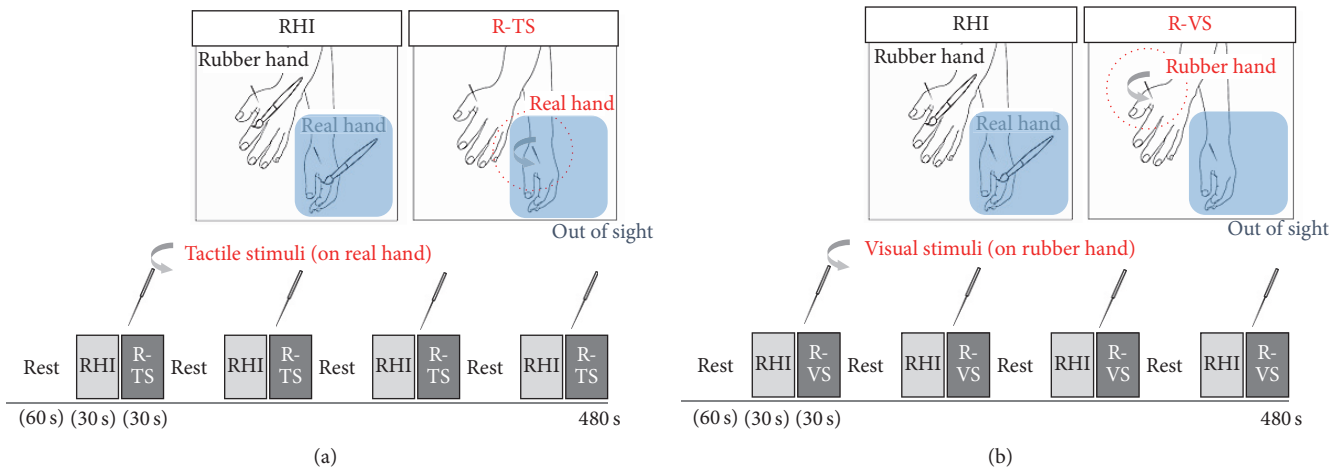

FIGURE 1: The two sessions involved the same degree of mechanical stimulation (needle rotation) in the real hand (reinstantiation by tactile stimuli or R-TS condition, (a)) and the rubber hand (reinstantiation by visual stimuli or R-VS condition, (b)). Each session included four blocks of brush strokes (30 s, at a frequency of 1 Hz, synchronously on the same location on the rubber and real hand) to induce the rubber hand illusion (RHI) and four subsequent blocks of tactile or visual stimuli (30 s, at a frequency of 1 Hz) immediately thereafter.

(SPM8; Wellcome Center for Neuroimaging, London, UK) implemented in Matlab 7.1 (MathWorks Inc., Natick, MA). All participants satisfied a motion threshold of <2 mm spatial displacement in any direction. The data were realigned and coregistered on a mean image, normalized to a template, and smoothed with an 8 mm full-width-at-half-maximum (FWHM) Gaussian kernel. The first four volumes of each session were discarded to allow for T1 equilibration.

For the first-level analysis, a general linear model (GLM) was applied to the preprocessed data. Movements during the scanning sessions were modeled as confounding regressors in the general linear model. RHI and needle rotations were modeled as boxcar functions, convolved with a standard hemodynamic response function that began at the onset of each stimulation, and contrast maps were generated (F-contrast for evaluating the effects of interest, T-contrasts for RHI and needle rotations). A second-level analysis (group analysis) of the stroking brushes during RHI was performed using a random-effects model. This study was performed using the standard summary statistics procedure to make random-effects inferences.

2.5. DCM. Our dynamic causal modeling proceeded in two steps. In the first step, we identified the underlying effective connectivity responsible for the rubber hand illusion *per se*. In the second step, we introduced the effects of acupuncture to identify changes in extrinsic coupling or connectivity within the architecture identified in the first step.

In the first step, we explored a number of architectures with bidirectional connections among the four nodes or regions, using the RHI effect as both a driving and a modulatory input. In other words, we modeled the differences between the brain states in the RHI conditions as a mixture of direct driving effects on SII and LOC and a context-sensitive change in coupling between regions. Crucially, we did not differentiate between the two different sorts of reinstantiation (tactile and visual) as RHI procedures before reinstantiation were identical in both sessions, leaving the reinstantiation effects to the second stage.

Having established the best architecture using Bayesian model selection, we then proceeded to the second step. In the second step, we were interested in identifying the regions and connections that differentiated between the tactile and visual reversals of the illusion. We adopted a conservative approach by applying DCM to both sessions separately and then comparing the effective connection strengths using classical statistics (ANOVA) at the between-subject level. This should be contrasted with the more usual approach of modeling both sessions within a single DCM and specifying where the reinstantiation effects could operate (through modulation of endogenous connectivity). We chose the former because it allows for potential effects of reversal on every connection included in the session-specific DCMs. Note that our inferences about the effects of reinstantiation on regional responses and coupling are assessed in relation to between-subject variability using classical statistics. This follows the normal summary statistic approach, in which the estimates from DCM were used to summarize the subject and session-specific neuronal responses. Crucially, we used Bayesian model averaging (within each session) to accommodate the uncertainty about how the reinstantiation effects were mediated. Under the null hypothesis that reinstantiation effects are the same, this session-specific Bayesian model averaging did not introduce any bias into the parameter estimates (i.e., summary statistics).

We performed a standard bilinear, one-state, deterministic DCM using center input using DCM12 implemented in SPM12. Four regions of interest (ROIs) in the right hemisphere (because the stroking brush and needle rotations were delivered to the left hand), the right PMv, the right IPS, the right SII, and the right LOC were selected for three different DCM analyses: (1) the RHI, (2) the R-TS condition, and (3) the R-VS condition. The selected ROIs were reported in a recent paper that provided relevant evidence supporting

changes in the effective connectivity between these regions [5].

2.5.1. Definition of the ROIs. The coordinates of the ROIs were based on the aforementioned whole brain GLM (i.e., SPM) analysis and effects of RHI from a previous study (R-TS session: the right SII: 54, −20, 22; the right LOC: 52, −68, 0; the right IPS: 38, −34, 50; and the right PMv: 48, 6, 42; R-VS session: the right SII: 58, −26, 20; the right LOC: 52, −66, 0; the right IPS: 30, −40, 52; and the right PMv: 52, 4, 38) [5]. After the group-level coordinates of each ROI were defined, a 15 mm radius sphere for all ROIs was created and applied as an inclusive mask on individual contrast images for RHI and needle rotations in the R-TS and R-VS sessions ($p < 0.001$, uncorrected). The nearest local maximum to the group-level coordinates within the mask was selected, ensuring that the individual coordinates were within 15 mm from the group coordinates.

The anatomical location of each volume of interest (VOI) was confirmed with neuroanatomical labels from the SPM Anatomy Toolbox [15] and the Talairach Atlas Daemon [16]. The first eigenvariates of all significant voxels within a 6 mm radius sphere centered on individual coordinates were extracted. Because there was no significant activation during needle rotations in one participant in each session, in total, four participants were excluded from the DCM analyses (two in the RHI session, one in the R-TS session, and one in the R-VS session).

2.5.2. DCM for the RHI. As the RHI with stroking brushes was the same in the two sessions, we used all time-series data during the RHI for both sessions for model specification in the DCM analysis during the RHI. In the first step, the endogenous connectivity for the RHI was established, including bidirectional connections between the IPS and the PMv, the IPS and the SII, the IPS and the LOC, and self-connections.

The modulatory effect on endogenous connectivity by the RHI was modeled to investigate bottom-up or top-down modulation: no modulatory effect (Model 1), modulation on bidirectional connections between the IPS-SII and the IPS-LOC (Model 2), modulation on bidirectional connections between the IPS-PMv, the IPS-SII, and the IPS-LOC (Model 3), modulation on bottom-up connections from the SII and the LOC to the IPS (Model 4), additional connections from the IPS to the PMv beyond Model 4 (Model 5), additional connections from the PMv to the IPS beyond Model 5 (Model 6), modulation on top-down connections from the IPS to the SII and the LOC (Model 7), additional connections from the PMv to the IPS beyond Model 7 (Model 8), and additional connections from the IPS to the PMv beyond Model 8 (Model 9). Connection parameters were estimated using a Bayesian scheme (Figure 2(a)).

The nine models from both sessions were compared using random-effects (RFX) Bayesian model selection (BMS) after estimation. The winning model, with the highest exceedance probability (Model 3; see Results) was selected as the baseline RHI model for analyses of both the R-TS and the R-VS conditions.

2.5.3. DCM for Recovery from the RHI with Needle Rotation. We evaluated three models for the R-TS and R-VS conditions. To investigate the changes of connectivity strength in the baseline brain network during the R-TS and during the R-VS conditions, the driving input of mechanical stimulation was added to the winning model for the RHI. The models for investigation were thus mechanical stimulation input influencing the activity in the SII (Model A), in the LOC (Model B), and in both the SII and the LOC (Model C) (Figure 2(b)).

We hypothesized that mechanical stimulation could change the brain network of the RHI by directly influencing the activity in the SII (Model A) in the R-TS condition and in both the SII and the LOC (Model C) in the R-VS condition. After estimation, the three models for each session were compared separately using RFX BMS, and the model with the highest exceedance probability was selected as the winning model (Model A for the R-TS condition and Model C for the R-VS condition; see Results).

2.5.4. Bayesian Model Averaging (BMA) and Statistical Analysis (Group Comparison). As the winning models from the session-specific DCM analyses differed, the parameter estimates from all the models of reinstantiation effects were obtained using Bayesian model averaging (BMA). Exceedance probabilities from BMA analysis of all endogenous connections, modulatory effects, and driving inputs from all participants were extracted and their significance was assessed using a one-sample t-test with Bonferroni correction for multiple comparisons. A one-way analysis of variance (ANOVA) was also used to compare the strength of estimated parameters in the three brain networks (RHI, R-TS, and R-VS) with Bonferroni correction.

3. Results

BMA was performed across all models to calculate parameter estimates (see Supplementary Table 1 available online at http://dx.doi.org/10.1155/2016/8307175). BMA accounts for individual variability in model fit by weighting parameter estimates by the posterior probability of each model.

3.1. The Winning Models. The BMS results showed that Model 3 was the winning model for the RHI (the highest exceedance probability in Model 3 for the RHI = 0.3767). Model A was the winning model for the R-TS condition, whereas Model C was the winning model for the R-VS condition (the highest exceedance probability in Model A for the R-TS condition = 0.7463 and the highest exceedance probability in Model C for the R-VS condition = 0.8053; Figure 2(c)).

3.2. BMA Parameter Estimates

3.2.1. DCM for the RHI. Analysis of the parameter estimates of the BMA results for endogenous connectivity showed significant positive connections from the IPS to the PMv ($p < 0.05$), from the IPS to the SII ($p < 0.001$), and from the LOC to the IPS ($p < 0.01$) and self-connections of the IPS ($p < 0.01$) and the SII ($p < 0.001$). In the RHI, the positive connectivity strengths from the IPS to the SII and from the IPS to the LOC were weakened significantly and became

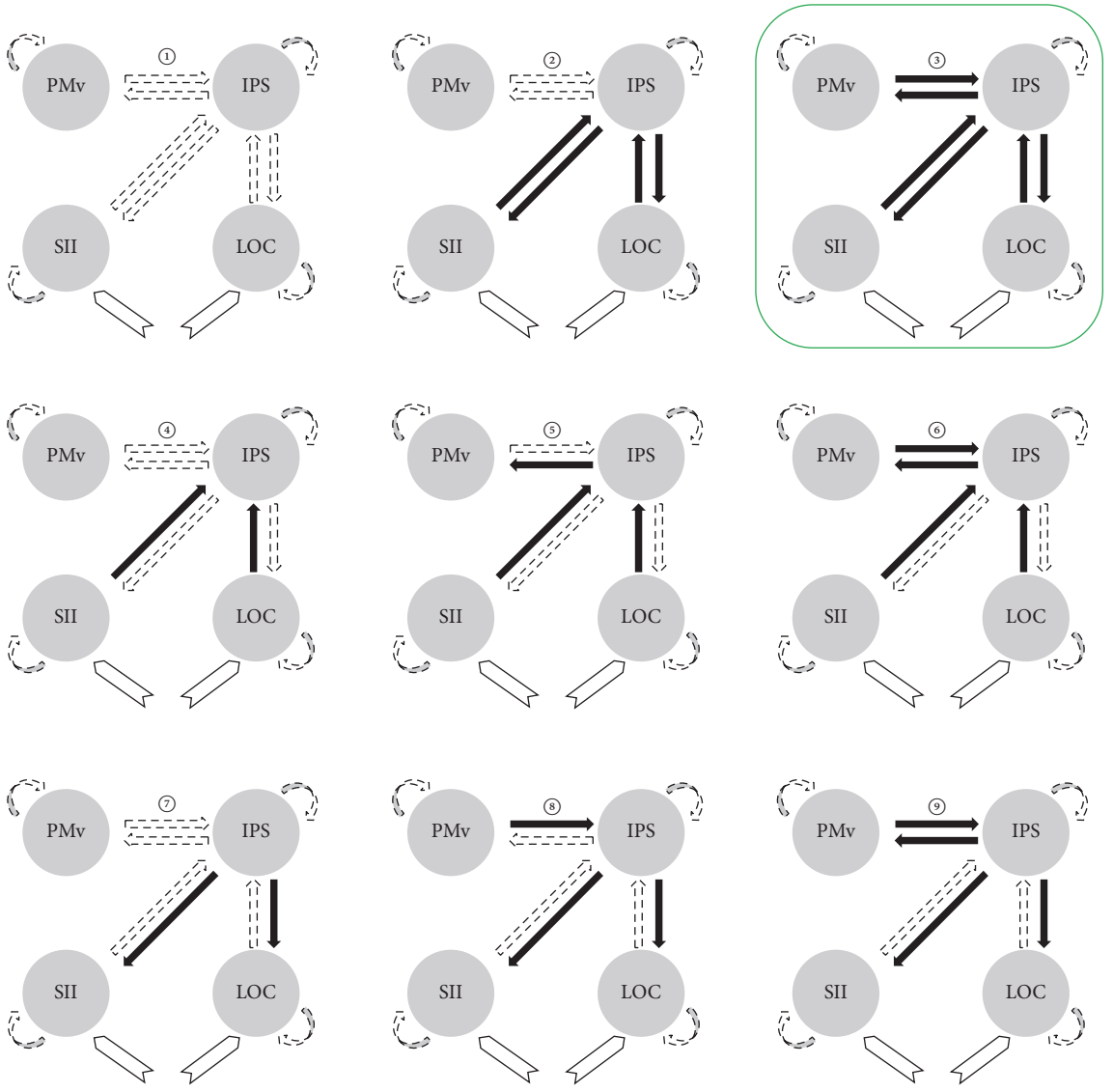

(a) DCM models for RHI

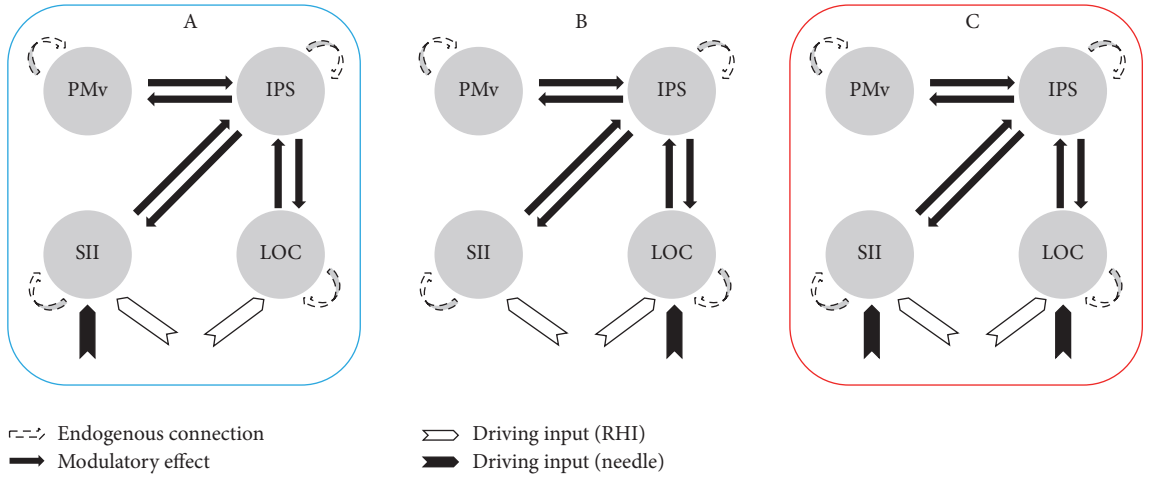

(b) DCM models for recovery from RHI by tactile or by visual stimuli

Figure 2: Continued.

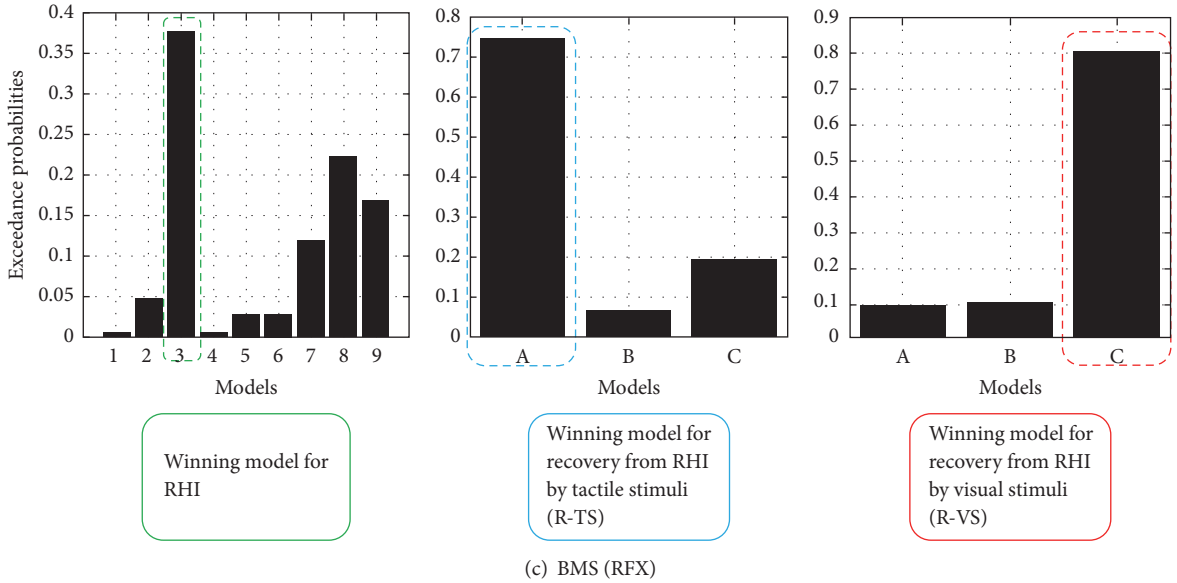

(c) BMS (RFX)

Figure 2: (a) Dynamic causal modeling (DCM) for the RHI (9 models). Blank arrow indicates endogenous connection, and solid arrow indicates modulatory effect. (b) DCM for recovery from the RHI by needle rotation in the real hand (R-TS, 3 models) and in the rubber hand (R-VS, 3 models). Winning models from the random-effects Bayesian model selection for each DCM analysis are marked with a box: Model 3 for the RHI, Model A for recovery from the RHI by tactile stimuli, and Model C for recovery from the RHI by visual stimuli. Winning Model 3 for the RHI was used in DCM analyses for R-TS and R-VS in which the driving inputs from mechanical stimulation were differentially defined as entering into the SII (Model A), into the LOC (Model B), and into the SII and the LOC (Model C). (c) Bayesian model selection (BMS), winning model, and parameter analysis.

negative ($p < 0.01$ and $p < 0.001$, resp.). Driving inputs in the RHI to both the SII and the LOC were also statistically significant ($p < 0.01$ and $p < 0.001$, resp.).

3.2.2. DCM of Recovery from the RHI with Tactile Stimuli. Analysis of the parameter estimates of the BMA results for endogenous connectivity showed a significant negative self-connection of the LOC ($p < 0.05$). By needle rotation in the real hand during the RHI, connections from the IPS to the SII and from the IPS to the LOC were weakened significantly and became negative ($p < 0.001$ and $p < 0.01$, resp.) and the positive connection from the IPS to the PMv was enhanced significantly ($p < 0.05$). Only the driving input of mechanical stimulation to the SII was statistically significant ($p < 0.001$; Figure 3(a)).

3.2.3. DCM of Recovery from the RHI by Visual Stimuli. Analysis of the parameter estimates for the BMA results for endogenous connectivity showed significant positive connections from the IPS to the PMv ($p < 0.001$) and from the IPS to the LOC ($p < 0.05$) and a negative connection of self-connections of the IPS ($p < 0.01$). By needle rotations in the rubber hand during RHI, connections from the IPS to the SII were weakened significantly and became negative ($p < 0.01$). Driving inputs in the RHI to both the SII and the LOC were statistically significant ($p < 0.001$ and $p < 0.01$, resp.; Figure 3(b)).

3.2.4. Comparing Effective Connectivity of Recovery from the RHI by Tactile Stimuli. In comparison with the RHI, the endogenous connections from the IPS to the SII and from the LOC to the IPS decreased significantly in the R-TS condition ($p < 0.05$). In comparison with the R-VS condition, the endogenous connection from the IPS to the PMv decreased significantly in the R-TS condition ($p < 0.05$). In comparison with the R-VS condition, the modulatory effect on the connection from the IPS to the PMv increased significantly in the R-TS condition ($p < 0.01$). In comparison with the R-VS condition, the driving input in the RHI to the SII decreased significantly in the R-TS condition, and the driving input of needle rotation to the LOC decreased significantly in the R-TS condition ($p < 0.05$; Figure 4).

4. Discussion

The present study showed that two different bottom-up information processes with tactile and visual information processing differentially modulated brain networks during RHI-induced disowned bodily states. Tactile information upon mechanical stimulation changed the brain network by directly influencing activity in the SII, whereas visual information on mechanical stimulation changed the brain network by influencing both the SII and the LOC. Importantly, the endogenous connectivity from the IPS to the PMv was reduced significantly in the R-TS versus the R-VS condition. However, the modulatory effect of tactile stimulation was significantly positive in this connection in the R-TS condition, indicating the important role of the connection from the IPS to the PMv in the RHI and in the reinstantiation of body ownership. To our knowledge, this is the first reported

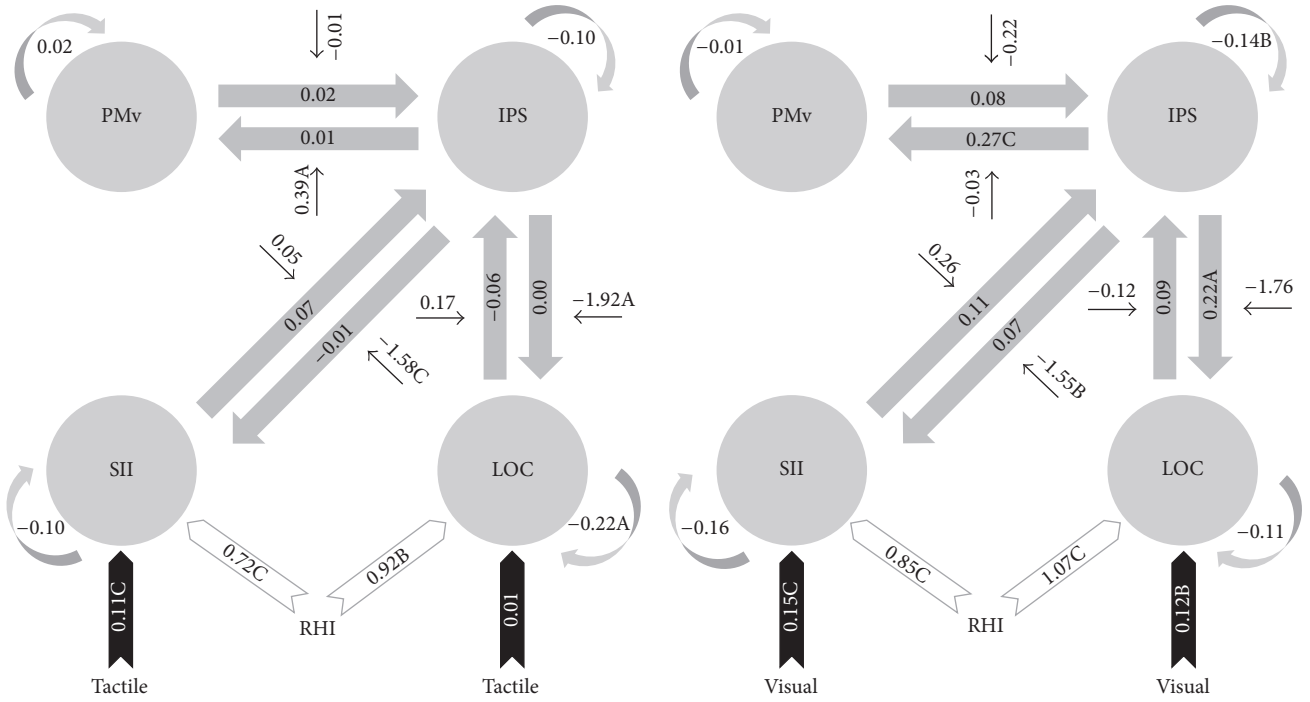

(a) R-TS (b) R-VS

Figure 3: (a) BMA results of recovery from the RHI by needle rotation in the real hand (R-TS condition). (b) BMA results of recovery from the RHI by needle rotation in the rubber hand (R-VS condition). Means of parameter estimates from all participants for endogenous connection (DCM.A), modulatory effect (DCM.B), and driving input (DCM.C) and statistical significance are shown. A one-sample t-test with zero was used to assess statistical significance and the Bonferroni correction was applied for multiple comparisons.

study to show the neural network involved in the mechanism underlying the recovery from disowned bodily states induced by the RHI.

In the current study, illusory ownership of a dummy arm was induced successfully by stroking the dummy body part together with the subject's own corresponding body part (0.94 ± 0.32 in R-TS session; 1.17 ± 0.34 in R-VS session) [13]. We first used standard GLM analyses and found that congruent visuotactile touch information following brush strokes selectively resulted in brain activation in the contralateral PMv, IPS, SII, and LOC. These findings were consistent with previous findings in which illusory body ownership was associated with temporoparietal multisensory brain regions [4, 5]. Subsequently, both of the different forms of needle stimulation (tactile and visual) on the body were determined to be effective methods for recovery from the disowned bodily states induced by the RHI. Based on the winning models from the model specification and estimation, the tactile input changed the brain network of illusory body ownership by directly influencing activity in the SII (Model A), whereas the visual input changed the brain network of illusory body ownership by influencing both the SII and the LOC (Model C; Figure 2(b)). Similarly, the two different stimuli differentially changed the activities in the corresponding nodes (driving inputs), leading to changes in the properties of the effective connectivity. The driving input of mechanical stimulation to the SII was significant when participants recovered from the RHI with tactile stimuli (Figure 3(a)). In contrast, the driving input of the RHI to both the SII and the LOC was significant when participants recovered from the RHI with visual stimuli (Figure 3(b)). Although the visual information was delivered from the rubber hand, the brain could still engage with somatosensory input (i.e., the SII) combined with visual input (i.e., the LOC). This can be interpreted as (1) an imagery effect of visual input on other objects or (2) the participants having illusory ownership of the rubber hand. It also supports our previous finding that needle rotations in the rubber hand produced substantial sensation ratings as well as activation in brain areas associated with enhanced bodily awareness of the hand [13]. Furthermore, group comparisons revealed that the driving input of the RHI to the SII decreased significantly in the R-TS session versus that in the R-VS session (red arrow to

SII, Figure 4), showing the stronger interference of RHI input to the SII with tactile stimulation. These findings suggest that two different bottom-up sensory information processes attributed to two different external sensory stimuli can result in brain network recovery of disowned bodily states induced by the RHI.

From our DCM results, the connection from the IPS to the PMv could be related to both the formation of illusory body ownership and its reinstantiation. Most accounts of body ownership have been linked to the integration of multimodal information in hierarchical cortical networks, predominantly the PMv and the IPS [17]. The IPS is known to counter prediction error by integrating multisensory touch information and recalibrating the coordinates of the somatosensory reference frame onto the visual reference frame [5]. Increased functional coupling between the IPS and the PMv is known to indicate potential information transfer about the peripersonal space from the parietal cortex to the frontal cortex [18]. The positive enhancement of effective connectivity from the IPS to the PMv by adding new tactile information to the subject's own hand in the R-TS session versus the R-VS session (Figure 4; blue arrow) might result from recalibration of the multimodal peripersonal space into the subject's own body [9]. Taken together, interactions of higher-level integrated brain regions, such as those between the IPS and the PMv, might be involved in the reinstantiation of body ownership from the condition of disowned bodily states. These findings highlight the functional role of connectivity between the parietal and frontal multimodal areas in the reinstantiation of body ownership.

Within the Bayesian theoretical and mathematical framework of the free-energy principle, the brain constantly interprets sensory information by minimizing the average of surprise (i.e., prediction errors) in all the sensory system [19]. Predictive coding suggests that probabilistic representations act as top-down influence on expectations explaining away bottom-up prediction errors between expected and actual sensory events [20]. In the aspect of the principles of free-energy and predictive coding, representations of one's self arise through the integration of sensory information, creating multimodal representations of the self under a hierarchical generative model of the world [21]. The perceptual illusion of body ownership is characterized as inferences of a common cause for visual, tactile, and proprioceptive sensations and modalities, and this can be explained by the Bayesian causal inference [22]. The brain network subserving body ownership is involved in detection of mismatches between the predictions of one's body model and the visuosomatosensory information provided [5]. The influence of ascending somatosensory prediction errors on top-down predictions reduced by the attenuation of somatosensory precision during the RHI [23]. Based on the DCM of electroencephalogram data, perception of the RHI was associated with stronger forward connectivity between visual region and the PMv [24]. In the current study, both needle rotations to rubber hand as visual stimuli and needle rotations to real hand as tactile stimuli could produce another mismatch between expected and actual sensory input, and the brain could reoptimize predictions through the dynamic updating of prior expectations.

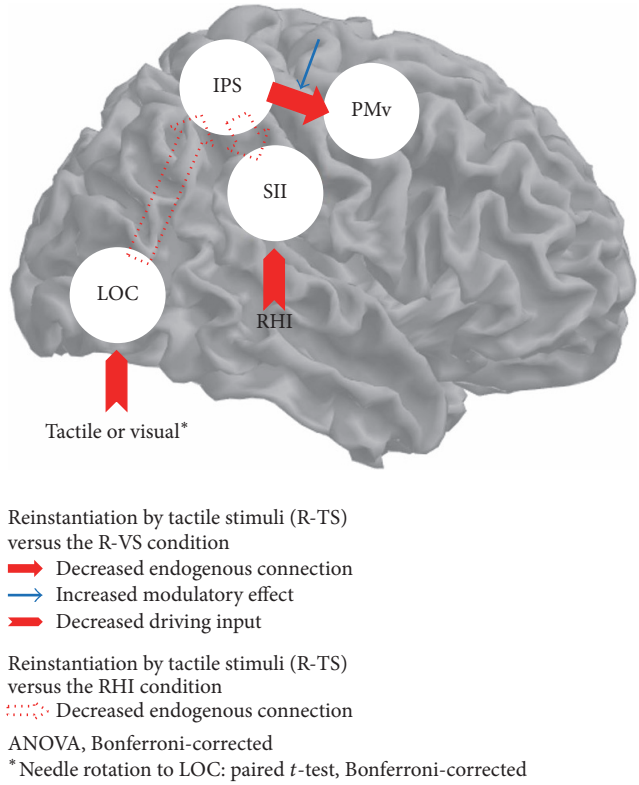

Figure 4: Significant changes in DCM parameter estimates during the R-TS condition versus the RHI (dotted-line arrow) and significant changes in DCM parameter estimates during the R-TS condition versus the R-VS condition (solid-line arrow). One-way analysis of variance (ANOVA) and Bonferroni *post hoc* analyses were used, and the Bonferroni correction was applied for multiple comparisons, except for the driving input of mechanical stimulation to the LOC (∗). As mechanical stimulation (tactile or visual stimuli) was modeled in two DCM analyses, paired t-tests with a Bonferroni correction were used.

The reduced endogenous connectivity between the IPS and the PMv in the current study might be associated with the restoration of increased bottom-up influence on the PMv through tactile information of needle stimulation. Our findings suggest that the changed functional architecture of multisensory integration during RHI could be differentially adjusted based on the different external information sources.

In conclusion, this investigation showed that connectivity patterns were differentially modulated for the reinstantiation of the body ownership by adding tactile and visual afferent inputs. Effective connectivity from the IPS to the PMv may be critical to the formation of and recovery from disowned bodily states. Our results thus provide new insight into the underlying neuronal mechanisms for the recovery of body ownership from disowned bodily states.

Competing Interests

The authors declare that there are no competing interests regarding the publication of this paper.

Acknowledgments

This research was supported by the Basic Science Research Program through the National Research Foundation of Korea (NRF) funded by the Ministry of Science, ICT & Future Planning (no. 2015R1D1A1A01058033) and the Korea Institute of Oriental Medicine (no. K15070).

References

[1] M. Botvinick and J. Cohen, "Rubber hands 'feel' touch that eyes see," *Nature*, vol. 391, no. 6669, p. 756, 1998.

[2] H. H. Ehrsson, C. Spence, and R. E. Passingham, "That's my hand! Activity in premotor cortex reflects feeling of ownership of a limb," *Science*, vol. 305, no. 5685, pp. 875–877, 2004.

[3] M. Tsakiris, "My body in the brain: a neurocognitive model of body-ownership," *Neuropsychologia*, vol. 48, no. 3, pp. 703–712, 2010.

[4] J. Limanowski, A. Lutti, and F. Blankenburg, "The extrastriate body area is involved in illusory limb ownership," *NeuroImage*, vol. 86, pp. 514–524, 2014.

[5] J. Limanowski and F. Blankenburg, "Network activity underlying the illusory self-attribution of a dummy arm," *Human Brain Mapping*, vol. 36, no. 6, pp. 2284–2304, 2015.

[6] G. L. Moseley, N. Olthof, A. Venema et al., "Psychologically induced cooling of a specific body part caused by the illusory ownership of an artificial counterpart," *Proceedings of the National Academy of Sciences of the United States of America*, vol. 105, no. 35, pp. 13169–13173, 2008.

[7] N. Barnsley, J. H. McAuley, R. Mohan, A. Dey, P. Thomas, and G. L. Moseley, "The rubber hand illusion increases histamine reactivity in the real arm," *Current Biology*, vol. 21, no. 23, pp. R945–R946, 2011.

[8] J. Limanowski and F. Blankenburg, "That's not quite me: limb ownership encoding in the brain," *Social Cognitive and Affective Neuroscience*, vol. 11, no. 7, pp. 1130–1140, 2016.

[9] G. Gentile, A. Guterstam, C. Brozzoli, and H. Henrik Ehrsson, "Disintegration of multisensory signals from the real hand reduces default limb self-attribution: an fMRI study," *The Journal of Neuroscience*, vol. 33, no. 33, pp. 13350–13366, 2013.

[10] Y. Chae, D.-S. Chang, S.-H. Lee et al., "Inserting needles into the body: a meta-analysis of brain activity associated with acupuncture needle stimulation," *The Journal of Pain*, vol. 14, no. 3, pp. 215–222, 2013.

[11] Y. Chae, I.-S. Lee, W.-M. Jung et al., "Decreased peripheral and central responses to acupuncture stimulation following modification of body ownership," *PLoS ONE*, vol. 9, no. 10, Article ID e109489, 2014.

[12] J. Lee, V. Napadow, J. Kim et al., "Phantom acupuncture: dissociating somatosensory and cognitive/affective components of acupuncture stimulation with a novel form of placebo acupuncture," *PLoS ONE*, vol. 9, no. 8, Article ID e104582, 2014.

[13] Y. Chae, I.-S. Lee, W.-M. Jung, K. Park, H.-J. Park, and C. Wallraven, "Psychophysical and neurophysiological responses to acupuncture stimulation to incorporated rubber hand," *Neuroscience Letters*, vol. 591, pp. 48–52, 2015.

[14] K. E. Stephan, W. D. Penny, R. J. Moran, H. E. M. den Ouden, J. Daunizeau, and K. J. Friston, "Ten simple rules for dynamic causal modeling," *NeuroImage*, vol. 49, no. 4, pp. 3099–3109, 2010.

[15] S. B. Eickhoff, K. E. Stephan, H. Mohlberg et al., "A new SPM toolbox for combining probabilistic cytoarchitectonic maps and functional imaging data," *NeuroImage*, vol. 25, no. 4, pp. 1325–1335, 2005.

[16] J. L. Lancaster, M. G. Woldorff, L. M. Parsons et al., "Automated Talairach Atlas labels for functional brain mapping," *Human Brain Mapping*, vol. 10, no. 3, pp. 120–131, 2000.

[17] V. I. Petkova, M. Björnsdotter, G. Gentile, T. Jonsson, T.-Q. Li, and H. H. Ehrsson, "From part- to whole-body ownership in the multisensory brain," *Current Biology*, vol. 21, no. 13, pp. 1118–1122, 2011.

[18] T. R. Makin, N. P. Holmes, and H. H. Ehrsson, "On the other hand: dummy hands and peripersonal space," *Behavioural Brain Research*, vol. 191, no. 1, pp. 1–10, 2008.

[19] K. Friston, "The free-energy principle: a unified brain theory?" *Nature Reviews Neuroscience*, vol. 11, no. 2, pp. 127–138, 2010.

[20] K. Friston and S. Kiebel, "Predictive coding under the free-energy principle," *Philosophical Transactions of the Royal Society B: Biological Sciences*, vol. 364, no. 1521, pp. 1211–1221, 2009.

[21] M. A. J. Apps and M. Tsakiris, "The free-energy self: a predictive coding account of self-recognition," *Neuroscience and Biobehavioral Reviews*, vol. 41, pp. 85–97, 2014.

[22] M. Samad, A. J. Chung, and L. Shams, "Perception of body ownership is driven by Bayesian sensory inference," *PLoS ONE*, vol. 10, no. 2, Article ID e0117178, 2015.

[23] D. Zeller, V. Litvak, K. J. Friston, and J. Classen, "Sensory processing and the rubber hand illusion—an evoked potentials study," *Journal of Cognitive Neuroscience*, vol. 27, no. 3, pp. 573–582, 2015.

[24] D. Zeller, K. J. Friston, and J. Classen, "Dynamic causal modeling of touch-evoked potentials in the rubber hand illusion," *NeuroImage*, vol. 138, pp. 266–273, 2016.

Hindawi Publishing Corporation
Neural Plasticity
Volume 2016, Article ID 5320641, 16 pages
http://dx.doi.org/10.1155/2016/5320641

Research Article

Inhibition of the cAMP/PKA/CREB Pathway Contributes to the Analgesic Effects of Electroacupuncture in the Anterior Cingulate Cortex in a Rat Pain Memory Model

Xiao-Mei Shao,[1] Jing Sun,[1] Yong-Liang Jiang,[1] Bo-Yi Liu,[1] Zui Shen,[1] Fang Fang,[2] Jun-Ying Du,[1] Yuan-Yuan Wu,[1] Jia-Ling Wang,[1] and Jian-Qiao Fang[1]

[1]*Department of Neurobiology and Acupuncture Research, The Third Clinical Medical College, Zhejiang Chinese Medical University, Hangzhou, China*
[2]*Department of Acupuncture and Moxibustion, Wenzhou Hospital Affiliated to Zhejiang University of Traditional Chinese Medicine, Wenzhou, China*

Correspondence should be addressed to Jian-Qiao Fang; fangjianqiao7532@163.com

Received 25 July 2016; Revised 30 September 2016; Accepted 24 October 2016

Academic Editor: Cun-Zhi Liu

Copyright © 2016 Xiao-Mei Shao et al. This is an open access article distributed under the Creative Commons Attribution License, which permits unrestricted use, distribution, and reproduction in any medium, provided the original work is properly cited.

Pain memory is considered as endopathic factor underlying stubborn chronic pain. Our previous study demonstrated that electroacupuncture (EA) can alleviate retrieval of pain memory. This study was designed to observe the different effects between EA and indomethacin (a kind of nonsteroid anti-inflammatory drugs, NSAIDs) in a rat pain memory model. To explore the critical role of protein kinase A (PKA) in pain memory, a PKA inhibitor was microinjected into anterior cingulate cortex (ACC) in model rats. We further investigated the roles of the cyclic adenosine monophosphate (cAMP), PKA, cAMP response element-binding protein (CREB), and cAMP/PKA/CREB pathway in pain memory to explore the potential molecular mechanism. The results showed that EA alleviates the retrieval of pain memory while indomethacin failed. Intra-ACC microinjection of a PKA inhibitor blocked the occurrence of pain memory. EA reduced the activation of cAMP, PKA, and CREB and the coexpression levels of cAMP/PKA and PKA/CREB in the ACC of pain memory model rats, but indomethacin failed. The present findings identified a critical role of PKA in ACC in retrieval of pain memory. We propose that the proper mechanism of EA on pain memory is possibly due to the partial inhibition of cAMP/PKA/CREB signaling pathway by EA.

1. Introduction

Pain memory is one of the pivotal pathogeneses of chronic pain, which is involved in sensory-discriminative, emotional affective, and cognitive evaluative pain [1, 2]. It is a nociceptive pain characterized by hyperalgesia and allodynia, resulting in formation of memories and negative emotions of pain in the brain [3–6]. This process consists of acquisition, consolidation, and retrieval of pain [7, 8]. Nociceptive sensory neurons acquire and transfer signals up to the related nuclei in the brain, including the anterior cingulate cortex (ACC), the prefrontal cortex, the hippocampus, the amygdala, and the insular cortex [1, 9–11], to form long-term memory with repeated and persistent stimulation from the emotional environment of short-term memory. Researchers have suggested that the activation of cyclic adenosine monophosphate (cAMP), protein kinase A (PKA), cAMP response element-binding protein (CREB), and their associated signaling pathways can regulate long-term synaptic plasticity to modulate both memory storage and retrieval [12, 13]. However, a clear understanding of the pain memory pathway in the ACC is still lacking.

The cAMP/PKA/CREB signaling pathway has been demonstrated to be crucial in memory formation and pain modulation [13–15]. Neuronal synaptic plasticity at the molecular, neuroanatomical and functional levels has been verified throughout the neuroaxis in response to persistent pain [1]. The activation of the cAMP/PKA/CREB signaling pathway can improve the recognition function [16] and exert an antidepressive action [17] through the enhancement of structural synaptic plasticity in the hippocampus [15, 18]. The ACC is an area that encodes pain averseness, thus

contributing to pain modulation [19, 20]. As we discovered in a previous study, the phosphorylation of CREB (p-CREB) results in a profound increase in pain memory in the ACC [21]. Thus, we assume that the pathway in pain memory induces a gradual activation of cAMP, PKA, and CREB after nociceptive stimulation in the ACC and that longer lasting forms of latent long-term central sensitization promote long-term memory formation through the cAMP/PKA/CREB signaling pathway.

Due to the growing importance of pain memory in chronic pain study, it is necessary to identify measures to alleviate pain memory. Indomethacin is often used to treat inflammatory pain. However, its usage is restricted due to its side-effects and poor efficacy. Till now, there are few studies about indomethacin on pain memory. Electroacupuncture (EA), a type of acupuncture with electronic stimulation, is widely applied as analgesic for chronic pain in clinical settings. Our previous work has indicated that EA treatment can alleviate the retrieval of pain memory [21]. Although some of the pain modulation mechanisms of the analgesic effects of EA and indomethacin have been demonstrated, their potential mechanisms underlying pain memory remain unclear.

In this study, we established an animal pain memory model using two injections of carrageenan [21, 22]. Animals were treated with EA and indomethacin to study the different effects and explore the mechanism of EA on pain memory. Our data confirmed the advantageous effect of EA and further proposed that the effect of EA is partially through the inhibition of the cAMP/PKA/CREB signaling pathway.

2. Materials and Methods

2.1. Subject. Male adult Sprague-Dawley rats (Sino-British SIPPR/BK Lab. Animal Ltd., Shanghai, China) weighing 180–200 g (6 weeks) were kept at a controlled room temperature (22°C) with a 12-h light-dark cycle and free access to rodent chow and water. All animal experiments were performed according to the National Institutes of Health Guide for the Care and Use of Laboratory Animals [21, 23].

2.2. Pain Memory Model. As described previously [21], the pain memory model induced by two injections of carrageenan was selected to complete the study. The first carrageenan injection was placed into the left hind paw plantar surface via the subcutaneous injection of 0.1 mL of 2% carrageenan (Sigma Chemical Co, St. Louis, MO, USA) to induce acute inflammatory pain. After a 14-day recovery period, the pain value of the left hind paw was recovered. Then the second carrageenan injection was placed into the right hind paw to induce another pain. At this time, the left hind paw, which did not receive the second injection of carrageenan, appeared to exhibit nociceptive hyperalgesia. In the present study, the hyperalgesia of the left hind paw was regarded as the retrieval of pain memory [21, 22].

2.3. Experimental Design. Three experiments were designed and administered to study the effects of EA and indomethacin on pain memory and explore the potential mechanisms with the cAMP/PKA/CREB signaling pathway.

In Experiment 1, all rats were divided randomly into 5 groups (n = 10/group): the control, model, indo (indomethacin), EA, and the sham EA groups. Saline (0.9%) or carrageenan (2%) was injected into the hind paws twice at a 14 d interval. The rats in the indo, EA, and sham EA groups were treated with indomethacin, EA, and sham EA, respectively (Figure 1). The aim of this experiment was to observe the different effects of the therapies on pain memory by detecting the pain behavioral response.

In Experiment 2 (Figure 2), the sections of right ACC in rats were implanted with stainless steel guided cannulae and divided into 2 groups (n = 5/group): the model + vehicle group (implanted rats treated with the vehicle) and the model + H89 (implanted rats treated with PKA inhibitor H89). This experiment was performed to identify the role of PKA in the retrieval of pain memory and to determine whether the EA had a similar effect with H89 in the retrieval of pain memory partially.

In Experiment 3, to explore the potential mechanisms of the different effects of EA, indomethacin, and sham EA on pain memory, the right ACC tissues of the rats from Experiment 1 were prepared. The grouping was the same as Experiment 1. Four of 10 rats in each group were further used for double-immunofluorescence labeling and six others were used for western blot assays.

2.4. Electroacupuncture. Without anesthesia, EA treatment was applied in rats of the EA group. In a previous study [21], we found that EA treatment at bilateral acupoints "Zusanli" (ST36) and the reference electrode (1 cm inferior of "Zusanli") were effective for impairing the retrieval of a pain memory. Therefore, we used the same methods including the acupoints and EA parameters in this study. The acupoints were needled with stainless acupuncture needles (0.25 mm in diameter × 13 mm in length) and electrically stimulated with a HANS Acupuncture Point Nerve Stimulator (LH-202H; Huawei Co., Ltd., Beijing, China). The parameters of EA were set as follows: 2/100 Hz of frequency with automatically shifting between 2 Hz and 100 Hz stimulation for 3 s each; a square wave current output (pulse width: 0.2 ms); an intensity range of about 1-2 mA adjusted to animals' local muscle contractions. The treatment was administered at 5 h, 1–5 d after the first carrageenan injection. To confirm the authenticity of the effects of EA, thin stainless acupuncture needles (0.18 mm in diameter × 13 mm in length) pierced the subcutaneous acupoints of the sham EA animals without electrical stimulation. The animals wore black hoods over their heads for a calming effect during the administration of EA. No signs of stress were observed. To maintain consistency, the rats in the model and control groups also wore black hoods at the same time.

2.5. Behavioral Pain Test. Mechanical allodynia, assessed by the paw withdrawal thresholds (PWTs), was used to evaluate the pain response. An UGO-Basile Dynamic Plantar Aesthesiometer (UGO 37450, Milan, Italy), with an improved calibrated von Frey filaments method [21, 24, 25], was operated by a trained investigator who was blind to the experimental allocation. One measurement was taken at 5 min intervals, for a total 5 measurements, and the last 4

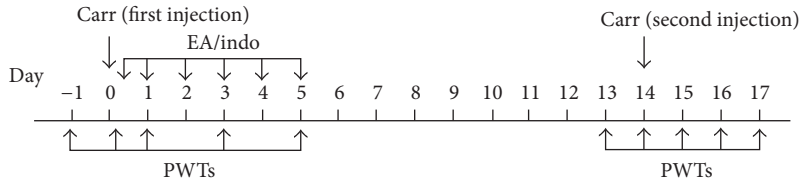

Figure 1: Flow chart of the procession of a pain memory model and intervening measures. The pain memory model was induced by two injections of carrageenan. The first inflammatory reaction was induced with carrageenan injection in the left hind paw at day 0. The paw withdrawal thresholds (PWTs) at days −1, 0, 1, 3, and 5 were recorded and that the one at day −1 was regarded as the baseline value. The EA/indo interventions were administered at 5 h, 1–5 d after the first carrageenan injection. The second inflammatory reaction was induced by injection in the right hind paw at day 14. The PWTs at day 13 through 17 were recorded and the one at day 13 was regarded as the new baseline value. The PWTs of the left (uninjected in the second injection of carrageenan) hind paw on day 15 through 17 manifested the memory of pain.

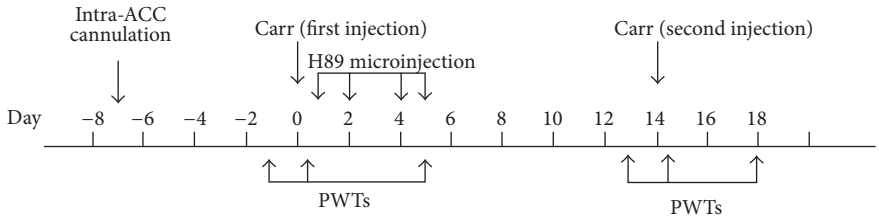

Figure 2: Flow chart of the PKA inhibitor intervention and PWTs detection in different time points. Before the establishment of pain memory model, intra-ACC cannulation was implanted. H89 microinjection was administered at 5 h and 1–5 d continually. The PWTs at days −1, 0, and 5 in the first injection time and days 13, 14, and 18 in the second injection time were recorded to evaluate pain.

were averaged as the PWTs value. All behavioral pain tests were performed between 9:00 and 15:00. All rats underwent habituation to the environment and testing procedure 2 days before the formal experiment.

2.6. Drug Administration. H89 (Sigma), a PKA inhibitor, was dissolved in dimethyl sulfoxide (DMSO) and water (10 μM, the ratio of DMSO and water is 1 : 999). Rats in the model + H89 group in Experiment 2 received H89 at a concentration of 10 μM via intra-ACC cannulation and brain microinjection. The specific times were the same as the times of EA administration in Experiment 1. Indomethacin (Yun Peng Co., Ltd., Shanxi, China) was dissolved in 0.9% saline and ingested by intragastric administration (3 mg/kg) for 6 times. The specific ingestion times were the same as the EA administration times.

2.7. Intra-ACC Cannulation and Microinjection. For PKA inhibitor infusion, intra-ACC cannulation and microinjection were performed as previously reported [20, 26]. Briefly, rats in Experiment 2 were anesthetized with 7% chloral hydrate (500 mg/kg, intraperitoneally) and fixed in a stereotaxic apparatus (RWD, Life Science Co., Ltd, Shenzhen, China). After the exposure of the skull around the bregma, the stainless steel guide cannula (3 mm long) was implanted according to the following coordinates in the right ACC: 3.2 mm anterior to the bregma, 0.6 mm on the right side of the midline, and 1.5 mm below the top of the skull [11, 21]. Then, the cannula was fixed to the skull with 3 screws and dental acrylic. A stylet 0.5 mm longer than the cannula was inserted to keep it in place prior to the microinjection. All rats were allowed at least 7 days to recover.

The intra-ACC microinjections were administered through the implanted guide cannulae using injection needles (3.5 mm long) that were connected by a polyethylene tube fitted to a 100 μL Hamilton microsyringe. The volume of the drug solution to be injected into the ACC of the rats in the model + H89 group was 1 μL and the duration of the drug infusion was 1 min. As a control, the vehicle containing DMSO was injected into the ACC of the rats in the model + vehicle group.

2.8. Tissue Preparation. At day 18, after the behavioral pain test, the rats were anesthetized with 10% chloral hydrate (350 mg/kg, intraperitoneally) and perfused via cardiac puncture with 0.9% saline. The right ACC tissues of the rats were removed immediately for the western blot assays. Subsequently, after perfusion with 4% paraformaldehyde, the whole brains of the other rats were harvested and post fixed by immersion in the same fixative for 24 h and dehydrated in a 15%–30% sucrose gradient for 24 h for immunofluorescence.

2.9. Double-Immunofluorescence Labeling. Immunofluorescence was used to evaluate the levels of cAMP, phosphorylation of PKA (p-PKA), and p-CREB expression in the right ACC. Furthermore, we used double-immunofluorescence labeling to demonstrate correlations among the above proteins as previous description [21]. Coronal brain slices 30 μm in thickness taken from the bregma at 3.2 mm containing the ACC were washed with 0.01 M PB saline (PBS, pH 7.4) and blocked with 5% goat serum. The tissue sections were

then incubated overnight with a rabbit anti-PKA (phospho T197) antibody (p-PKA, 1 : 200; Abcam, Boston, MA, USA) and either a mouse anti-cAMP antibody (1 : 1000; Abcam) or a mouse anti-phospho-CREB (Ser133) polyclonal antibody (p-CREB, 1 : 200; Millipore, Billerica, MA, USA). After rinsing in PBS, the sections were incubated in a goat-anti-mouse Alexa Fluor 488-conjugated secondary antibody (1 : 200; Jackson Immuno Labs, West Grove, PA, USA) and a goat anti-rabbit Alexa Fluor 594-conjugated secondary antibody (1 : 200; Abcam). Fluorescence signals were detected by a Nikon A1R laser scanning confocal microscope. The positive cells were counted and analyzed by NIS elements AR software.

2.10. Western Blot. Western blot was used to detect the protein expression levels of cAMP, p-PKA, and p-CREB in the right ACC. The tissues were weighed and homogenized in RIPA buffer (Beyotime P0013B, Haimen, Jiangsu, China) plus protease inhibitors. After centrifugation, a BCA protein assay kit (Beyotime P0012S, Haimen, Jiangsu, China) was used to determine the protein concentrations. Protein samples (20 μg) from each group were separated by 10% SDS-PAGE and transferred onto polyvinylidene fluoride membranes (Bio-Rad, Hercules, CA, USA). The membranes were blocked in 5% nonfat milk followed by incubation with primary antibodies: rabbit anti-p-PKA (1 : 5000; Abcam), rabbit anti-p-CREB (1 : 1000; Millipore), and rabbit anti-β-actin (1 : 5000; Abcam). Then, the membranes were incubated with secondary anti-rabbit HRP-conjugated IgG antibody (1 : 20000, Abcam). The immunoreactive bands were visualized by using an Immun-Star™ HRP Chemiluminescence Kit (Bio-Rad). The relative intensity of each band for β-actin was measured by an ImageQuant LAS 4000 system (GE Healthcare, Hino, Japan) and was analyzed by ImageQuant TL software (version 7.0, GE Healthcare).

2.11. Statistical Analysis. The data are expressed as the means ±SEM. Comparisons among different groups were performed by one-way, repeated-measures analysis of variance (ANOVA). For post hoc analysis, the least significant difference (LSD) and Dunnett's test were used for equal or unequal variances, respectively, as examined by the homogeneity of the variance test. Comparisons between two groups were evaluated using independent-sample t tests or paired-sample t tests. All statistical analyses were considered significant at the level of $p < 0.05$.

3. Results

3.1. Electroacupuncture Alleviated the Retrieval of Pain Memory in Model Rats. The pain memory model that we used in this experiment was described by Kissin et al. [22] and had been used successfully in previous experiments [21]. The PWTs were detected after two carrageenan injections separated by a 14 d interval in Experiment 1. Firstly, we measured the PWTs at the first injection time point to observe the effects of EA on acute inflammatory pain. As expected, the baseline values of all of the groups were similar. At 4 h after the carrageenan injection, the PWTs of the left hind paw in all groups except the control were significantly decreased compared with the control group ($p < 0.01$). After treatments, at 5 h and 1–5 d after the first carrageenan injection continuously, the PWTs of the left hind paw in the EA and indo groups increased significantly at 3 d and 5 d compared with the model group ($p < 0.01$). There were no significant differences between the two groups. The PWTs of the EA group also significantly increased compared with the sham EA group at 5-d time point ($p < 0.01$). Compared with the baseline values, the PWTs of each time point in the model, indo, EA, and sham EA groups significantly decreased ($p < 0.01$), except in the EA and indo group at the 5-d time point (Figure 3(a)). The noninjected (right) hind paw showed normal and stable levels of PWTs values with treatment at the same time points (Figure 3(b)).

Next, we investigated the analgesic effects of the preadministration of EA on pain memory by recording the PWTs of the left hind paws at the second injection time point. Note that the PWTs of all groups returned to their baseline values after a 14 d interval. Figure 3(c) presents the different changes in the PWTs of the noninjected (left) hind paws from the 5 groups at 4 h, 1 d, 2 d, and 3 d after the second carrageenan injection into the right hind paw. The values of the control group remained normal, whereas the model group exhibited a profound decrease from the 1 d to the 3 d time point compared with the control group ($p < 0.01$). This was regarded as the retrieval of pain memory. However, the PWTs in the EA group did not decrease and maintained similar levels with those of the control group. The values from the indo and sham EA groups also decreased. When compared with the model, indo, and sham EA groups, the PWTs of the EA group significantly increased at 3 d time point ($p < 0.01$). Compared with the baseline values of the model group, decreased PWTs were observed at 1 d to 3 d ($p < 0.01$). Similar decreased values appeared at 2 d and 3 d in the indo and sham EA groups compared with their baseline values ($p < 0.01$). However, there was no significant difference among values at different time points in the EA group. Because there was no intervention at the second injection time point, the injected (right) hind paws of the model, indo, EA, and sham EA groups showed significantly decreased PWTs values at 4 h after injection until 3 d compared with the control group and their separated baseline values ($p < 0.01$). The preadministration of EA had no effect on PWTs compared with the model group (Figure 3(d)).

3.2. Intra-ACC Microinjection of a PKA Inhibitor Blocked the Occurrence of Pain Memory. To elucidate the key role of PKA in the retrieval of pain memory, as well as to explore the potential mechanism of EA treatment, a PKA inhibitor (H89) was delivered into the ACC by intra-ACC cannulation and microinjection. The pain memory model with a vehicle group was set up as the control group to compare with the H89 group. The procedures were similar to those in Experiment 1: the pain memory model was established in the two groups of rats and was followed by a PKA inhibitor intervention at the same time points with EA treatment. As shown in Figure 4(c), the vehicle-injected rats presented with pain memory via

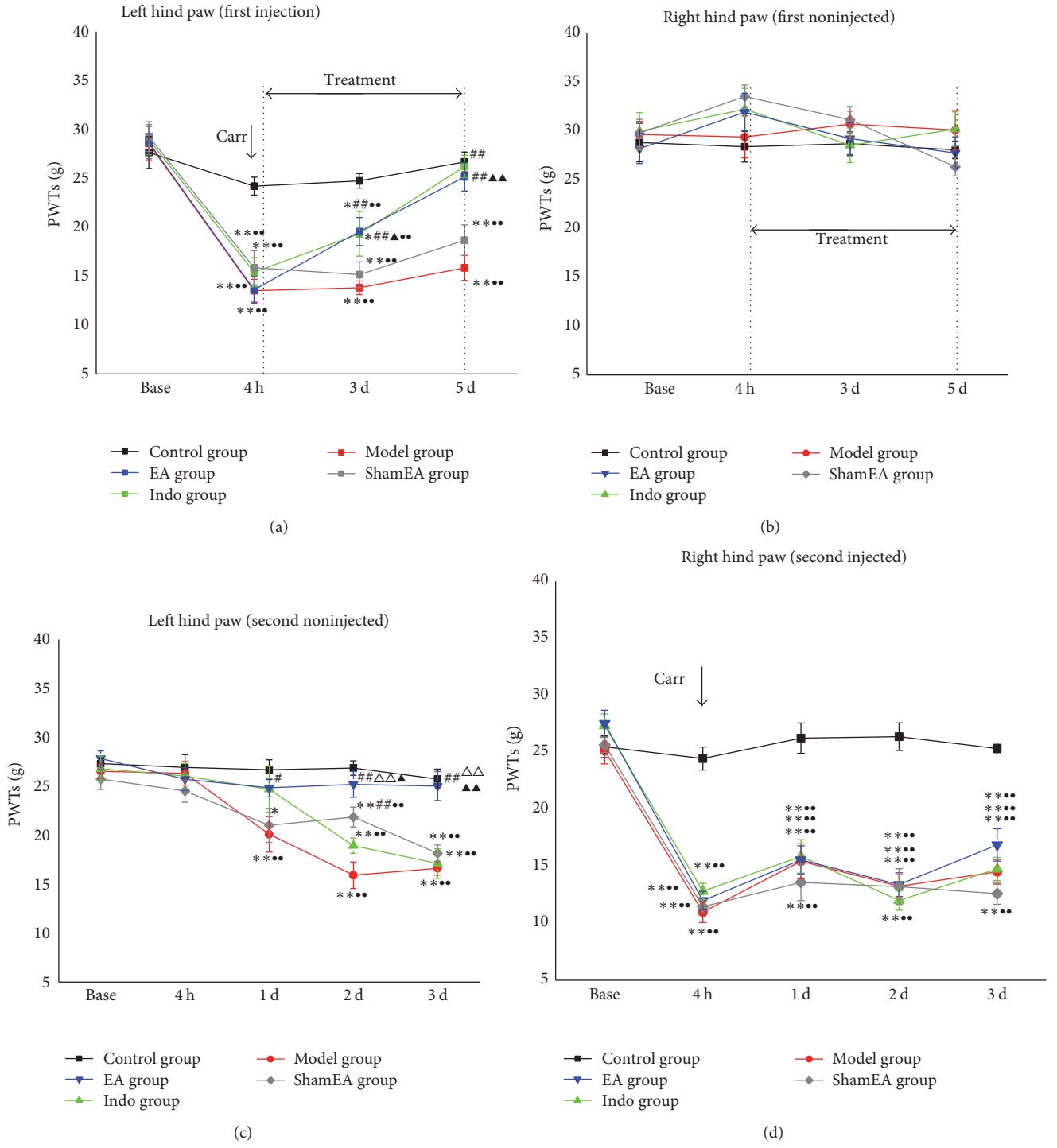

Figure 3: EA alleviated the retrieval of pain memory. The rats in the pain memory model were divided into the control, model, indo, EA, and sham EA groups, and the mechanical allodynia in each group was examined ($n = 10$). (a) On the left hind paw (first injected), EA or indomethacin treatment increased the PWTs significantly compared with the model group. (b) There was no significant difference in all groups at the same period. (c) On the left hind paw (second noninjected), the PWTs in the model group decreased significantly compared with the control group and its baseline. EA treatment administered at the first injection time point inhibited this progress. (d) The second injection of carrageenan into the right hind paw significantly decreased the PWTs of the carrageenan-injected groups compared with the control group and their baselines. Error bars indicate the SEM. $^{*}p < 0.05$ and $^{**}p < 0.01$, versus the control group; $^{\#}p < 0.05$ and $^{\#\#}p < 0.01$, versus the model group; $^{\triangle\triangle}p < 0.01$, versus the indo group; $^{\blacktriangle}p < 0.05$ and $^{\blacktriangle\blacktriangle}p < 0.01$, versus the sham EA group; $^{\bullet\bullet}p < 0.01$, versus baseline.

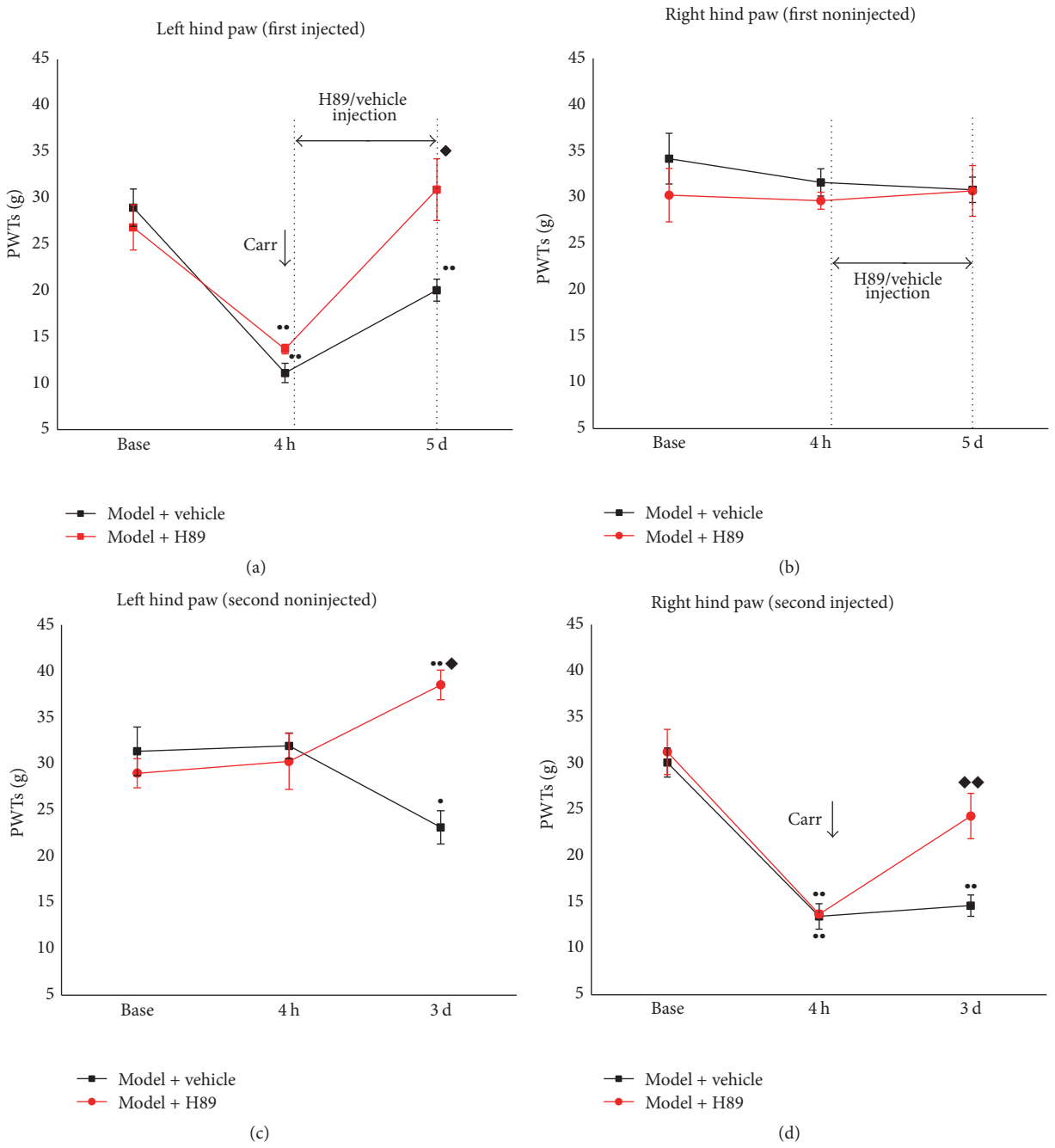

Figure 4: The effects of the PKA inhibitor of pain memory model. The rats were divided into the model + vehicle and the model + H89 groups and the mechanical allodynia was examined ($n = 7$). (a) In the left hind paw (first injected), the PKA inhibitor intervention significantly increased the PWTs from acute inflammatory pain. (b) In the right hind paw (first noninjected), the PWTs of the two groups were not significantly different. (c) In the left hind paw (second noninjected), PKA inhibitor intervention significantly increased the PWTs from pain memory. (b) In the right hind paw (second injected), PKA inhibitor intervention significantly increased the PWTs compared with the model + vehicle group. Error bars indicated SEM. $^{\blacklozenge}p < 0.05$ and $^{\blacklozenge\blacklozenge}p < 0.01$, versus the model + vehicle group; $^{\bullet}p < 0.05$ and $^{\bullet\bullet}p < 0.01$, versus baseline.

decreased PWTs in the left hind paw 3 d after the second carrageenan injection was administered into the right hind paw compared with baseline ($p < 0.05$). H89 inhibited the retrieval of pain memory significantly, with increased PWTs compared with the model + vehicle group and its baseline values ($p < 0.01$). In Figure 4(d), the PWTs of the right hind paw (the second injection) of the H89-treated rats showed an increase at 3 d after the carrageenan injection ($p < 0.01$).

3.3. Electroacupuncture Reduced the Activation of cAMP, PKA, CREB, in the ACC in Model Rats. It has been shown that the cAMP/PKA/CREB signaling pathway is crucial to

pain [14, 27] and memory formation in the ACC [26], which may occur via brain neural synaptic plasticity. To explore the different effects of EA and indomethacin on the cAMP/PKA/CREB signaling pathway in pain memory, we first examined the changes in cAMP, p-PKA, and p-CREB protein expression separately in the ACC via immunofluorescence and western blot assays. The numbers of cAMP-positive cells in the model group increased significantly compared with those of the control group ($p < 0.05$). After treatment with EA, indomethacin, or sham EA, the EA treatment profoundly decreased the number of positive cells compared with those in the model ($p < 0.05$), indo ($p < 0.01$), and sham EA ($p < 0.05$) groups. However, indomethacin and the sham EA treatment did not show this effect (Figures 5(a)-5(b)).

Because resting PKA and CREB contribute minimally to the synaptic plasticity of the learning and memory processes, the phosphorylation levels of PKA and CREB were examined. After the successful establishment of a pain memory, the amount of phosphorylated PKA (p-PKA) in the model group clearly increased compared with control group ($p < 0.01$). After EA but not indomethacin or sham EA treatment, the number of positive cells in EA group decreased compared with the model ($p < 0.05$) and indo ($p < 0.05$) groups (Figures 6(a)-6(b)). The western blot results also indicated similar trends in p-PKA expression (Figure 6(c)). Quantitative analysis indicated that the relative intensity of p-PKA/β-actin was significantly increased in the model group compared with the control group ($p < 0.05$, Figure 6(d)). Compared with model group, EA group showed reduced relative intensity of p-PKA/β-actin ($p < 0.05$, Figure 6(d)).

CREB is a key nuclear transcription factor for memory formation [13, 15]. Phosphorylation of CREB in the model group was increased compared with the control group ($p < 0.01$, Figures 7(a)-7(b)). The positive numbers of phosphorylated CREB (p-CREB) in EA group were decreased significantly compared with the model ($p < 0.01$), indo ($p < 0.01$), and sham EA ($p < 0.05$) groups. Indomethacin and sham EA treatment also resulted in decreased values of p-CREB ($p < 0.05$, Figures 7(a)-7(b)). The western blot quantitative analysis indicated that the relative intensity of p-CREB/β-actin was increased in the model group compared with the control group ($p < 0.05$) and that EA treatment significantly reduced the intensity of p-CREB/β-actin compared with the model ($p < 0.05$) and indo ($p < 0.05$) groups (Figures 7(c)-7(d)).

3.4. Colocalization of cAMP and p-PKA Was Reduced by Electroacupuncture in the ACC of Pain Memory Model Rats. Next, we detected the colocalization of cAMP and p-PKA in the ACC to elucidate whether cAMP was coexpressed with p-PKA in the pain memory model and the different effect of EA treatment on the coexpression. Double-immunofluorescence labeling for cAMP and p-PKA showed that cAMP colocalized with p-PKA in the ACC of pain memory model rats (Figure 8(a)). Because cAMP exists in the cytoplasm but p-PKA exists in the cytoplasm and nucleus, their colocalization occurs in the same plane but not at the same site (Figure 8(b)). The amount of colocalized cAMP and p-PKA increased in the model, indo, and sham EA groups compared with the control group ($p < 0.01$). A decreased amount of cAMP coexpressed with p-PKA was observed in the EA group compared with the model, indo, and sham EA groups ($p < 0.05$) (Figure 8(c)).

3.5. Colocalization of p-PKA and p-CREB Was Reduced by Electroacupuncture in the ACC of Pain Memory Model Rats. As described above, the colocalization of p-PKA and p-CREB in the ACC was detected to observe the effect of EA on the coexpression of p-PKA and p-CREB. Double labeling showed that p-PKA and p-CREB were coexpressed in the nuclei of the ACC (Figure 9(a)). CREB is activated in the nucleus of the ACC via cAMP/PKA signaling in pain memory. Figure 9(b) presents the overlap of p-PKA and p-CREB colocalization on the same plane and same site. The amount of colocalization of p-PKA and p-CREB of the model ($p < 0.05$), indo ($p < 0.01$) and sham EA ($p < 0.01$) groups had a profound increase compared with the control group. EA treatment decreased the colocalization of p-PKA and p-CREB compared with the model ($p < 0.05$), indo ($p < 0.01$), and sham EA ($p < 0.01$) groups.

4. Discussion

The key findings of this study are that EA can alleviate the pain memory induced by two carrageenan injections, whereas indomethacin failed to do so. Furthermore, pain memory can be blocked by PKA blockage, which may indicate the relationship between pain memory and the cAMP/PKA/CREB pathway. EA can inhibit the cAMP/PKA/CREB signaling pathway partially, but NSAIDs cannot. To our knowledge, this is by far the first study that investigated the different effects and mechanisms of EA and NSAIDS on pain memory.

Pain perception is determined by 3 dimensions consisting sensory-discriminative, affective-motivational, and evaluative-cognitive modulations. Nociception activate the above 3 dimensions of pain control system for the formation of pain memory through integrated process in brain nucleus. The sensory-discriminative and affective-motivational information of nociception could induce a profound process, like the recognition, memory, attention, expectation, and so on. It should also be noted that pain sensory could be affected by pain memory vice versa [28]. Through the top-down manipulation, the information from evaluative-cognitive modulation could exert pain perception on the others [3, 29]. Actually, pain memory is a complex perception experience.

In clinic, physicians have found that pain memory is accompanied by complex regional pain syndrome [6], phantom pain [30], postoperative pain [31], and long histories of chronic pain [32]. To explore the effective therapy and the potential mechanisms of pain memory, affective-motivational and evaluative-cognitive pain have increasingly gained researchers' attentions [2, 3, 26, 28, 33]. EA, an effective pain treatment that is considered to be a mind-body therapy, has a wide range of data supporting its analgesic role and capacity to regulate mood disorder and memory [2, 23, 34, 35]. In our previous studies, we have found that the retrieval of pain memory can be alleviated by pretreatment with EA, which is partially attributed to the downregulated expression

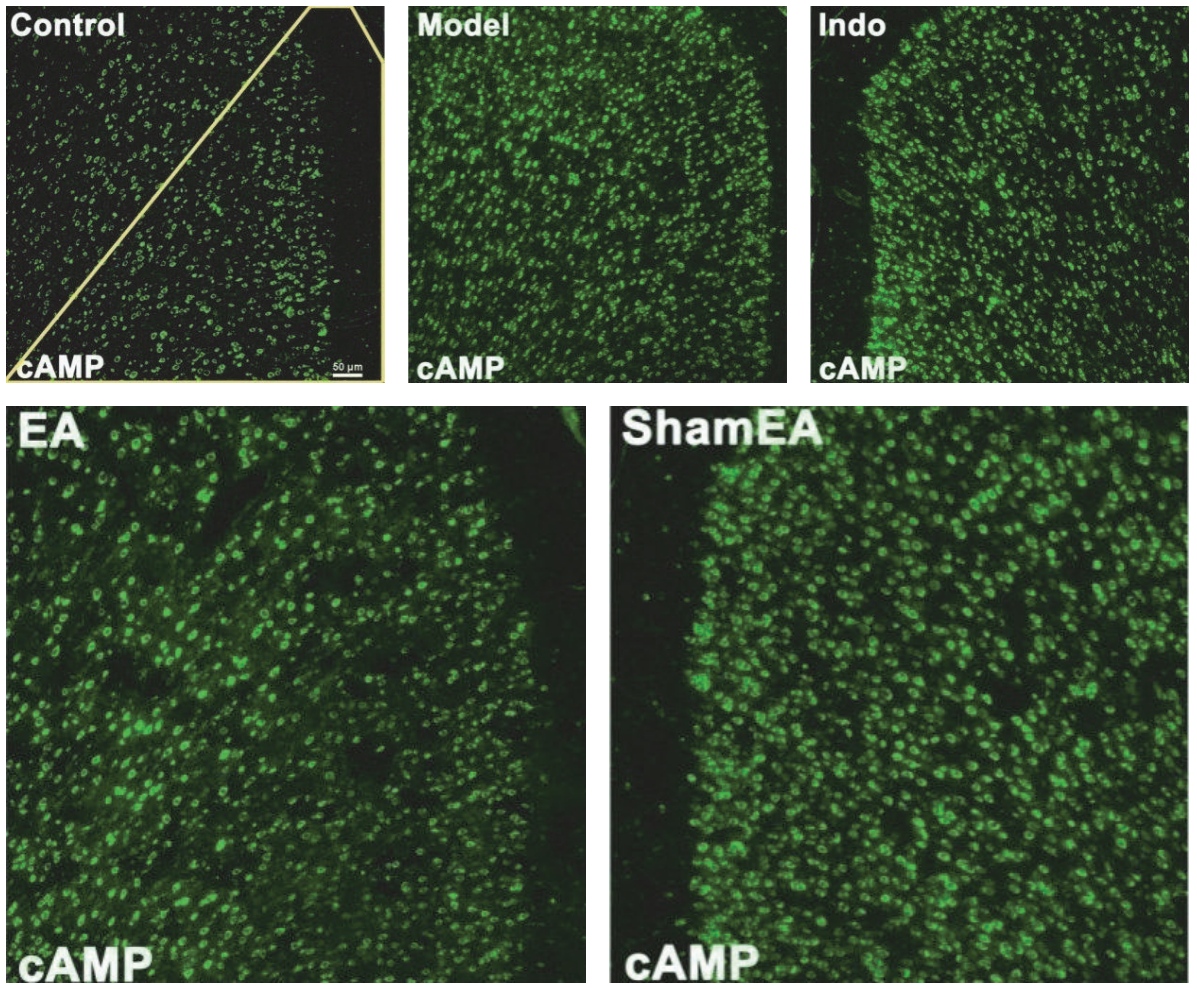

(a)

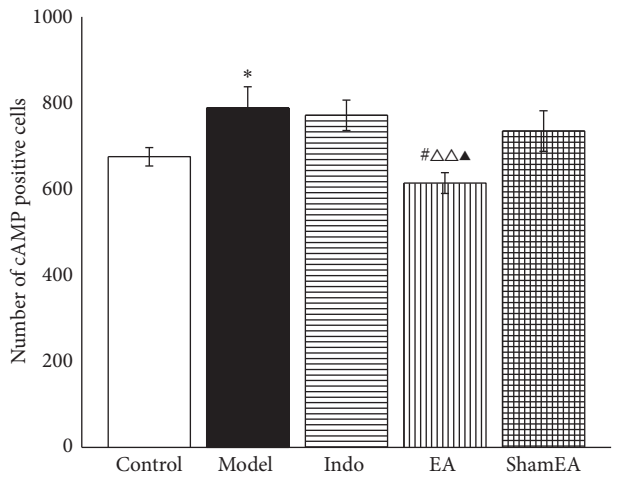

(b)

Figure 5: EA inhibited the activation of cAMP in the ACC of pain memory model rats. The right ACC tissues from the control, model, indo, EA, and sham EA groups were prepared and labeled with immunofluorescence ($n = 3$, five slides for each rat). (a) Views of cAMP-positive cells (scale bar, 50 μm). The yellow line indicates the field in which the positive cells were counted. (b) Quantification of cAMP-positive cells showed that EA treatment at the first injection time point significantly reduced the activation of cAMP. Error bars indicated SEM. $^{*}p < 0.05$, versus the control group; $^{\#}p < 0.05$, versus the model group; $^{\triangle\triangle}p < 0.01$, versus the indo group; $^{\blacktriangle}p < 0.05$, versus the sham EA group.

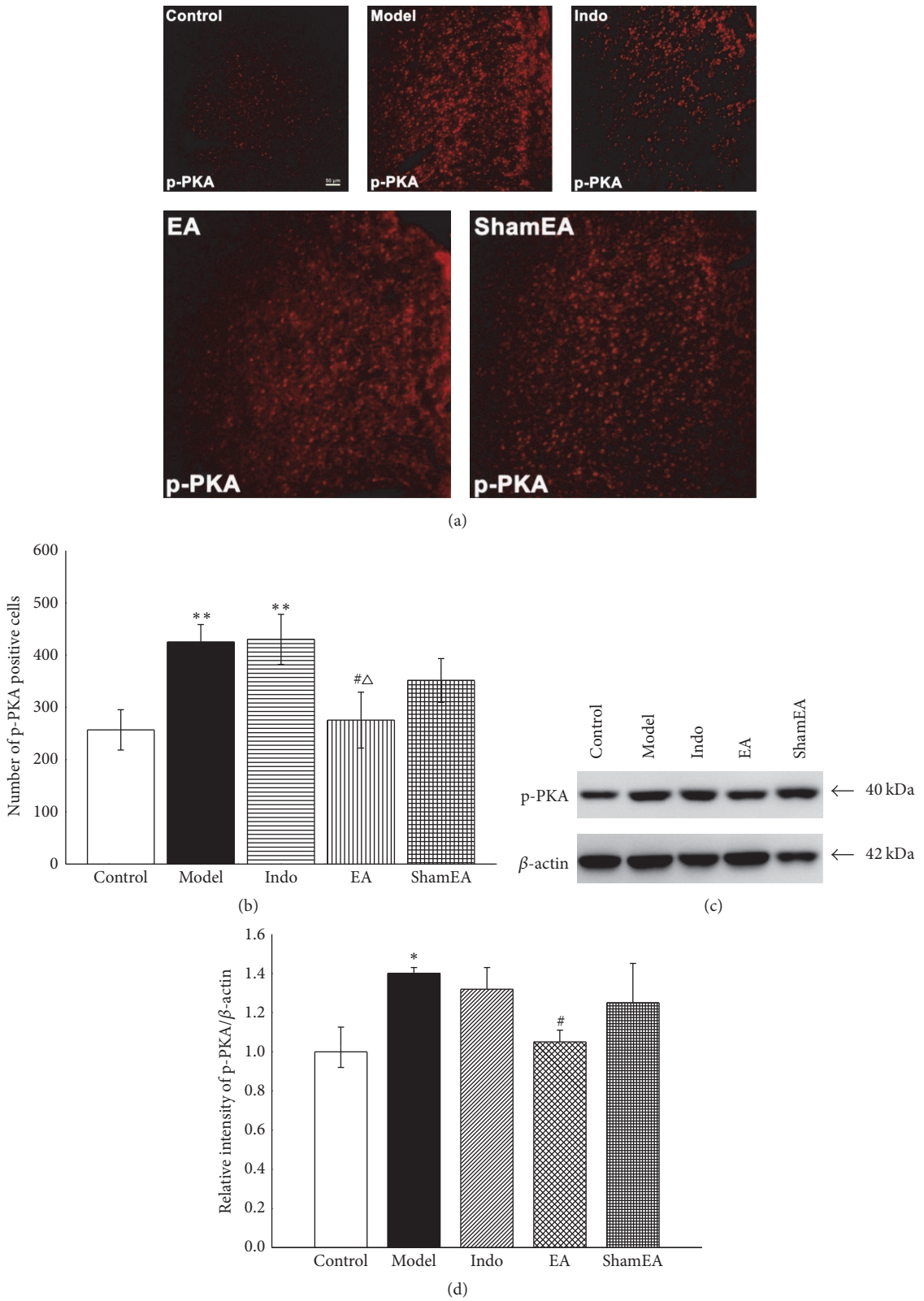

Figure 6: EA decreased the phosphorylation of PKA in the ACC of pain memory model rats. The right ACC tissues of different groups were prepared and labeled with immunofluorescence ($n = 3$, five slides for each rat). Total protein extracts from the ACC tissues were detected by western blotting ($n = 6$). (a) Views of p-PKA-positive cells in the ACC (scale bar, 50 μm). (b) Quantification of p-PKA-positive cells showed that EA treatment at the first injection time point significantly reduced the amount of positive p-PKA. (c) Western blotting analysis of p-PKA in the different groups. (d) Quantitative analysis using the western blot assay showed that EA significantly reduced the phosphorylation levels of PKA. Error bars indicated SEM. $^{*}p < 0.05$ and $^{**}p < 0.01$, versus the control group; $^{\#}p < 0.05$, versus the model group; $^{\triangle}p < 0.05$, versus the indo group.

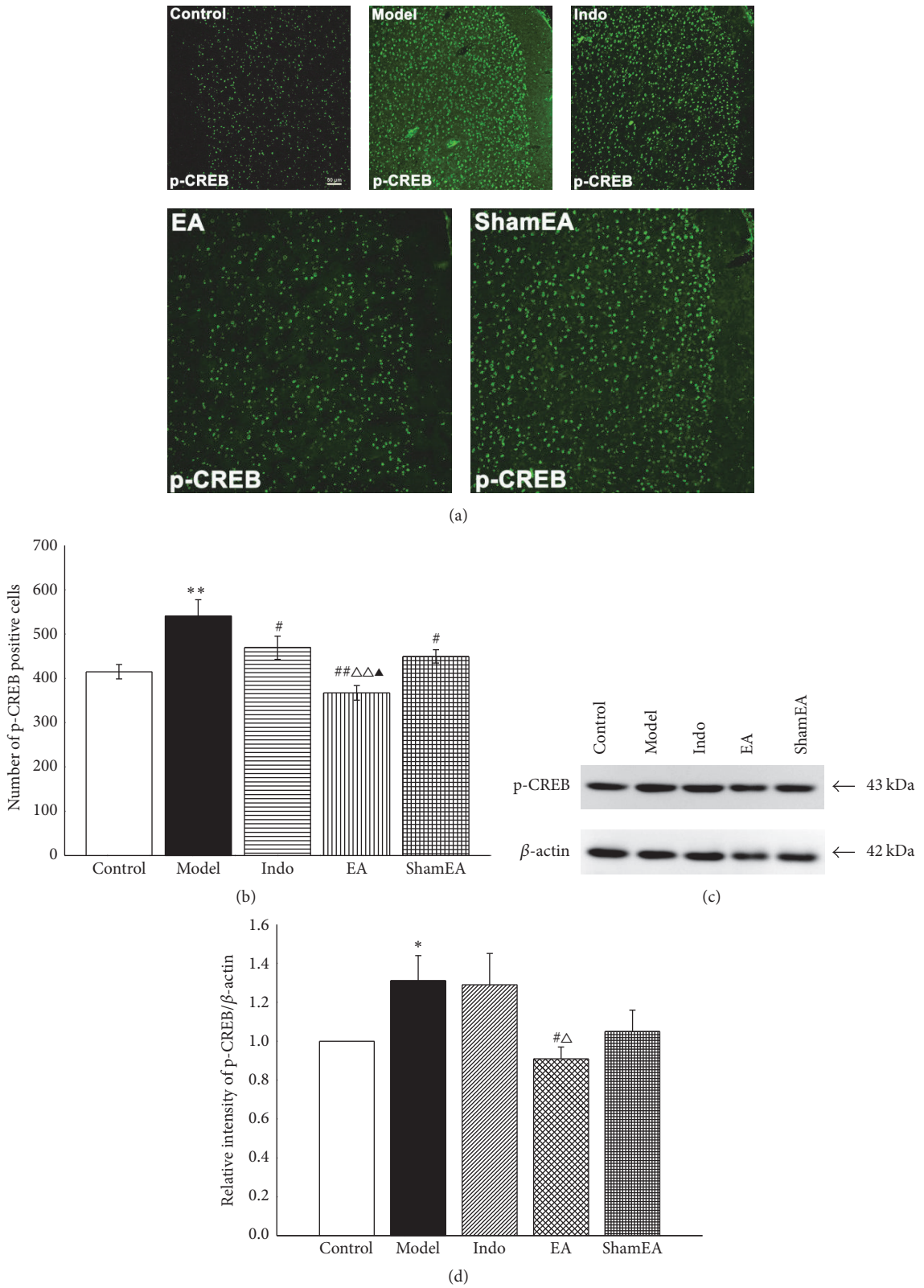

Figure 7: EA decreased CREB phosphorylation in the ACC of pain memory model rats. The right ACC tissues of different groups were prepared and labeled with immunofluorescence ($n = 3$, five slides for each rat). Total protein extracts from the ACC tissues were detected by western blotting ($n = 6$). (a) Views of p-CREB-positive cells in the ACC (scale bar, 50 μm). (b) Quantification of p-CREB-positive cells showed that EA treatment at first injection time point significantly reduced the amount of positive p-CREB. (c) Western blotting analysis of p-CREB in the different groups. (d) Quantitative analysis using the western blot assay showed that EA significantly reduced phosphorylation level of CREB. Error bars indicated SEM. $^{*}p < 0.05$ and $^{**}p < 0.01$, versus the control group; $^{\#}p < 0.05$ and $^{\#\#}p < 0.01$, versus the model group; $^{\triangle}p < 0.05$ and $^{\triangle\triangle}p < 0.01$, versus the indo group; $^{\blacktriangle}p < 0.05$, versus the sham EA group.

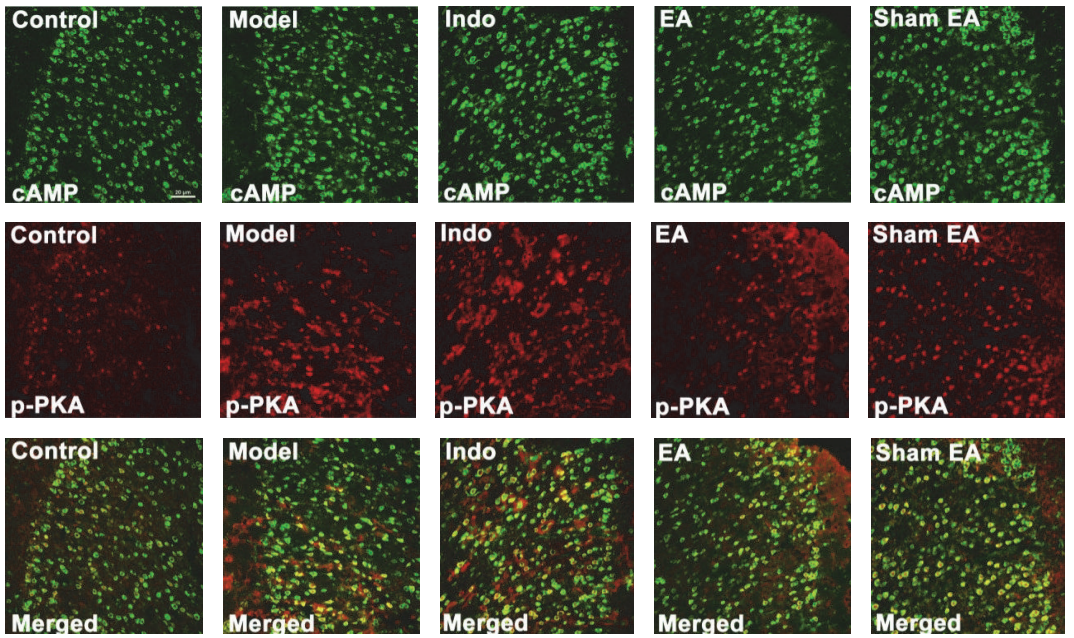

(a)

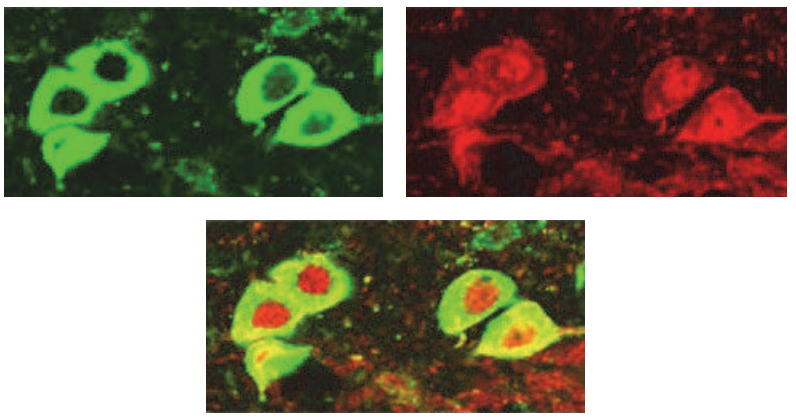

(b)

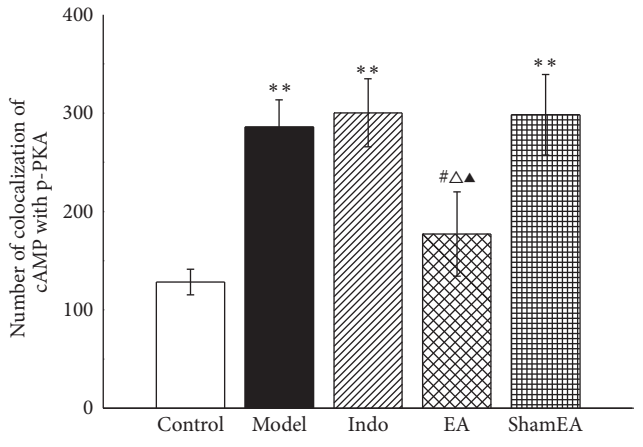

(c)

Figure 8: EA inhibited the colocalization of cAMP with p-PKA in the ACC of pain memory model rats. The right ACC tissues from each group were prepared and labeled with double-immunofluorescence ($n = 3$, five slides for each rat). (a) Views of the colocalization of cAMP with p-PKA (scale bar, 20 μm). (b) The magnified image shows the colocalization of cAMP with p-PKA. (c) Double-labeled immunofluorescence analysis demonstrated that EA significantly reduced the amount of colocalized cAMP and p-PKA. Error bars indicated SEM. $^{**}p < 0.01$, versus the control group; $^{\#}p < 0.05$, versus the model group; $^{\triangle}p < 0.05$, versus the indo group; $^{\blacktriangle}p < 0.05$, versus the sham EA group.

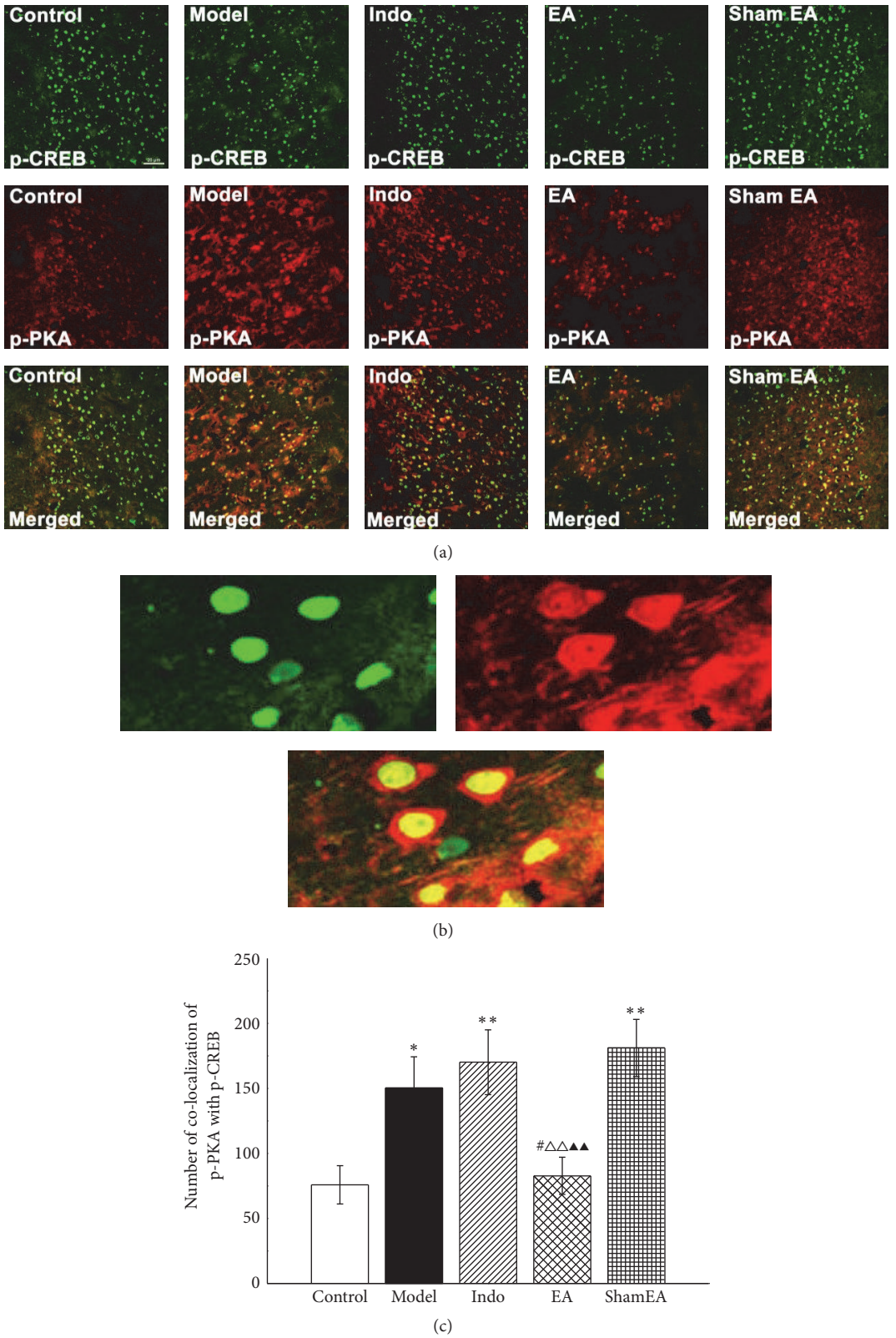

Figure 9: EA inhibited the colocalization of p-PKA with p-CREB in the ACC of pain memory model rats. The right ACC tissues from each groups were prepared and labeled with double-immunofluorescence ($n = 3$, five slides for each rat). (a) Views of the colocalization of p-PKA with p-CREB (scale bar, 20 μm). (b) The magnified image shows the colocalization of p-PKA with p-CREB. (c) Double-labeled immunofluorescence analysis demonstrated that EA significantly reduced the numbers of colocalized p-PKA and p-CREB. Error bars indicated SEM. $^{*}p < 0.05$ and $^{**}p < 0.01$, versus the control group; $^{\#}p < 0.05$, versus the model group; $^{\triangle\triangle}p < 0.01$, versus the indo group; $^{\blacktriangle\blacktriangle}p < 0.01$, versus the sham EA group.

of p-CREB [21]. In the present study, our results have identified different effects of EA and NSAIDS on pain memory. The retrieval of pain memory was demonstrated by the decreased PWTs of uninjected hind paw in the second carrageenan injection. EA blocked the retrieval of pain memory by showing unchanged PWTs values, while NSAIDs treatment did not. It is suggested that the mechanism of EA on pain memory is different from NSAIDs. EA intervention not only has relieved the acute inflammatory pain, but also inhibited the retrieval of pain memory integrated in high-level central neural system. Therefore, EA has an advantage over NSAIDs in treating inflammatory pain accompanied with pain memory.

It has shown that neuronal synaptic plasticity promoted the memory and chronic pain [36, 37]. Thus, we inferred that the potential mechanism of pain memory is closely related with neuronal synaptic plasticity and long-term central sensitization. Some studies have reported that the cAMP/PKA/CREB signaling pathway critically contributes to the neuronal synaptic plasticity in the processes of pain and memory [15, 27, 38]. Being a crucial second messenger, cAMP is involved in varies types of learning and memory processes and long-term synaptic plasticity [17, 39]. Years ago, it was found that increased levels of cAMP in sensory neurons indeed lead to a transient enhancement of transmitter release in the synaptic connection between sensory and motor neurons, which was regarded as a biochemical mechanism for short-term and long-term changes [13, 40]. Some studies have suggested that signaling pathways involving cAMP participate in inflammation and injury sensitization [41, 42]. Here, our study found an increased number of cAMP-positive cells in the ACC of pain memory model rats. Furthermore, when compared with indomethacin and sham EA intervention, EA treatment showed a profound advantage in reducing the number of cAMP-positive cells. In all, these results showed that the role of cAMP as a relative upstream protein in pain memory can be inhibited by EA treatment.

Thus, it would be interesting to determine whether the decreased release of cAMP by EA treatment can affect downstream processes. Reports from earlier studies have demonstrated that cAMP mediates almost all of its actions through PKA [13, 40]. When cAMP increases in cells, the cAMP-binding regulatory subunit of PKA is freed from the catalytic subunit of PKA and is allowed to phosphorylate its substrates [43]. A similar experiment performed in 1980 injected a catalytic subunit of PKA directly into the sensory neurons and found that PKA also sufficiently enhances transmitter release for synaptic plasticity in long-term memory [13, 44]. The inhibition of PKA activity reduces the phosphorylation of CREB [26, 45]. Other studies have indicated that different degrees of emotional/fear memories can be abolished by PKA deficiencies and that the cAMP/PKA signaling pathway is important for memory consolidation [15, 39]. The mechanical allodynia caused by inflammation and nerve injury can be inhibited by microinjections of PKA inhibitor [19, 46]. In Experiment 2 (Figure 4) of the present study, the behavioral test demonstrated that PKA inhibitor diminished the mechanical allodynia in the pain memory model. Regarding the protein expression of PKA in the ACC, the results of this study indicated that pain memory is induced by the phosphorylation of PKA, whereas EA inhibits this process. The effects of the PKA inhibitor suggested that EA treatment has a similar effect with PKA inhibitor.

cAMP and PKA serve as important proteins for the formation of memory [14, 17]. With regard to short-term memory switching to long-term memory, the synthesis of new proteins is required [13]. CREB, a cellular transcription factor that binds the cAMP response element, has a pivotal role in memory storage [9]. The activation of CREB is also closely related to pain [10, 47]. After its phosphorylation by PKA and other proteins, CREB functions as a transcriptional activator to modulate pain, long-term memory, and other physiological and pathological processes. Evidence from our previous study has shown that the phosphorylation of CREB in the ACC of pain memory model rats is significantly related to the retrieval of pain memory, and EA can influence the number of positive cells and active levels of p-CREB in the ACC [21]. In CFA-induced chronic pain rats, the levels of phosphorylated CREB are enhanced in the ACC, which suggests that the presence of synaptic plasticity is related to memories [48, 49]. The CREB-mediated response to stimuli, which acts a downstream of the cAMP/PKA pathway, can be modulated by PKA and its phosphorylation. Active levels of p-CREB in this study demonstrated that p-CREB indeed plays a key role in the retrieval of pain memory. Indomethacin and sham EA reduced the number of positive cells to some extent. However, EA treatment reduced the number of active cells and the phosphorylation levels of CREB to a much greater extent.

To verify the effects of EA treatment on pain memories were mediated through the cAMP/PKA/CREB signaling pathway; the coexpression of both cAMP and p-CREB with p-PKA in the ACC was assessed by double-immunofluorescence labeling. Our results showed that cAMP and p-PKA are coexpressed in cells but not at the same site because of their different distributions. This result indicated that the persistent increase in cAMP induces a longer enhancement of transmitter release in the synaptic connections in neurons and causes the catalytic subunit of PKA to become activated and phosphorylated [13]. Subsequently, the increased p-PKA transmits to the nucleus, where it phosphorylates the transcription factor CREB and activates the gene expression required for the formation of long-term memory [50]. The images from our study showed the coexpression of p-PKA and p-CREB at the same site in cell nuclei. Our data indicated that the amounts of coexpressed p-PKA and cAMP as well as p-CREB were increased in the pain memory model, even under conditions of indomethacin or sham EA treatments, but EA treatment could reverse this effect. In all, these results suggested that the analgesic effects of EA may be mediated via the cAMP/PKA/CREB signaling pathway, which contributes to the allodynia caused by pain memory.

5. Conclusions

This study is the first to demonstrate that the analgesic effect of EA in a rat pain memory model is different from that of the NSAIDs. EA has an advantage over NSAIDs in treating chronic inflammatory pain accompanied with pain memory. The present findings further identify that PKA in ACC plays

a critical role in pain memory retrieval. We propose that the proper mechanism of EA on pain memory is possibly due to the partial inhibition of cAMP/PKA/CREB signaling pathway by EA. Therefore, EA may be a preferred therapy for chronic pain induced by pain memory in clinic.

Competing Interests

The authors declare that there are no competing interests regarding the publication of this paper.

Authors' Contributions

Xiao-Mei Shao and Jing Sun contributed equally to this work as co-first authors. Xiao-Mei Shao designed and performed experimental protocols, data analysis, and manuscript writing. Jing Sun performed the animal experiments, molecular techniques, and data analysis and wrote the manuscript and participated in the design of the experiments. Yong-Liang Jiang and Bo-Yi Liu participated in the design of the experiments, data analysis, and writing of the paper. Zui Shen performed the animal experiments, western blotting, and associated analyses. Fang Fang and Jia-Ling Wang performed the animal experiments, immunofluorescence, and associated analysis. Jun-Ying Du and Yuan-Yuan Wu participated in the experiments and supervised behavioral monitoring. Jian-Qiao Fang designed the study, performed experimental protocols described in this paper, and wrote the initial draft of the paper. All authors read and approved the final manuscript.

Acknowledgments

This study was supported by the National Nature Science Foundation of China (81574056), the Zhejiang Provincial Natural Science Foundation of China (LY15H270009), the Special Financial Grant from the China Postdoctoral Science Foundation (2016T90552), the Key Science and Technology Innovation Team of Zhejiang Province (2013TD15), the Class General Financial grant from the China Postdoctoral Science Foundation (2015M580527), and the Project Supported by Zhejiang Province Top Key Discipline of Chinese Medicine-Acupuncture & Tuina.

References

[1] S. Alvarado, M. Tajerian, M. Suderman et al., "An epigenetic hypothesis for the genomic memory of pain," *Frontiers in Cellular Neuroscience*, vol. 9, no. 3, article 88, 2015.

[2] Y. Zhang, X. Meng, A. Li et al., "Electroacupuncture alleviates affective pain in an inflammatory pain rat model," *European Journal of Pain*, vol. 16, no. 2, pp. 170–181, 2012.

[3] Y. Ma, S. Wang, Y. Tian, L. Chen, G. Li, and J. Mao, "Disruption of persistent nociceptive behavior in rats with learning impairment," *PLoS ONE*, vol. 8, no. 9, Article ID e74533, 2013.

[4] N. Y. Shin, D.-H. Kang, J. H. Jang et al., "Impaired recognition of social emotion in patients with complex regional pain syndrome," *The Journal of Pain*, vol. 14, no. 11, pp. 1304–1309, 2013.

[5] G. Miguez, M. A. Laborda, and R. R. Miller, "Classical conditioning and pain: conditioned analgesia and hyperalgesia," *Acta Psychologica*, vol. 145, no. 1, pp. 10–20, 2014.

[6] M. Tajerian, D. Leu, Y. Zou et al., "Brain neuroplastic changes accompany anxiety and memory deficits in a model of complex regional pain syndrome," *Anesthesiology*, vol. 121, no. 4, pp. 852–865, 2014.

[7] O. K. Melemedjian, D. V. Tillu, M. N. Asiedu et al., "BDNF regulates atypical PKC at spinal synapses to initiate and maintain a centralized chronic pain state," *Molecular Pain*, vol. 9, no. 1, article 12, 2013.

[8] J. Bouffard, L. J. Bouyer, J.-S. Roy, and C. Mercier, "Tonic pain experienced during locomotor training impairs retention despite normal performance during acquisition," *The Journal of Neuroscience*, vol. 34, no. 28, pp. 9190–9195, 2014.

[9] K. A. Morris and P. E. Gold, "Age-related impairments in memory and in CREB and pCREB expression in hippocampus and amygdala following inhibitory avoidance training," *Mechanisms of Ageing and Development*, vol. 133, no. 5, pp. 291–299, 2012.

[10] H. Imbe, A. Kimura, T. Donishi, and Y. Kaneoke, "Repeated forced swim stress enhances CFA-evoked thermal hyperalgesia and affects the expressions of pCREB and c-Fos in the insular cortex," *Neuroscience*, vol. 259, no. 11, pp. 1–11, 2014.

[11] E. Navratilova, J. Y. Xie, D. Meske et al., "Endogenous opioid activity in the anterior cingulate cortex is required for relief of pain," *The Journal of Neuroscience*, vol. 35, no. 18, pp. 7264–7271, 2015.

[12] S. K. Sharma, M. W. Bagnall, M. A. Sutton, and T. J. Carew, "Inhibition of calcineurin facilitates the induction of memory for sensitization in Aplysia: requirement of mitogen-activated protein kinase," *Proceedings of the National Academy of Sciences of the United States of America*, vol. 100, no. 8, pp. 4861–4866, 2003.

[13] E. R. Kandel, "The molecular biology of memory: CAMP, PKA, CRE, CREB-1, CREB-2, and CPEB," *Molecular Brain*, vol. 5, no. 1, article 14, 2012.

[14] L.-H. Hang, J.-P. Yang, D.-H. Shao, Z. Chen, and H. Wang, "Involvement of spinal PKA/CREB signaling pathway in the development of bone cancer pain," *Pharmacological Reports*, vol. 65, no. 3, pp. 710–716, 2013.

[15] W. Wu, X. Yu, X.-P. Luo, S.-H. Yang, and D. Zheng, "Tetramethylpyrazine protects against scopolamine-induced memory impairments in rats by reversing the cAMP/PKA/CREB pathway," *Behavioural Brain Research*, vol. 253, no. 8, pp. 212–216, 2013.

[16] Q.-Q. Li, G.-X. Shi, J.-W. Yang et al., "Hippocampal cAMP/PKA/CREB is required for neuroprotective effect of acupuncture," *Physiology and Behavior*, vol. 139, no. 12, pp. 482–490, 2015.

[17] M. H. Kim and Y. H. Leem, "Chronic exercise improves repeated restraint stress-induced anxiety and depression through 5HT1A receptor and cAMP signaling in hippocampus," *Journal of Exercise Nutrition and Biochemistry*, vol. 18, no. 1, pp. 97–104, 2014.

[18] H. Qu, M. Zhao, S. Zhao et al., "Forced limb-use enhances brain plasticity through the cAMP/PKA/CREB signal transduction pathway after stroke in adult rats," *Restorative Neurology and Neuroscience*, vol. 32, no. 5, pp. 597–609, 2014.

[19] T. Chen, K. Koga, G. Descalzi et al., "Postsynaptic potentiation of corticospinal projecting neurons in the anterior cingulate cortex after nerve injury," *Molecular Pain*, vol. 10, article 33, 2014.

[20] N. Hamzeh-Gooshchi, E. Tamaddonfard, and A. A. Farshid, "Effects of microinjection of histamine into the anterior cingulate cortex on pain-related behaviors induced by formalin in rats," *Pharmacological Reports*, vol. 67, no. 3, pp. 593–599, 2015.

[21] J. Sun, X.-M. Shao, F. Fang, Z. Shen, Y.-Y. Wu, and J.-Q. Fang, "Electroacupuncture alleviates retrieval of pain memory and its effect on phosphorylation of cAMP response element-binding protein in anterior cingulate cortex in rats," *Behavioral and Brain Functions*, vol. 11, article 9, 2015.

[22] I. Kissin, C. F. Freitas, and E. L. Bradley Jr., "Memory of pain: the effect of perineural resiniferatoxin," *Anesthesia & Analgesia*, vol. 103, no. 3, pp. 721–728, 2006.

[23] J.-Q. Fang, J.-Y. Du, Y. Liang, and J.-F. Fang, "Intervention of electroacupuncture on spinal p38 MAPK/ATF-2/VR-1 pathway in treating inflammatory pain induced by CFA in rats," *Molecular Pain*, vol. 9, no. 1, article 13, 2013.

[24] S. R. Chaplan, F. W. Bach, J. W. Pogrel, J. M. Chung, and T. L. Yaksh, "Quantitative assessment of tactile allodynia in the rat paw," *Journal of Neuroscience Methods*, vol. 53, no. 1, pp. 55–63, 1994.

[25] F. X. Wu, R. R. Pan, W. F. Yu, and R. Y. Liu, "The antinociception effect of dezocine in a rat neuropathic pain model," *Translational Perioperative and Pain Medicine*, vol. 1, no. 1, pp. 5–8, 2014.

[26] H. Cao, Y.-J. Gao, W.-H. Ren et al., "Activation of extracellular signal-regulated kinase in the anterior cingulate cortex contributes to the induction and expression of affective pain," *The Journal of Neuroscience*, vol. 29, no. 10, pp. 3307–3321, 2009.

[27] J. H. Bo, W. Zhang, X. F. Sun et al., "The cyclic AMP response element-binding protein antisense oligonucleotide induced anti-nociception and decreased the expression of KIF17 in spinal cord after peripheral nerve injury in mice," *International Journal of Clinical and Experimental Medicine*, vol. 7, no. 12, pp. 5181–5191, 2014.

[28] J. S. Grimes, S. K. Creech, E. E. Young, E. G. Vichaya, and M. W. Meagher, "Distraction speeds the decay of shock-induced hypoalgesia: evidence for the contribution of memory systems in affective pain modulation," *The Journal of Pain*, vol. 10, no. 3, pp. 282–292, 2009.

[29] T. Koyama, J. G. McHaffie, P. J. Laurienti, and R. C. Coghill, "The subjective experience of pain: where expectations become reality," *Proceedings of the National Academy of Sciences of the United States of America*, vol. 102, no. 36, pp. 12950–12955, 2005.

[30] S. Prakash and P. Golwala, "Phantom headache: pain-memory-emotion hypothesis for chronic daily headache?" *Journal of Headache and Pain*, vol. 12, no. 3, pp. 281–286, 2011.

[31] R. H. Terry, C. A. Niven, E. E. Brodie, R. B. Jones, and M. A. Prowse, "Memory for pain? A comparison of nonexperiential estimates and patients' reports of the quality and intensity of postoperative pain," *Journal of Pain*, vol. 9, no. 4, pp. 342–349, 2008.

[32] D. S. Choi, D. Y. Choi, R. A. Whittington, and S. S. Nedeljković, "Sudden amnesia resulting in pain relief: the relationship between memory and pain," *Pain*, vol. 132, no. 1-2, pp. 206–210, 2007.

[33] H. Cao, W.-H. Ren, M.-Y. Zhu, Z.-Q. Zhao, and Y.-Q. Zhang, "Activation of glycine site and GluN2B subunit of NMDA receptors is necessary for ERK/CREB signaling cascade in rostral anterior cingulate cortex in rats: Implications for affective pain," *Neuroscience Bulletin*, vol. 28, no. 1, pp. 77–87, 2012.

[34] H. Y. Kim, J. Wang, I. Lee, H. K. Kim, K. Chung, and J. M. Chung, "Electroacupuncture suppresses capsaicin-induced secondary hyperalgesia through an endogenous spinal opioid mechanism," *Pain*, vol. 145, no. 3, pp. 332–340, 2009.

[35] X. Li, F. Guo, Q. Zhang et al., "Electroacupuncture decreases cognitive impairment and promotes neurogenesis in the APP/PS1 transgenic mice," *BMC Complementary and Alternative Medicine*, vol. 14, article 37, 2014.

[36] R.-R. Ji, T. Kohno, K. A. Moore, and C. J. Woolf, "Central sensitization and LTP: do pain and memory share similar mechanisms?" *Trends in Neurosciences*, vol. 26, no. 12, pp. 696–705, 2003.

[37] S. J. Kang, M.-G. Liu, T. Chen et al., "Plasticity of metabotropic glutamate receptor- dependent long-term depression in the anterior cingulate cortex after amputation," *The Journal of Neuroscience*, vol. 32, no. 33, pp. 11318–11329, 2012.

[38] M. Zhuo, "Cortical excitation and chronic pain," *Trends in Neurosciences*, vol. 31, no. 4, pp. 199–207, 2008.

[39] E. Nassireslami, P. Nikbin, B. Payandemehr et al., "A cAMP analog reverses contextual and tone memory deficits induced by a PKA inhibitor in Pavlovian fear conditioning," *Pharmacology Biochemistry and Behavior*, vol. 105, pp. 177–182, 2013.

[40] M. Brunelli, V. Castellucci, and E. R. Kandel, "Synaptic facilitation and behavioral sensitization in Aplysia: possible role of serotonin and cyclic AMP," *Science*, vol. 194, no. 4270, pp. 1178–1181, 1976.

[41] R. M. Edelmayer, J.-D. Brederson, M. F. Jarvis, and R. S. Bitner, "Biochemical and pharmacological assessment of MAP-kinase signaling along pain pathways in experimental rodent models: a potential tool for the discovery of novel antinociceptive therapeutics," *Biochemical Pharmacology*, vol. 87, no. 3, pp. 390–398, 2014.

[42] C. L. Ross, T. Teli, and B. S. Harrison, "Effect of electromagnetic field on cyclic adenosine monophosphate (cAMP) in a human mu-opioid receptor cell model," *Electromagnetic Biology and Medicine*, vol. 35, no. 3, pp. 206–213, 2015.

[43] M. Baudonnat, J.-L. Guillou, M. Husson et al., "Disrupting effect of drug-induced reward on spatial but not cue-guided learning: implication of the striatal protein kinase A/cAMP response element-binding protein pathway," *The Journal of Neuroscience*, vol. 31, no. 46, pp. 16517–16528, 2011.

[44] V. F. Castellucci, E. R. Kandel, and J. H. Schwartz, "Intracellular injection of the catalytic subunit of cyclic AMP-dependent protein kinase simulates facilitation of transmitter release underlying behavioral sensitization in Aplysia," *Proceedings of the National Academy of Sciences of the United States of America*, vol. 77, no. 12, pp. 7492–7496, 1980.

[45] S.-P. Fu, W. Wang, B.-R. Liu et al., "β-Hydroxybutyric sodium salt inhibition of growth hormone and prolactin secretion via the cAMP/PKA/CREB and AMPK signaling pathways in dairy cow anterior pituitary cells," *International Journal of Molecular Sciences*, vol. 16, no. 2, pp. 4265–4280, 2015.

[46] Y. Fu, J. Han, T. Ishola et al., "PKA and ERK, but not PKC, in the amygdala contribute to pain-related synaptic plasticity and behavior," *Molecular Pain*, vol. 4, article 26, 2008.

[47] Y.-X. Yao, Y.-F. Zhang, Y. Yang, S.-H. Guo, Z. Jiang, and Z.-Q. Zhao, "Spinal synaptic scaffolding protein Homer 1b/c regulates CREB phosphorylation and c-fos activation induced by inflammatory pain in rats," *Neuroscience Letters*, vol. 559, no. 12, pp. 88–93, 2014.

[48] H. Ikeda, K. Mochizuki, and K. Murase, "Astrocytes are involved in long-term facilitation of neuronal excitation in the anterior cingulate cortex of mice with inflammatory pain," *Pain*, vol. 154, no. 12, pp. 2836–2843, 2013.

[49] F.-L. Chen, Y.-L. Dong, Z.-J. Zhang et al., "Activation of astrocytes in the anterior cingulate cortex contributes to the affective component of pain in an inflammatory pain model," *Brain Research Bulletin*, vol. 87, no. 1, pp. 60–66, 2012.

[50] B. J. Bacskai, B. Hochner, M. Mahaut-Smith et al., "Spatially resolved dynamics of cAMP and protein kinase a subunits in Aplysia sensory neurons," *Science*, vol. 260, no. 5105, pp. 222–226, 1993.

Hindawi Publishing Corporation
Neural Plasticity
Volume 2016, Article ID 3131586, 9 pages
http://dx.doi.org/10.1155/2016/3131586

Research Article

Musical Electroacupuncture May Be a Better Choice than Electroacupuncture in a Mouse Model of Alzheimer's Disease

Jing Jiang,[1] Gang Liu,[2] Suhua Shi,[3] and Zhigang Li[1]

[1]*Beijing University of Chinese Medicine, Beijing 100029, China*
[2]*Community Health Service Center of Dongcheng District, Beijing 100010, China*
[3]*Third Affiliated Hospital of Beijing University of Chinese Medicine, Beijing 100029, China*

Correspondence should be addressed to Zhigang Li; lizhigang620@126.com

Received 22 May 2016; Revised 17 September 2016; Accepted 20 October 2016

Academic Editor: Jian Kong

Copyright © 2016 Jing Jiang et al. This is an open access article distributed under the Creative Commons Attribution License, which permits unrestricted use, distribution, and reproduction in any medium, provided the original work is properly cited.

Objectives. To compare musical electroacupuncture and electroacupuncture in a mouse model of Alzheimer's disease. *Methods*. In this study, 7.5-month-old male senescence-accelerated mouse prone 8 (SAMP8) mice were used as an Alzheimer's disease animal model. In the normal control paradigm, 7.5-month-old male SAMR1 mice were used as the blank control group (N group). After 15 days of treatment, using Morris water maze test, micro-PET, and immunohistochemistry, the differences among the musical electroacupuncture (MEA), electroacupuncture (EA), Alzheimer's disease (AD), and normal (N) groups were assessed. *Results*. The Morris water maze test, micro-PET, and immunohistochemistry revealed that MEA and EA therapies could improve spatial learning and memory ability, glucose metabolism level in the brain, and Aβ amyloid content in the frontal lobe, compared with the AD group ($P < 0.05$). Moreover, MEA therapy performed better than EA treatment in decreasing amyloid-beta levels in the frontal lobe of mice with AD. *Conclusion*. MEA therapy may be superior to EA in treating Alzheimer's disease as demonstrated in SAMP8 mice.

1. Introduction

Alzheimer's disease (AD) is a central nervous degenerative disease with memory impairment, aphasia, agnosia, and executive dysfunction, as well as personality and behavior changes [1]. Pathological features of AD include β amyloid (Aβ) deposition and neurofibrillary tangles, leading to progressive neuronal damage, and ultimately atrophy of the cortex and subcortical structures [2]. Magnetic resonance imaging (MRI) studies demonstrated that the hippocampus is a region affected early in AD patients [3]. However, relatively few studies are available assessing changes in other brain regions in AD patients, especially the frontal lobe. Interestingly, evaluating 41 patients with AD, Harwood et al. found that the insight and cognitive impairment as well as functional deficits in AD are associated with the glucose metabolic rate in the frontal cortex [4].

We previously demonstrated that treatment with electroacupuncture could effectively improve the spatial learning and memory ability as well as glucose metabolism in the hippocampus of animals with AD [5]. Other studies suggested that music therapy could contribute to a supplementary treatment of AD [6]. In China, an innovative therapy combined electroacupuncture and music therapy, and the term musical electroacupuncture (MEA) was coined. MEA has been clinically used to treat some neurological and psychotic disorders. Addition of musical therapy helps overcome acupuncture intolerability; therefore, the MEA therapy in a way is superior to traditional electroacupuncture [7].

In the current study, we aimed to address two questions: (1) what happens in the frontal lobe during MEA? Do these changes differ from those observed in other brain regions? (2) Are there differences between the two therapies for AD treatment? To this end, senescence-accelerated mouse prone 8 (SAMP8) mice were selected as an AD animal model, and the differences between techniques were assessed. First, Morris' water maze test was used to evaluate behavioral changes in the model animals. Then, micro-PET assessment

of a region of interest (ROI) and glucose metabolism evaluation in different brain regions were performed. Finally, immunohistochemistry (IHC) was used to assess the changes of amyloid-β1-42 deposition in the frontal lobe after the treatments.

2. Materials and Methods

2.1. Animals. Senescence-accelerated mouse prone 8 (SAMP8) and cognate normal senescence-accelerated mouse-R1 (SAMR1) breeding pairs were kindly provided by Professor Takeda at Kyoto University, Japan [8]. All animals were male and specific pathogen-free (SPF), weighing 30 ± 2 g. They were housed in a barrier facility at the Experimental Animal Centre of First Teaching Hospital of Beijing University of Traditional Chinese Medicine, under controlled temperature (24 ± 2°C) and 12 h/12 h dark-light cycle, with sterile drinking water and standard pellet diet *ad libitum*. All experiments were performed according to the National Institute of Health Guide for the Care and Use of Laboratory Animals (NIH publications number 80-23). Thirty 7.5-month-old male SAMP8 mice were divided into three groups (n = 10 per group), including SAMP8 Alzheimer's disease control (AD), electroacupuncture (EA), and musical electroacupuncture (MEA) groups. Ten 7.5-month-old male SAMR1 mice composed the normal control (N) group.

2.2. Acupuncture. Electroacupuncture and musical electroacupuncture treatments were performed 20 minutes per day, once daily for 15 days (no treatment on day 8). Prescription of acupuncture points included DU20 *Baihui*, DU 26 *Shuigou*, and EX-HN3 *Yintang* (significant extra points); the locations of these points were according to the National Acupuncture Society for Experimental Research developed by the "laboratory animal acupuncture atlas." *Huatuo* card 30# (0.5 inch) needles were used for treatment. The pricking method was used for DU 26 *Shuigou* and the flat thorn method for DU20 *Baihui* and EX-HN3 *Yintang*. Needle depth was 0.5 cm and taped.

In the EA group, the needle handle was connected to the HANS-LH202 electroacupuncture device (Peking University Institute of Science Nerve and Beijing Hua Wei Industrial Development Company), with sparse wave at 2 Hz, 2 V, and 0.6 mA.

In the MEA group, the needle handle was connected to the ZJ-12H musical electroacupuncture device (Developed by Chinese Acupuncture Society and manufactured by Harbin Zhihou Medical Devices Co., Ltd.). Clear rhythm, moderate speed, and music prescription intensity (*curing dementia prescription*) were selected; music intensity was adjusted so that the animals remained quiet during the treatment.

In the N and AD groups, no treatment was carried out, with grabbing and fixing the mice in order to ensure the same treatment conditions, once daily for 15 days.

2.3. Morris' Water Maze Test. Morris' water maze consisted of a circular tank (diameter, 90 cm; height, 50 cm), filled with water to a depth of 29 cm, maintained at 24 ± 1°C, and rendered opaque with blue-black ink. A removable circular platform (diameter, 9.5 cm; height, 28 cm) with the top surface 1 cm below the water was located inside the pool. The pool area was conceptually divided into four quadrants (NE, NW, SW, and SE) of equal size. Data were collected by a video camera (TOTA-450d, Japan), which was fixed to the ceiling and connected to a video recorder with an automated tracking system (China Daheng Group, Beijing, China).

In the behavioral test, mice were placed in the pool of water containing a platform just below the surface of the water. They escaped from the maze once they find the platform. Distal visual cues are arrayed around the room, and, in general, mice are able to find the location of the hidden platform based on these cues.

2.3.1. Hidden Platform Test. This test assesses the ability of mice to find the platform under conditions where they cannot directly see the latter but must either remember it based on external cues or perform a search. The platform was placed 1 cm under the water surface; the water was rendered opaque by a suspension of dark blue, nontoxic tempera paint. The platform was placed in a different location from that used in the visible platform testing. Each mouse was released from one of the 4 locations and had 60 s to search for the hidden platform. At the end of each trial, the mouse was placed on the platform or allowed to stay there for 15 s. Prominent spatial cues were arrayed around the room. The investigator also constituted a powerful spatial cue and always sat in the same location during each trial after releasing the mouse. Six trials per day for 5 consecutive days were performed with the platform location kept constant. The time that the mouse took to find the platform was recorded and represented escape latency.

2.3.2. Probe Trial. The day after completion of the hidden platform test, the platform was removed; each mouse was placed in the pool once for 60 s, starting from the same starting location used first in the hidden platform test. The time spent swimming in the quadrant that contained the platform was recorded. This is considered the most specific test for spatial memory. The time spent in the platform quadrant was recorded, and the percentage of total time spent swimming to the platform quadrant was derived.

2.4. Micropositron Emission Tomography. Four animals were randomly selected from each group for micro-PET detection. The ^{18}F-FDG PET tracer was provided by the Chinese Medicine Research Institute PET Room; PET imaging was carried out on a Siemens INVEON PET/CT imaging system. Before the experiments, mice (7.5 months, 28~32 g) were submitted to blood glucose monitoring and showed levels in the normal range (7.0~10.1 mmol/L). Therefore, they could be assessed by micro-PET. Mice were deprived of water 6 h before assessment. The animals were placed in the suction chamber, inhaling oxygen mixed with 1.5% isoflurane for anesthesia. After complete anesthesia, approximately 14.8~16.5 MBq ^{18}F-FDG PET were injected via the tail vein. After ^{18}F-FDG PET tracer uptake for 60 min, the mice were

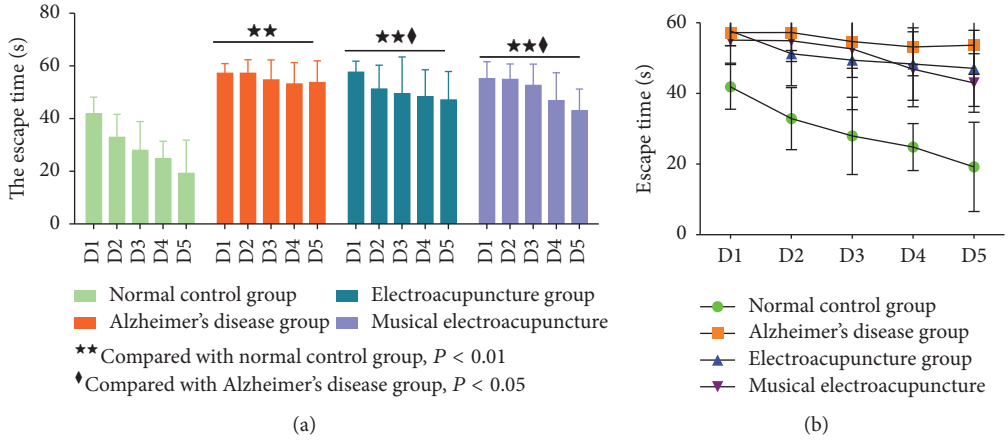

Figure 1

placed in the prone position, parallel to the scanner long axis, with the head located within the scanner field of view. Then, micropositron emission tomography began to collect images. The mice were anesthetized by inhalation of oxygen mixed with 1.5% isoflurane (1 L/min).

2.4.1. Micropositron Emission Tomography Image Reconstruction. Filtered back projection (FBP) and CT photon attenuation correction were used for image reconstruction. Dynamic micro-PET image frames were taken at 30 s/frames.

2.4.2. Region of Interest Selection. Three-dimensional regions of interest were selected in the hippocampus, in transverse, coronal, and sagittal planes. The uptake rate per gram in each region of interest was calculated.

2.5. Immunohistochemistry. After the Morris water maze test, the remaining six mice in each group (four were used in micro-PET) were anesthetized by intraperitoneal injection of 10% chloral hydrate at 0.35 mL/100 g body weight. Three minutes later, the chest was opened and the heart exposed; intubation was performed from the left ventricle to the ascending aorta with quick injection of 100 mL saline. Then, the right atrial appendage was cut, and 4% paraformaldehyde was injected until the liver turned white with clear fluid flowing out from the right atrial appendage. After the perfusion, the mouse was decapitated and the whole brain extracted and placed on ice. The brain was then placed into 4% paraformaldehyde for paraffin embedding.

For histochemistry, paraffin embedded brain tissue sections were deparaffinized with xylene and hydrated with graded alcohol. Then, the sections were treated with citric acid antigen repair buffer and washed with PBS (pH 7.4) every 5 min three times with shaking. After incubation with 3% hydrogen peroxide for 20 min in the dark to quench endogenous peroxidase, the sections were incubated with anti-Aβ1-42 antibody (1 : 50, ab10148, Abcam) overnight. Then, secondary antibodies were added for 30 min at room temperature, and detection was performed with DAB. Finally, the sections were dehydrated with graded alcohol and mounted. Micrographs of brain tissue samples were obtained at 400x magnification, and integral optical density (IOD) values were calculated using Image-Pro Plus 6.0 software.

2.6. Statistical Analysis. Data are mean ± SD for each group. For the Morris water maze test, the escape latency time of the hidden platform trial was analyzed by the Huynh-Feldt test, while one-way ANOVA was conducted on probe trial, micro-PET test, and immunohistochemical data. LSD test was used to compare group pairs. Statistical significance was set at $P < 0.05$. All statistical analyses were performed with the SPSS software V.17.0 (SPSS, USA).

3. Results

3.1. Effects of Electroacupuncture and Musical Electroacupuncture on Spatial Learning and Memory Ability of SAMP8 Mouse in Morris' Water Maze Test. The effects of electroacupuncture and musical electroacupuncture in spatial location ability of SAMP8 mice in the WMW test are shown in Figure 1(a). With training time extension, escape latency in all groups showed a downward trend (Figure 1(b)). The AD group showed a marked retardation in escape latency compared with the N group ($P = 0.00$), probably due to memory deficits resulting from the rapid aging process impairing learning and memory. Compared with the AD group, escape latency in the EA ($P = 0.031$) and MEA ($P = 0.023$) groups was significantly reduced ($P < 0.05$). As shown in Figures 1(a) and 1(b), the MEA group performed better than the EA group, although there was no statistically significant difference ($P = 0.895$).

To assess therapeutic effects on spatial memory ability, performance on day 6 was examined by analyzing the percentages of swimming time in the expected platform position. A higher percentage of time spent in the platform quadrant is interpreted as a higher level of memory retention [9]. In this trial, compared with the AD group, the EA ($P = 0.045$) and MEA ($P = 0.035$) groups showed increased time spent in the platform quadrant ($P < 0.05$). What is more, percentages of time spent in the platform quadrant were similar between the EA and MEA groups ($P = 0.907$, Figure 2).

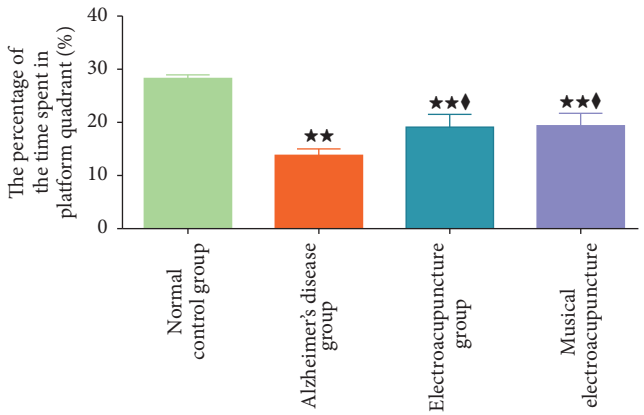

★★Compared with normal control group, $P < 0.01$
♦Compared with Alzheimer's disease group, $P < 0.05$

Figure 2

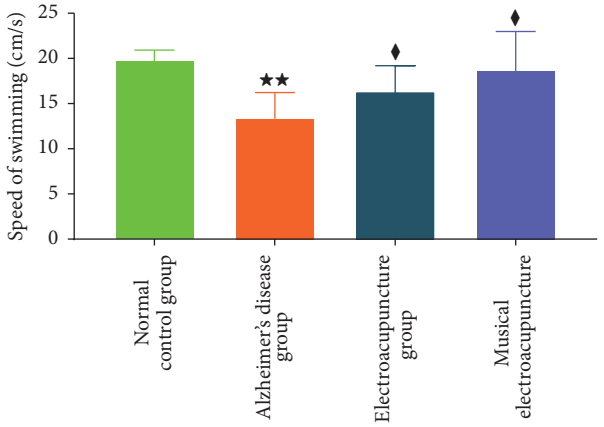

★★Compared with normal control group, $P < 0.01$
♦Compared with Alzheimer's disease group, $P < 0.05$

Figure 3

Besides the escape time, the average animal swimming speed is also associated with spatial learning and memory ability. In some cases, swimming speed in the normal control group was slower, with the escape time longer than in the Alzheimer's disease group. Thus, escapes times cannot serve as the only indicator of learning ability and memory. The average swimming speed before getting on the platform is an important indicator of exercise ability and can reflect individual differences in experimental animals.

Compared with the N group, the swimming speed in AD group was significantly reduced ($P = 0.00$), indicating lower exercise ability for SAMP8 mice compared with SAMR1 animals. Compared with the AD group, electroacupuncture and musical electroacupuncture both increased the swimming speed of SAMP8 mice (EA, $P = 0.023$; MEA, $P = 0.009$). What is more, the MEA group performed better than the EA group (Figure 3).

3.2. PET Images and ^{18}F-FDG Uptake Rate in Different Brain Regions. Micro-PET images were obtained from the hippocampus, frontal lobe, and cerebral cortex of each mouse. The same color standard and code were used from top to bottom to display the metabolic rate of glucose. After treatment with electroacupuncture and musical electroacupuncture, ^{18}F-FDG levels in each brain region assessed were higher than values obtained for the nontherapy group (Figures 4(a), 4(b), and 4(c)).

To obtain acute differences in glucose metabolism among groups, the uptake rate of ^{18}F-FDG per gram of different brain regions was assessed. After treatment with electroacupuncture and musical electroacupuncture, uptake rates of ^{18}F-FDG per gram in the hippocampus (EA, $P = 0.039$; MEA, $P = 048$), cerebral cortex (EA, $P = 0.14$; MEA, $P = 0.047$), and frontal lobe (EA, $P = 0.045$; MEA, $P = 0.031$) were higher than those obtained for the Alzheimer's disease group (Figures 5(a), 5(b), and 5(c)). In the frontal lobe, the uptake rate of ^{18}F-FDG for the MEA group was higher than that of the EA group, while, in the other two regions, the EA group showed higher values.

3.3. Protein Expression of Amyloid-β1-42 in the Frontal Lobe. After the behavioral tests and imaging, brain tissue samples were analyzed by immunohistochemistry to assess the effects of the two therapeutic variants on amyloid-β1-42 accumulation due to neuronal damage and memory impairment. Compared with the N group, IOD of amyloid-β1-42 in the frontal lobe was significantly higher in the AD group ($P = 0.00$), EA ($P = 0.00$), and MEA ($P = 0.007$) groups. Meanwhile, IOD of amyloid-β1-42 in frontal lobe samples from the AD group was significantly higher than those of the EA ($P = 0.00$) and MEA ($P = 0.00$) groups. Interestingly, IOD of amyloid-β1-42 in frontal lobe samples from the MEA group was significantly lower than that of the EA group ($P = 0.01 < 0.05$) (Figures 6 and 7).

4. Discussions

4.1. Senescence-Accelerated Mouse Prone 8 (SAMP8) Is an Ideal Animal Model for Alzheimer's Disease. The senescence-accelerated mouse (SAM) is an accelerated aging model that was established through phenotypic selection from a common genetic pool of the AKR/J mouse strain [10]. These animals develop deficits in learning and memory relatively early in their lifespan [11]. It was shown that senescence-accelerated mouse (SAMP8), as a model of aging, displays many features known to occur in the early stage of AD such as increased oxidative stress, amyloid-beta level alteration, and tau phosphorylation [12]. What is more, published data [13] and our previous research [5] demonstrated that SAMP8 could undergo acupuncture therapy to improve learning and memory ability. In this study, therefore, SAMP8 mice were selected as an ideal animal model for Alzheimer's disease.

4.2. An Innovative Therapy for Alzheimer's Disease: Musical Electroacupuncture Therapy. Music therapy is a nonpharmacological treatment for the behavioral and psychological symptoms of Alzheimer's disease [14]. Appropriate music formulation could provide a form of relief to the AD patient and may stimulate cognitive activities so that areas subject to

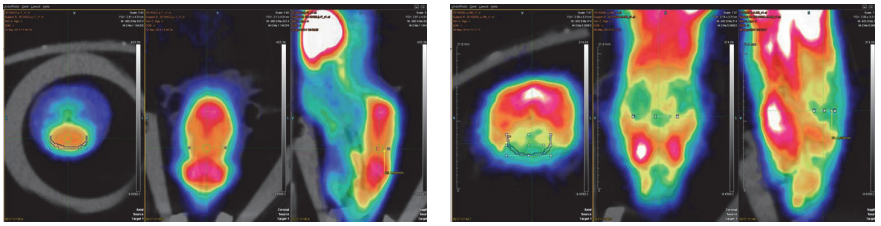

Normal group Alzheimer's disease group

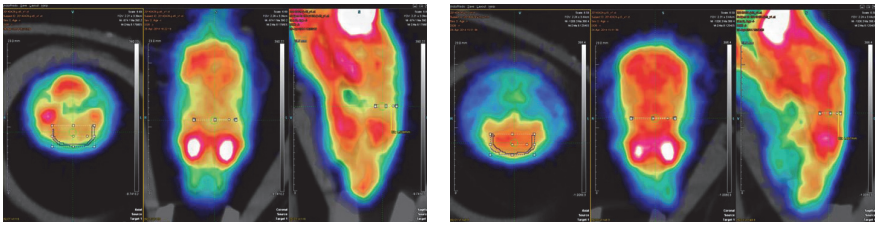

Electroacupuncture group Musical electroacupuncture group

(a)

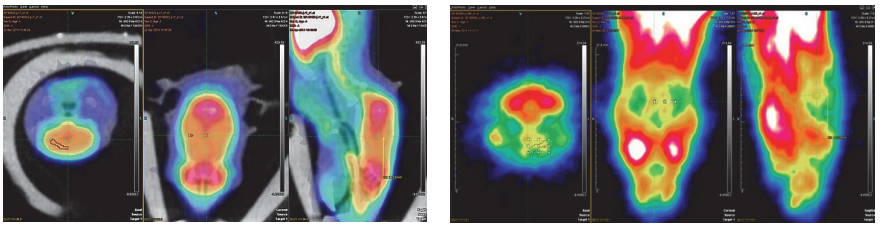

Normal group Alzheimer's disease group

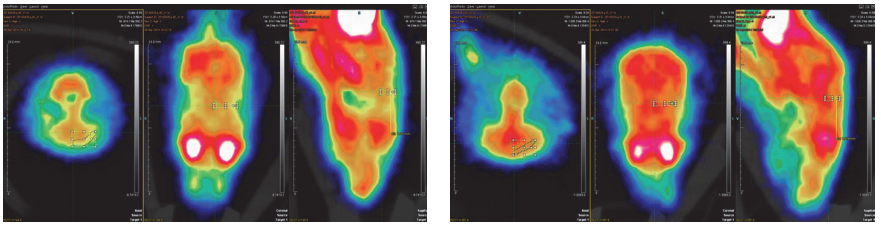

Electroacupuncture group Musical electroacupuncture group

(b)

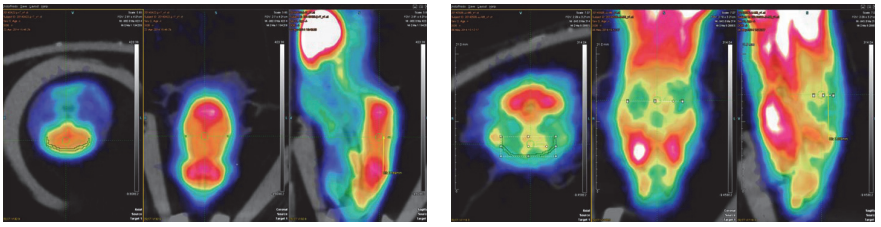

Normal group Alzheimer's disease group

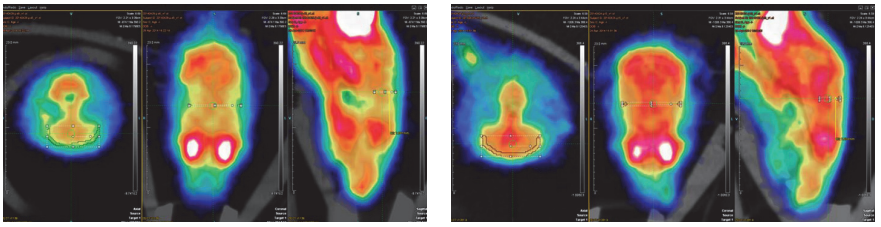

Electroacupuncture group Musical electroacupuncture group

(c)

Figure 4: (a) The micro-PET images of the frontal lobe. (b) The micro-PET images of the hippocampus. (c) The micro-PET images of the cerebral cortex.

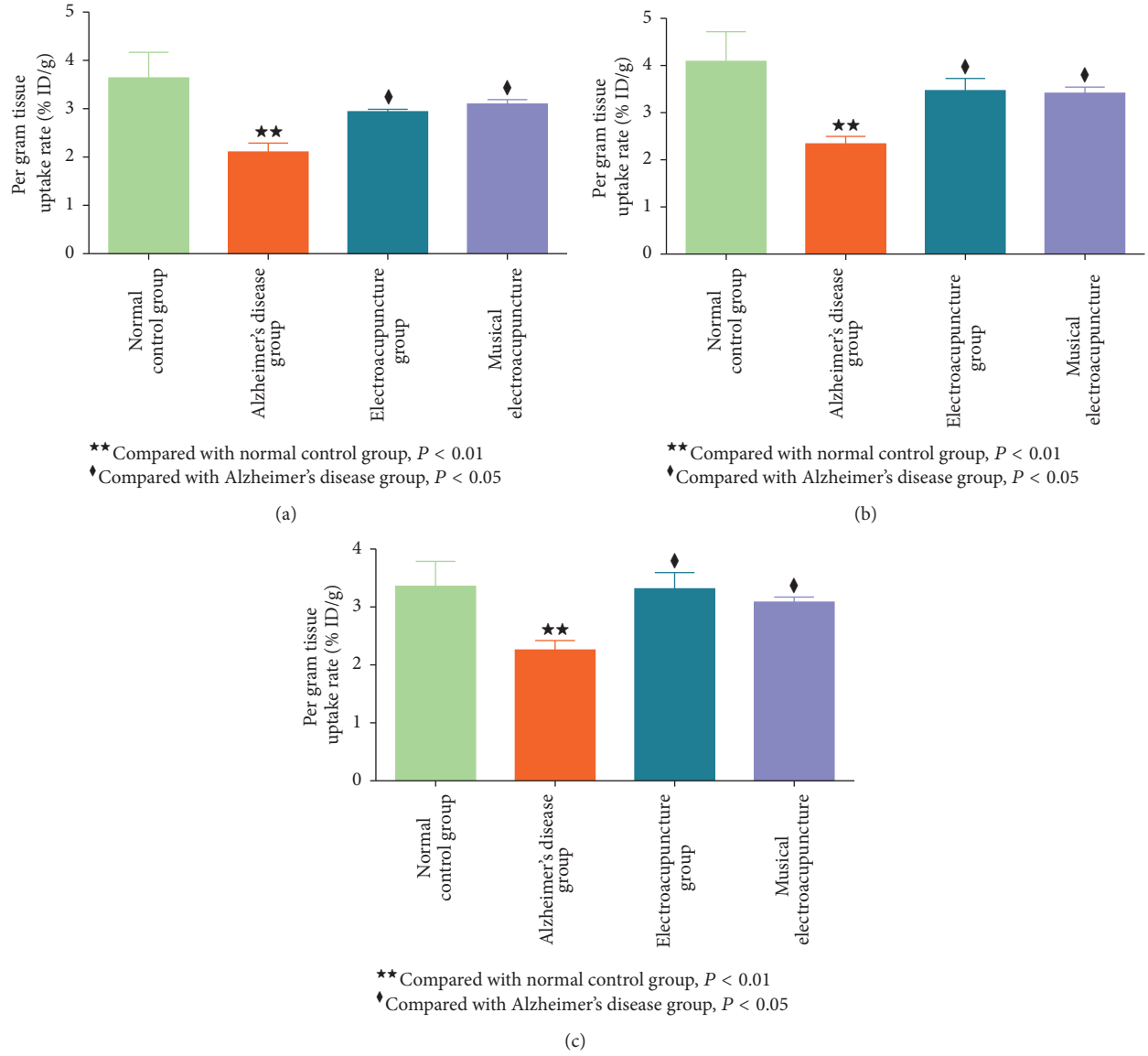

Figure 5: (a) The uptake rate of ^{18}F-FDG per gram in the frontal lobe of each group. (b) The uptake rate of ^{18}F-FDG per gram in the hippocampus of each group. (c) The uptake rate of ^{18}F-FDG per gram in the cerebral cortex of each group.

progressive degeneration are maintained [15]. In the recent ten years, increasing evidence suggests that proper music formulation could improve AD symptoms [16–21], especially for mild cases [22].

Besides, since music therapy is nonpharmacological, it is often used in combination with other therapies. Interestingly, a research on cerebral palsy combined acupuncture treatment and music therapy. Interestingly, the combined therapy showed improved outcome compared with monotherapies [23].

Therefore, in this research, we introduced musical electroacupuncture for AD treatment. Musical electroacupuncture (MEA) combines music therapy and electroacupuncture; during symptomatic selection of music, the sound wave could be turned into a pulse current [24]. Therefore, the effects of MEA on the human auditory organ and acupoints were separately assessed. Specifically, the fundamental characteristics and advantages included two aspects: music therapy and irregular pulse current [7].

Electroacupuncture (EA) is widely used in clinical practice and research and in experimental investigations into the mechanisms of acupuncture [25]. This therapy has been applied for AD treatment and could improve the cognitive function [26] and brain energy metabolism [5, 27]. Therefore, EA is considered an effective therapeutic intervention for AD [28]. However, the concept of *EA tolerance* had been demonstrated three decades ago [29]. The mechanism of *EA tolerance* is that the central nervous system releases analgesic

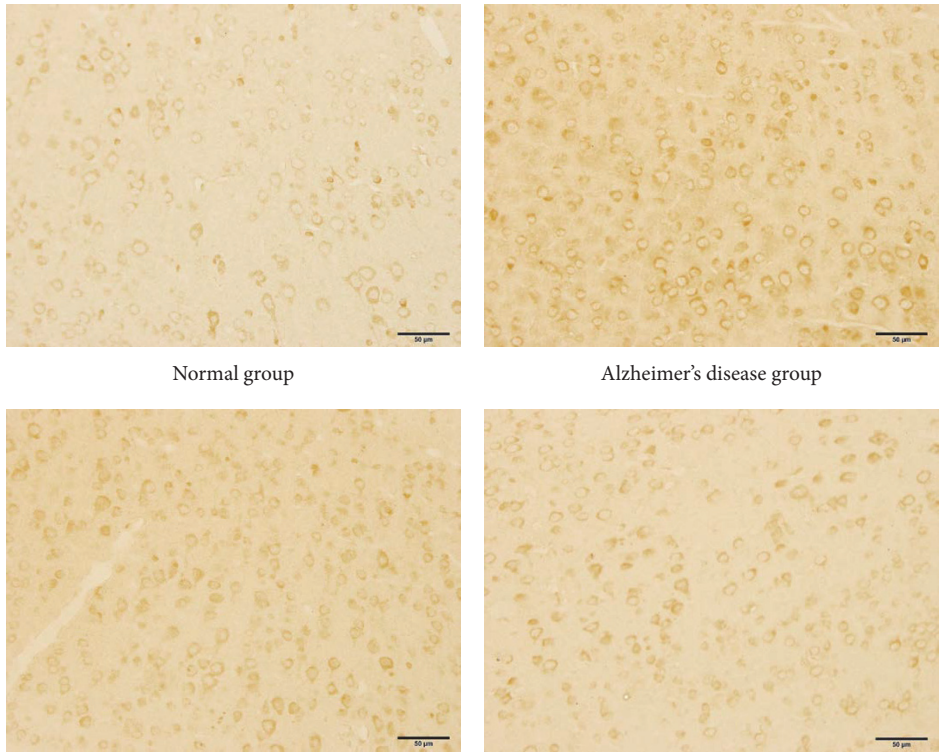

Figure 6: The IHC images of frontal lobe.

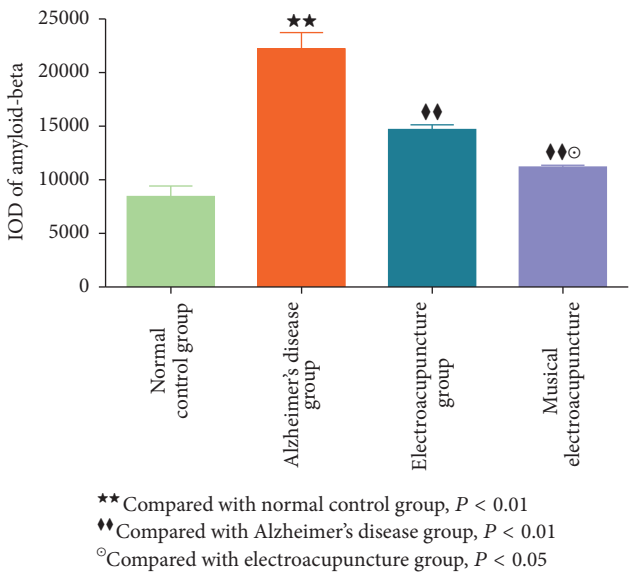

Figure 7: The IOD of amyloid-beta in frontal lobe of each group.

substances (including brain norepinephrine and endogenous antiopioid substances) as well as large amounts of endogenous monoamine. Among them, cholecystokinin octapeptide (CCK-8) is by far the most recognized antiopioid contributing to *EA tolerance* [30], which is caused by long-term use of the same frequency in EA. Since AD treatment requires a long-term course, it likely results in *EA tolerance* [31]. Therefore, we assessed MEA in this study for AD treatment. MEA therapy was full of Chinese characteristic musical therapy. It transformed musical rhythms into constantly changing frequencies and waveforms to overcome the shortcomings of human body's tolerance of general electroacupuncture. Meanwhile, patients were allowed to listen to relieving music, which plays a role of music therapy [32]. MEA therapy is not novel in Chinese clinical and fundamental research. It was shown that such therapy performs better than traditional electroacupuncture in relieving pains [33], improving the symptoms of dermatosis (urticarial disease [34], chloasma [35]), alleviating nervous system diseases such as depression [36–38], insomnia [39], and anxiety [40, 41]. However, there was seldom research on dementia. Therefore, introducing this therapy for Alzheimer's disease constitutes an innovation.

4.3. Difference between MEA and EA in the Frontal Lobe of SAMP8 Mice. Studies assessing the pathogenesis of AD are currently more focused on the temporal lobe, parietal cortex, and hippocampus, with few analyzing changes in the frontal lobe [42]. Recent studies found that transgenic mice with Alzheimer's disease show early cognitive decline related to frontal atrophy, with the changes taking place even earlier than in the hippocampus [43].

As shown above, although the MEA therapy performed better than EA in the Morris water maze test, differences were not statistically significant. In micro-PET, EA therapy showed higher glucose metabolism improvement in the hippocampus

and cerebral cortex compared with MEA. Only in the frontal lobe, MEA therapy was better than EA, but the difference was not significant. These findings prompted the question whether MEA therapy was more inclined to play a role in the frontal lobe.

To address this, amyloid-beta levels were assessed in the frontal lobe of SAMP8 mice, and the results confirmed the above notion. Comparing the different therapies in IOD of amyloid-beta in the frontal lobe, MEA therapy performed significantly better than EA ($P < 0.05$). Therefore, MEA indeed is inclined to play a role in the frontal lobe.

5. Conclusions

Using behavioral tests, *in vivo* imaging, and protein detection, the differences between MEA and EA therapy for AD treatment were assessed in SAMP8 mice. Interestingly, both EA and MEA could improve spatial learning and memory ability, improving glucose metabolism in different brain regions and amyloid-beta expression in the frontal lobe. What is more, the MEA therapy performed better than EA in decreasing amyloid-beta amounts in the frontal lobe. However, further studies are required to further explain this phenomenon.

Competing Interests

The authors declare that there is no conflict of interests regarding the publication of this paper.

Acknowledgments

This research was supported by the *National Natural Science Foundation of China* (no. 81273825).

References

[1] C. Ballard, S. Gauthier, A. Corbett, C. Brayne, D. Aarsland, and E. Jones, "Alzheimer's disease," *The Lancet*, vol. 377, no. 9770, pp. 1019–1031, 2011.

[2] V. H. Finder, "Alzheimer's disease: a general introduction and pathomechanism," *Journal of Alzheimer's Disease*, vol. 22, no. 3, pp. S5–S19, 2010.

[3] A. Tarroun, M. Bonnefoy, J. Bouffard-Vercelli, C. Gedeon, B. Vallee, and F. Cotton, "Could linear MRI measurements of hippocampus differentiate normal brain aging in elderly persons from Alzheimer disease?" *Surgical and Radiologic Anatomy*, vol. 29, no. 1, pp. 77–81, 2007.

[4] D. G. Harwood, D. L. Sultzer, D. Feil, L. Monserratt, E. Freedman, and M. A. Mandelkern, "Frontal lobe hypometabolism and impaired insight in Alzheimer disease," *American Journal of Geriatric Psychiatry*, vol. 13, no. 11, pp. 934–941, 2005.

[5] J. Jiang, K. Gao, Y. Zhou et al., "Electroacupuncture treatment improves learning-memory ability and brain glucose metabolism in a mouse model of Alzheimer's disease: using Morris water maze and micro-PET," *Evidence-Based Complementary and Alternative Medicine*, vol. 2015, Article ID 142129, 7 pages, 2015.

[6] C.-H. Li, C.-K. Liu, Y.-H. Yang, M.-C. Chou, C.-H. Chen, and C.-L. Lai, "Adjunct effect of music therapy on cognition in Alzheimer's disease in Taiwan: a pilot study," *Neuropsychiatric Disease and Treatment*, vol. 11, pp. 291–296, 2015.

[7] W. Fan, X. Chunlan, D. Guirong, and D. Hongsheng, "Music acupuncture therapy research status and prospects," *Journal of Chinese Acupuncture-Moxibustion*, vol. 12, pp. 1247–1250, 2014.

[8] J. E. Morley, H. J. Armbrecht, S. A. Farr, and V. B. Kumar, "The senescence accelerated mouse (SAMP8) as a model for oxidative stress and Alzheimer's disease," *Biochimica et Biophysica Acta—Molecular Basis of Disease*, vol. 1822, no. 5, pp. 650–656, 2012.

[9] K. Bromley-Brits, Y. Deng, and W. Song, "Morris Water Maze test for learning and memory deficits in Alzheimer's disease model mice," *Journal of Visualized Experiments*, no. 53, Article ID e2920, 2011.

[10] D. A. Butterfield and H. F. Poon, "The senescence-accelerated prone mouse (SAMP8): a model of age-related cognitive decline with relevance to alterations of the gene expression and protein abnormalities in Alzheimer's disease," *Experimental Gerontology*, vol. 40, no. 10, pp. 774–783, 2005.

[11] J. F. Flood and J. E. Morley, "Learning and memory in the SAMP8 mouse," *Neuroscience and Biobehavioral Reviews*, vol. 22, no. 1, pp. 1–20, 1997.

[12] M. Pallas, A. Camins, M. A. Smith, G. Perry, H.-G. Lee, and G. Casadesus, "From aging to Alzheimer's disease: unveiling 'The switch' with the senescence-accelerated mouse model (SAMP8)," *Journal of Alzheimer's Disease*, vol. 15, no. 4, pp. 615–624, 2008.

[13] G. Li, X. Zhang, H. Cheng et al., "Acupuncture improves cognitive deficits and increases neuron density of the hippocampus in middle-aged SAMP8 mice," *Acupuncture in Medicine*, vol. 30, no. 4, pp. 339–345, 2012.

[14] N. J. Glynn, "The music therapy assessment tool in Alzheimer's patients," *Journal of Gerontological Nursing*, vol. 18, no. 1, pp. 3–9, 1992.

[15] D. Aldridge, "Alzheimer's Disease: rhythm, timing and music as therapy," *Biomedicine and Pharmacotherapy*, vol. 48, no. 7, pp. 275–281, 1994.

[16] M. Satoh, T. Yuba, K. Tabei et al., "Music therapy using singing training improves psychomotor speed in patients with Alzheimer's disease: a neuropsychological and fMRI study," *Dementia and Geriatric Cognitive Disorders Extra*, vol. 5, no. 3, pp. 296–308, 2015.

[17] G. E. Lancioni, M. F. O'Reilly, N. N. Singh et al., "Assessing the impact and social perception of self-regulated music stimulation with patients with Alzheimer's disease," *Research in Developmental Disabilities*, vol. 34, no. 1, pp. 139–146, 2013.

[18] J. J. M. Garćia, R. Iodice, J. Carro, J. Sánchez, F. Palmero, and A. M. Mateos, "Improvement of autobiographic memory recovery by means of sad music in Alzheimer's disease type dementia," *Aging Clinical and Experimental Research*, vol. 24, no. 3, pp. 227–232, 2012.

[19] H. Fukui, A. Arai, and K. Toyoshima, "Efficacy of music therapy in treatment for the patients with Alzheimer's disease," *International Journal of Alzheimer's Disease*, vol. 2012, Article ID 531646, 6 pages, 2012.

[20] J. Witzke, R. A. Rhone, D. Backhaus, and N. A. Shaver, "How sweet the sound: research evidence for the use of music in Alzheimer's dementia," *Journal of Gerontological Nursing*, vol. 34, no. 10, pp. 45–52, 2008.

[21] H. B. Svansdottir and J. Snaedal, "Music therapy in moderate and severe dementia of Alzheimer's type: A Case-Control

Study," *International Psychogeriatrics*, vol. 18, no. 4, pp. 613–621, 2006.

[22] M. Irish, C. J. Cunningham, J. B. Walsh et al., "Investigating the enhancing effect of music on autobiographical memory in mild Alzheimer's disease," *Dementia and Geriatric Cognitive Disorders*, vol. 22, no. 1, pp. 108–120, 2006.

[23] H.-B. Yu, Y.-F. Liu, and L.-X. Wu, "Acupuncture combined with music therapy for treatment of 30 cases of cerebral palsy," *Journal of Traditional Chinese Medicine*, vol. 29, no. 4, pp. 243–248, 2009.

[24] Z. Jin, Z. Yihong, and B. Yan, "Research of musical eletro-acupuncture," *Chinese Acu-Mox*, vol. 8, pp. 585–588, 2005.

[25] D. Mayor, "An exploratory review of the electroacupuncture literature: clinical applications and endorphin mechanisms," *Acupuncture in Medicine*, vol. 31, no. 4, pp. 409–415, 2013.

[26] W. Dong, W. Guo, X. Zheng et al., "Electroacupuncture improves cognitive deficits associated with AMPK activation in SAMP8 mice," *Metabolic Brain Disease*, vol. 30, no. 3, pp. 777–784, 2015.

[27] W. Dong, W. Guo, F. Wang et al., "Electroacupuncture upregulates SIRT1-dependent PGC-1α expression in SAMP8 Mice," *Medical Science Monitor*, vol. 21, pp. 3356–3362, 2015.

[28] F. Wang, H. Zhong, X. Li et al., "Electroacupuncture attenuates reference memory impairment associated with astrocytic NDRG2 suppression in APP/PS1 transgenic mice," *Molecular Neurobiology*, vol. 50, no. 2, pp. 305–313, 2014.

[29] J. S. Han, X. Z. Ding, and S. G. Fan, "Cholecystokinin octapeptide (CCK-8): antagonism to electroacupuncture analgesia and a possible role in electroacupuncture tolerance," *Pain*, vol. 27, no. 1, pp. 101–115, 1986.

[30] J.-T. Bian, M.-Z. Sun, and J.-S. Han, "Reversal of electroacupuncture tolerance by cck-8 antiserum: an electrophysiological study on pain-related neurons in nucleus parafascicularis of the rat," *International Journal of Neuroscience*, vol. 72, no. 1-2, pp. 15–29, 1993.

[31] L. Mei, S. F. Pu, and J. S. Han, "Effect of electroacupuncture tolerance by different frequencies on the opioid inhibition to cardiovascular activity in the spinal cord of rats," *Neuropeptides*, vol. 26, no. 4, pp. 221–224, 1994.

[32] W. Canhua, B. Shengzhao, H. Yangming, and X. Wenwen, "Embedded music electro-acupuncture instrument design and efficacy evaluation prescription," *Modernization of Traditional Chinese Medicine and Material Medical*, no. 10, pp. 2278–2281, 2014.

[33] D. Hongsheng, P. Hao, and D. Guirong, "Comparative research of music electro-acupuncture and pulse electro-acupuncture in analgesic effect," *Acupuncture Research*, vol. 02, pp. 83–87, 2005.

[34] Z. Jing, Y. Taipeng, Y. Cong, W. Mei, and Yan, "Clinical observation of musical electro-acupuncture treatment of chronic urticaria (35 cases)," *Medicine of Harbin*, vol. 02, pp. 48–49, 2010.

[35] M. Cheng, X. Yue, and Z. Zhenkun, "Clinical observation of 120 cases of chloasma treated by musical electro-acupuncture," *Chinese Primary Health Care*, vol. 07, pp. 81–82, 2007.

[36] T. Yinshan, J. Qian, C. Jin et al., "Musical EA and pulse EA of the chronic stress depression rats in different brain regions monoamine neurotransmitter expression," *Journal of Clinical Acupuncture*, vol. 03, pp. 52–55, 2014.

[37] Y. Fang, F. Fuzhen, and L. Jinying, "Comparison of the efficacy of pulse EA and musical EA in depressive patients with gastrointestinal symptoms after stroke," *Journary of Nanjing University of Traditional Chinese Medicine*, vol. 03, pp. 225–228, 2014.

[38] J. Qian, M. Xuhui, T. Yinshan, D. Xiaofeng, and L. Zhigang, "Music EA and pulse EA against acts of Chronic Stress Depression Rats and hippocampal astrocytes influence," *CJTCMP*, vol. 03, pp. 648–651, 2013.

[39] X. Jing, *Clinical study music electro-acupuncture treatment of insomnia [M.S. thesis]*, Heilongjiang College of Chinese Medicien, 2013.

[40] Z. Hong, Z. Zheng, and D. Hong, "Music electro-acupuncture treatment of anxiety 157 cases," *Journal of Shanghai Acupuncture-Moxibustion*, vol. 1, pp. 22–23, 2002.

[41] H. Shuxia, L. Guizhen, and L. Mingxia, "Efficacy of plus psychological counseling treating anxiety musical EA," *Journary of Rehabilitation and Wellness*, vol. 4, pp. 160–162, 1994.

[42] I. D. Ionov, "Specific mechanism for blood inflow stimulation in brain area prone to Alzheimer's disease lesions," *International Journal of Neuroscience*, vol. 117, no. 10, pp. 1425–1442, 2007.

[43] A. Herrero-San Martin, A. Villarejo-Galende, A. Rábano-Gutiérrez, C. Guerrero-Márquez, J. Porta-Etessam, and F. Bermejo-Pareja, "Frontal variant of Alzheimer's disease. Two pathologically confirmed cases and a literature review," *Revista de Neurologia*, vol. 57, no. 12, pp. 542–548, 2013.

Hindawi Publishing Corporation
Neural Plasticity
Volume 2016, Article ID 6521026, 11 pages
http://dx.doi.org/10.1155/2016/6521026

Research Article

Electroacupuncture Reduces the Effects of Acute Noxious Stimulation on the Electrical Activity of Pain-Related Neurons in the Hippocampus of Control and Neuropathic Pain Rats

Jun-Ying Wang,[1,2] Renbo Chen,[3] Shu-Ping Chen,[1] Yong-Hui Gao,[1] Jian-Liang Zhang,[1] Xiu-Mei Feng,[1] Yaxia Yan,[1] Jun-Ling Liu,[1] Ingrid Gaischek,[2] Daniela Litscher,[2] Lu Wang,[2] Irmgard Th. Lippe,[4] and Gerhard Litscher[1,2]

[1] *Department of Physiology, Institute of Acupuncture and Moxibustion, China Academy of Chinese Medical Sciences, Beijing 100700, China*
[2] *Research Unit for Complementary and Integrative Laser Medicine, Research Unit of Biomedical Engineering in Anesthesia and Intensive Care Medicine, and TCM Research Center Graz, Medical University of Graz, 8036 Graz, Austria*
[3] *Department of Chronic Diseases, Institute of Basic Research in Clinical Medicine, China Academy of Chinese Medical Sciences, Beijing 100700, China*
[4] *Institute of Experimental and Clinical Pharmacology, Medical University of Graz, 8036 Graz, Austria*

Correspondence should be addressed to Jun-Ling Liu; 13521898023@163.com
and Gerhard Litscher; gerhard.litscher@medunigraz.at

Received 12 April 2016; Revised 29 July 2016; Accepted 27 September 2016

Academic Editor: Stuart C. Mangel

Copyright © 2016 Jun-Ying Wang et al. This is an open access article distributed under the Creative Commons Attribution License, which permits unrestricted use, distribution, and reproduction in any medium, provided the original work is properly cited.

To study the effects of acupuncture analgesia on the hippocampus, we observed the effects of electroacupuncture (EA) and mitogen-activated protein kinase (MEK) inhibitor on pain-excited neurons (PENs) and pain-inhibited neurons (PINs) in the hippocampal area CA1 of sham or chronic constrictive injury (CCI) rats. The animals were randomly divided into a control, a CCI, and a U0126 (MEK1/2 inhibitor) group. In all experiments, we briefly (10-second duration) stimulated the sciatic nerve electrically and recorded the firing rates of PENs and PINs. The results showed that in both sham and CCI rats brief sciatic nerve stimulation significantly increased the electrical activity of PENs and markedly decreased the electrical activity of PINs. These effects were significantly greater in CCI rats compared to sham rats. EA treatment reduced the effects of the noxious stimulus on PENs and PINs in both sham and CCI rats. The effects of EA treatment could be inhibited by U0126 in sham-operated rats. The results suggest that EA reduces effects of acute sciatic nerve stimulation on PENs and PINs in the CA1 region of the hippocampus of both sham and CCI rats and that the ERK (extracellular regulated kinase) signaling pathway is involved in the modulation of EA analgesia.

1. Introduction

Peripheral nerve injuries produce acute pain and often induce neuropathic pain, a severe clinical problem and chronic debilitating condition that affects the nervous system. Neuropathic pain is relatively common and impairs the quality of life of sufferers. In the past few decades, neuropathic pain animal models have been used to study pain mechanisms and analgesia effects. Chronic constrictive injury (CCI) has been the common neuropathic pain model since 1988 [1, 2].

The hippocampus, a part of the limbic system, has the function of learning, memory, emotion, and affect and also has relationships with chronic and acute pain. It has been reported that hippocampal formation plays an important role in pain information processing, including anatomical features, behavioral experiments, electrophysiology, functional imaging, and other molecular research [3]. Humans suffering from chronic or severe pain had smaller hippocampal volumes. Hippocampal N-acetylaspartate/creatine decreased in elderly patients suffering from acute pain [4, 5]. Neuropathic pain induced hippocampal interleukin-1 beta (IL-1β) mRNA levels upregulation, and the changes of IL-1β mRNA expression correlated with the injured side of the hippocampus [6]. Xiao et al. [7], Yang et al. [8], and Li et al. [9]

reported in a series of studies that acetylcholine (ACh) influences the pain-induced discharge frequency and the electric activities of pain-related neurons in the hippocampus of rats.

Acupuncture has been widely applied in China and other Asian countries for thousands of years to ameliorate a number of diseases, including acute and chronic pain. Acupuncture analgesia has been gradually accepted by people due to its advantages, but its mechanism has not yet been clarified in detail. Mounting evidence from many laboratories over the past years suggests that acupuncture has effects on the hippocampus. Traditional acupuncture treatments significantly decreased functional magnetic resonance imaging (fMRI) signals [10] and the metabolism in the hippocampus [11]; 2 Hz electrical acupoint stimulation-induced analgesia has negative correlations with the averaged fMRI activation levels of the bilateral hippocampus [12]. Electroacupuncture (EA) could modulate the function of interneurons in the hippocampus, significantly enhancing long-term potentiation (LTP) [13]. In some of our previous studies, chronic pain had an effect on the hippocampal cholinergic system, and EA treatment relieved pain by regulating hippocampal cholinergic neurons [14]. EA had an obvious analgesic effect and in CCI rats significantly diminished the injury-induced increase in synaptic cleft width and thinning of the postsynaptic density [15, 16]. It also activated the extracellular regulated protein kinases (ERK) signaling pathway in the hippocampus [17]. Previous studies suggested that ERK/mitogen-activated protein kinase (MEK) play an essential role in neuropathic pain [18]. In the spinal cord, CCI-induced neuropathic pain activated the ERK- and cAMP-response element binding protein (CREB) signaling pathway [19]. However, it remains largely unknown how the ERK is involved in pain modulation in the hippocampus.

On the basis of these studies, the objective of this research is to investigate the effects of EA and the ERK signaling pathway on the acute pain-induced responses of pain-related neurons in the hippocampus of Wistar rats under both control and neuropathic pain conditions.

2. Materials and Methods

2.1. Animals and Groups. Adult male Wistar rats, weighing from 220 g to 280 g ($n = 43$), purchased from Beijing Union Medical College, were acclimatized to standard laboratory conditions (12-hour light and dark cycle) at the Beijing Acupuncture and Moxibustion Institute for a week and given free access to standard chow pellet diet and water. The rats were randomly divided into three groups: (1) sham/control group: $n = 15$ (sham-operated rats); (2) CCI group, $n = 13$; (3) U0126 (ERK1/2 inhibitor) group, $n = 15$; U0126 (2.26 μL, 10 μg) was injected to the rats. With the automatic injector, the liquid was intracerebroventricularly (i.c.v.) administered within 2 min. All surgical interventions and postoperative animal care were performed in accordance with the Guidelines for Declaration of the National Institutes of Health *Guide for the Care and Use of Laboratory Animals* (publication number 80-23, revised 1996).

2.2. Tracheal Intubation and Chronic Constrictive Injury. The rats were anesthetized by a mixture of a solution of urethane (28 mg/100 g) plus chloralose (3.3 mg/100 g). Rectal body temperature was monitored throughout the experiment, and a heating pad was used to maintain the temperature of the animals at 37.0°C ± 0.5°C.

The rats were fixed on the back and the hair on the neck was shaved. The trachea was exposed by blunt dissection through neck muscles after cutting off the neck skin above the manubrium. A T-shaped incision was sheared at the bottom of the thyroid isthmus, and then tracheal intubation was performed using special intubation designed by the laboratory of the Institute of Acupuncture and Moxibustion. In the prone position, the left sciatic nerve was isolated (the chronic constrictive injured nerve in the CCI group) and covered with liquid paraffin.

As described by Bennett and Xie [2], CCI was used as the neuropathic pain model. The left sciatic nerve was exposed and tied around four times by gut suture. The sciatic nerve in the sham group was exposed but not tied. Local application of antibiotics (sodium penicillin, 9000–10000 U/rat) was used to avoid postoperative infection. All models were established by the same experimenter to avoid experimental variability. The electrophysiological experiments were carried out 12 days after the operation.

2.3. Recording Neuronal Discharge. The rats were anesthetized by a mixture of urethane (28 mg/100 g) and chloralose (3.3 mg/100 g). The head of the rat was fixed on the stereotaxic apparatus (SR-6R, Nihon Kohden, Tokyo, Japan). With the aid of the stereotaxic atlas of the rat brain, two small skull windows were opened and covered with warm liquid paraffin at the positions for inserting recording electrodes and microsyringe (KDS-310-PLUS, KD Scientific, Holliston, MA, USA). A glass microelectrode (5 MΩ, filled with 3 mol/L KCl) was inserted into the right hippocampal CA1 area (AP: 3.2–3.6 mm; ML: 2.5–3.0 mm; DV: 2.5–3.2 mm) by a micromanipulator (SM-21, Nihon Kohden, Tokyo, Japan) as recording electrode [20]. Another micromanipulator was used to insert the microsyringe into the lateral ventricle (AP: 1.0 mm; ML: 1.3–2.0 mm; DV: 3.0 mm) [21] to inject the experimental drug (MEK1/2 inhibitor). The neuronal discharges were monitored by an oscilloscope (VC-10, Nihon Kohden, Tokyo, Japan) at the same time. After recording spontaneous neural discharge for 5 min as control, the sciatic nerve was stimulated by a double stainless electrode (delay 0, interval 50 msec, duration 0.3 msec, and current intensity 5 mA) for 10 s as noxious stimulation. If there was no change in the neural discharge after noxious stimulation, the neural discharges were not recorded anymore. When the discharge frequency returned to control level (about 10 min after giving the noxious stimulation), the sciatic nerve was given another noxious stimulation for 10 s. At the end of noxious stimulation, bilateral "Zusanli" (ST36) and "Yanglingquan" (GB34) acupoints were punctured with stainless-steel acupuncture needles (gauge 28, 0.20 mm in diameter) to a depth of about 4 mm, respectively, and stimulated electrically using a HANS EA Stimulator for 1 min, and U0126 was administered intracerebroventricularly for 2 min at the

same time. "Zusanli" (ST36) and "Yanglingquan" (GB34) are the main points for treating sciatica and other types of leg pain according to the theory of traditional Chinese medicine. Our previous results also suggested that EA at "Zusanli" (ST36) and "Yanglingquan" (GB34) has cumulative analgesic effects for neuropathic pain [14–17]. The complete recording duration was about 30 min.

2.4. Definition of Neurons. The response of the neurons to noxious stimuli can have three forms: excitement, inhibition, and no response. Neurons that respond to nociceptive stimulation are defined as pain-related neurons, neurons excited after noxious stimuli are called pain-excited neurons (PENs) [22], and the inhibited neurons are defined as pain-inhibited neurons (PINs) [23]. The discharge frequencies before the noxious stimulus served as control (corresponding to 100%) to observe the changes of discharge frequencies of pain-related neurons. We analyzed the electrical activities of pain-related neurons whose discharge frequencies increased or decreased by more than 20% after noxious stimuli.

2.5. Statistical Analysis. The experimental data were scanned on a computer with Spike II (CED Instruments, Cambridge, United Kingdom) after management and analyzed with Spike II software. All data were expressed as mean ± SEM (standard error of the mean). Statistical differences were evaluated by one-way ANOVA. Significance was determined at the level of $P < 0.05$.

3. Results

29 pain-related neurons were recorded in the control group ($n = 15$). The electric activities of 17 PENs (58.6%) were increased while those of 12 PINs (41.4%) were decreased after noxious stimuli. In the CCI group ($n = 13$), we recorded 18 pain-related neurons, 14 of which were PENs (78%) and 4 were PINs (22%), so the number of recorded PINs in the control group was larger than in the CCI group. The U0126 group ($n = 15$) showed 15 pain-related neurons, among which there were 9 PENs (60%) and 6 PINs (40%).

3.1. EA Regulated the Effects of Acute Noxious Stimulation on the Firing Rates of Pain-Related Neurons in the Hippocampus of Sham Rats. In sham rats, brief sciatic nerve stimulation significantly increased the electrical activities of 17 hippocampal PENs in the control group (134.53 ± 18.50%) and EA group (126.1 ± 8.97%), and there was no difference between the two groups ($P > 0.05$, Figure 1(c)). EA reduced the excitatory effects of brief sciatic nerve stimulation on the firing rates of 17 PENs. At 2 min after the noxious stimuli, the discharge frequency changes of hippocampal PENs in the EA group (121.18 ± 7.45%) were markedly lower than those in the control group (168.68 ± 10.64%, $P < 0.05$). At 4 min after the noxious stimuli, although the firing rates of hippocampal PENs in the control group (145.08 ± 7.22%) were still increased, the firing rates of hippocampal PENs in the EA group (108.65 ± 4.48%) had almost returned to normal level. No significant difference was found between the control group (116.86 ± 8.21%, 103.22 ± 2.13%) and the EA group (102.14 ± 6.03%, 97.65 ± 4.12%) at 8 and 10 min after the noxious stimuli. The electric activities of PENs in the control group almost returned to normal level at 8 min after the noxious stimuli. It is suggested that EA played an inhibiting role in regulating excitatory effects of the acute noxious stimulus on the electrical activity of PENs in sham rats.

The electric activities of 12 hippocampal PINs were decreased by the brief sciatic nerve stimulation in sham rats (Figure 1(d)), and the frequency changes in the control group were larger than those in the EA group. At 0 minutes (immediately) after brief sciatic nerve stimulation, the firing rates in the control group (67.88% ± 6.00) were lower than those in the EA group (93.35% ± 6.46, $P < 0.05$). The frequencies of PINs in the control group were still decreased at 2 min (54.35% ± 4.97), 4 min (53.01% ± 6.12), and 6 min (67.93% ± 7.64) and returned to normal level at 10 min (94.96% ± 6.11) after the stimulation. The frequencies of PINs in the EA group were still at a low level at 2 min (74.36% ± 6.28) and 4 min (87.37% ± 3.78) and returned to normal level at 6 min (100.59% ± 8.80), earlier than in the control group. In comparison with the control group, the frequency changes of PINs in the EA group were higher ($P < 0.05$) at 2, 4, and 6 min after giving the noxious stimuli. Those findings suggested that EA played an exciting role in regulating inhibitory effects of the acute noxious stimulus on the electrical activity of PINs in sham rats.

3.2. EA Regulated the Effects of Acute Noxious Stimulation on the Firing Rates of Pain-Related Neurons in the Hippocampus of CCI Rats. The electric activities of 14 hippocampal PENs reached 216.46±25.40% in the CCI group and 219.57±44.15% in the CCI + EA group after the noxious stimulus. There was no significant difference between the two groups ($P > 0.05$, Figure 2(c)) of CCI rats. Similar to the sham rats, the discharge frequencies of 14 PENs were decreased after EA treatment. The frequency changes of hippocampal PENs in the CCI group (193.54 ± 21.50%) were markedly higher than those in the CCI + EA group (139.40% ± 12.78, $P < 0.05$) at 2 min after the noxious stimuli. The firing rates of PENs in the CCI + EA group (116.99% ± 20.90) returned to normal level and were observably lower than those in the CCI group (188.82% ± 16.16, $P < 0.05$) at 6 min. The frequency changes of PENs in the CCI + EA group were 105.87% ± 13.26 and 99.58% ± 9.06 at 8 min and 10 min after the brief sciatic nerve stimulation, which are lower than those in the CCI group (167.27% ± 14.86, 148.82% ± 20.71, $P < 0.05$). It is suggested that EA treatment also reduced the excitatory effects of brief nerve stimulation on the firing rate of PENs in CCI rats.

The discharge frequencies of 4 hippocampal PINs were decreased significantly in both the CCI (56.44% ± 8.68) and the CCI + EA (68.27% ± 7.96) group after brief sciatic nerve stimulation (Figure 2(d)). There was no significant difference between the two groups at 0, 2, and 4 min. At 6 min after giving the noxious stimuli, the frequencies of PINs in the CCI group (59.82% ± 9.57) were still inhibited, and the frequency of PINs in the CCI + EA group (81.40% ± 16.29) had almost returned to normal level. At 8 and 10 min after giving the noxious stimuli, the frequency changes of hippocampal PINs

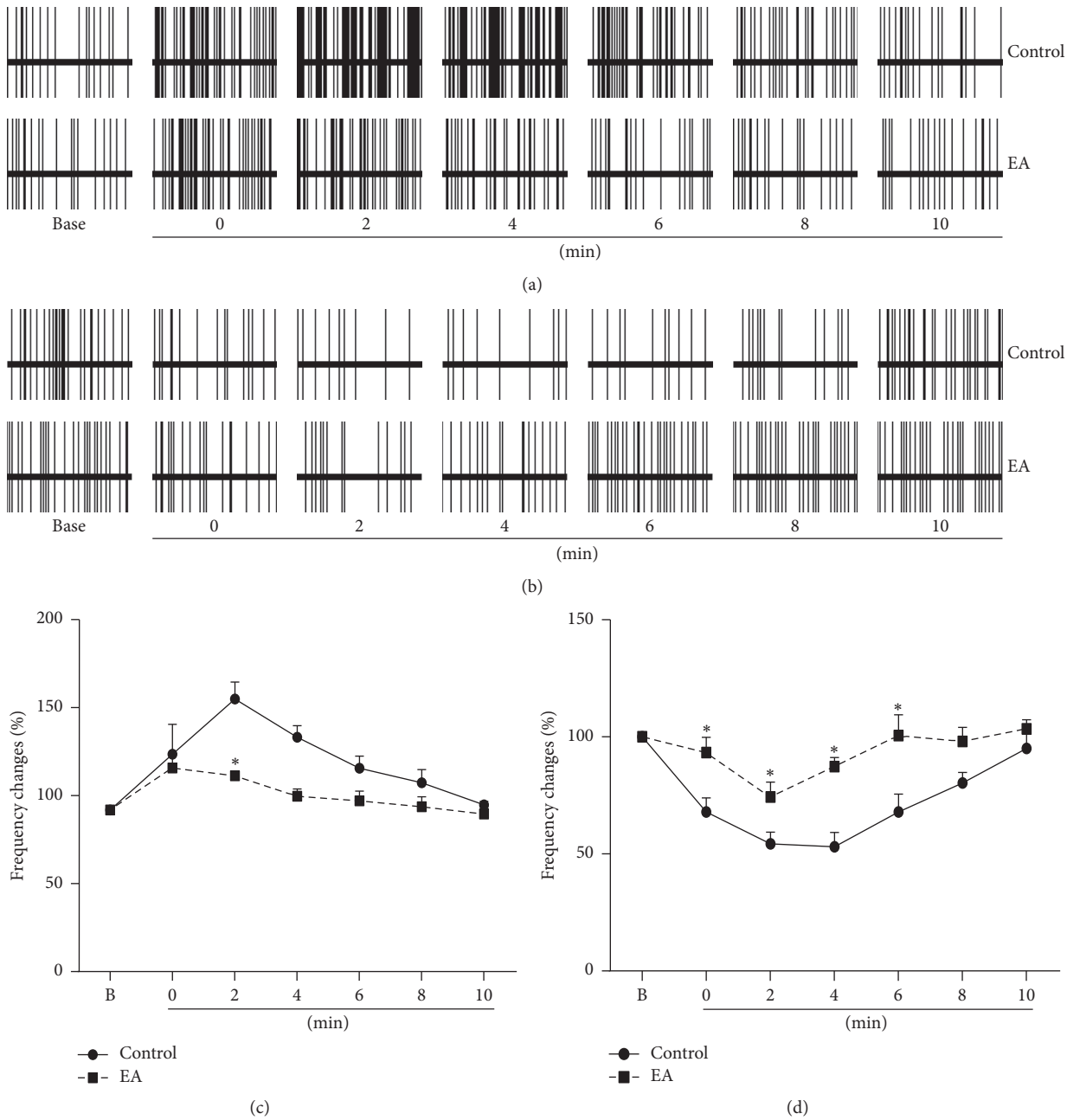

Figure 1: EA reduced the excitatory and inhibitory effects of brief sciatic nerve stimulation on the firing rates of PENs and PINs, respectively, in sham rats. (a) Example of EA reducing the effects of acute noxious stimulation on discharges of hippocampal PENs in the sham group. (b) Example of EA reducing the effects of acute noxious stimulation on discharges of hippocampal PINs in the sham group. (c) EA reduced the effects of acute noxious stimulation on the firing rates of hippocampal PENs ($n = 17$) at different times after the noxious stimuli in sham rats. (d) EA reduced the effects of acute noxious stimulation on the firing rates of hippocampal PINs ($n = 12$) at different times after the noxious stimuli in sham rats. The 10-second stimulation of the sciatic nerve occurred immediately before 0 min, not at 0 min. B on the x-axis stands for the background firing rate before the noxious stimulus. $*$: compared with the control group, $P < 0.05$.

reached 70.65 ± 10.31% and 77.94 ± 2.67%, respectively, in the CCI group; however, the frequencies in the CCI + EA group were still at the normal level (100.30% ± 15.36, 96.69% ± 5.66). The discharge frequency changes of the CCI and the CCI + EA group showed no significant differences at 10 min. Although the number of recorded PINs was small, it is also suggested that EA treatment reduced the effect of brief sciatic nerve stimulation on the frequency of PINs in CCI rats.

3.3. Contrasting the Effect of Acute Noxious Stimulation on Frequency Changes of Pain-Related Neurons between Sham and CCI Rats after Noxious Stimuli and EA Treatment. The discharges of 17 PENs and 12 PINs were recorded in the

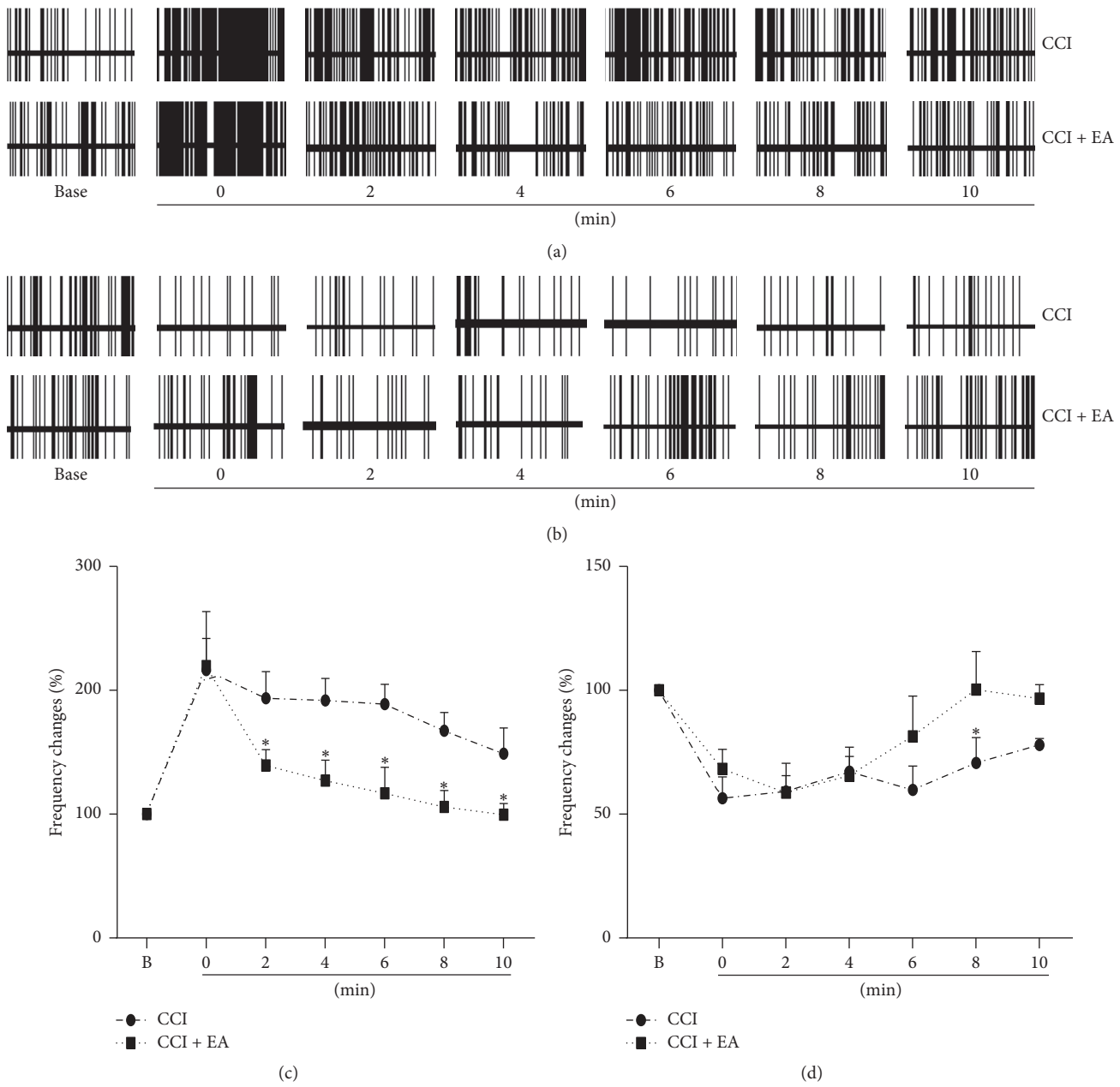

Figure 2: EA reduced the excitatory effects of brief sciatic nerve stimulation on the firing rate of PENs and had a similar reducing effect on PINs in CCI rats. (a) Example of EA reducing the effects of acute noxious stimulation on discharges of hippocampal PENs in CCI rats. (b) Example of EA regulating the effects of acute noxious stimulation on discharges of hippocampal PINs in CCI rats. (c) EA reduced the effects of acute noxious stimulation on the firing rates of hippocampal PENs ($n = 14$) at different times after the noxious stimuli in CCI rats. (d) EA reduced the effects of acute noxious stimulation on the firing rates of hippocampal PINs ($n = 4$) at different times after the noxious stimuli in CCI rats. B on the X-axis stands for the background firing rate before the noxious stimulus. $*$: compared with the CCI group, $P < 0.05$.

hippocampus of 15 sham rats, and those of 14 PENs and 4 PINs were recorded in the CCI rats. At 2 min, there was no difference between sham and CCI rats in the frequency changes ($P > 0.05$, Figure 3(a)); however, brief sciatic nerve stimulation induced bigger frequency changes of PENs in the CCI rats than in the sham rats ($P < 0.05$) from 4 min to 8 min. The discharge frequencies of PENs in the CCI rats were still increased at 10 min, while the discharge frequencies of PENs in the sham rats had almost returned to normal level at 8 min after the acute noxious stimuli.

The discharge frequency changes of PINs in the CCI group were slightly higher than in the control group at 2 and 10 min after the noxious stimuli ($P > 0.05$, Figure 3(b)). This might be associated with the small number of PINs recorded in the CCI group.

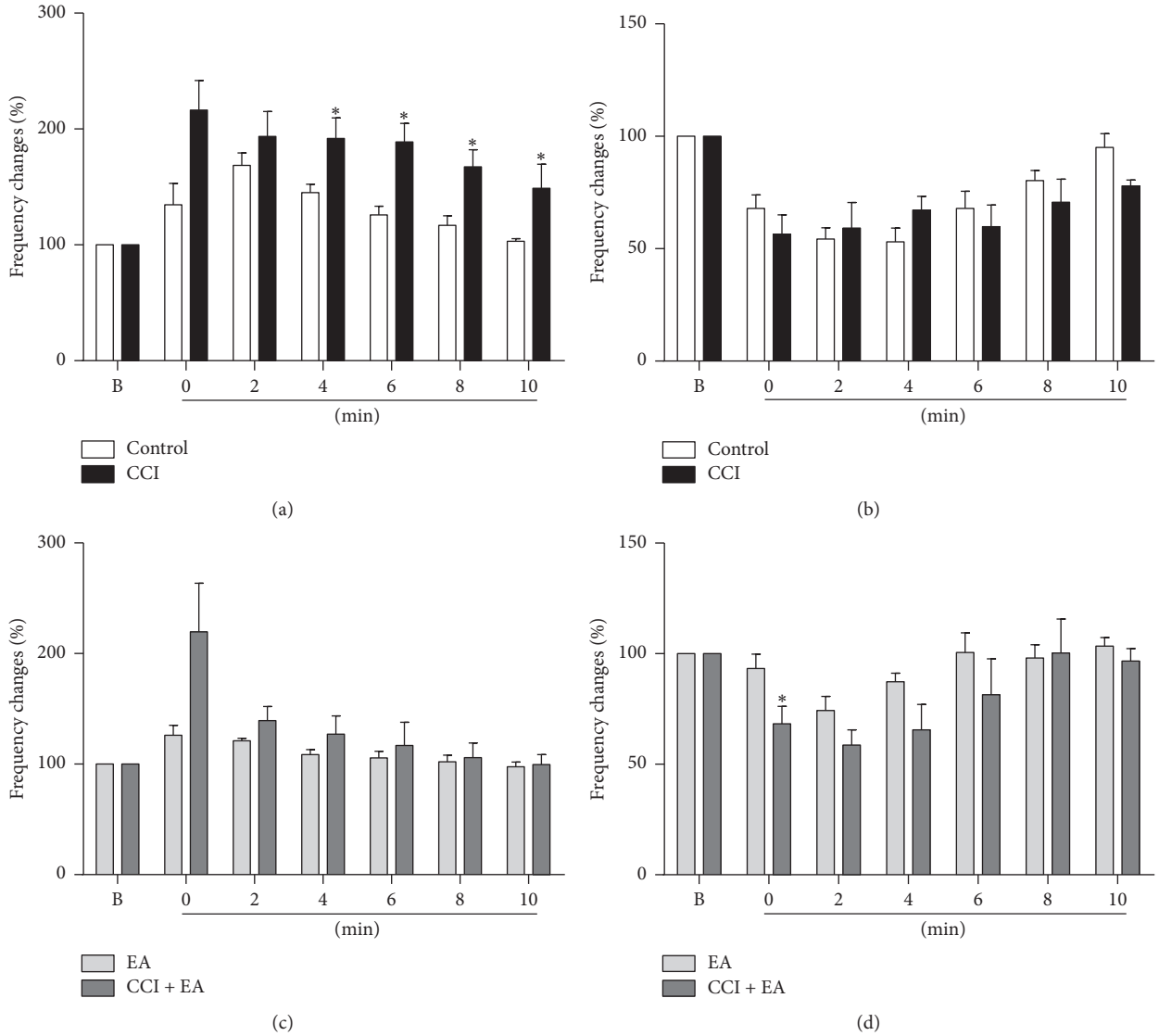

Figure 3: The differences in effects of acute noxious stimulation on the firing rate between sham and CCI rats. The brief sciatic nerve stimulation had a greater excitatory effect on the firing rate of PENs in CCI compared to sham rats (a) and a similar effect on PINs in both CCI and sham rats (b). Also, EA blocked the excitatory effect of the acute noxious stimulus on the firing rate of PENs in both sham and CCI rats (c) and produced slightly less blocking of the inhibitory effect of noxious stimulation on PINs in CCI rats compared to sham rats (d). ∗: compared with the control group, $P < 0.05$.

Compared with the EA group, the discharge frequency changes of PENs in the CCI + EA group were slightly increased ($P > 0.05$, Figure 3(c)), and those of PINs in the CCI + EA group were mildly decreased ($P > 0.05$, Figure 3(d)) from 2 to 10 min after the noxious stimuli. EA suppressed the excitatory and inhibitory effects of the acute noxious stimulus on the electric activities of PENs and PINs in both sham and CCI rats.

3.4. The Effect of the MEK U0126 Inhibitor on EA Treatment in the Hippocampus of Sham Rats. Compared with the EA group, the discharge frequency changes of 9 hippocampal PENs in the U0126 group were not significant ($P > 0.05$, Figure 4(b)) at 0 min. Compared with the EA group, the discharge frequency changes of hippocampal PENs in the U0126 group (195.20 ± 22.98%) increased significantly ($P < 0.05$) at 2 min after the noxious stimuli (after injection of U0126). From 4 to 8 min after giving the noxious stimuli, the discharge frequency changes of PENs in the U0126 group (165.80 ± 39.32%, 188.32 ± 25.35%, and 181.14 ± 43.41%) were still higher than those in the EA group ($P < 0.05$). At 10 min after giving the noxious stimuli, no significant differences were found between the U0126 group (118.34% ± 20.80) and the EA group. There was no significant difference between the U0126 group and the EA group in the discharge frequency changes of 6 hippocampal PINs ($P > 0.05$) at 0 min. The discharge frequency changes of hippocampal PINs in the U0126 group (55.6% ± 13.27) were bigger compared to those in the EA group at 2 min after the noxious stimuli (and after injection of U0126). During a period of 6 to

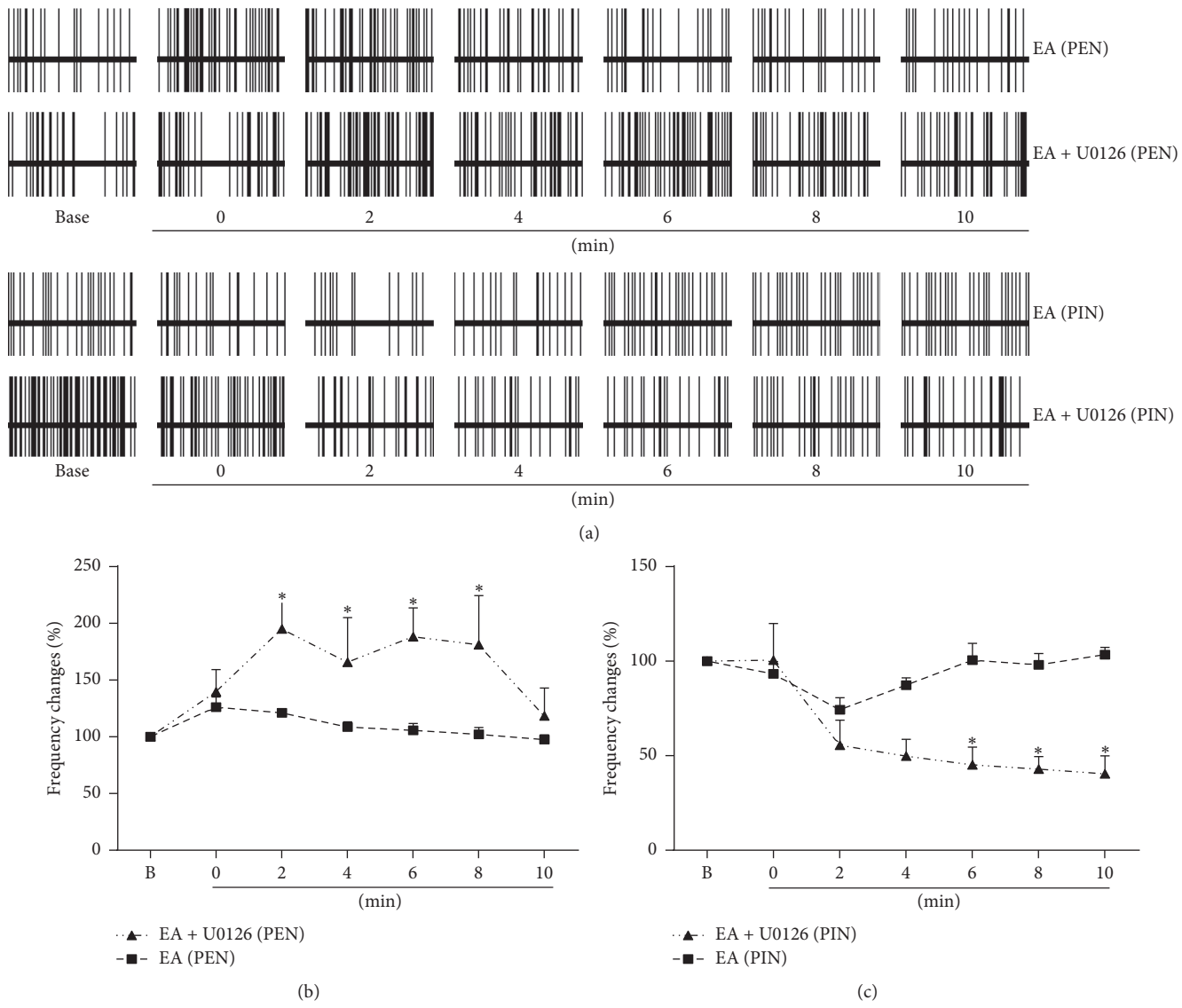

Figure 4: EA was ineffective in the presence of U0126. (a) Example of the effect of U0126 + EA and EA only on the impact of brief sciatic nerve stimulation on the firing rates of hippocampal PENs ($n = 9$) and PINs ($n = 6$). (b) Combination of U0126 and EA increased the discharge frequency changes of PENs caused by acute noxious stimulation to a larger extent than that observed in the EA group. (c) Combination of U0126 and EA decreased the discharge frequency changes of PINs caused by acute noxious stimulation to a larger extent than that observed in the EA group. ∗: compared with EA group, $P < 0.05$.

10 min, the discharge frequency changes of PINs in the U0126 group exhibited obvious differences when compared with the same period in the EA group ($P < 0.05$). The electrical activities of PINs gradually returned to baseline levels at 6 min after the noxious stimuli in the EA group, while those in the U0126 group did not. Combination of U0126 + EA in sham rats produced effects markedly greater than those observed when brief sciatic nerve stimulation was performed alone (without drugs), so it may be assumed that U0126 increased the effect of noxious stimulation through a pathway other than that of the EA pathway, thus masking the effect of EA. It is suggested that the MEK1/2 inhibitor U0126 blocked the EA effect on acute noxious stimulation.

4. Discussion

Pain is an unpleasant sensory and emotional experience associated with actual or potential tissue damage, or described in terms of such damage. There are two kinds of pain: acute and chronic. Acute pain is very common in clinical practice, including pain in the perioperative setting [24], pain in patients with severe or concurrent medical illnesses (such as arthritis [25]), pain related to cancer or cancer treatment, and labor pain. Acute pain including neuropathic pain [26] affects bodily health and the quality of life. Tens of thousands of people are affected by acute pain, and the treatment costs amount to billions of dollars every year. To enhance the quality of life and maintain the patient's function

ability, clinical medicine is used to treat acute pain, but these medications have substantial side effects [27]. Acupuncture analgesia has its advantages, such as an obvious analgesic effect and little side effects, but its mechanism of action is not clarified at the moment. As a part of the limbic system, the hippocampus is associated with memory, but also with pain and acupuncture analgesia. The dorsal hippocampal dopamine receptors exert an analgesic effect during the orofacial pain test [28]; microinjections of nonsteroidal anti-inflammatory drugs [29] or 2-AG [30] into the hippocampus induce antinociception. A recent study indicates that persistent peripheral nociception induced by subcutaneous injection of bee venom upregulated mTOR target p70 S6 kinase signaling and facilitated long-term potentiation which could be reversed by mTOR inhibitor in the hippocampus [31].

In our experiment, we observed that the discharge frequencies of hippocampal CA1 pain-related neurons (PENs or PINs) were changed after brief electrical impulses applied to the sciatic nerve. The electric activities of PENs and PINs returned to normal level at 8 and 10 min after the noxious stimuli, respectively. Xiao et al. [7], Yang et al. [8], Li et al. [9], and Jiao et al. [32] focused on electric activities of pain-related neurons in the hippocampus after noxious stimuli for many years. In the hippocampal CA1 and CA3 area and dentate gyrus, cholinergic neurons and muscarinic receptors have effects on the electric activities of PENs and PINs, so that they are involved in pain modulation [7–9, 32]. Glutamate and its receptors, noradrenaline (NE), phentolamine, and alpha-adrenoceptors also have effects on pain modulation by regulating electric activities of PENs and PINs in the hippocampal CA3 region [33, 34]. These studies reported the effects of pain-induced discharges of hippocampal neurons, but few research papers pay attention to electric activities of hippocampal neurons in a chronic pain state. Hains et al. reported that after spinal cord contusion injury the changes of the spontaneous discharge and afterdischarge of extracellular neurons in the thalamus are related to an upregulated sodium channel expression [35]. In CCI rats, the acute noxious stimulation evoked greater changes of electric activities of PENs and PINs, and the recorded number of hippocampal PENs was obviously bigger and that of PINs smaller compared with sham rats. It took more time for the pain-related neurons to return to normal level in the CCI rats than in sham rats. This might be because the effect of brief sciatic nerve stimulation on firing rates of PENs and PINs was enhanced under the advanced CCI situation. The CCI rats may have experienced more pain than the sham rats after the short noxious stimulation. The CCI rats were in a state of hyperalgesia, an increased response to noxious stimuli, which means the same intensity of electrical stimulation causes more pain intensity and finally a prolonged time of recovery to normal.

Shi et al. [36] reported that pain-related neurons were involved in the modulation of EA analgesia, and EA stimulation resulted in an inhibiting effect on the electrical activity of PENs and an activating effect on the electrical activity of PINs. After EA at the acupoint "Hegu," or dolantin given intravenously, Gao et al. stimulated the head of the caudate nucleus, eliciting an inhibitory effect on PENs and a reduction of inhibition or release on PINs [37]. EA has been shown to suppress PENs and excite PINs, which can be taken as an electrophysiological index for EA analgesia [38, 39]. Yang et al. also reported that EA treatment could play an inhibiting role in mediating the evoked discharge of PENs and an activating role in that of PINs, and cholecystokinin-8's (CCK-8) B receptor antagonist could be antagonistic to the effect of CCK on EA analgesia [40]. Our results (comp. Figure 1) showed that, in the hippocampal CA1 area, EA inhibited the excitatory effect of brief sciatic nerve stimulation on the electric activities of PENs and activated the inhibitory effect of brief sciatic nerve stimulation on electric activities of PINs in sham rats, which caused the firing rates of PENs and PINs to return to normal level at 6 min after the noxious stimuli, earlier than in the control group. These findings suggest that the analgesic effect of EA is related to the electric activities of pain-related neurons in the CA1 area, which were affected by noxious stimulation. EA reduced the effect of acute noxious stimulation on the electric activities of PENs and PINs. The electric activities of PENs and PINs play an important role in mediating EA analgesia, as reported before.

In CCI rats, EA also had an effect on the firing rate of PENs and PINs similar to that evoked by acute noxious stimuli, but the electric activities returned to normal level at 6 or 8 min after administration of the noxious stimulus. It is suggested that the effect of EA treatment is closely related to the severity of pain.

Intrathecal administration of the inhibitor of the MAPK family members MEK1/2, such as U0126, PD198306, and PD98059, had analgesic effects and significantly potentiated the effectiveness of opioids in neuropathy in the spinal cord [41–43]. U0126 downregulated the increased late responses and afterdischarge induced by melittin (a pain-related peptidergic component) in wide-dynamic-range neurons of the spinal cord [44]. Accumulating evidence showed that ERK expression increased at the peripheral nerve and spinal cord horn [45–47]. Phospho-ERK (pERK) in the spinal cord is activated immediately in neurons (<6 h), then in microglia on days 1 and 3 and both in astrocytes and in microglia on day 10, and finally in satellite cells on days 10 and 21 after spinal nerve ligation, and this activation contributes to mechanical allodynia [46]. PD 98059 may modulate the nociceptive factors and antinociceptive factors that are released by glial cells, which have a close relationship with reduced symptoms of neuropathy [43, 46]. These reports suggested that MEK1/2 inhibitors have an analgesic effect on neuropathic models in the primary injury and that neuropathic pain is associated with the activity of the MAPK/ERK signal pathway within the spinal cord. Few studies focused on the relationship between the expression of ERK and the hippocampus in chronic neuropathic pain, and an agreement has not been reached [48, 49]. There were no significant changes in hippocampal pERK after formalin injection [50]. Electroacupuncture had inhibiting effects on the ERK signal pathway on the spinal dorsal horn. The phosphorylation of the ERK signal transduction pathway was enhanced by EA in depression rat tissue [51]; however, there was no report on the study of EA analgesia on the hippocampus ERK signal pathway. Our

previous results showed that in the hippocampus the ERK signal pathway was inhibited in chronic neuropathic rats, and after acupuncture treatment the ERK signaling pathway was activated [16]. U0126 is a specific inhibitor of MEK, both MEK1 and MEK2. Our experimental results showed that, compared with the EA group, brief sciatic nerve stimulation produced a greater excitatory and inhibitory effect on the firing rate of PENs and PINs in U0126 + EA group, suggesting that U0126 suppressed the effect of EA on the analgesic pathway. It is suggested that involvement of the activation of ERK signaling pathway in the hippocampal CA1 region in EA treatment induced pain relief.

5. Conclusions

In CCI rats, acute noxious stimulation required a longer time for the firing rate of pain-related neurons to return to normal level; EA treatment could suppress the effect of the noxious stimulus on PENs and PINs in both sham and CCI rats, which suggests a close relationship with the EA analgesic effect; and the ERK signal pathway is probably involved in pain and EA analgesia.

Competing Interests

None of the authors declares any competing interests related to this paper.

Acknowledgments

This work was supported by the National Natural Science Foundation of the People's Republic of China (81202762, 30472241, Key Project: 90709031) and the Ministry of Science and Technology of PRC ("973" Project, 2013CB531904). In Austria, the work was supported by the Austrian Federal Ministry of Science, Research and Economy and the German Academy of Acupuncture (DAA). Ass. Professor Dr. Jun-Ying Wang received a 3-month scholarship from the Austrian Eurasia-Pacific Uninet for a research stay at the TCM Research Center at the Medical University of Graz.

References

[1] Y.-W. Chen, J.-I. Tzeng, K.-S. Liu, S.-H. Yu, C.-H. Hung, and J.-J. Wang, "Systemic diphenidol reduces neuropathic allodynia and TNF-alpha overexpression in rats after chronic constriction injury," *Neuroscience Letters*, vol. 552, pp. 62–65, 2013.

[2] G. J. Bennett and Y.-K. Xie, "A peripheral mononeuropathy in rat that produces disorders of pain sensation like those seen in man," *Pain*, vol. 33, no. 1, pp. 87–107, 1988.

[3] M.-G. Liu and J. Chen, "Roles of the hippocampal formation in pain information processing," *Neuroscience Bulletin*, vol. 25, no. 5, pp. 237–266, 2009.

[4] A. A. Mutso, D. Radzicki, M. N. Baliki et al., "Abnormalities in hippocampal functioning with persistent pain," *The Journal of Neuroscience*, vol. 32, no. 17, pp. 5747–5756, 2012.

[5] M. E. Zimmerman, J. W. Pan, H. P. Hetherington, M. L. Lipton, K. Baigi, and R. B. Lipton, "Hippocampal correlates of pain in healthy elderly adults: A Pilot Study," *Neurology*, vol. 73, no. 19, pp. 1567–1570, 2009.

[6] A. del Rey, H.-J. Yau, A. Randolf et al., "Chronic neuropathic pain-like behavior correlates with IL-1β expression and disrupts cytokine interactions in the hippocampus," *Pain*, vol. 152, no. 12, pp. 2827–2835, 2011.

[7] Y. Xiao, X.-F. Yang, and M.-Y. Xu, "Effect of acetylcholine on pain-related electric activities in hippocampal CA1 area of normal and morphinistic rats," *Neuroscience Bulletin*, vol. 23, no. 6, pp. 323–328, 2007.

[8] X. F. Yang, Y. Xiao, and M.-Y. Xu, "Both endogenous and exogenous ACh plays antinociceptive role in the hippocampus CA1 of rats," *Journal of Neural Transmission*, vol. 115, no. 1, pp. 1–6, 2008.

[9] G.-Z. Li, Q.-C. Liang, Y.-H. Jin et al., "The effect of acetylcholine on pain-related electric activities in the hippocampal CA3 of rats," *Journal of Neural Transmission*, vol. 118, no. 4, pp. 555–561, 2011.

[10] K. K. S. Hui, J. Liu, N. Makris et al., "Acupuncture modulates the limbic system and subcortical gray structures of the human brain: evidence from fMRI studies in normal subjects," *Human Brain Mapping*, vol. 9, no. 1, pp. 13–25, 2000.

[11] J. Yang, F. Zeng, Y. Feng et al., "A PET-CT study on the specificity of acupoints through acupuncture treatment in migraine patients," *BMC Complementary and Alternative Medicine*, vol. 12, article 123, 2012.

[12] W.-T. Zhang, Z. Jin, G.-H. Cui et al., "Relations between brain network activation and analgesic effect induced by low vs. high frequency electrical acupoint stimulation in different subjects: a functional magnetic resonance imaging study," *Brain Research*, vol. 982, no. 2, pp. 168–178, 2003.

[13] X. He, T. Yna, R. Chen, and D. Ran, "Acute effects of electro-acupuncture (EA) on hippocampal long term potentiation (LTP) of perforant path-dentate gyrus granule cells synapse related to memory," *Acupuncture & Electrotherapeutics Research*, vol. 37, no. 2-3, pp. 89–101, 2012.

[14] J. Wang, J. Liu, S. Chen, Y. Gao, F. Meng, and L. Qiao, "Acupuncture effects on the hippocampal cholinergic system in a rat model of neuropathic pain," *Neural Regeneration Research*, vol. 7, no. 3, pp. 212–218, 2012.

[15] Q. Xu, S. Chen, and Y. Gao, "Observation on the analgesic effect of repeated electroacupuncture and its relation to the expression of synaptophysin in rat's hippocampus and hypothalamus," *Chinese Journal of Rehabilitation Medicine*, vol. 24, no. 6, pp. 498–501, 2009.

[16] Q. L. Xu, T. Liu, S. P. Chen et al., "The cumulative analgesic effect of repeated electroacupuncture involves synaptic remodeling in the hippocampal CA3 region," *Neural Regeneration Research*, vol. 7, no. 18, pp. 1378–1385, 2012.

[17] J.-Y. Wang, S.-P. Chen, Y.-H. Gao, L.-N. Qiao, J.-L. Zhang, and J.-L. Liu, "Effect of repeated electroacupuncture intervention on hippocampal ERK and p38MAPK signaling in neuropathic pain rats," *Evidence-Based Complementary and Alternative Medicine*, vol. 2015, Article ID 641286, 10 pages, 2015.

[18] Y. Jeon, C.-E. Kim, D. Jung et al., "Curcumin could prevent the development of chronic neuropathic pain in rats with peripheral nerve injury," *Current Therapeutic Research—Clinical and Experimental*, vol. 74, pp. 1–4, 2013.

[19] M. Han, R.-Y. Huang, Y.-M. Du, Z.-Q. Zhao, and Y.-Q. Zhang, "Early intervention of ERK activation in the spinal cord can block initiation of peripheral nerve injury-induced neuropathic pain in rats," *Sheng Li Xue Bao*, vol. 63, no. 2, pp. 106–114, 2011.

[20] G. Paxinos and G. Walsop, *The Rat Brain in Stereotaxic Coordinates*, Academic Press, San Diego, Calif, USA, 2nd edition, 1979.

[21] L. J. Pellegrino, A. S. Pellegrino, and A. J. Cushman, *A Stereotaxic Atlas of the Rat Brain*, Plenum Press, New York, NY, USA, 2nd edition, 1979.

[22] X. T. Zhang, "The integration of thalamus in the process of acupuncture analgesia," *Scientia Sinica Mathematio*, vol. 1, pp. 28–52, 1973.

[23] M. Z. Sun, L. S. Chen, H. L. Gu, J. Cheng, and L. S. Yue, "Effect of acupuncture on unit discharge in nucleus parafascicularis of rat thalamus," *Sheng Li Xue Bao*, vol. 32, pp. 207–213, 1980.

[24] J. Dong, W. Li, and Y. Wang, "The effect of pregabalin on acute postoperative pain in patients undergoing total knee arthroplasty: a meta-analysis," *International Journal of Surgery*, vol. 34, pp. 148–160, 2016.

[25] M. Abdullah, M. L. Mahowald, S. P. Frizelle, C. W. Dorman, S. C. Funkenbusch, and H. E. Krug, "The effect of intra-articular vanilloid receptor agonists on pain behavior measures in a murine model of acute monoarthritis," *Journal of Pain Research*, vol. 9, pp. 568–570, 2016.

[26] M. Zimmermann, "Pathobiology of neuropathic pain," *European Journal of Pharmacology*, vol. 429, no. 1–3, pp. 23–37, 2001.

[27] J. E. Holden and J. A. Pizzi, "The challenge of chronic pain," *Advanced Drug Delivery Reviews*, vol. 55, no. 8, pp. 935–948, 2003.

[28] A. Shamsizadeh, P. Pahlevani, A. Haghparast, M. Moslehi, L. Zarepour, and A. Haghparast, "Involvement of dopamine receptors within the dorsal hippocampus in suppression of the formalin-induced orofacial pain," *Pharmacology Biochemistry and Behavior*, vol. 114-115, pp. 37–42, 2013.

[29] G. Gurtskaia, N. Tsiklauri, I. Nozadze, M. Nebieridze, and M. G. Tsagareli, "Antinociceptive tolerance to NSAIDs microinjected into dorsal hippocampus," *BMC Pharmacology and Toxicology*, vol. 15, article 10, 2014.

[30] K. Rea, G. K. Ford, W. M. Olango, B. Harhen, M. Roche, and D. P. Finn, "Microinjection of 2-arachidonoyl glycerol into the rat ventral hippocampus differentially modulates contextually induced fear, depending on a persistent pain state," *The European Journal of Neuroscience*, vol. 39, no. 3, pp. 435–443, 2014.

[31] D. Lyu, W. Yu, N. Tang et al., "The mTOR signaling pathway regulates pain-related synaptic plasticity in rat entorhinal-hippocampal pathways," *Molecular Pain*, vol. 9, no. 1, article 64, 2013.

[32] R. Jiao, C. Yang, Y. Zhang, M. Xu, and X. Yang, "Cholinergic mechanism involved in the nociceptive modulation of dentate gyrus," *Biochemical and Biophysical Research Communications*, vol. 379, no. 4, pp. 975–979, 2009.

[33] H. Jin, Y. Teng, X. Zhang, C. Yang, M. Xu, and L. Yang, "Noradrenergic mechanism involved in the nociceptive modulation of hippocampal CA3 region of normal rats," *Neuroscience Letters*, vol. 574, pp. 31–35, 2014.

[34] X. Ma, T.-F. Shi, M. Zhang et al., "Modulatory role of glutamic acid on the electrical activities of pain-related neurons in the hippocampal CA3 region," *Neuroscience Letters*, vol. 513, no. 1, pp. 67–71, 2012.

[35] B. C. Hains, C. Y. Saab, and S. G. Waxman, "Changes in electrophysiological properties and sodium channel Nav1.3 expression in thalamic neurons after spinal cord injury," *Brain*, vol. 128, part 10, pp. 2359–2371, 2005.

[36] T. F. Shi, C. X. Yang, D. X. Yang et al., "L-364,718 potentiates electroacupuncture analgesia through Cck-A receptor of pain-related neurons in the nucleus parafascicularis," *Neurochemical Research*, vol. 36, no. 1, pp. 129–138, 2011.

[37] M. L. Gao, J. M. Zhang, and Y. R. Liu, "The effect of electrical stimulation of the head of caudate nociceptive neuronal activities in the mesencephalon reticular formation and its relation to the acupuncture effect," *Zhen Ci Yan Jiu*, vol. 14, no. 4, pp. 414–419, 1989.

[38] J.-T. Bian, M.-Z. Sun, and J.-S. Han, "Reversal of electroacupuncture tolerance by cck-8 antiserum: an electrophysiological study on pain-related neurons in nucleus parafascicularis of the rat," *The International Journal of Neuroscience*, vol. 72, no. 1-2, pp. 15–29, 1993.

[39] X. X. Chi, M. Z. Sun, and J. Zhang, "The effect of electroacupuncture on pain excited neurons, pain inhibited neurons and tail flick latency in caudate nucleus in rats," *Chinese Journal of Applied Physiology*, vol. 12, pp. 49–52, 1996.

[40] C.-X. Yang, T.-F. Shi, Q.-C. Liang et al., "Cholecystokinin-8 antagonizes electroacupuncture analgesia through its B receptor in the caudate nucleus," *Neuromodulation*, vol. 13, no. 2, pp. 93–98, 2010.

[41] K. Popiolek-Barczyk, W. Makuch, E. Rojewska, D. Pilat, and J. Mika, "Inhibition of intracellular signaling pathways NF-κB and MEK1/2 attenuates neuropathic pain development and enhances morphine analgesia," *Pharmacological Reports*, vol. 66, no. 5, pp. 845–851, 2014.

[42] A. Ciruela, A. K. Dixon, S. Bramwell, M. I. Gonzalez, R. D. Pinnock, and K. Lee, "Identification of MEK1 as a novel target for the treatment of neuropathic pain," *British Journal of Pharmacology*, vol. 138, no. 5, pp. 751–756, 2003.

[43] E. Rojewska, K. Popiolek-Barczyk, N. Kolosowska et al., "PD98059 influences immune factors and enhances opioid analgesia in model of neuropathy," *PLoS ONE*, vol. 10, no. 10, Article ID e0138583, 2015.

[44] Y.-Q. Yu, F. Zhao, and J. Chen, "Activation of ERK1/2 in the primary injury site is required to maintain melittin-enhanced wind-up of rat spinal wide-dynamic-range neurons," *Neuroscience Letters*, vol. 459, no. 3, pp. 137–141, 2009.

[45] S. Sun, Y. Yin, X. Yin et al., "Anti-nociceptive effects of Tanshinone IIA (TIIA) in a rat model of complete Freund's adjuvant (CFA)-induced inflammatory pain," *Brain Research Bulletin*, vol. 88, no. 6, pp. 581–588, 2012.

[46] Z.-Y. Zhuang, P. Gerner, C. J. Woolf, and R.-R. Ji, "ERK is sequentially activated in neurons, microglia, and astrocytes by spinal nerve ligation and contributes to mechanical allodynia in this neuropathic pain model," *Pain*, vol. 114, no. 1-2, pp. 149–159, 2005.

[47] X. Xu, H. Chen, B.-Y. Ling, L. Xu, H. Cao, and Y.-Q. Zhang, "Extracellular signal-regulated protein kinase activation in spinal cord contributes to pain hypersensitivity in a mouse model of type 2 diabetes," *Neuroscience Bulletin*, vol. 30, no. 1, pp. 53–66, 2014.

[48] M.-G. Liu, R.-R. Wang, X.-F. Chen, F.-K. Zhang, X.-Y. Cui, and J. Chen, "Differential roles of ERK, JNK and p38 MAPK in pain-related spatial and temporal enhancement of synaptic responses in the hippocampal formation of rats: multi-electrode array recordings," *Brain Research*, vol. 1382, pp. 57–69, 2011.

[49] S.-W. Guo, M.-G. Liu, Y.-L. Long et al., "Region- or state-related differences in expression and activation of extracellular signal-regulated kinases (ERKs) in naïve and pain-experiencing rats," *BMC Neuroscience*, vol. 8, article 53, 2007.

[50] S.-S. Choi, Y.-J. Seo, E.-J. Shim et al., "Involvement of phosphorylated Ca^{2+}/calmodulin-dependent protein kinase II and phosphorylated extracellular signal-regulated protein in the mouse formalin pain model," *Brain Research*, vol. 1108, no. 1, pp. 28–38, 2006.

[51] W. Y. Bao, W. D. Li, J. Lu, Y. Z. Song, and Y. Tu, "Effects of electro-acupuncture on ERK signal pathway in the brain of depression rats induced by chronic stress," *China Journal of Traditional Chinese Medicine and Pharmacy*, vol. 29, pp. 2009–2011, 2014.

Hindawi Publishing Corporation
Neural Plasticity
Volume 2016, Article ID 1437148, 14 pages
http://dx.doi.org/10.1155/2016/1437148

Research Article

Electroacupuncture Treatment Alleviates Central Poststroke Pain by Inhibiting Brain Neuronal Apoptosis and Aberrant Astrocyte Activation

Gui-Hua Tian,[1,2,3] Shan-Shan Tao,[4] Man-Tang Chen,[4] Yu-Sang Li,[4] You-Ping Li,[3] Hong-Cai Shang,[1] Xiao-Yi Tang,[1,2] Jian-Xin Chen,[1] and He-Bin Tang[4]

[1]*Key Laboratory of Chinese Internal Medicine of MOE, Beijing Dongzhimen Hospital, Beijing University of Chinese Medicine, Beijing 100700, China*
[2]*Department of Tuina and Pain, Beijing Dongzhimen Hospital, Beijing University of Chinese Medicine, Beijing 100700, China*
[3]*Chinese Evidence-Based Medicine Center, West China Hospital, Sichuan University, Sichuan 610041, China*
[4]*Department of Pharmacology, School of Pharmaceutical Sciences, South-Central University for Nationalities, No. 182, Minyuan Road, Wuhan 430074, China*

Correspondence should be addressed to He-Bin Tang; hbtang2006@mail.scuec.edu.cn

Received 20 July 2016; Revised 30 August 2016; Accepted 1 September 2016

Academic Editor: Jian Kong

Copyright © 2016 Gui-Hua Tian et al. This is an open access article distributed under the Creative Commons Attribution License, which permits unrestricted use, distribution, and reproduction in any medium, provided the original work is properly cited.

Electroacupuncture (EA) is reported to effectively relieve the central poststroke pain (CPSP). However, the underlying mechanism remains unclear. The present study investigated the detailed mechanisms of action of EA treatment at different frequencies for CPSP. A CPSP model was established with a single collagenase injection to the left ventral posterolateral nucleus of the thalamus. The EA-treated groups then received EA treatment at frequency of 2, 2/15, or 15 Hz for 30 min daily for five days. The pain-related behavioral responses, neuronal apoptosis, glial activation, and the expression of pain signal transmission-related factors (β-catenin, COX-2, and NK-1R) were assessed using behavioral tests, Nissl staining, TUNEL staining, and immunohistochemical staining, respectively. The low-frequency EA treatment significantly (1) reduced brain tissue damage and hematoma sizes and (2) inhibited neuronal apoptosis, thereby exerting abirritative effects. Meanwhile, the high-frequency EA treatment induced a greater inhibition of the aberrant astrocyte activation, accompanied by the downregulation of the expressions of COX-2, β-catenin, and subsequently NK-1R, thereby alleviating inflammation and producing strong analgesic effects. Together, these findings suggest that CPSP is closely related to pathological changes of the neocortex and hippocampus. EA treatments at different frequencies may exert abirritative effects by inhibiting brain neuronal apoptosis and aberrant astrocyte activation in the brain.

1. Introduction

As a type of the neuropathic pain, central poststroke pain (CPSP) is one of the most troublesome sequelae of stroke, which can be caused by a primary lesion that affects the central somatosensory system following intracerebral hemorrhagic stroke [1]. In the clinic, patients exhibit thermal and mechanical hyperalgesia, which produces a low quality of life. A demographic census shows that the incidence of CPSP in stroke patients was approximately 7.3%–10.5% [2]. However, recent studies on neuropathic pain mainly focus on the peripheral nervous system instead of the injury to the central nervous system, particularly the CPSP [3].

In Western medicine, CPSP is mainly treated with drugs, including analgesics, antidepressants, and anticonvulsants, which may produce resistance and addiction [4]. As an important part of Chinese traditional medicine, acupuncture treatment obtains consistent international affirmation for its reliable analgesic effect. Electroacupuncture (EA) is a form of acupuncture in which a small electric current is passed

between pairs of acupuncture needles. There are some reports showing that EA could be a good treatment to alleviate neuropathic pain by regulating the sympathetic nerve [5] and has the advantages of simple operation, small damage, light side effect, reasonable cost, and hence easy acceptance by patients. Currently, the EA treatment for CPSP has achieved remarkable efficacy in the clinic. For example, acupuncture at "Zusanli" and "Baihui" can significantly reduce the pain threshold of CPSP patients [3]. However, while the EA treatment for CPSP may be effective, the mechanisms underlying its therapeutic effects are not fully understood.

It has been known that CPSP is related to intracerebral hemorrhage and thalamus infarction. When blood suddenly bursts into brain tissues, the hematoma physically disrupts and seriously damages the neurons and astrocytes, producing great suffering and economic burdens to the patients [6]. After destruction of brain tissue, astrocytes will be aberrantly activated and can facilitate the synthesis and release of various pain signal transduction-related mediators, such as Akt, extracellular signal regulated kinase, β-catenin, nuclear factor kappa B, cyclooxygenase-2 (COX-2), and neurokinin 1 receptor (NK-1R) [6, 7], which further promote local neuroinflammation. Following astrocytes activation and the initiation of neuroinflammation, the inflammatory mediators can enhance pain-related signal transmission and induce central sensitization to generate pain.

It was speculated that these pain signal transmission-related mediators may be associated with CPSP; therefore, the present study was designed to investigate the inhibitory effects of EA treatments at different frequency patterns on neuronal apoptosis and astrocyte activation in the brain using a rat CPSP model and to reveal the changes in the expression of various pain signal transmission-related mediators (COX-2, β-catenin, and NK-1R) in different regions of the brain after EA treatment at different frequency patterns.

2. Material and Methods

Adult male Sprague-Dawley (SD) rats (250–300 g; $n = 75$) were obtained from the experimental animal center of Hubei Province. The care and use of animals and all experimental protocols (Permit number: 2011-SCUEC-AEC-001) for this study were performed according to the Guide for Animal Experimentation, South-Central University for Nationalities, and the Committee of Research Facilities for Laboratory Animal Sciences, South-Central University for Nationalities, China.

The experimental CPSP model was induced by single collagenase injection into the left ventral posterolateral nucleus of the rat thalamus, as previously reported [8]. All surgeries were performed under trichloroacetaldehyde monohydrate (450 mg/kg, i.p.) anesthesia and placed in a stereotaxic frame. Under stereotaxic guidance, collagenase (type IV; 0.025 U in 0.25 μL cerebrospinal fluid; Sigma-Aldrich, St. Louis, MO, USA) or cerebrospinal fluid (0.25 μL, containing 126.0 mM NaCl, 3.0 mM KCl, 1.4 mM Na_2PO_4, 1.0 mM $MgSO_4$, 26.0 mM $NaHCO_3$, 10.0 mM glucose, and 2.5 mM $CaCl_2$, pH 7.4) was injected into the left ventral posterolateral nucleus of the thalamus (A: −3.8 mm; L: 3.3 mm from bregma; and V: 6.0 mm). Sham was injected with an equal volume of the cerebrospinal fluid vehicle. The needle was left in place for 5 min to allow for diffusion of collagenase away from the injection site and then withdrawn gently. All SD rats were randomly and double-blindly divided into seven groups: a control group (intragastric administration of saline; $n = 15$), a sham group (intragastric administration of saline after the injection of cerebrospinal fluid; $n = 5$), a model group (intragastric administration of saline after the injection of collagenase; $n = 15$), a fluoxetine group (intragastric administration of fluoxetine after the injection of collagenase; 5 mL/kg, 0.4 mg/mL; $n = 10$; a positive drug to treat the stroke through improving infarct volumes and neurobehavioral, Patheon France, Bourgoin-Jallieu, France), and EA-treated groups (2, 15, and 2/15 Hz groups; $n = 10$ for each group).

Rats were loosely immobilized on a wood plate and two stainless steel acupuncture needles were inserted into two acupoints ST36 and GV20 with a depth of 5 mm. In the EA treatment groups, the rats received EA administration on the left "Zusanli" (ST36, 5 mm lateral to the anterior tubercle of tibia) and "Baihui" (GV20, located at the midmost point between the bilateral parietal bones, forward insertion) once every day, starting from 24 h after the termination of collagenase injection for 5 days. EA (1 mA) was administered at different frequencies (2, 15, or 2/15 Hz) for 30 min every day. The EA's current was delivered with a modified current-constant Han's Acupuncture Point Nerve Stimulator (HANA-100A, Huawei Co., Ltd., Beijing, China) where the needles were connected with the electrical stimulation [9].

Hyperalgesia to thermal stimulation was measured using a plantar test (Model 37370, Ugo Basile, Varese, Italy) according to a previously described method [10]. Subsequent readings of the same paw were carried out at 0, 1, 3, and 5 day(s) after the operation. The process was repeated three times, and the mean values were taken as the threshold values.

Hyperalgesia to pressure stimulation was measured in the hindpaws of lightly restrained alert rats using a hand-held measuring instrument (HR/SLY-HFM/402359, Beijing, China) referred to in a previously described method [10]. The forces required for mechanical hyperalgesia were displayed on the instrument, when the rats withdrew the paws after the stimulation. The process was repeated three times, and the mean values were taken as the threshold values.

Hyperalgesia to cold stimulation was measured with an ice-cold metal aluminum platform according to a previously described method [10]. The latency before the first response (licking, paw movements, and little leaps) to cold stimulation was recorded with a cut-off time of 60 s. The process was repeated three times, and the mean values were taken as the threshold values.

To examine the brain neuronal cell damage of CPSP rats, the rats were sacrificed via intracardial perfusion on the 5th or 7th day after the operation, and their brains were dissected and rapidly fixed for 24 h at 22°C with 4% paraformaldehyde (Sigma). The 4 μm brain sections were washed by a series of grade ethanol for 5 min each time and incubated in Nissl

staining solutions (Beyotime Institute of Biotechnology, Nantong, China) for 30 min at room temperature according to the manufacturer's instructions. The brain neuronal cell apoptosis was analyzed using a Nuance Multispectral Imaging System (Cambridge Research and Instrumentation Inc., Woburn, MA, USA) with instructions followed closely [11].

To examine the expressions of several pain signal transmission-related factors in CPSP rats, the 4 μm brain sections were incubated overnight at 4°C with rabbit anti-COX-2 antibody (1 : 200 dilution; Cayman Chemical, Ann Arbor, MI), rabbit anti-glial fibrillary acidic protein (GFAP) antibody (1 : 400 dilution; Sigma Chemical Co., St. Louis, MO, USA), rabbit anti-β-catenin (1 : 400 dilution, Cayman), or rabbit-anti-NK-1R antibody (1 : 2000 dilution, Sigma) according to the manufacturer's instructions (Histofine Simple Stain Rat MAX-PO (MULTI) kit; Nichirei, Tokyo) [12].

To examine the apoptosis in CPSP rat brain sections, the 4 μm brain sections were incubated with TdT-mediated dUTP Nick-End Labeling (TUNEL) reaction mixture containing biotin-labeled dUTPs at 37°C for 45 min according to the manufacturer's instructions (Boster Biochemical Techniques Co., Ltd., Wuhan, China). In a negative control, the TUNEL reaction mixture was replaced with PBS. Sections of the positive control sections were pretreated with DNase I for 10 min followed by TUNEL staining [11].

Finally, multispectral imaging analysis of all slides in each experiment was performed by using an Eclipse Ti microscope (Nikon, Tokyo) with a Nuance Multispectral Imaging System (Cambridge Research and Instrumentation Inc., Woburn, MA, USA) according to a previously described method [12].

On the 5th day, rats were sacrificed via decollation. The cortex of the damage area and the whole hippocampus tissues were rapidly dissected out and then put into the liquid nitrogen and stored in −80°C. Then the tissues were homogenized in ice-cold cell lysis buffers (Beyotime Institute of Biotechnology, Haimen, Jiangsu, China) containing 1% phenylmethanesulfonylfluoride (Beyotime Institute of Biotechnology) and 1% phosphatase inhibitor cocktail (Roche Diagnostics GmbH, Mannheim, Germany), respectively. The protein concentration of each fraction was determined using a Lowry protein assay. Equal amounts of protein were separated and transferred to polyvinylidene fluoride membranes. Then, the membranes were incubated with primary antibodies: rabbit anti-NK-1R antibody (1 : 3000 dilution, Sigma), rabbit anti-β-catenin antibody (1 : 500 dilution, Cayman), rabbit anti-GFAP-antibody (1 : 2000 dilution, Sigma), rabbit anti-COX-2 antibody (1 : 200 dilution, Cayman), and rabbit anti-β-tubulin antibody (1 : 5000 dilution; ABclonal Biotech Co., Ltd., Baltimore Avenue, USA) overnight at 4°C. After reaction with a horseradish peroxidase-conjugated anti-rabbit secondary antibody (1 : 2000 dilution; Cell Signaling Technology, Beverly, MA), the proteins were detected using an ECL detection reagent according to a previously described method [13].

The results are shown as the means ± SEM. The statistical analysis was performed by one- or two-way ANOVA, as indicated in the text, using InStat software (GraphPad Prism 5, USA). A p value less than 0.05 was considered to be statistically significant.

3. Results

As shown in Figure 1(a) and Figure I (online-only Supplementary Material available at http://dx.doi.org/10.1155/2016/1437148), on the 5th day, there was a significant difference in the thermal pain threshold between the model group (14.5 ± 1.7 s) and the control group (25.2 ± 0.9 s). The thermal pain thresholds of the rats in the fluoxetine-treated and different frequency EA-treated groups were increased (19.3 ± 3.5 s for fluoxetine; 18.4 ± 1.4 s, 22.2 ± 3.1 s, and 22.3 ± 2.3 s for 2, 2/15, and 15 Hz, resp.) compared to the rats in the model group, which also showed that the efficacy of the EA treatment, particularly the high-frequency EA treatment, was better than fluoxetine. Similar to the changes in the thermal pain thresholds, there appeared to be a decreasing trend in the cold pain threshold after the EA treatment (Figure 1(b)). However, regarding the mechanical pain threshold, the efficacies of fluoxetine and the different frequencies of EA treatment were nearly identical (92.4 ± 5.6 s for fluoxetine; 89.6 ± 10.5%, 89.2 ± 6.3%, and 97.6 ± 4.8% of the control for 2, 2/15, and 15 Hz, resp.; Figure 1(c)). Taken together, the results shown in Figures 1(a), 1(b), and 1(c) indicated that fluoxetine and EA treatment could relieve CPSP, while the administration of high-frequency EA led to the best performance.

Regarding the neuropathological changes in the brain, on the 5th day after the collagenase injection into the thalamus, the brains exhibited obvious cerebral hemorrhages, neuronal cell damage, and aberrant glial cell activation compared to those in the control group. After the treatment with fluoxetine or different patterns of EA, increased Nissl body staining, decreased hematoma sizes, and relieved inflammation were observed, which indicated that the EA treatment for CPSP was effective (Figure 1(d)). It is also important to note that the changes on the above parameters made by EA treatments exceed fluoxetine, demonstrating a better efficacy of EA treatments. Moreover, among EA treatments, the low-frequency one exhibited the best efficacy in improving the neuropathological changes in the brain.

To further analyze the correlations between EA administration and the cellular apoptosis in brain tissues, a TUNEL assay and a multispectral imaging analysis were performed to quantify the relative rates of cellular apoptosis. As shown in Figure 2(a), glial cell apoptosis was noticeable around the damaged area in the model group (375.3 ± 44.3% of the control) compared to the control group (100.0 ± 19.9%). After EA treatment at the corresponding frequencies, apoptosis was downregulated (184.4 ± 16.6%, 210.8 ± 35.7%, and 222.0 ± 78.2% of the control for 2, 2/15, and 15 Hz, resp.), and the efficacy was better than that of the fluoxetine group (254.1 ± 20.9% of the control).

As shown in Figure 2(b), apoptosis was observed in the neocortex and hippocampus sections from the model group (188.8 ± 29.9% and 185.9 ± 14.5% of the control, resp.). After the EA treatment, the relative cellular apoptosis rate in both the neocortex and hippocampus of the CPSP rats sharply decreased and the low-frequency EA treatment exhibited the best efficacy (102.3 ± 23.1% of the control and 141.4 ± 10.9% of the control, resp.), which was closely followed by

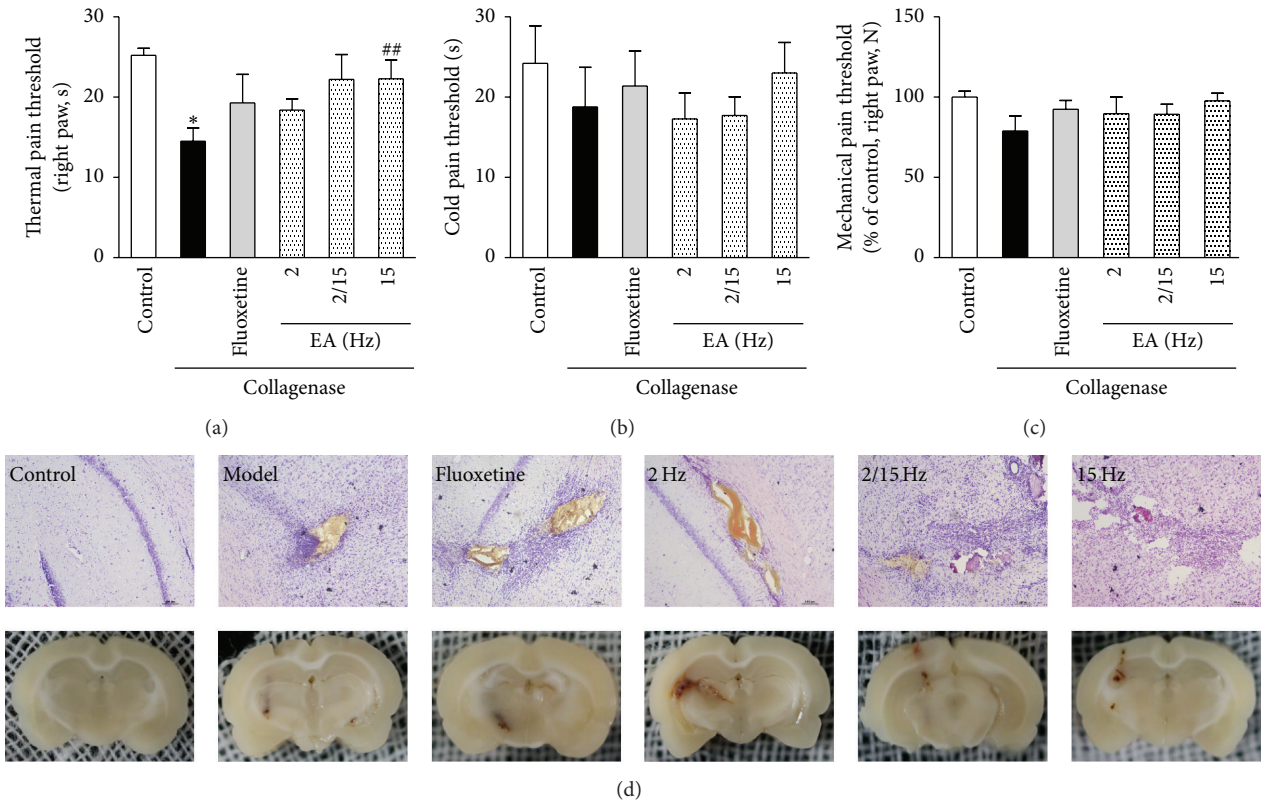

Figure 1: Effects of the different frequency EA treatments on pain-related behavioral responses and neuropathological changes in the brains of the CPSP rats. Changes in the thermal (a), cold (b), and mechanical (c) hyperalgesia in the contralateral paw of CPSP rats that had been treated with or without EA at different frequencies. (d) Representative photomicrographs of Nissl staining in equivalent coronal sections of the brains of the CPSP rats on the 5th day after the operation. $*$ denotes $p < 0.05$ versus the control; ## denotes $p < 0.01$ versus the model ($n = 5$ in each group; one-way analysis of variance, followed by the Newman-Keuls *post hoc* test).

the fluoxetine group (114.2 ± 19.2% and 159.8 ± 8.4% of the control, resp.).

As shown in Figure 3(a), the astrocytes in the model group were hypertrophic and showed a remarkable increase in the number of cells. On the contrary, there were fewer and smaller astrocytes in the fluoxetine- and EA-treated groups.

In Figure 3(b), the expression of GFAP in the model group (716.9 ± 22.6% of the control) was significantly increased after the collagenase injection compared to the control group (100.0 ± 34.8%). After the EA treatment, GFAP expression (466.9 ± 75.6%, 531.7 ± 38.0%, and 430.5 ± 52.9% of the control for 2, 2/15, and 15 Hz, resp.) decreased, and the high-frequency EA was more effective. In addition, the efficacy of the fluoxetine group (567.3 ± 46.0% of the control) was marginally reduced compared to the EA-treated groups.

Aberrant GFAP expression was observed in the neocortex and hippocampal sections from the model group (1419.4 ± 36.3% and 1491.7 ± 43.8% of the control, resp.). After the EA treatment, GFAP expression was sharply decreased, and the high-frequency EA treatment exhibited highest efficiency (586.4 ± 33.2% and 509.0 ± 47.2% of the control, resp.). Moreover, the efficacy of the fluoxetine group (938.2 ± 48.3% and 797.8 ± 50.1% of the control, resp.) was marginally reduced compared to the EA-treated groups.

To further confirm the inhibitory effect of the EA treatment on GFAP expression, Western blotting analysis was performed using the proteins extracted from the neocortex and hippocampus of the rats in the same groups (Figure 3(c)). GFAP expression was also significantly increased in the neocortex and hippocampus from the rats in the model group (180.6 ± 7.1% and 180.3 ± 12.6% of the control, resp.). After the EA treatment, the GFAP expression levels in the neocortex and hippocampus were decreased (107.9 ± 8.8% and 82.7 ± 17.1% of the control, resp.), and the high-frequency EA treatment exhibited better efficacy. In addition, GFAP expression in the tissues from the fluoxetine group (148.8 ± 5.7% and 125.9 ± 9.2% of the control, resp.; Figure 3(d)) was increased compared to those in the EA groups. As a result, the EA treatment, particularly the high-frequency EA treatment, attenuates aberrant glial activation, thereby reducing neuronal cell damage.

As shown in Figure 4(a), there were a massive inflammatory infiltration and a large number of COX-2-positive cells around the damaged brain tissue after the collagenase injection compared to the control group. After an intragastric administration of fluoxetine or the EA treatment, a reduced number of COX-2-positive cells were observed in brain tissues, and the inflammation was relatively reduced compared to the control group, which indicated that the EA treatments

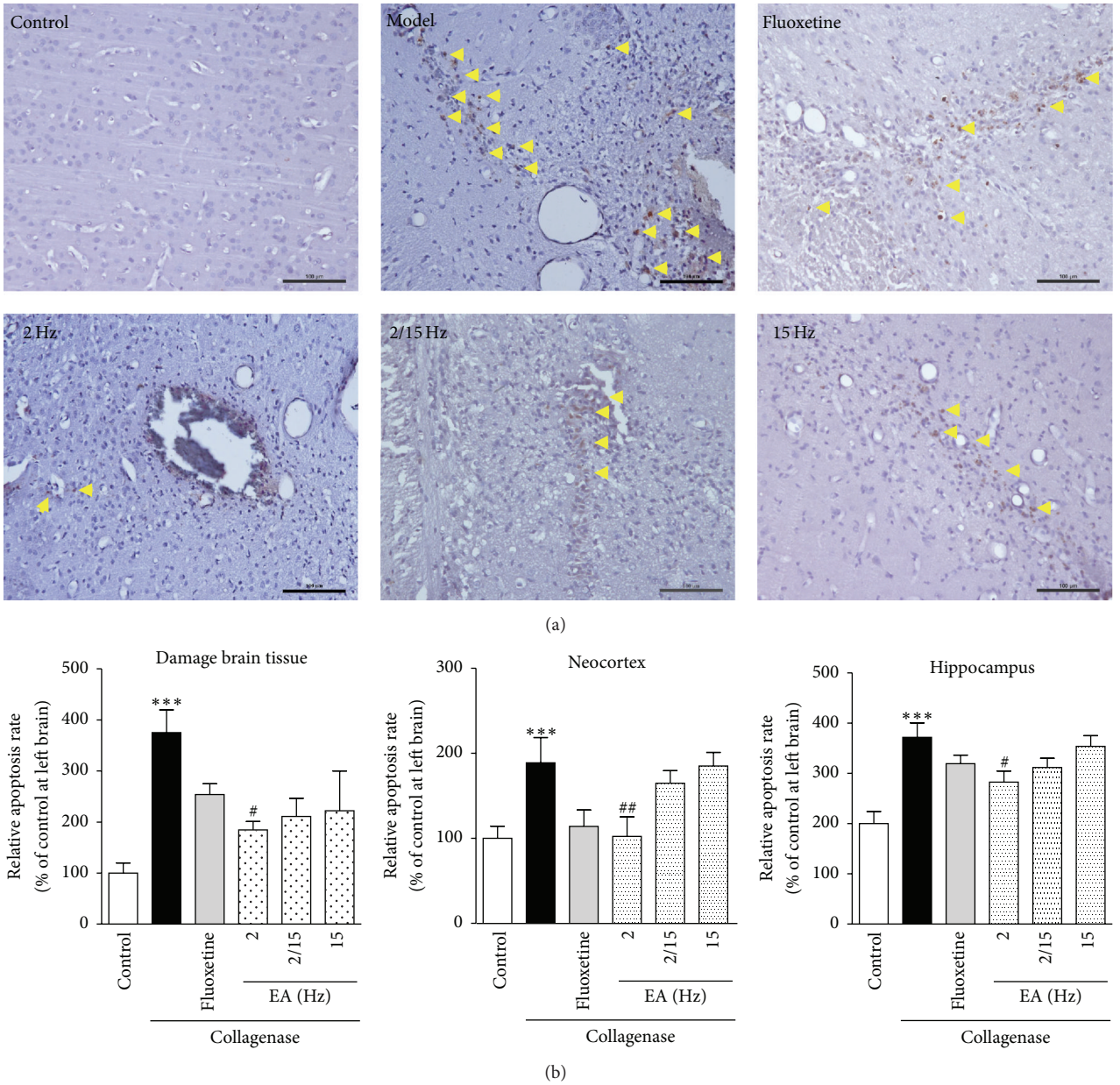

Figure 2: Effects of the different frequency EA treatments on neuronal apoptosis in the brains of the CPSP rats. (a) Representative photomicrographs of TUNEL staining in the brains of the CPSP rats that had been treated with or without EA on the 5th day after the operation. The yellow arrows denote neuronal cell apoptosis. (b) Determination of neuronal cell apoptosis rate in the brains of the CPSP rats (ipsilateral brain section) using a multispectral analysis. $***$ denotes $p < 0.001$ versus the control; # and ## denote $p < 0.05$ and 0.01 versus the model ($n = 5$ in each group; one-way analysis of variance, followed by the Newman-Keuls *post hoc* test).

with different frequency patterns were effective at alleviating CPSP. We further quantified COX-2 expression using a multispectral quantitative technology. COX-2 expression (322.0 ± 35.0%, 330.3 ± 27.5%, and 316.2 ± 73.6% of the control for 2, 2/15, and 15 Hz, resp.) decreased after the EA treatment compared to the model group (494.0 ± 60.4% of the control) and was slightly better than the fluoxetine group (349.7 ± 27.9% of the control).

Moreover, we quantified COX-2 expression in the the neocortex and hippocampus. The EA treatment decreased COX-2 expression in the neocortex (179.5 ± 34.1%, 229.8 ± 26.8%, and 176.5 ± 35.1% of the control for 2, 2/15, and 15 Hz, resp.) compared to that in the model group (499.2 ± 24.3% of the control), and the efficacy of the high-frequency EA treatment was better than the EA treatments of other patterns and fluoxetine (309.7 ± 15.4% of the control). However, the phenomenon was not evident in the hippocampus (Figure 4(b)).

As shown in Figure 4(c), we further investigated the inhibitory effects of the EA treatment on COX-2 expression

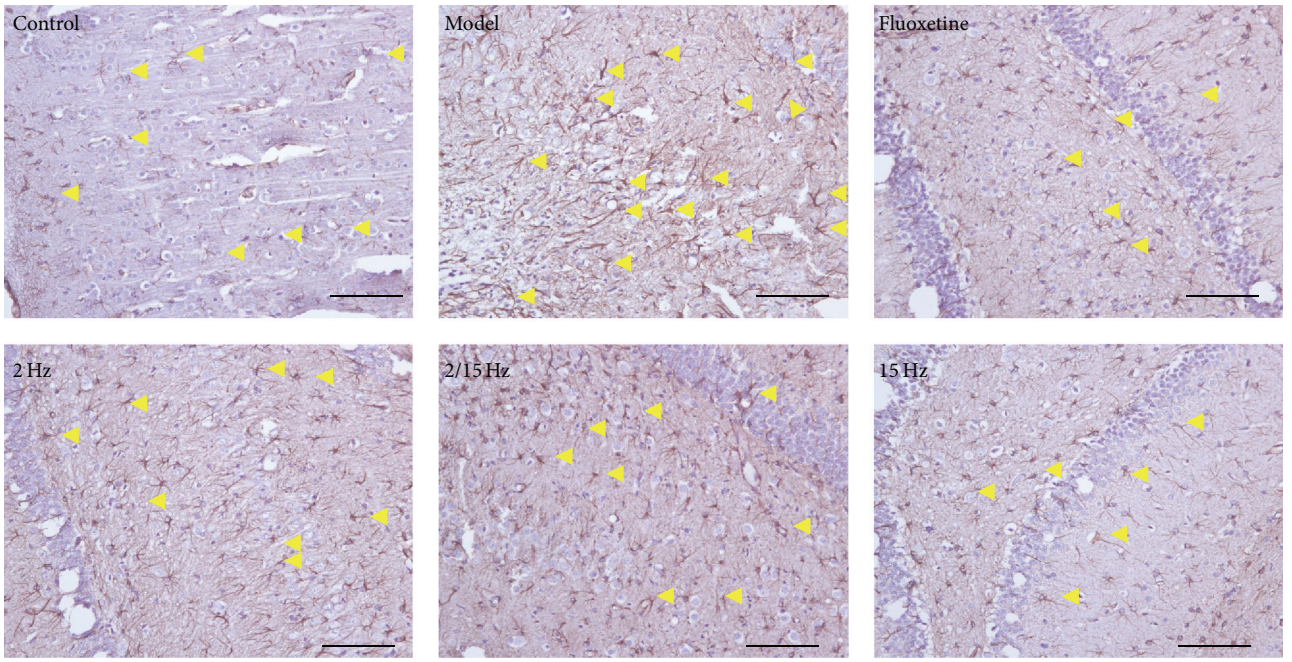

(a)

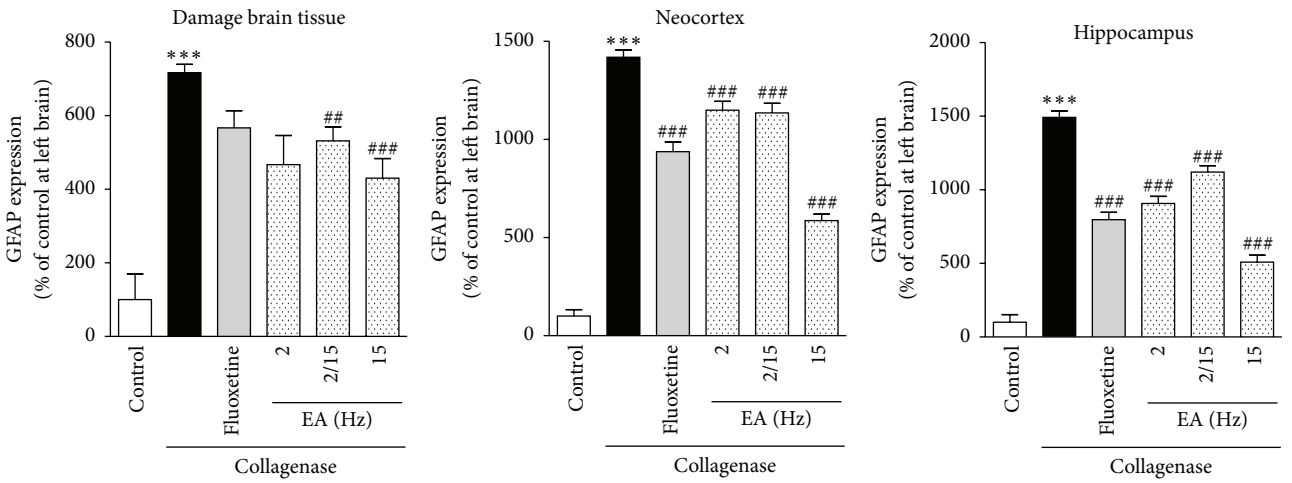

(b)

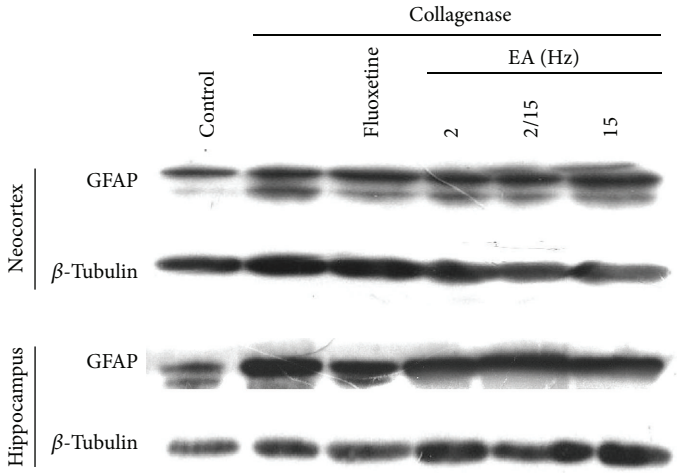

(c)

Figure 3: Continued.

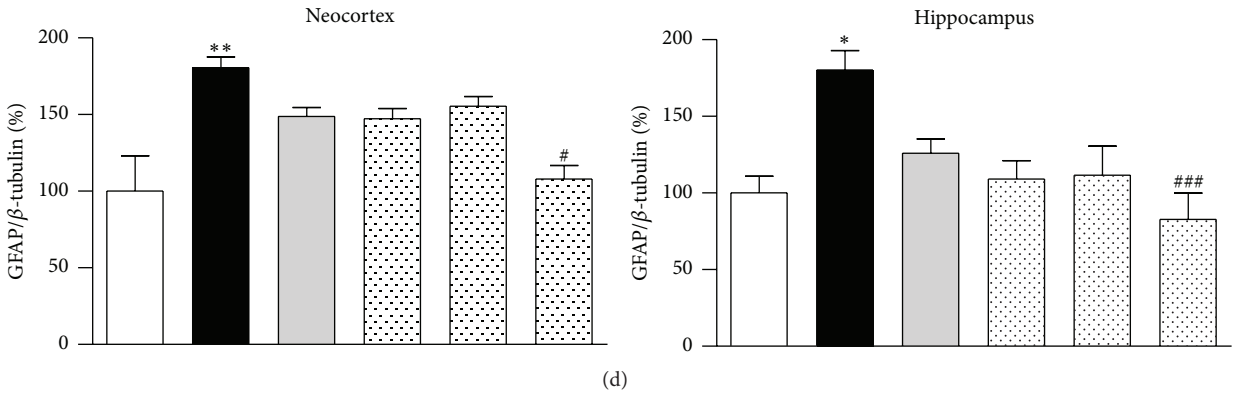

Figure 3: Effects of the different frequency EA treatments on GFAP expression in the brains of the CPSP rats. (a) Representative photomicrographs of immunohistochemical staining of GFAP expression in the brains of the CPSP rats that had been treated with or without EA on the 5th day after the operation. The yellow arrows denote glia cells. (b) Determination of GFAP expression in the brains of the CPSP rats using a multispectral analysis (ipsilateral brain section). (c) Representative Western blots of ipsilateral GFAP expression in the neocortex and hippocampus of the CPSP rats. (d) Western blot determination of (c). ∗, ∗∗, and ∗∗∗ denote $p < 0.05$, 0.01, and 0.001 versus the control; #, ##, and ### denote $p < 0.05$, 0.01, and 0.001 versus the model ($n = 5$ in each group; one-way analysis of variance, followed by the Newman-Keuls *post hoc* test), respectively.

by Western blotting analysis using the proteins extracted from the neocortex and hippocampus of the rats in the same groups. As expected, the EA treatments of different patterns and fluoxetine significantly decreased the COX-2 expression levels in the neocortex (142.4 ± 6.7%, 114.4 ± 12.3%, and 108.7 ± 19.8% of the control for 2, 2/15, and 15 Hz, resp.; 158.5 ± 8.1% of the control for fluoxetine) compared to the model group (163.9 ± 8.9% of the control), and the high-frequency EA treatment exhibited better efficacy (Figure 4(d)). Therefore, we could conclude that the EA treatment, particularly the high-frequency EA treatment, could inhibit COX-2 expression to attenuate the inflammation induced by the collagenase injection.

Next, the effects of the EA treatment on the expression of β-catenin in the CPSP rats were investigated. As shown in Figure 5(a), a large number of β-catenin-positive cells were observed around the damaged brain tissues, particularly in the cytoplasm and cell nucleus of the CPSP rats compared to the control group. After the EA treatment, the number of β-catenin-positive cells was relatively reduced compared to that in the control or fluoxetine groups, which indicated that the EA treatment was effective on CPSP. We further quantified β-catenin expression using a multispectral quantitative technology. As shown in Figure 5(b), β-catenin expression (121.7 ± 15.8%, 123.0 ± 13.1%, and 117.5 ± 12.9% of the control for 2, 2/15, and 15 Hz, resp.) decreased after the EA treatment compared to the model group (137.4 ± 26.7% of the control) and the fluoxetine group (131.8 ± 24.2% of the control), confirming that the high-frequency EA treatment exhibited better efficacy.

Moreover, β-catenin expressions in the different brain regions, such as the neocortex and hippocampus, were quantified and compared. Compared to the model group (252.9 ± 26.2% of the control), the high-frequency EA treatment (167.8 ± 17.6% of the control) inhibited β-catenin expression in the hippocampus of the CPSP rats, and the high-frequency EA treatment exhibited better efficacy (Figure 5(b)).

To further study β-catenin expression after the EA treatment, we evaluated the efficacy of EA treatment by Western blotting analysis using the proteins extracted from the neocortex and hippocampus of the rats from the same groups (Figure 5(c)). β-Catenin expression decreased in the neocortex and hippocampus of the 15 Hz group (neocortex: 78.9 ± 10.0%; hippocampus: 60.4 ± 8.2% of the control) after the EA treatment and the expression was further reduced in the fluoxetine group (neocortex: 106.2 ± 19.4% of the control; hippocampus: 107.4 ± 7.9% of the control) compared to the model group (neocortex: 129.2 ± 12.4% of the control; hippocampus: 114.8 ± 13.3% of the control). Moreover, the high-frequency EA treatment exhibited better efficacy (Figure 5(d)). Consequently, the high-frequency EA treatment inhibited β-catenin expression and produced analgesic effects.

As shown in Figure 6(a), a large number of NK-1R-positive cells were observed around the damaged brain tissues after the collagenase injection compared to the control groups, particularly the model group. However, a smaller number of NK-1R-positive cells were observed in the fluoxetine group compared to the model group. After the EA treatment, the number of NK-1R-positive cells was relatively reduced compared to the fluoxetine group, which indicated that the EA treatment for CPSP was effective. To further demonstrate the expression, NK-1R expression was further quantified using a multispectral quantitative technology. As shown in Figure 6(b), NK-1R expression (592.0 ± 41.9%, 553.4 ± 31.9%, and 528.5 ± 88.1% of the control for 2, 2/15, and 15 Hz, resp.) decreased after the EA treatment compared to the model group (695.2 ± 10.8% of the control). The level of NK-1R expression in the fluoxetine group (640.5 ± 97.1% of the control) was between that of the model group and that

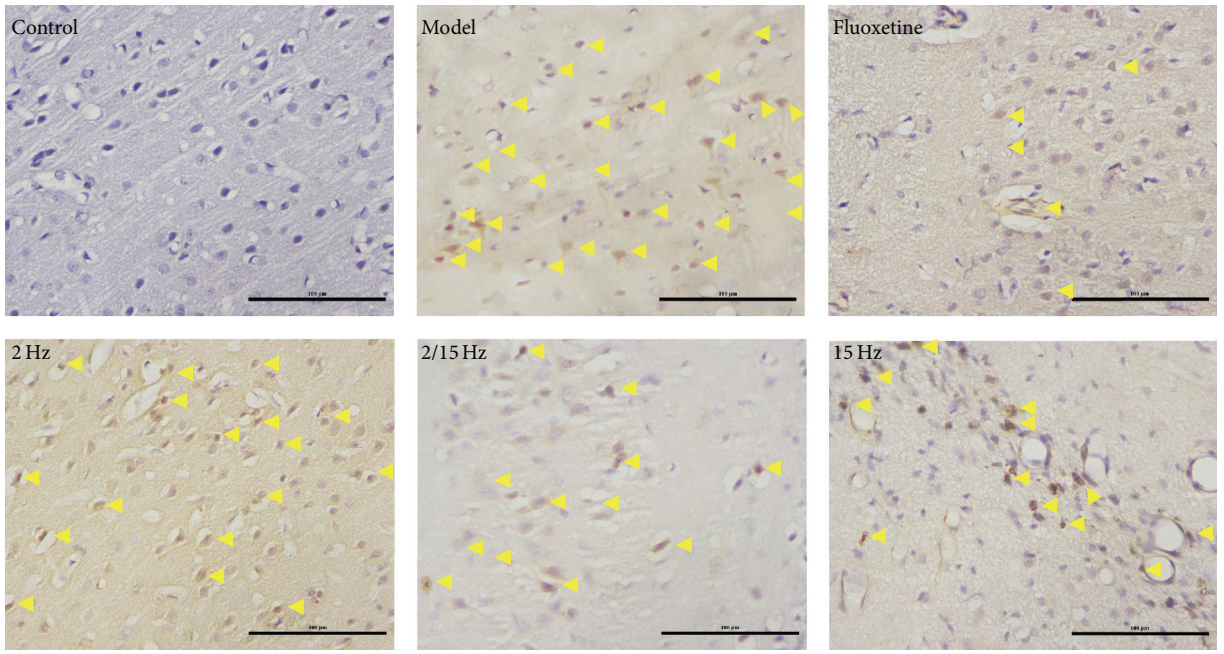

(a)

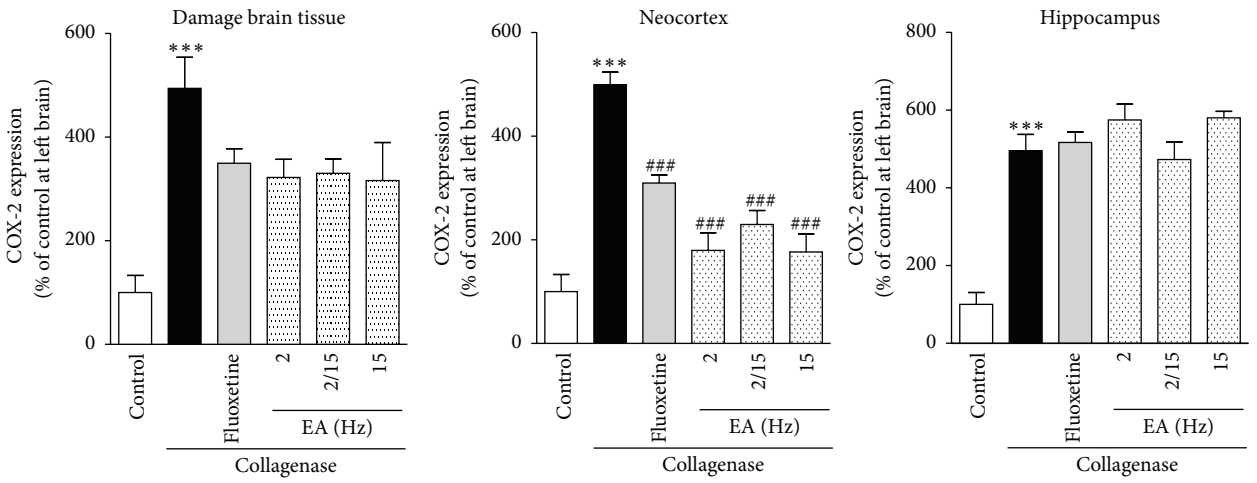

(b)

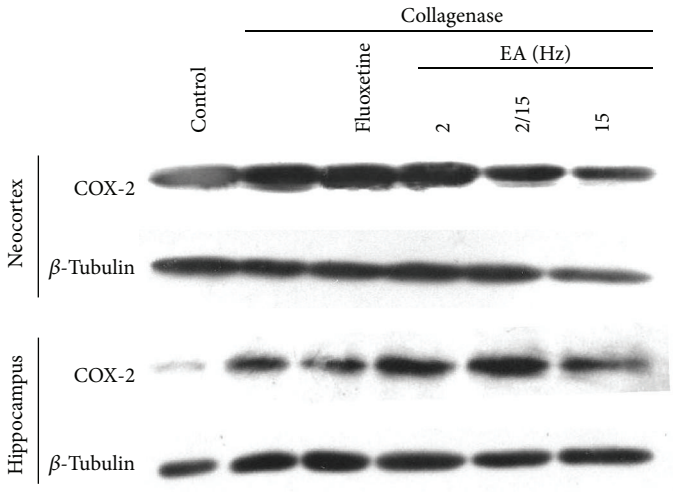

(c)

Figure 4: Continued.

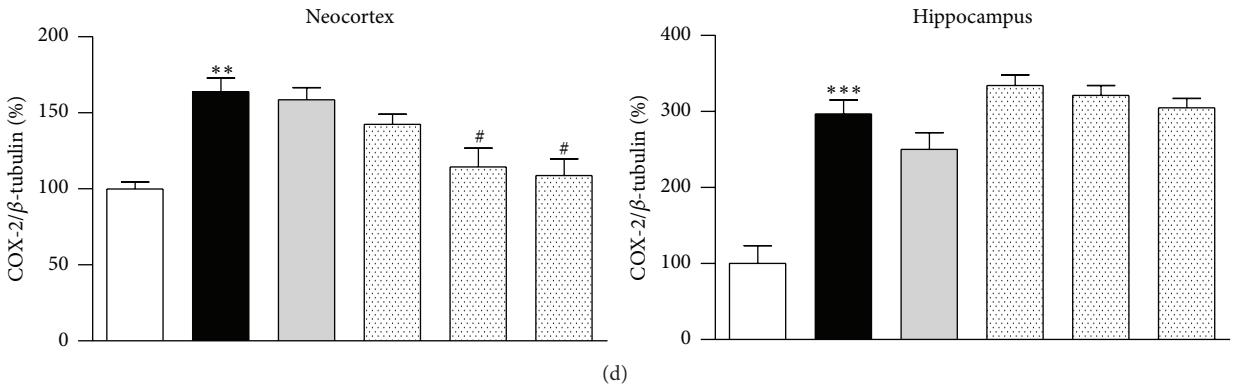

Figure 4: Effects of the different frequency EA treatments on COX-2 expression in the brains of the CPSP rats. (a) Representative photomicrographs of immunohistochemical staining of COX-2 expression in the brains of the CPSP rats that had been treated with or without EA on the 5th day after the operation. (b) Determination of COX-2 expression in the brains of the CPSP rats using a multispectral analysis (ipsilateral brain section). (c) Representative Western blots of COX-2 expression in the ipsilateral neocortex and hippocampus of the CPSP rats. (d) Western blot determination of (c). ∗∗ and ∗∗∗ denote $p < 0.01$, 0.001 versus the control; # and ### denote $p < 0.05$, 0.001 versus the model ($n = 5$ in each group; one-way analysis of variance, followed by the Newman-Keuls *post hoc* test).

of the EA groups, which showed that the high-frequency EA treatment exhibited better efficacy.

Moreover, we quantified NK-1R expressions in different brain regions, such as the neocortex and hippocampus, respectively. NK-1R expression was significantly decreased in the neocortex and hippocampus (neocortex: 528.5 ± 88.1% of the control; hippocampus: 635.3 ± 53.2% of the control) of the EA-treated groups compared to the model group (neocortex: 1232.0 ± 60.4% of the control; hippocampus: 1516.3 ± 62.6% of the control), and the effect of fluoxetine (neocortex: 1220.6 ± 54.4% of the control; hippocampus: 1399.1 ± 59.6% of the control) was not as significant as the EA treatments. Therefore, the high-frequency EA treatment exhibited better efficacy (Figure 6(b)).

To further study NK-1R expression after the EA treatment, the efficacy of EA treatment was evaluated by Western blotting analysis using the proteins extracted from the neocortex and hippocampus of the rats in the same groups (Figure 6(c)). NK-1R expression was significantly decreased in the neocortex and hippocampus of the 15 Hz group (neocortex: 85.3 ± 8.7% of the control; hippocampus: 56.1 ± 8.6% of the control) after EA treatment compared to the model group (neocortex: 268.7 ± 12.4% of the control; hippocampus: 150.3 ± 9.8% of the control), whereas NK-1R expression in the fluoxetine group (neocortex: 212.0 ± 26.0% of control; hippocampus: 121.3 ± 8.9% of control) was higher than that of the EA groups. It was speculated that the high-frequency EA treatment exhibited better efficacy (Figure 6(d)). Hence, the high-frequency EA treatment could significantly downregulate NK-1R expression, thus exerting a direct analgesic effect.

4. Discussion

In the present study, we confirmed that low-frequency and high-frequency EA treatments exert analgesic effects by inhibiting neuronal cell apoptosis and aberrant astrocyte activation in the brain. Different regions of the brain, particularly the neocortex and hippocampus, are related to the generation of CPSP.

It is known that some kinds of medicine can relieve CPSP in some degree [4] and acupuncture, which has been used in China and other Asian countries for the past 3,000 years, represents a potentially valuable adjunct therapy to the existing strategies for pain relief. Some researchers have studied the process of pain and showed that neuronal cell apoptosis and abnormal astrocyte activation play an important role in pain. A growing body of evidence supports the role of astrocytes in the development of persistent pain and hypersensitivity after injury [14]. Researchers have proved that the molecular and cellular alterations in the primary sensory neurons and the neurons in the spinal dorsal horn play important roles in the pathogenesis of neuropathic pain after peripheral nerve injury [15]. However, the mechanism by which the neuronal cell apoptosis and abnormal astrocyte activation promote CPSP is not clear. As expected, we have confirmed that neuronal cell apoptosis and abnormal astrocyte activation in the brain indeed occurred in CPSP (Figures 2 and 3), and the low-frequency EA was effective at relieving neuronal cell apoptosis, while the high-frequency EA was effective at inhibiting the abnormal astrocyte activation. Moreover, the EA treatment could relieve the CPSP and its efficacy was better than that of fluoxetine (a positive drug to treat the stroke through improving infarct volumes and neurobehavioral [16]; Figure 1).

As an inducible enzyme that is pivotal in the inflammatory response, COX-2 converts arachidonic acid to prostaglandins, which are necessary for the biosynthesis and release of substance P during the development of inflammation [12]. Moreover, nerve injury evoked a positive feedback loop between COX-2 and β-catenin for the biosynthesis and release of substance P, which may contribute to the responses related to neuropathic pain [17]. Thus, we could speculate that the possible mechanism by which the EA

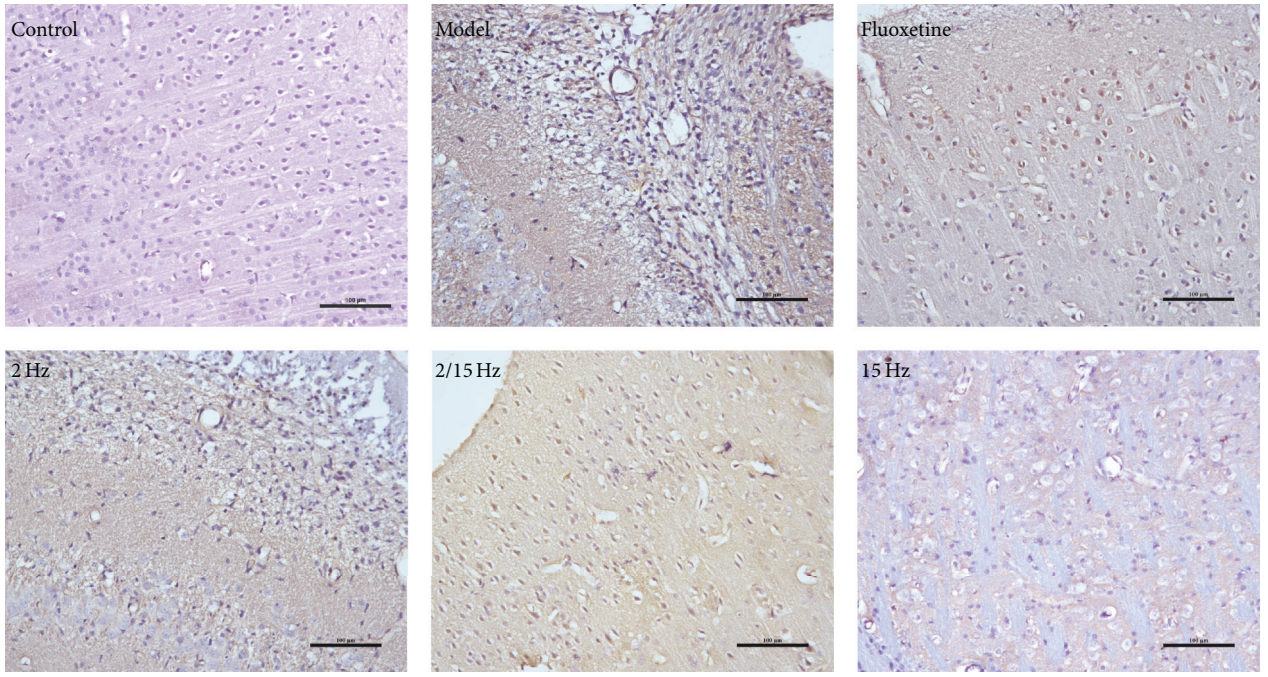

(a)

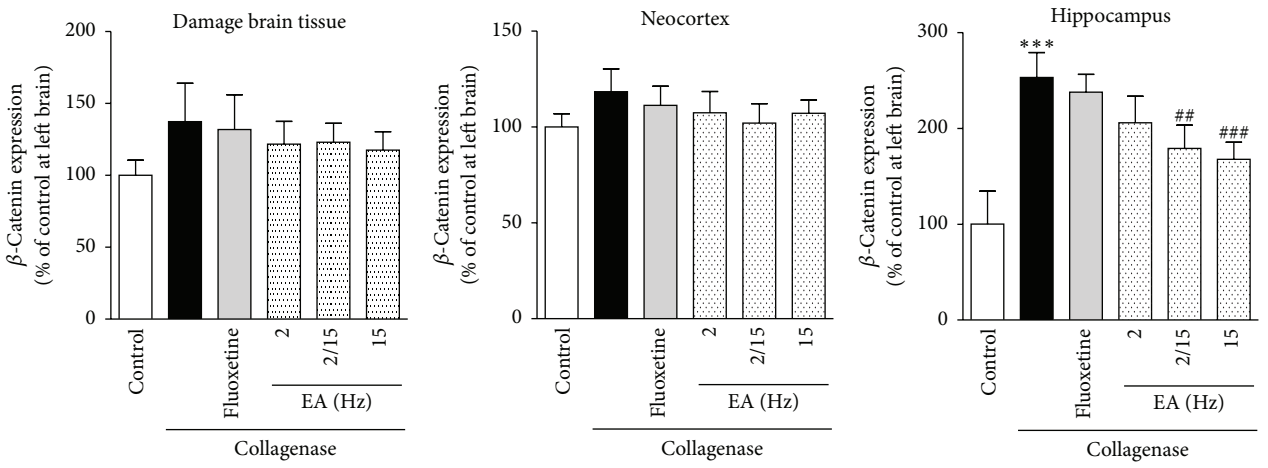

(b)

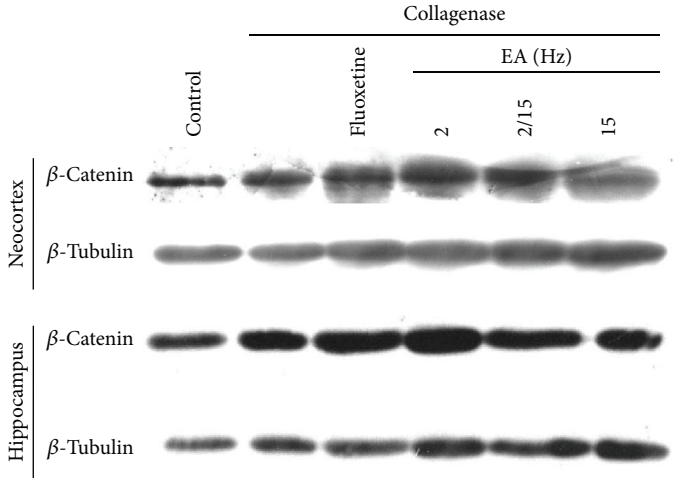

(c)

Figure 5: Continued.

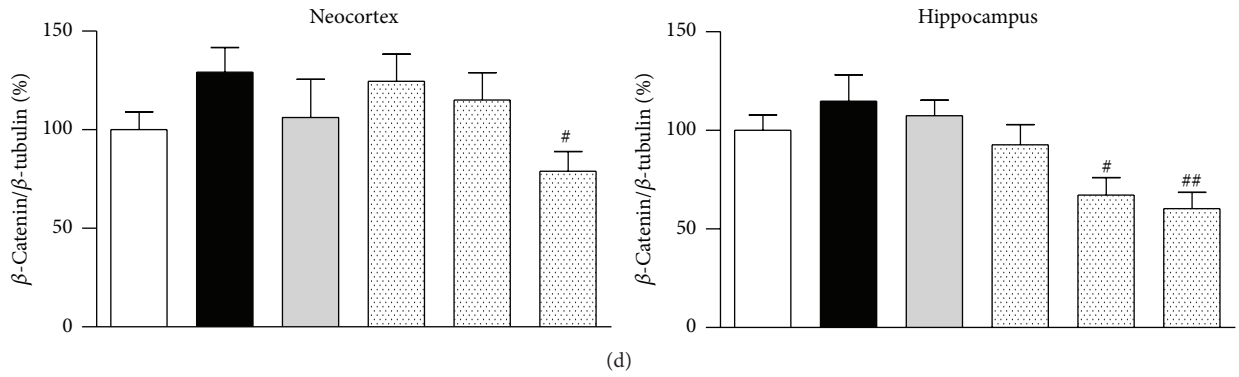

Figure 5: Effects of the different frequency EA treatments on β-catenin expression in the brains of the CPSP rats. (a) Representative photomicrographs of immunohistochemical staining of β-catenin in the brains of the CPSP rats that had been treated with or without EA on the 5th day after the operation. (b) Determination of β-catenin expression in the brains of the CPSP rats brain using a multispectral analysis (ipsilateral brain section). (c) Representative Western blots of β-catenin expression in the ipsilateral neocortex and hippocampus of the rats. (d) Western blot determination of (c). $***$ denotes $p < 0.001$ versus the control; #, ##, and ### denote $p < 0.05$, 0.01, and 0.001 versus the model ($n = 5$ in each group; one-way analysis of variance, followed by the Newman-Keuls *post hoc* test).

treatment improved CPSP was through the downregulation of β-catenin expression to exert an analgesic effect.

In addition, NK-1R is an endogenous receptor for substance P. The binding of substance P to NK-1R is thought to be related to the transmission of pain signals [18]. Preclinical studies show that NK-1R antagonists exert an analgesic effect, and clinical studies in humans have shown that these antagonists are generally ineffective for the treatment of pain [19]. The upregulated NK-1R expression in the CPSP rats could be attenuated by the EA treatment (Figure 6), suggesting that the EA treatment can relieve CPSP better than NK-1R antagonists.

Moreover, some previous studies have demonstrated that the low-frequency EA treatment for CPSP inhibits neuronal cell apoptosis. Wang et al. indicated that different frequency EAs were spatially specific, and the 2 Hz EA treatment regulated more genes, which were associated with apoptosis [20]. Compared to the above observations, our present findings strongly suggested that low-frequency EA was effective at alleviating CPSP by inhibiting neuronal cell apoptosis. Xiang et al. described that the different frequencies of EA were mediated by different opioid receptors in specific areas of the central nervous system [21]; therefore, the different frequency EA treatments may have different roles in various pathways. Some other studies have proved that the analgesia induced by high-frequency EA (>100 Hz) is mainly mediated by the release of dynorphins and κ receptors [22]. In the present study, we have demonstrated that the high-frequency EA treatment exerted a greater analgesic effect mainly by regulating the expression of pain signal transmission-related mediators (β-catenin, COX-2, and NK-1R). Based on the above discussion, we are interested in exploring the therapeutic effect of EA at an alternating frequency (2/15 Hz). Unfortunately, the therapeutic effect of the 2/15 Hz EA treatment is worse than that of the 2 Hz or 15 Hz EA treatments, which will be further investigated in a future study.

Dejerine and Roussy firstly described that CPSP had a thalamic origin, which was characterized by neuropathic pain emerging from thalamic lesions, such as infarctions and bleeds [23]. The hippocampus is the most sensitive area to cerebral hemorrhage and has important roles in learning and memory, which has a close relationship with cognitive function. In addition, the prefrontal cortex is known to participate in executive function, emotions, and pain. Some studies have shown that prefrontal cortical dysfunction occurs in chronic pain patients [24]. Therefore, in our study, we investigated the expression levels of GFAP, β-catenin, COX-2, and NK-1R in the neocortex and hippocampus to explore their relationships with pain. Abnormal astrocyte activation has been observed in the cortex in other models of neuropathic pain [25], but not in rat CPSP model. However, GFAP expression was downregulated in the neocortex and hippocampus after the EA treatment (Figure 3). Many lines of experimental evidence emphasized the significance of blocking the COX-2 pathway in therapeutic strategies for global cerebral ischemia. COX-2 expression was dramatically increased in the injured hippocampus of animal models following global cerebral ischemia [26]. We indeed found that EA could downregulate COX-2 expression to exert an analgesic effect in the hippocampus (Figure 4). Growing evidence showed that an NK-1R antagonist could disrupt the binding of substance P to NK-1R, which significantly improved the motor and cognitive outcomes and inhibited dyskinesia in a hemi-Parkinsonian rat model [27]. Moreover, the NK-1R antagonist reduced brain edema and axonal injury in experimental models of traumatic brain injury [28]. Similar to the NK-1R antagonist, the NK-1R expression was indeed downregulated after the EA treatment (Figure 6). In a previous study, treatment with lithium ions decreased β-catenin expression in the ischemic cortex, when assessed 3 days after an endothelin-1 injection [29]. EA treatment downregulated β-catenin expression in both the cortex and hippocampus (Figure 5). Thus, we may conclude that the EA

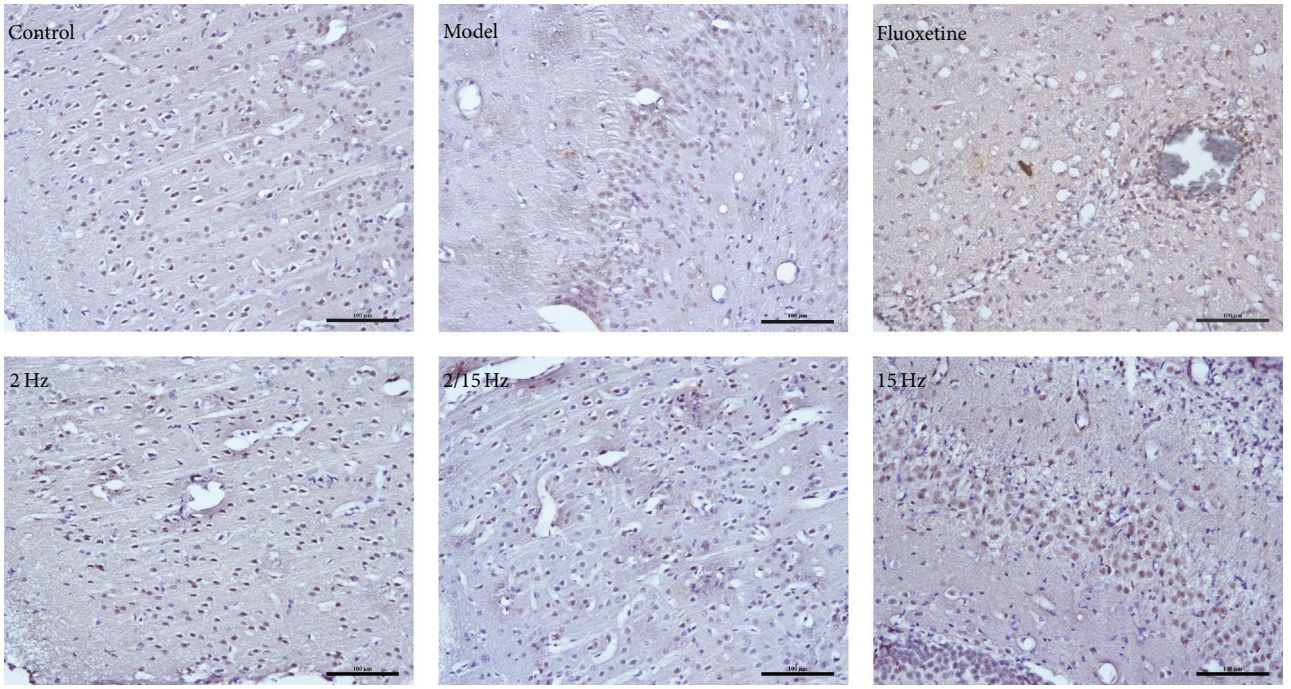

(a)

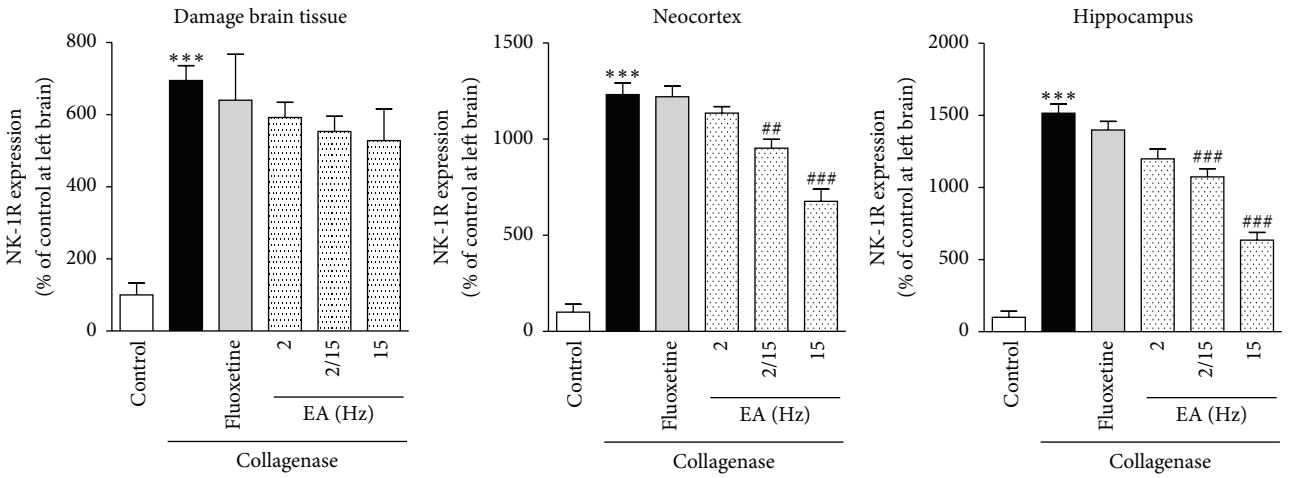

(b)

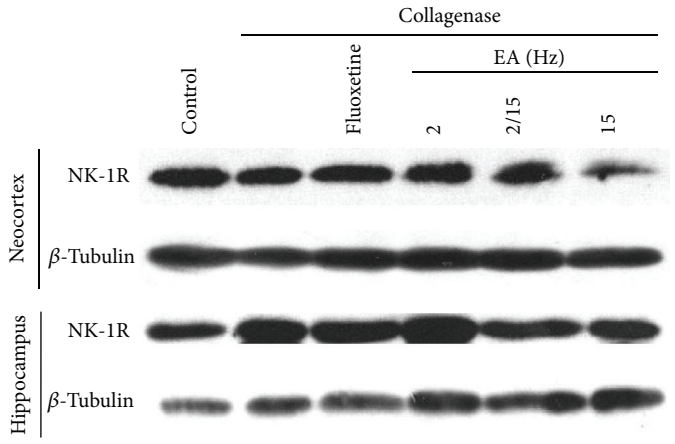

(c)

Figure 6: Continued.

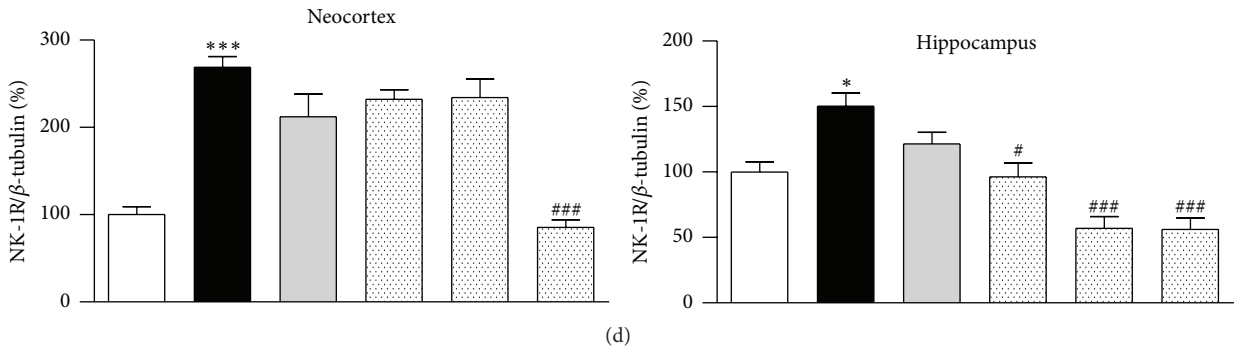

Figure 6: Effects of the different frequency EA treatments on NK-1R expression in the brains of the CPSP rats. (a) Representative photomicrographs of immunohistochemical staining of NK-1R expression in the brains of the CPSP rats that had been treated with or without EA on the 5th day after the operation. (b) Determination of NK-1R expression in the brains of the CPSP rats using a multispectral analysis (ipsilateral brain section). (c) Representative Western blots of NK-1R expression in the ipsilateral neocortex and hippocampus of the CPSP rats. (d) Western blot determination of (c). $*$ and $***$ denote $p < 0.05$ and 0.001 versus the control; #, ##, and ### denote $p < 0.05$, 0.01, and 0.001 versus the model ($n = 5$ in each group; one-way analysis of variance, followed by the Newman-Keuls *post hoc* test).

treatment for CPSP could downregulate the expression of some pain signal transmission-related mediators in different brain regions, particularly the neocortex and hippocampus.

In summary, our studies strongly confirmed that the EA treatment was effective at alleviating CPSP, and different regions of the brain, particularly the neocortex and hippocampus, have a significant relationship with the generation of pain. Low-frequency and high-frequency EA treatments may exert abirritation effects by inhibiting neuronal apoptosis and aberrant astrocyte activation. However, this finding was observed only by histomorphology and still must be verified at the protein and nucleic acid levels. Moreover, additional investigations are required to fully elucidate the signaling pathways. Nevertheless, the present findings may elucidate the mechanism of EA treatment for CPSP from a novel perspective.

Competing Interests

The authors declare that there is no conflict of interests regarding the publication of this paper.

Authors' Contributions

Gui-Hua Tian and Shan-Shan Tao contributed equally to this work.

Acknowledgments

Funding for this work was provided by the National Natural Science Foundation of China (81403468 and 81573887), Beijing Nova Program (XX2014B049), and the Fundamental Research Funds for the Central Universities of China (CZZ15007).

References

[1] F. Blasi, F. Herisson, S. Wang, J. Mao, and C. Ayata, "Late-onset thermal hypersensitivity after focal ischemic thalamic infarcts as a model for central post-stroke pain in rats," *Journal of Cerebral Blood Flow and Metabolism*, vol. 35, no. 7, pp. 1100–1103, 2015.

[2] H. Klit, N. B. Finnerup, G. Andersen, and T. S. Jensen, "Central poststroke pain: a population-based study," *Pain*, vol. 152, no. 4, pp. 818–824, 2011.

[3] S.-Y. Cho, J.-Y. Park, W.-S. Jung et al., "Bee venom acupuncture point injection for central post stroke pain: a preliminary single-blind randomized controlled trial," *Complementary Therapies in Medicine*, vol. 21, no. 3, pp. 155–157, 2013.

[4] M.-M. Backonja, G. Irving, and C. Argoff, "Rational multidrug therapy in the treatment of neuropathic pain," *Current Pain and Headache Reports*, vol. 10, no. 1, pp. 34–38, 2006.

[5] L. Lao, R.-X. Zhang, G. Zhang, X. Wang, B. M. Berman, and K. Ren, "A parametric study of electroacupuncture on persistent hyperalgesia and Fos protein expression in rats," *Brain Research*, vol. 1020, no. 1-2, pp. 18–29, 2004.

[6] X.-L. Yang, C. K. Kim, T. J. Kim et al., "Anti-inflammatory effects of fimasartan via Akt, ERK, and NFκB pathways on astrocytes stimulated by hemolysate," *Inflammation Research*, vol. 65, no. 2, pp. 115–123, 2016.

[7] M. J. Pérez-Álvarez, M. D. C. Maza, M. Anton, L. Ordoñez, and F. Wandosell, "Post-ischemic estradiol treatment reduced glial response and triggers distinct cortical and hippocampal signaling in a rat model of cerebral ischemia," *Journal of Neuroinflammation*, vol. 9, article 157, 2012.

[8] C. L. MacLellan, G. Silasi, C. C. Poon et al., "Intracerebral hemorrhage models in rat: comparing collagenase to blood infusion," *Journal of Cerebral Blood Flow and Metabolism*, vol. 28, no. 3, pp. 516–525, 2008.

[9] H. Xu, Y. Zhang, H. Sun, S. Chen, and F. Wang, "Effects of acupuncture at gv20 and st36 on the expression of matrix metalloproteinase 2, aquaporin 4, and aquaporin 9 in rats subjected to cerebral ischemia/reperfusion injury," *PLoS ONE*, vol. 9, no. 5, Article ID e97488, 2014.

[10] L. S. C. Nicol, J. M. Dawes, F. L. Russa et al., "The role of G-protein receptor 84 in experimental neuropathic pain," *Journal of Neuroscience*, vol. 35, no. 23, pp. 8959–8969, 2015.

[11] G. Huang, J. Zhou, W. Zhan et al., "The neuroprotective effects of intraperitoneal injection of hydrogen in rabbits with cardiac arrest," *Resuscitation*, vol. 84, no. 5, pp. 690–695, 2013.

[12] Y.-S. Li, J.-X. Wang, M.-M. Jia, M. Liu, X.-J. Li, and H.-B. Tang, "Dragon's blood inhibits chronic inflammatory and neuropathic pain responses by blocking the synthesis and release of substance P in rats," *Journal of Pharmacological Sciences*, vol. 118, no. 1, pp. 43–54, 2012.

[13] X.-J. Li, Y.-M. Mu, T.-T. Li et al., "Gynura procumbens reverses acute and chronic ethanol-induced liver steatosis through MAPK/SREBP-1c-dependent and -independent pathways," *Journal of Agricultural and Food Chemistry*, vol. 63, no. 38, pp. 8460–8471, 2015.

[14] C.-Y. Chiang, B. J. Sessle, and J. O. Dostrovsky, "Role of astrocytes in pain," *Neurochemical Research*, vol. 37, no. 11, pp. 2419–2431, 2012.

[15] M. Tsuda and K. Inoue, "Neuron-microglia interaction by purinergic signaling in neuropathic pain following neurodegeneration," *Neuropharmacology*, vol. 104, pp. 76–81, 2016.

[16] T. Siepmann, A. I. Penzlin, J. Kepplinger et al., "Selective serotonin reuptake inhibitors to improve outcome in acute ischemic stroke: possible mechanisms and clinical evidence," *Brain and Behavior*, vol. 5, no. 10, article e00373, 2015.

[17] Y.-S. Li, Y. Xi, X.-J. Li et al., "Up-regulation of the biosynthesis and release of substance P through Wnt/β-catenin signaling pathway in rat dorsal root ganglion cells," *PLoS ONE*, vol. 10, no. 6, Article ID e0129701, 2015.

[18] X.-J. Li, M.-M. Jia, Y.-S. Li, Y.-L. Yang, X.-Q. Mao, and H.-B. Tang, "Involvement of substance P/neurokinin-1 receptor in the analgesic and anticancer activities of minimally toxic fraction from the traditional Chinese medicine Liu-Shen-Wan *in vitro*," *Biological and Pharmaceutical Bulletin*, vol. 37, no. 3, pp. 431–438, 2014.

[19] D. Borsook, J. Upadhyay, M. Klimas et al., "Decision-making using fMRI in clinical drug development: revisiting NK-1 receptor antagonists for pain," *Drug Discovery Today*, vol. 17, no. 17-18, pp. 964–973, 2012.

[20] K. Wang, R. Zhang, F. He et al., "Electroacupuncture frequency-related transcriptional response in rat arcuate nucleus revealed region-distinctive changes in response to low- and high-frequency electroacupuncture," *Journal of Neuroscience Research*, vol. 90, no. 7, pp. 1464–1473, 2012.

[21] X.-H. Xiang, Y.-M. Chen, J.-M. Zhang, J.-H. Tian, J.-S. Han, and C.-L. Cui, "Low- and high-frequency transcutaneous electrical acupoint stimulation induces different effects on cerebral μ-opioid receptor availability in rhesus monkeys," *Journal of Neuroscience Research*, vol. 92, no. 5, pp. 555–563, 2014.

[22] J.-S. Han, "Acupuncture: neuropeptide release produced by electrical stimulation of different frequencies," *Trends in Neurosciences*, vol. 26, no. 1, pp. 17–22, 2003.

[23] R. G. Dejerine, "Le syndrome thalamique," *Revue Neurologique*, vol. 14, p. 12, 1906.

[24] A. V. Apkarian, Y. Sosa, S. Sonty et al., "Chronic back pain is associated with decreased prefrontal and thalamic gray matter density," *Journal of Neuroscience*, vol. 24, no. 46, pp. 10410–10415, 2004.

[25] A. Yamashita, A. Hamada, Y. Suhara et al., "Astrocytic activation in the anterior cingulate cortex is critical for sleep disorder under neuropathic pain," *Synapse*, vol. 68, no. 6, pp. 235–247, 2014.

[26] T. Sasaki, K. Kitagawa, K. Yamagata et al., "Amelioration of hippocampal neuronal damage after transient forebrain ischemia in cyclooxygenase-2-deficient mice," *Journal of Cerebral Blood Flow & Metabolism*, vol. 24, no. 1, pp. 107–113, 2004.

[27] E. Thornton, M. M. Hassall, F. Corrigan, and R. Vink, "The NK1 receptor antagonist N-acetyl-l-tryptophan reduces dyskinesia in a hemi-parkinsonian rodent model," *Parkinsonism and Related Disorders*, vol. 20, no. 5, pp. 508–513, 2014.

[28] J. J. Donkin, A. J. Nimmo, I. Cernak, P. C. Blumbergs, and R. Vink, "Substance P is associated with the development of brain edema and functional deficits after traumatic brain injury," *Journal of Cerebral Blood Flow and Metabolism*, vol. 29, no. 8, pp. 1388–1398, 2009.

[29] F. Mastroiacovo, C. L. Busceti, F. Biagioni et al., "Induction of the Wnt antagonist, Dickkopf-1, contributes to the development of neuronal death in models of brain focal ischemia," *Journal of Cerebral Blood Flow and Metabolism*, vol. 29, no. 2, pp. 264–276, 2009.

Hindawi Publishing Corporation
Neural Plasticity
Volume 2016, Article ID 7308261, 8 pages
http://dx.doi.org/10.1155/2016/7308261

Research Article

Electroacupuncture Exerts Neuroprotection through Caveolin-1 Mediated Molecular Pathway in Intracerebral Hemorrhage of Rats

Hui-Qin Li, Yan Li, Zi-Xian Chen, Xiao-Guang Zhang, Xia-wei Zheng, Wen-ting Yang, Shuang Chen, and Guo-Qing Zheng

Department of Neurology, The Second Affiliated Hospital and Yuying Children's Hospital of Wenzhou Medical University, Wenzhou, China

Correspondence should be addressed to Guo-Qing Zheng; gq_zheng@sohu.com

Received 20 June 2016; Accepted 25 August 2016

Academic Editor: Cun-Zhi Liu

Copyright © 2016 Hui-Qin Li et al. This is an open access article distributed under the Creative Commons Attribution License, which permits unrestricted use, distribution, and reproduction in any medium, provided the original work is properly cited.

Spontaneous intracerebral hemorrhage (ICH) is one of the most devastating types of stroke. Here, we aim to demonstrate that electroacupuncture on Baihui (GV20) exerts neuroprotection for acute ICH possibly via the caveolin-1/matrix metalloproteinase/blood-brain barrier permeability pathway. The model of ICH was established by using collagenase VII. Rats were randomly divided into three groups: Sham-operation group, Sham electroacupuncture group, and electroacupuncture group. Each group was further divided into 4 subgroups according to the time points of 6 h, 1 d, 3 d, and 7 d after ICH. The methods were used including examination of neurological deficit scores according to Longa's scale, measurement of blood-brain barrier permeability through Evans Blue content, *in situ* immunofluorescent detection of caveolin-1 in brains, western blot analysis of caveolin-1 in brains, and *in situ* zymography for measuring matrix metalloproteinase-2/9 activity in brains. Compared with Sham electroacupuncture group, electroacupuncture group has resulted in a significant improvement in neurological deficit scores and in a reduction in Evans Blue content, expression of caveolin-1, and activity of matrix metalloproteinase-2/9 at 6 h, 1 d, 3 d, and 7 d after ICH ($P < 0.05$). In conclusion, the present results suggested that electroacupuncture on GV20 can improve neurological deficit scores and reduce blood-brain barrier permeability after ICH, and the mechanism possibly targets caveolin-1/matrix metalloproteinase/blood-brain barrier permeability pathway.

1. Introduction

Intracerebral hemorrhage (ICH) is one of the leading causes of human death with high morbidity, fatality, and disability, which accounts for 10%~15% of all strokes worldwide [1]. The overall incidence of ICH was 24.6 per 100 000 person-years and the median case fatality at 1 month was 40.4% [2]. Even surviving the ictus, most patients' neurological deficits remain and no more than 40% patients are independent at 6 months [2]. Over the past twenty years, more and more animal and clinical studies have been done to identify the mechanism underlying ICH-induced brain injury, which is considered to be composed of primary injury and secondary injury [3]. According to the primary injury, we should remove the clot or prevent the expansion of haematoma to reduce the physical effects of the haematoma. However, the usefulness of clot evacuation is uncertain for most ICH patients, and there is high thromboembolic risk with hemostatic agents such as recombinant activated factor VII and no clear clinical benefit to ICH patients without coagulopathy [4]. In addition, although there are a cluster of potential therapeutic targets for preventing ICH secondary brain injury, the relevant recommendations are merely symptomatic and supportive [4]. Therefore, more and more patients resort to complementary and alternative medicines (CAM) for ICH.

Acupuncture, as one form of CAM, has a long history worldwide [5] and its efficacy for treating stroke is acknowledged [6]. Scalp acupuncture (SA) is a new branch

of acupuncture that developed according to traditional acupuncture science in combination with modern anatomy, neurophysiology, and bioholographic theory [7]. It belongs to micropuncture system, in which filiform needle is utilized to penetrate specific stimulation areas of the scalp [8]. Historically, SA has been used to treat various diseases for thousands of years through needling and stimulating the specific areas of the scalp, but SA develops so fast in recent decades. In 1983, Western Pacific Ocean Region Committee of World Health Organization (WHO) entrusted China Acupuncture Association to prepare the scheme of Standard Nomenclature of SA lines. In 1984, 1985, and 1987, after the discussion in the standardization working group, consensus of opinion had been reached and named as "A Proposed Standard International Acupuncture Nomenclature: 3.6 Scalp Acupuncture Lines." In 1989, this scheme was formally adopted in a science group meeting held by WHO. In 1991, the formal version of SA lines was published [9]. A meta-analysis in our group has showed that SA probably can improve neurological deficits in acute ICH patients [10]. In addition, the GV20 is supposed to be the most important acupuncture point for acute ICH in the rat models [11]. However, the underlying mechanism of SA for acute ICH is not completely clear.

Blood-brain barrier (BBB) plays a key role in the ICH secondary brain injury. A range of factors such as thrombin, chemokines, and matrix metalloproteinases (MMPs) have been implicated in induction of BBB disruption [12–14]. Therefore, preventing BBB disruption like blocking multiple pathways or blocking the common end pathway is a main method to prevent ICH damage. Caveolin-1 (Cav-1) is the main structural protein of caveolae in the cell plasma membrane [15]. It is particularly abundant in endothelial cells, fibroblasts, epithelial cells, and smooth muscle cells [16]. Cav-1 has many important functions such as regulating various signaling molecules, participating in cellular cholesterol transport, and maintaining homeostasis [17]. Cav-1 is also considered as regulation of expression of tight junction-associated proteins in brain microvascular endothelial cells [18]. What is more, Cav-1 has been reported to play an important role in regulating BBB permeability in experimental cerebral ischemia/reperfusion injury [19, 20]. These evidences suggest that Cav-1 could play an important role in brain damage after stroke.

MMPs are a cluster of proteolytic zinc-containing enzymes that can degrade the extracellular matrix around cerebral blood vessels and neurons [21]. Furthermore, MMPs could increase BBB permeability by degrading tight junction proteins [22]. It is considered that activation of MMPs is a key step in the BBB opening [22]. Administration of MMPs inhibitor, BB-1101, could significantly reduce the brain water and sodium content in the ICH models [23]. Our previous study showed that MMPs activity could be regulated by Cav-1 and the BBB permeability could be regulated via Cav-1/MMPs pathway [19]. Thus, in the present study, we hypothesized that electroacupuncture (EA) on Baihui (GV20) exerts neuroprotection for acute ICH possibly via the Cav-1/MMP/BBB permeability pathway.

2. Materials and Methods

2.1. Ethics Statement. All animal experiments were conducted in accordance with the Guide for the Care and Use of Laboratory Animals issued by the US National Institutes of Health (publication number 85-23). All of animal experimental protocols were approved and regulated by the local ethic committee of the Wenzhou Medical University on the use of live animals in teaching and research (number wydw2014-0104). All the animals were sacrificed by anesthesia at the end of the experiment.

2.2. Animals, Grouping, and Induction of ICH Model. Male adult Sprague-Dawley (SD) rats were obtained from Shanghai Laboratory Animal Center (number, SCXK, Shanghai, 2013-148). Rats were randomly divided into three groups: Sham-operation group, Sham electroacupuncture (EA) group, and EA group. Each group was further divided into 4 subgroups according to the time points of 6 h, 1 d, 3 d, and 7 d after ICH. The model of ICH was established as previously described by using collagenase VII [24]. Briefly, SD rats were anaesthetized with 10% chloral hydrate intraperitoneal injection (400 mg/kg). After shaving and regular sterilization, the rats were placed in the stereotactic frame. The scalp was incised longitudinally with 0.8 cm long incision in the midline, and a 0.8 mm burr hole was made in the skull using a dental drill at the point that was 0.2 mm posterior and 2.9 mm lateral to bregma. A sterile needle of 0.7 mm in diameter was then punctured down into a point that was 6 mm ventral to the right caudate nucleus. Normal saline 3 μL containing collagenase VII 0.6 U/μL was injected into right caudate nucleus of rat in Sham EA group and EA group. Then the needle was removed and the scalp sutured together. All rats were allowed free access to food and water. For the Sham-operation group, the same procedure was carried out in the rats without injection of collagenase VII.

2.3. EA Treatment. The EA treatment was conducted according to the methodological standards published in our group previously [25]. After the animal was fastened to a frame, a sterile acupuncture needle with a diameter of 0.25 mm was inserted into GV20 towards Qubin (GB7), and another needle was inserted into wet gauze fastened to the tail. Then both of the needles were connected to the type G-6805 EA stimulator. The needles were stimulated with intensity of 0.2 mA, frequency of 2 Hz, and stimulation duration of 30 min. EA treatment in each group was performed after ICH and once daily until the rats were sacrificed. Thus, the times of EA treatment for ICH rats in 6 h, 1 d, 3 d, and 7 d group were once, twice, four times, and eight times, respectively. The animals in Sham EA group were fastened to the frame with Sham EA on therapeutic acupoints plus no penetration plus no electrical stimulation. Treatment in each group was performed once a day until the rats were sacrificed.

2.4. Neurological Deficit Scores. Neurological deficit scores were evaluated at 6 h, 1 d, 3 d, and 7 d after ICH by an investigator who was blind to the experiment design according

to the five-point scale described previously by Longa et al. [26] as follows: score 0 indicated no neurological deficit; score 1 mild focal neurological deficit (with contralateral forelimb flexion); score 2 moderate focal neurological deficit (circling to the contralateral side); score 3 severe focal neurological deficit (falling to the contralateral side); score 4 no spontaneous activity with a depressed level of consciousness or death. Rats with higher score showed more severity of neurological deficits. Only rats with score of 1 to 3 at 6 h after ICH were considered successful models and used in the current study.

2.5. Measurement of BBB Permeability. Evans Blue (EB) content in the brain tissue was used to investigate the effect of EA on BBB permeability. After being anesthetized, the rats were intravenously injected with 2% EB dye at a dose of 4 mL·kg^{-1} via the femoral vein. Ninety minutes later, the rats were perfused with 250 mL of normal saline through the left ventricle and then the brains were removed and dissected. Each hemisphere was weighed, put into 3 mL of methanamide, and then heated in 37°C water for 24 h. Samples were then centrifuged for 20 min at 5000 rpm followed by 10 min at 10,000 rpm. The absorbance of the supernatant was measured at 632 nm wavelength with a spectrophotometer.

2.6. In Situ Immunofluorescent Detection of Cav-1 in Brains. Frozen coronal sections with the hematoma were used for *in situ* detection of Cav-1 with immunofluorescent chemistry. The sections were treated with buffer containing 0.2% Triton (Sigma) and 50 mM phosphate-buffered saline (PBS) for 5 min, antigen retrieval buffer for 5 min, 10% donkey serum for 1 h, and then polyclonal rabbit Cav-1 (1 : 400; CST) overnight at 4°C. After rinsing with PBS, the slides were incubated with Alexa 488 goat anti-rabbit secondary antibody (1 : 400; Invitrogen), a kind of fluorophore-labeled donkey anti-rabbit IgG (H+L) antibodies, for 1 h at 37°C. The Alexa Fluor® dyes to which these antibodies are conjugated provide for extraordinarily bright antibody conjugates. Sections were mounted with antifade mounting medium (Beyotime). Images were acquired using fluorescent microscope (Nikon) at a constant exposure.

2.7. Western Blot Analysis of Cav-1 in Brains. Rats were deeply anesthetized and were transcardially perfused with normal saline. Then brains were quickly removed from the skull and stored at −80°C until next steps. Denatured protein samples from the whole frozen coronal sections were resolved in sodium dodecyl sulfate-polyacrylamide gels and transferred to polyvinylidene fluoride membranes (Invitrogen). After blocking, membranes were incubated overnight at 4°C with polyclonal rabbit Cav-1 (1 : 1000; CST) followed by incubation with the goat anti-rabbit horseradish peroxidase-conjugated secondary antibodies (1 : 5000; boyun biotech). Chemiluminescence was detected using ECL advance western blotting detection reagents under the imaging system (MicroChemi).

2.8. In Situ Zymography for Measuring MMP-2/9 Activity in Brains. Rats were deeply anesthetized and transcardially perfused with normal saline followed by 4% paraformaldehyde. Brains were then postfixed overnight in 4% paraformaldehyde at 4°C. Tissue was frozen in optimum cutting temperature compound and stored at −80°C until sectioning. Tissue was cut into coronal 6 μm thick sections using a cryotome (Thermo Shandon). Gelatinolytic activities of MMP-2/9 in frozen brain sections were measured with *in situ* zymography using EnzCheck collagenase kit (Invitrogen) following the manufacturer's instructions. Frozen brain sections were incubated with the 1x reaction buffer containing 0.8 mg/mL of FITC-labeled DQ gelatin at 37°C overnight. The gelatin was cleaved by MMP-2/9 and yielded the peptides whose fluorescence intensity was detected as the representatives of gelatinolytic activities of MMP-2/9. Fluorescence intensity was measured with a fluorescence microscope at a constant exposure.

2.9. Statistics Analysis. All the data were presented as means ± standard (mean ± SD) deviation. Statistics analysis was performed by SPSS 15.0 statistical software. For multiple group experiments, comparisons were made using one-way analysis of variance (ANOVA) and followed by Dunnett test for comparison of two groups within the multiple groups. The significance level was set at $P < 0.05$.

3. Results

3.1. EA Improved Neurological Function. Sham-operated rats did not show visible neurological deficits. Neurological scores increased at 6 h after ICH, peaked at 1 d, and then descended gradually. Compared with Sham-operation group, Sham EA group has significant differences at the time point of 6 h, 1 d, 3 d, and 7 d after ICH ($P < 0.05$). Compared with Sham EA group, EA group has significant differences at 6 h, 1 d, 3 d, and 7 d after ICH ($P < 0.05$). Compared with Sham-operation group, EA group has significant differences at 6 h, 1 d, and 3 d after ICH ($P < 0.05$) (Figure 1).

3.2. EA Reduced BBB Disruption. EB content in the brain increased at 6 h after ICH and peaked at 1 d and then descended gradually but still remained higher than normal at 7 d. Compared with Sham-operation group, Sham EA group has significant differences at the time point of 6 h, 1 d, 3 d, and 7 d after ICH ($P < 0.05$). Compared with Sham EA group, EA group has significant differences at 6 h, 1 d, 3 d, and 7 d after ICH ($P < 0.05$). Compared with Sham-operation group, EA group has significant differences at 6 h and 1 d after ICH ($P < 0.05$) (Figure 2).

3.3. EA Downregulated the Expression of Cav-1. With immunofluorescence and western blot, the results showed that the expression of caveolin-1 increased at 6 h after ICH and peaked at 1 d and then descended gradually but still remained higher than normal at 7 d. Compared with Sham-operation group, Sham EA group has significant differences at the time point of 6 h, 1 d, 3 d, and 7 d after

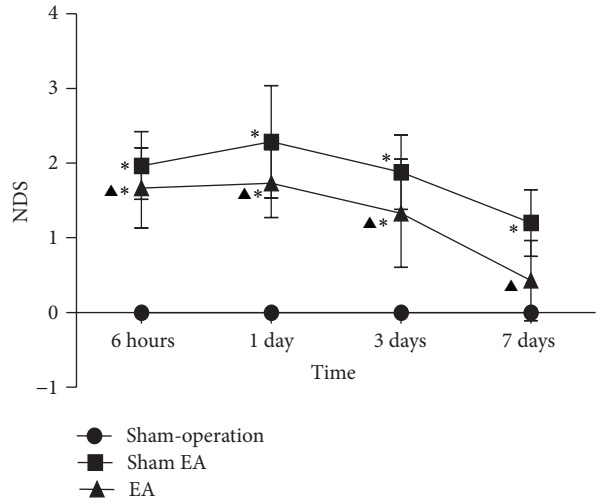

Figure 1: Effects of EA on neurological deficits after ICH in rats (mean ± SD, $n = 24$). NDS in Sham-operation group, Sham EA group, and EA group at 6 h, 24 h, 3 d, and 7 d. One-way analysis of variance (ANOVA) was used for multiple group experiments comparison and followed by Dunnett test for comparison of two groups within the multiple groups. $^{*}P < 0.05$, compared with Sham-operated group. $^{\blacktriangle}P < 0.05$ compared with Sham EA group.

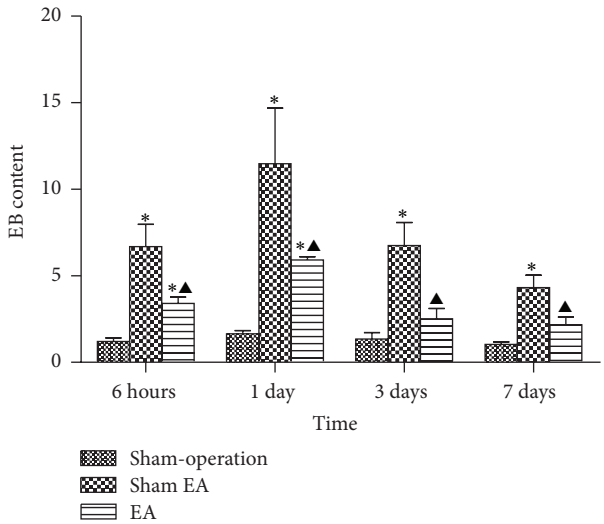

Figure 2: Effects of EA on BBB permeability after ICH in rats (mean ± SD, $n = 6$). Evans Blue leakage experiments for determining BBB permeability after acute ICH in rats in 4 subgroups at 6 h, 24 h, 3 d, and 7 d. One-way analysis of variance (ANOVA) was used for multiple group experiments comparisons and followed by Dunnett test for comparison of two groups within the multiple groups. $^{*}P < 0.05$, compared with Sham-operated group. $^{\blacktriangle}P < 0.05$, compared with Sham EA group.

ICH ($P < 0.05$). Compared with Sham EA group, EA group has significant differences at 6 h, 1 d, 3 d, and 7 d after ICH ($P < 0.05$). Compared with Sham-operation group, EA group has significant differences at 6 h, 1 d, 3 d, and 7 d after ICH ($P < 0.05$) (Figures 3 and 4).

3.4. EA Decreased the Activity of MMP-2/9. The MMP-2/9 activity was detected by *in situ* zymography. The result showed that MMP-2/9 activity increased at 6 h after ICH and thereafter remained higher than normal without any trend to decrease or increase. Compared with Sham EA group, EA group and Sham-operation group both have significant differences at the time point of 6 h, 1 d, 3 d, and 7 d after ICH ($P < 0.05$). Compared with Sham-operation group, EA group has differences at 1 d after ICH ($P < 0.05$) (Figure 5).

4. Discussion

The present study showed that EA on GV20 could improve neurological function and reduce BBB permeability in acute ICH of rats. This study also provided the mechanism that EA could downregulate the expression of Cav-1 and the activity of MMP-2/9 in a rat model of ICH. These data support the hypothesis that EA exerts neuroprotection via Cav-1/MMPs/BBB permeability pathway in acute ICH.

EA is an extension technique of acupuncture based on traditional acupuncture combined with modern electrotherapy. There are various advantages of EA as its readily quantifiable stimulation parameters of frequency, intensity, and duration [27]. GV20 acupoint belongs to the Du meridian (the government vessel). It locates at the intersection of the line connecting the apexes of the two auricles and the median line of the head, 7 cun directly above the posterior hairline and 5 cun behind the anterior hairline according to the acupuncture theory and the WHO definition [28]. Based on the TCM theory, Baihui is located on the highest place of the head, where all the yang meridians meet [29]. The function of GV20 can tonify yang, lift the spirits, ascend the function of the spleen, eliminate interior wind, clear the mind, and promote resuscitation [30]. Thus, the GV20 is used specifically to treat psychiatric and neurological disorders such as stroke, dizziness, headache, and anxiety. Our previous study revealed that GV20 based acupuncture can substantially reduce neurological deficit and brain edema and may have potential neuroprotective role in animal models of ICH and stroke [11]. Moreover, needling through GV20 towards GB7, as one type of GV20-based scalp penetration needling, is not only one of the most important branches of SA for stroke but also the most commonly used acupuncture method with the advantage of easy positioning [7]. Thus, scalp acupuncture at GV20 towards GB7 is used to treat experimental ICH in the present study.

Preclinical models of ICH are essential for understanding the basic mechanisms of hemorrhage damage and functional recovery thereafter as well as for the initial testing of potential therapies. Up to now, there are three main models commonly used to understand the physiology behind ICH-microballoon insertion, autologous blood injection, and collagenase injection model. Each model has its own advantages and disadvantages. Microballoon insertion can demonstrate the mass effect of a presupposed volume, but it cannot produce such factors as the toxicity of blood elements and cause BBB disruption [31]. Injection of autologous blood with a controlled size of mass can be used for study of

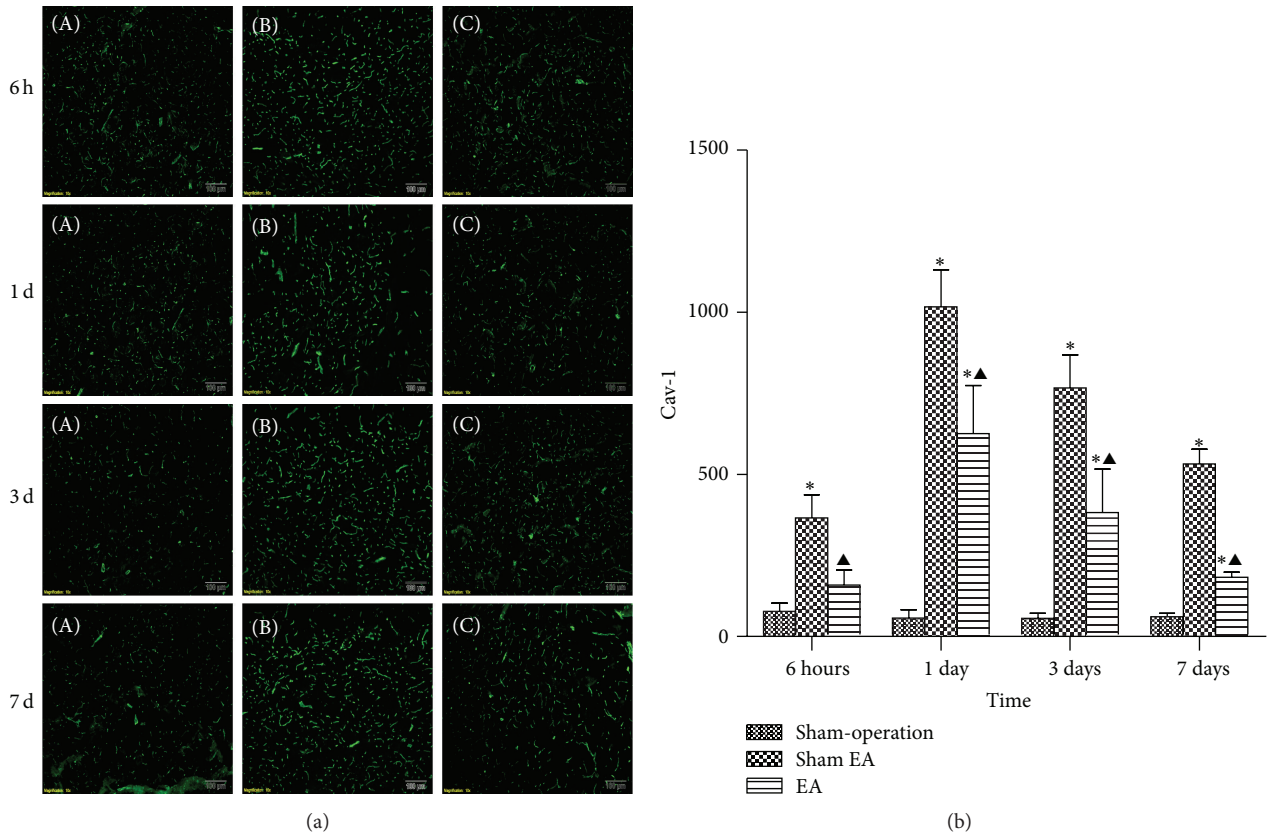

FIGURE 3: Effects of EA on the *in situ* expression of Cav-1 after ICH in rats (mean ± SD, $n = 6$). (a) Expression of Cav-1 in focal rat brain coronal frozen sections. (A) Sham-operation group; (B) Sham EA group; (C) ICH plus EA group. (b) Quantitative analysis for the results of groups at 6 h, 24 h, 3 d, and 7 d, respectively. One-way analysis of variance (ANOVA) was used for multiple group experiments comparisons and followed by Dunnett test for comparison of two groups within the multiple groups. $^{*}P < 0.05$, compared with Sham-operated group. $^{\blacktriangle}P < 0.05$ compared with Sham EA group.

mass effect and the effects of blood products. However, the disadvantage is that it fails to mimic the growing hemorrhagic mass, which often occurs in the pathological process of ICH [32]. The collagenase injection model overcomes the above disadvantages and mimics spontaneous ICH more successfully only with disadvantage of diffusing bleeding from small blood vessels rather than bleeding from the arterial source that happens in ICH patients [31]. Thus, we used the collagenase injection model for present study.

Cav-1 plays an important role in brain injury. In our group, we revealed that Cav-1 KO mice with a loss of Cav-1 had remarkably higher BBB permeability than wild-type mice during ischemia-reperfusion injury. In addition, the molecular mechanisms of maintaining BBB integrity in which Cav-1 plays an important role through inhibition of MMPs activity and protection of TJ protein during cerebral ischemia-reperfusion injury have been reported in our previous study [19]. However, up to now there are seldom published data concerning the expression and function of Cav-1 in acute ICH. One study reported that Cav-1 was upregulated at 1 d after ICH in mice [33], whereas another study reported that Cav-1 was downregulated at 1 d but upregulated at 3 d and 7 d after ICH in rats [34]. Therefore, there is no conclusion whether the expression of Cav-1 in acute ICH is increased or decreased. Our experimental results indicate that the expression of Cav-1 began to increase at 6 h after ICH, reached its peak at 1 d, and then decreased, but it remained to be higher than that of Sham-operation group until 7 d. It indicates that ICH resulted in an upregulation of Cav-1 in brain. In addition, compared with Sham EA group, the EA treatment group at all of the observed time points had significant difference, indicating that EA treatment at GV20 can reduce the expression of Cav-1 in acute stage of ICH to exert neuroprotective function in rat model of ICH.

It is known that both of MMP-2 and MMP-9 expression are increased after ICH [35, 36]. In clinical studies, the levels of MMP-2 and MMP-9 were both found to increase after acute ICH, and the increased MMP-9 was associated with perihematomal edema and neurological worsening within the acute stage [37, 38]. The present study indicated that ICH significantly increased the activities of MMP-2/9 at all of the observed time points and EA treatment remarkably inhibited the ICH-induced activities of MMP-2/9 in the brain.

Taken together, the present study demonstrated that EA on GV20 can improve neurological function deficits and

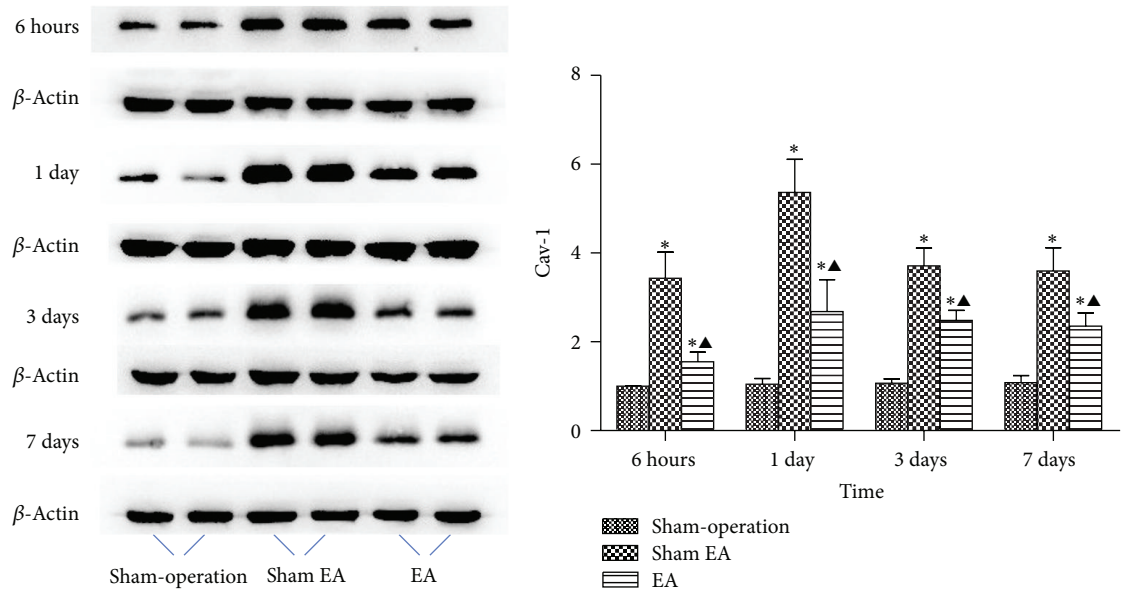

FIGURE 4: Western blot analysis on the overall expressions of Cav-1 in brain from rats (mean ± SD, $n = 6$). (a) Expression of Cav-1 in brain. (b) Representative statistic results. One-way analysis of variance (ANOVA) was used for multiple group experiments comparisons and followed by Dunnett test for comparison of two groups within the multiple groups. $^{*}P < 0.05$, compared with Sham-operated group. $^{\blacktriangle}P < 0.05$ compared with Sham EA group.

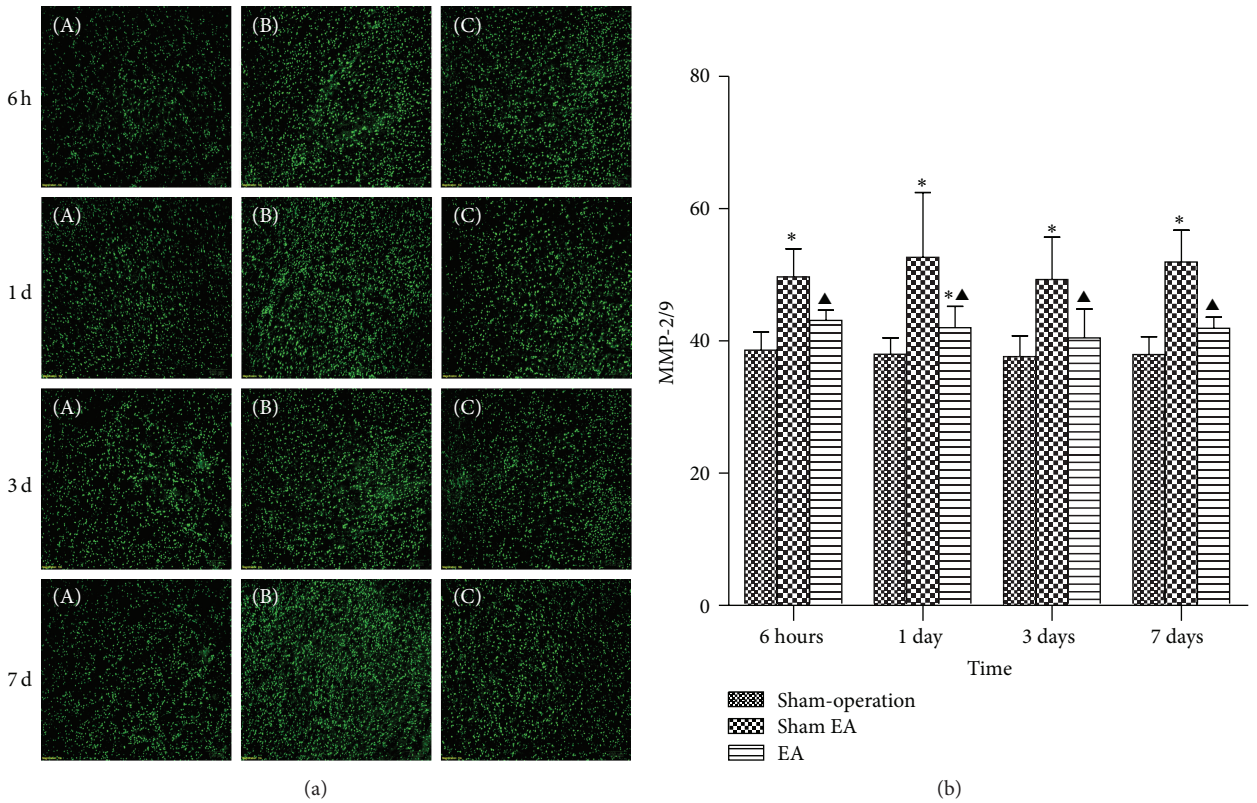

FIGURE 5: Representative MMPs activity in focal rat brain coronal frozen sections (mean ± SD, $n = 6$). (a) Representative MMPs activity in focal rat brain coronal frozen sections. (A) *In situ* MMPs activity in Sham-operation group; (B) Sham EA group; (C) ICH plus EA group. (b) Quantitative analysis for the results of groups, respectively. One-way analysis of variance (ANOVA) was used for multiple group experiments comparisons and followed by Dunnett test for comparison of two groups within the multiple groups. $^{*}P < 0.05$, compared with Sham-operated group. $^{\blacktriangle}P < 0.05$ compared with Sham EA group.

reduce BBB permeability after ICH, and the mechanism possibly targets Cav-1/MMP/BBB permeability pathway.

Competing Interests

None of the authors have potential competing interests to be disclosed.

Authors' Contributions

Hui-Qin Li, Yan Li, and Zi-Xian Chen contributed equally to this work.

Acknowledgments

This project was supported by the grant of National Natural Science Foundation of China (81573750/81473491/81173395/H2902); the Young and Middle-Aged University Discipline Leaders of Zhejiang Province, China (2013277); Zhejiang Provincial Program for the Cultivation of High-level Health Talents (2015).

References

[1] A. I. Qureshi, A. D. Mendelow, and D. F. Hanley, "Intracerebral haemorrhage," *The Lancet*, vol. 373, no. 9675, pp. 1632–1644, 2009.

[2] C. J. van Asch, M. J. Luitse, G. J. Rinkel, I. van der Tweel, A. Algra, and C. J. Klijn, "Incidence, case fatality, and functional outcome of intracerebral haemorrhage over time, according to age, sex, and ethnic origin: a systematic review and meta-analysis," *The Lancet Neurology*, vol. 9, no. 2, pp. 167–176, 2010.

[3] R. F. Keep, Y. Hua, and G. Xi, "Intracerebral haemorrhage: mechanisms of injury and therapeutic targets," *The Lancet Neurology*, vol. 11, no. 8, pp. 720–731, 2012.

[4] L. B. Morgenstern, J. C. Hemphill III, C. Anderson et al., "Guidelines for the management of spontaneous intracerebral hemorrhage: a guideline for healthcare professionals from the American Heart Association/American Stroke Association," *Stroke*, vol. 41, no. 9, pp. 2108–2129, 2010.

[5] A. Vickers and C. Zollman, "ABC of complementary medicine: acupuncture," *BMJ*, vol. 319, no. 7215, pp. 973–976, 1999.

[6] "NIH consensus conference. Acupuncture," *JAMA*, vol. 280, no. 17, pp. 1518–1524, 1998.

[7] Z. Liu, L. Guan, Y. Wang, C.-L. Xie, X.-M. Lin, and G.-Q. Zheng, "History and mechanism for treatment of intracerebral hemorrhage with scalp acupuncture," *Evidence-Based Complementary and Alternative Medicine*, vol. 2012, Article ID 895032, 9 pages, 2012.

[8] Y. Wang, J. Shen, X. M. Wang et al., "Scalp acupuncture for acute ischemic stroke: a meta-analysis of randomized controlled trials," *Evidence-Based Complementary and Alternative Medicine*, vol. 2012, Article ID 480950, 9 pages, 2012.

[9] WHO Scientific Group on International Acupuncture Nomenclature, *A Proposed Standard International Acupuncture Nomenclature: Report of a WHO Scientific Group*, World Health Organization, Geneva, Switzerland, 1991.

[10] G.-Q. Zheng, Z.-M. Zhao, Y. Wang et al., "Meta-analysis of scalp acupuncture for acute hypertensive intracerebral hemorrhage," *Journal of Alternative and Complementary Medicine*, vol. 17, no. 4, pp. 293–299, 2011.

[11] H.-Q. Li, J.-H. Li, A.-J. Liu, M.-Y. Ye, and G.-Q. Zheng, "GV20-based acupuncture for animal models of acute intracerebral haemorrhage: a preclinical systematic review and meta-analysis," *Acupuncture in Medicine*, vol. 32, no. 6, pp. 495–502, 2014.

[12] D.-Z. Liu, B. P. Ander, H. Xu et al., "Blood-brain barrier breakdown and repair by Src after thrombin-induced injury," *Annals of Neurology*, vol. 67, no. 4, pp. 526–533, 2010.

[13] R. F. Keep, J. Xiang, S. R. Ennis et al., "Blood-brain barrier function in intracerebral hemorrhage," *Acta Neurochirurgica, Supplementum*, no. 105, pp. 73–77, 2008.

[14] K. R. Lee, N. Kawai, S. Kim, O. Sagher, and J. T. Hoff, "Mechanisms of edema formation after intracerebral hemorrhage: effects of thrombin on cerebral blood flow, blood-brain barrier permeability, and cell survival in a rat model," *Journal of Neurosurgery*, vol. 86, no. 2, pp. 272–278, 1997.

[15] B. Razani, S. E. Woodman, and M. P. Lisanti, "Caveolae: from cell biology to animal physiology," *Pharmacological Reviews*, vol. 54, no. 3, pp. 431–467, 2002.

[16] P. E. Scherer, R. Y. Lewis, D. Volonté et al., "Cell-type and tissue-specific expression of caveolin-2. Caveolins 1 and 2 co-localize and form a stable hetero-oligomeric complex in vivo," *The Journal of Biological Chemistry*, vol. 272, no. 46, pp. 29337–29346, 1997.

[17] M. P. Lisanti, PE. Scherer, Z. Tang, and M. Sargiacomo, "Caveolae caveolin and caveolin-rich membrane domains: a signalling hypothesis," *Trends in Cell Biology*, vol. 4, no. 7, pp. 231–235, 1994.

[18] L. Song, S. Ge, and J. S. Pachter, "Caveolin-1 regulates expression of junction-associated proteins in brain microvascular endothelial cells," *Blood*, vol. 109, no. 4, pp. 1515–1523, 2007.

[19] Y. Gu, G. Zheng, M. Xu et al., "Caveolin-1 regulates nitric oxide-mediated matrix metalloproteinases activity and blood-brain barrier permeability in focal cerebral ischemia and reperfusion injury," *Journal of Neurochemistry*, vol. 120, no. 1, pp. 147–156, 2012.

[20] S. Fu, Y. Gu, J.-Q. Jiang et al., "Calycosin-7-O-β-D-glucoside regulates nitric oxide /caveolin-1/matrix metalloproteinases pathway and protects blood-brain barrier integrity in experimental cerebral ischemia-reperfusion injury," *Journal of Ethnopharmacology*, vol. 155, no. 1, pp. 692–701, 2014.

[21] Y. Gu, C. M. Dee, and J. Shen, "Interaction of free radicals, matrix metalloproteinases and caveolin-1 impacts blood-brain barrier permeability," *Frontiers in Bioscience*, vol. 3, no. 4, pp. 1216–1231, 2011.

[22] Y. Yang, E. Y. Estrada, J. F. Thompson, W. Liu, and G. A. Rosenberg, "Matrix metalloproteinase-mediated disruption of tight junction proteins in cerebral vessels is reversed by synthetic matrix metalloproteinase inhibitor in focal ischemia in rat," *Journal of Cerebral Blood Flow and Metabolism*, vol. 27, no. 4, pp. 697–709, 2007.

[23] G. A. Rosenberg and M. Navratil, "Metalloproteinase inhibition blocks edema in intracerebral hemorrhage in the rat," *Neurology*, vol. 48, no. 4, pp. 921–926, 1997.

[24] G.-Q. Zheng, X.-T. Wang, X.-M. Wang et al., "Long-time course of protease-activated receptor-1 expression after intracerebral hemorrhage in rats," *Neuroscience Letters*, vol. 459, no. 2, pp. 62–65, 2009.

[25] G.-Q. Zheng, "Methodological standards for experimental research on stroke using scalp acupuncture," *Acupuncture & Electro-Therapeutics Research*, vol. 34, no. 1-2, pp. 1–13, 2009.

[26] E. Z. Longa, P. R. Weinstein, S. Carlson, and R. Cummins, "Reversible middle cerebral artery occlusion without craniectomy in rats," *Stroke*, vol. 20, no. 1, pp. 84–91, 1989.

[27] H. M. Langevin, R. Schnyer, H. MacPherson et al., "Manual and electrical needle stimulation in acupuncture research: pitfalls and challenges of heterogeneity," *Journal of Alternative and Complementary Medicine*, vol. 21, no. 3, pp. 113–128, 2015.

[28] World Health Organization (WHO), *Guidelines on Basic Training and Safety in Acupuncture*, World Health Organization (WHO), Geneva, Switzerland, 1999.

[29] E.-Y. Shen, F.-J. Chen, Y.-Y. Chen, and M.-F. Lin, "Locating the acupoint Baihui (GV20) beneath the cerebral cortex with MRI reconstructed 3D neuroimages," *Evidence-Based Complementary and Alternative Medicine*, vol. 2011, Article ID 362494, 6 pages, 2011.

[30] Y. C. Cheong, S. Dix, E. Hung Yu Ng, W. L. Ledger, and C. Farquhar, "Acupuncture and assisted reproductive technology," *The Cochrane Database of Systematic Reviews*, no. 7, Article ID CD006920, 2013.

[31] A. Manaenko, H. Chen, J. H. Zhang, and J. Tang, "Comparison of different preclinical models of intracerebral hemorrhage," in *Intracerebral Hemorrhage Research: From Bench to Bedside*, J. Zhang and A. Colohan, Eds., vol. 111 of *Acta Neurochirurgica Supplementum*, pp. 9–14, 2011.

[32] G. A. Rosenberg, M. Grossetete, and S. Mun-Bryce, "Experimental models in intracerebral hemorrhage," *Handbook of Clinical Neurology*, vol. 92, pp. 307–324, 2009.

[33] C.-F. Chang, S.-F. Chen, T.-S. Lee, H.-F. Lee, S.-F. Chen, and S.-K. Shyue, "Caveolin-1 deletion reduces early brain injury after experimental intracerebral hemorrhage," *The American Journal of Pathology*, vol. 178, no. 4, pp. 1749–1761, 2011.

[34] M.-D. Wang, Y. Wang, Y.-P. Xia et al., "High serum MiR-130a levels are associated with severe perihematomal edema and predict adverse outcome in acute ICH," *Molecular Neurobiology*, vol. 53, no. 2, pp. 1310–1321, 2016.

[35] Y. Li, M. E. Ogle, G. C. T. Wallace, Z. Y. Lu, S. P. Yu, and L. Wei, "Erythropoietin attenuates intracerebral hemorrhage by diminishing matrix metalloproteinases and maintaining blood-brain barrier integrity in mice," *Acta Neurochirurgica*, vol. 105, supplement, pp. S105–S112, 2008.

[36] C. Power, S. Henry, M. R. Del Bigio et al., "Intracerebral hemorrhage induces macrophage activation and matrix metalloproteinases," *Annals of Neurology*, vol. 53, no. 6, pp. 731–742, 2003.

[37] J. Alvarez-Sabín, P. Delgado, S. Abilleira et al., "Temporal profile of matrix metalloproteinases and their inhibitors after spontaneous intracerebral hemorrhage: relationship to clinical and radiological outcome," *Stroke*, vol. 35, no. 6, pp. 1316–1322, 2004.

[38] S. Abilleira, J. Montaner, C. A. Molina, J. Monasterio, J. Castillo, and J. Alvarez-Sabín, "Matrix metalloproteinase-9 concentration after spontaneous intracerebral hemorrhage," *Journal of Neurosurgery*, vol. 99, no. 1, pp. 65–70, 2003.

Hindawi Publishing Corporation
Neural Plasticity
Volume 2016, Article ID 2371875, 9 pages
http://dx.doi.org/10.1155/2016/2371875

Research Article

Effects of Electroacupuncture at Governor Vessel Acupoints on Neurotrophin-3 in Rats with Experimental Spinal Cord Injury

Yu-ping Mo,[1,2] Hai-jiang Yao,[2,3] Wei Lv,[2] Liang-yu Song,[2] Hong-tao Song,[4] Xiao-chen Yuan,[5] Ying-qiu Mao,[6] Quan-kai Jing,[2] Su-hua Shi,[7] and Zhi-gang Li[2]

[1]*Department of Rehabilitation, The Third People's Hospital of Shenzhen, No. 29 Bulan Road, Longgang District, Shenzhen 518112, China*
[2]*School of Acupuncture, Moxibustion and Tuina, Beijing University of Chinese Medicine, No. 11 North Third Ring Road East, Chaoyang District, Beijing 100029, China*
[3]*Treatment Center of TCM, Beijing Bo'ai Hospital, China Rehabilitation Research Center, School of Rehabilitation Medicine, Capital Medical University, No. 10 Jiaomen North Road, Fengtai District, Beijing 100068, China*
[4]*Department of Traditional Chinese Medicine, Inner Mongolia People's Hospital, No. 20 Zhao Wudaroad, Hohhot, Inner Mongolia Autonomous Region 010017, China*
[5]*Institute of Microcirculation, Chinese Academy of Medical Sciences & Peking Union Medical College, No. 5 Dong Dan San Tiao Street, Dongcheng District, Beijing 100005, China*
[6]*Research and Experimental Center, Beijing University of Chinese Medicine, No. 11 North Third Ring Road East, Chaoyang District, Beijing 100029, China*
[7]*Department of Rehabilitation, The Third Affiliated Hospital of Beijing University of Chinese Medicine, No. 51 An Wai Xiao Guan Street, Chaoyang District, Beijing 100029, China*

Correspondence should be addressed to Su-hua Shi; molly-flower@163.com and Zhi-gang Li; lizhigang620@126.com

Received 20 March 2016; Revised 27 June 2016; Accepted 17 July 2016

Academic Editor: Ke-Lun Wang

Copyright © 2016 Yu-ping Mo et al. This is an open access article distributed under the Creative Commons Attribution License, which permits unrestricted use, distribution, and reproduction in any medium, provided the original work is properly cited.

In an effort to explore new, noninvasive treatment options for spinal cord injuries (SCI), this study investigated the effects of electroacupuncture (EA) for SCI rat models. SCI was induced by a modified Allen's weight-drop method. We investigated the response of EA at Dazhui (GV 14) and Mingmen (GV 4) acupoints to understand the effects and mechanisms of EA in neuroprotection and neuronal function recovery after SCI. BBB testing was used to detect motor function of rats' hind limbs among groups, and EA was shown to promote the recovery of SCI rats' motor function. Nissl staining showed a restored neural morphology and an increase in the quantity of neurons after EA. Also, the antiapoptosis role was exposed by TUNEL staining. Western blotting analysis was used to determine the protein expression of neurotrophin-3 (NT-3) in spinal cord tissue. Compared to the sham group, the expression levels of NT-3 were significantly decreased and EA was shown to upregulate the expression of NT-3. The present study suggests that the role of EA in neuroprotection and dorsal neuronal function recovery after SCI in rats, especially EA stimulation at GV 14 and GV 4, can greatly promote neuronal function recovery, which may result from upregulating the expression of NT-3.

1. Introduction

Spinal cord injury (SCI) is an accidental tragedy, causing unexpected suffering physically and emotionally, and is costly to patients [1]. Traumatic SCI can cause disorders of somatesthesia and locomotion below the level of injury. SCI induces primary mechanical damage and causes secondary damage to the spinal cord. Primary damage occurs by mechanical tissue disruption immediately subsequent to trauma. Secondary damage is mediated by complex cellular and molecular processes [2].

At present, mainstream treatments for SCI include pharmacotherapies, neurotrophic factors, cell-transplantation, gene therapy, and biological materials transplantation [3, 4]. Traditional Chinese Medicine (TCM) treatments were also reported and used [3, 4]. Pharmacotherapy includes

methylprednisolone and GM1 [3]. Neurotrophic factors include nerve growth factor (NGF) and brain-derived neurotrophic factor (BDNF) [5].

Acupuncture is a therapeutic technique used in TCM. Since its development several thousand years ago, acupuncture has made many contributions to health care and medical treatment. Electroacupuncture (EA) is a type of therapy in which a needle inserted into an acupoint is attached to a trace pulse current with the purpose of producing a synthetic electric needling stimulation. The application of EA for the treatment of SCI has shown promising results in the alleviation of the patients' suffering [6]. Previous studies have shown that applications of EA for the treatment of SCI have been proven to contribute to neurologic and functional recoveries in SCI [7–9].

TCM believes that Governor Vessel injury is the main reason of SCI. Malnutrition of tendons and muscles due to obstruction of qi and blood induces disuse and atrophy. Therefore, Governor Vessel acupoints are the first choices for treating SCI. "Dazhui" (GV 14) is the confluence of Governor Vessel and the hand and foot three Yang meridians. Acupuncture stimulation in GV 14 can activate and inspire Yang-qi in the whole body to dredge the meridians. "Mingmen" (GV 4) is also a Governor Vessel acupoint and is the intersection of the Governor Vessel and Belt Vessel. It gathers genuine-Yin and genuine-Yang, which are the root of Yuan-qi and the gateway of life. Stimulating GV 4 can regulate channels and activate collaterals, tonify Yang, and strengthen the kidneys. In previous experiments using SCI rat models, acupuncture stimulation in GV 14 and GV 4 has been adopted [10].

EA on the Governor Vessel has been shown to alleviate secondary damage after SCI in both patients and animal models [10, 11]. Therapeutic effects has been reported by a review [12] which showed that acupuncture stimulation on Governor Vessel could promote motor function recovery after SCI and improve restoration of bladder function. Evidence from both clinical trials and basic researches supports EA on Governor Vessel for restoration of motor function, bladder function, and sensory function of limbs after SCI [10, 13–15].

Neurotrophic factors (NTFs) are protein molecules which are essential to neuron survival and growth [16]. NGF, BDNF, neurotrophin 3 (NT-3), and neurotrophin 4/5 (NT-4/5) have been determined as NTFs. NT-3 is crucial to neuron survival, differentiation, and formation of neural circuits during neural development [17, 18]. NT-3 is also an important factor in the microenvironment for spinal cord repair [16]. It plays an influential role in preventing neuron death in injured spinal cord, maintaining neuron survival and promoting axon regeneration [16]. Exogenous NT-3 also promotes adult stem cell survival and differentiation after transplantation into an injured spinal cord [19]. Previous research found that EA on Governor Vessel promoted secretion of NT-3 at the injured area and adjacent tissues 14 days after SCI [7, 20]. However whether NT-3 is altered prior to this time is not known.

This study aims to explore whether EA can promote a suitable microenvironment for recovery of neurological function after SCI by increasing endogenous NT-3 secretion and expression at the injured area and adjacent tissues after performing EA on the Governor Vessel during the early phase of SCI.

2. Experimental Procedures

2.1. Animal and Experimental Groups. All experiments were approved by the Institutional Animal Care and Use Committee of Beijing University of Chinese Medicine. 165 rats (Sprague-Dawley, male, 180 to 220 g) were randomly assigned into three groups at a ratio of 1 : 1 : 1. The sham-operation group (S) received only a laminectomy. The remaining two groups were modeled as spinal cord injury at the T10 spinal segment. The control group (C) received no treatment. The EA group received EA treatment at GV 14 and GV 4 acupoints. Rats in the control group and EA group were randomly placed into the following subgroups: 1 d, 3 d, and 7 d. There were 20 rats per group in 3 d and 7 d, respectively, and 15 rats in group 1 d. Each of the animals was housed in separated cages with free access to food and water. Room temperature was set at 25 ± 3°C.

2.2. Spinal Cord Injury. The surgical procedure for inducing SCI was conducted according to established methods [21]. The rats were anesthetized with 10% chloral hydrate (3.5 mg/kg, intraperitoneal), and a laminectomy was performed at the T9–T11 level, exposing the underlying cord without disrupting the dura. Spinal cord contusion was induced using a weight-drop apparatus, where a guided 5 g rod was dropped from a height of 80 mm onto the exposed cord, representing moderate SCI. The absorbable gelatin sponge was placed at the site of the SCI for hemostasis and was sutured to the vertebral column. Afterwards, the skin and musculature were sutured. Laminectomy was performed on the sham-operation group without SCI. All SCI animal models included in the study met the following injury criteria: spinal cord ischemia and edema around the wound, formation of tail sway reflex, flicking of both body and legs, and the appearance of sluggish paralysis (Figure 1). All the animals were returned to separated cages with sufficient water and food and were then treated everyday with an intraperitoneal injection of gentamicin at a dose of 2000 μ, twice daily. No analgesics were used. Rats that underwent SCI received specialized care consisting of manual bladder expression three times daily and cleansing for the duration of the experiment.

2.3. Acupuncture Application. GV 14 and GV 4 acupoints were utilized during EA treatment. The GV 14 acupoint is located in the posterior midline and in the depression below the spinous process of the 7th cervical vertebra in prone position. GV 4 is also located in the posterior midline and in the depression below the spinous process of the 2nd lumbar vertebra in prone position. Rats were placed within a cloth bag without anesthesia during EA administration. Sham and control animals were captured for bondage when the EA group received treatment, for a duration of 20 minutes each time, to ensure the same processing conditions. Sterilized

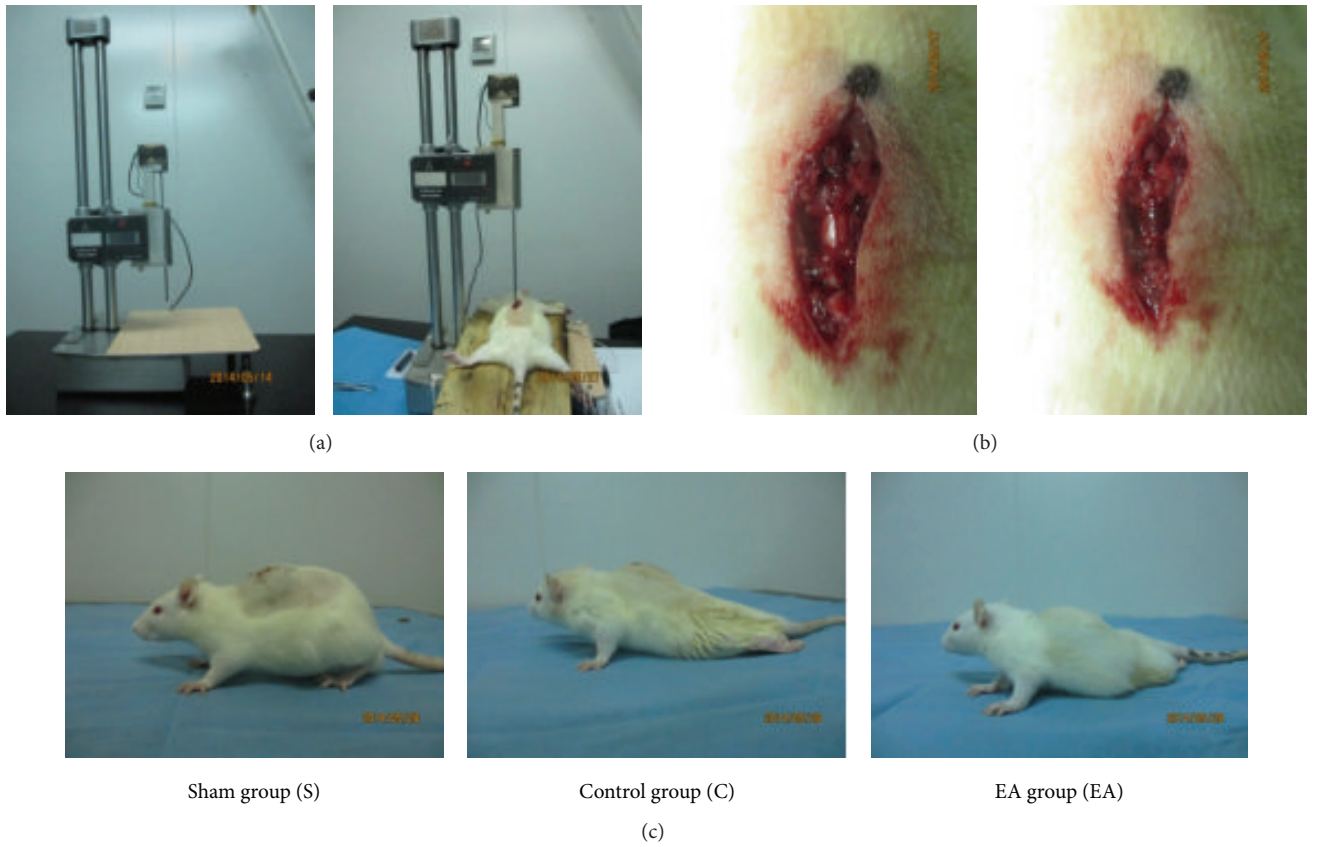

Figure 1: (a) Modified Allen's weight-drop apparatus; (b) before and after SCI; (c) the hind limbs condition of each group after SCI.

disposable stainless steel needles (0.30 ∗ 25 mm, Zhongyan Taihe brand, Beijing Zhongyan Taihe Medical Instrument Co., Ltd., Beijing, China) were inserted into GV 14 (oblique downwardly) and GV 4 (oblique upwardly), respectively, as deep as 5–7 mm for both points. Following the insertions, electrodes were connected to the handle of the needles (electric acupuncture apparatus used: LH202 acupoint nerve stimulator, Beijing Huawei Industrial Development Co., Ltd., Beijing, China). Electric simulation parameters were at a frequency of 2 Hz and an intensity of 1 mA for 20 minutes. The rats received EA treatment 2 hours after the SCI model was established and anesthesia recovery. One hour before euthanasia, at the 24th hour of postsurgery, the rats in 1 d EA group were given the 2nd treatment. The rats in 3 d and 7 d EA group were given the same treatment once per day until they were euthanized at the appointed time. The sham and control animals did not receive treatment. Finally, 11 rats per group were analyzed. 6 rats per group were perfused to fixation and fresh tissue was taken from the other 5 rats per group. All the above procedures were conducted after anesthesia.

2.4. Behavioral Testing. Rats from the sham group, the control group, and the EA group were assessed for hind limb motor function at 1 d, 3 d, and 7 d after injury by two blinded observers using the Basso, Beattie, and Bresnahan (BBB) hind limb locomotor rating scale test. The BBB rating scale is a 21-point system based on operationally defined behavioral features, which follow the recovery progression from complete paralysis to normal locomotion. The rating scale ranges from 0 to 21, with a score of 0 indicating complete hind limb paralysis and a score of 21 denoting completely normal locomotor function.

2.5. Nissl Staining. Six of eleven rats in each group were euthanized at the specified time of postsurgery and perfused transcardially with 0.9% sodium chloride and then with 4% paraformaldehyde in 1x phosphate buffered saline (4% PFA) for 30 min. Spinal cords were surgically removed and kept in 4% PFA for postfix overnight. After dehydration, the spinal cords were embedded with paraffin, and serial coronal sections with thickness of 4 μm were obtained. To assess the histopathologic change, each one of six sections obtained was subjected to Nissl staining. Surviving neurons were characterized by blue staining Nissl bodies. Quantification was performed by counting the quantity of survival neurons in five randomly chosen fields within each slide from each section in the same part of the structure at 400x with an Olympus (BX53, Japan) optic microscope. Two observers, blind to the experiment, counted the surviving neurons.

2.6. TUNEL Staining. To detect apoptosis, each one of six coronal sections obtained in the above experimental procedure was further subjected to terminal deoxynucleotidyl

transferase mediated dUTP nick end labeling (TUNEL) staining. To assess the apoptotic cells, we measured 6 samples in one section chosen at random from each spinal cord. Apoptotic cells were characterized by dark brown staining of nucleus and nuclear membrane. Quantification was performed by counting the quantity of positive cells in five randomly chosen fields within each slide from each section in the same part of the structure at 400x with an Olympus (BX53, Japan) optic microscope. The index of apoptosis was calculated as the ratio of overall apoptotic cells. Two observers, blind to the experiment, counted the apoptotic cells.

2.7. Western Blotting. The remaining five of eleven rats in each group were deeply anesthetized with 10% chloral hydrate and euthanized at the appointed time. A 1 cm spinal cord segment centered at the injury epicenter was quickly dissected. Spinal cord protein homogenates were prepared by rapid homogenization in a 50 μL lysis buffer. Samples were centrifuged at 10000 r/min for 10 min at 4°C. Protein concentrations were determined using the Bradford method [22]. For electrophoresis, protein samples (40 μg each) were dissolved in the sample buffer and heated to 100°C for 5 min. Samples were then resolved on 10% SDS-PAGE and transferred to PVDF membranes. The membranes were blocked in TBS-T containing 5% nonfat dry milk for 1 h, followed by incubation with NT-3 (1 : 500, ABcam, UK) at 4°C overnight. After being washed, the membranes were incubated with HRP-Goat-Anti-Mouse IgG (1 : 5000, ZSGB-BIO, Beijing, China). Proteins were visualized by ECL Chemiluminescence (Santa Cruz, USA). All Western blot experiments were repeated for at least 3 times. GAPDH (reduced glyceraldehyde-phosphate dehydrogenase) served as an internal control. The gray values of target proteins were divided by that of internal control to correct the error, which resulted due to the relative content of the target protein in the sample.

2.8. Statistical Analyses. No rats died in 1 d; while in 3 d, 2 rats died in the sham group, 3 rats died in the control group, and 1 rat died in the EA group; in 7 d, no rats died in the sham group, 7 rats died in the control group, and 5 rats died in the EA group. Lastly, 11 rats per group were randomly selected to enter into statistics. Data were presented as means ± SD (Standard Deviation). SPSS 20.0 (SPSS Inc., Chicago, USA) was deployed for data analysis with a one-way ANOVA method after the test of normal distribution and homogeneity of variance, followed by a post hoc multiple comparison. Between the two groups, we used Fisher's LSD (Least Significant Difference) method to compare any differences. Statistical significance was set to $p < 0.05$.

3. Results

3.1. Effects of EA on Behavioral Testing after SCI. We used the BBB hind limb locomotor rating scale test to assess neurological function at 1 d, 3 d, and 7 d after SCI. The mean BBB scores (Table 1) of the control group were lower than the sham group at 1 d, 3 d, and 7 d after SCI ($p < 0.01$). The mean BBB scores (Table 1) of the EA group were higher than the control group at 7 d after SCI ($p < 0.01$). The mean BBB scores in the control group increased from 0.6364 at 1 d to 2.0909 at 7 d (Table 1). The mean BBB scores in the EA group increased from 0.6364 at 1 d to 4.0909 at 7 d (Table 1). The BBB scores of the sham group were at the highest level because nerve function was not damaged [23]. These results suggested that EA plays an important role in improvement of neurological function.

Table 1: Behavioral testing after SCI in the following groups ($n = 11$ per group): sham, control, and EA. $^{**}p < 0.01$, as compared with sham group; $^{\#\#}p < 0.01$, as compared with control group (S: sham group; C: control group; EA: electroacupuncture group).

Group	BBB scores		
	1 d	3 d	7 d
S	21 ± 0.00	21 ± 0.00	21 ± 0.00
C	0.6364 ± 0.15**	1.3636 ± 0.15**	2.0909 ± 0.21**
EA	0.6364 ± 0.15**	2.0909 ± 0.25**	4.0909 ± 0.21$^{**\#\#}$

3.2. Effects of EA on Neuron Survival after SCI. In the sham group, neurons exhibited a large amount of densely stained toluidine blue granules in the cytoplasm (Figure 2) [24]. However, in the control group, the Nissl bodies dramatically decreased or even disappeared in the neurons at 1 d (Figure 2). At 3 d, the motor neurons of the gray matter showed obvious atrophy, some neurons dissolved, and the quantity of the Nissl bodies was significantly reduced or even disappeared in the control group (Figure 2). At 7 d, a small number of neurons' Nissl bodies appeared again in the control group (Figure 2). In the EA group the quantity of Nissl bodies was restored compared with that of the control group and displayed patch morphology [24]. The histomorphology had no change in EA group at 1 d; neurons also had varying degrees of reducing as dyeing was lighter (Figure 2). At 3 d, neuronal atrophy and reduction still existed, but the condition was better than in the control group, and Nissl bodies were faintly visible in the EA group (Figure 2). At 7 d, the Nissl bodies of the remaining neurons appeared again after receiving EA treatment, and the quantity was significantly larger than that of the control group (Figure 2). EA group showed significantly preserved neurons compared with that of the control group at 1 d, 3 d, and 7 d after SCI (Figure 2; Table 2) (data are presented as mean ± SD, $^{**}p < 0.01$, versus sham group; $^{\#}p < 0.05$; $^{\#\#}p < 0.01$, versus control group; $n = 6$ animals per group). These results suggested that rats had a lower number of surviving neurons after SCI, and EA can improve survival.

3.3. Effects of EA on the Inhibition of Apoptotic Cell Death after SCI. In the sham group, there were almost no TUNEL positive cells (Figure 3). In the control group, positive cells appeared and mainly distributed in the damaged area and its edge at 1 d after SCI (Figure 3). The positive cells significantly increased and widely distributed in both the white and gray matter of the control group at 3 d after SCI (Figure 3)

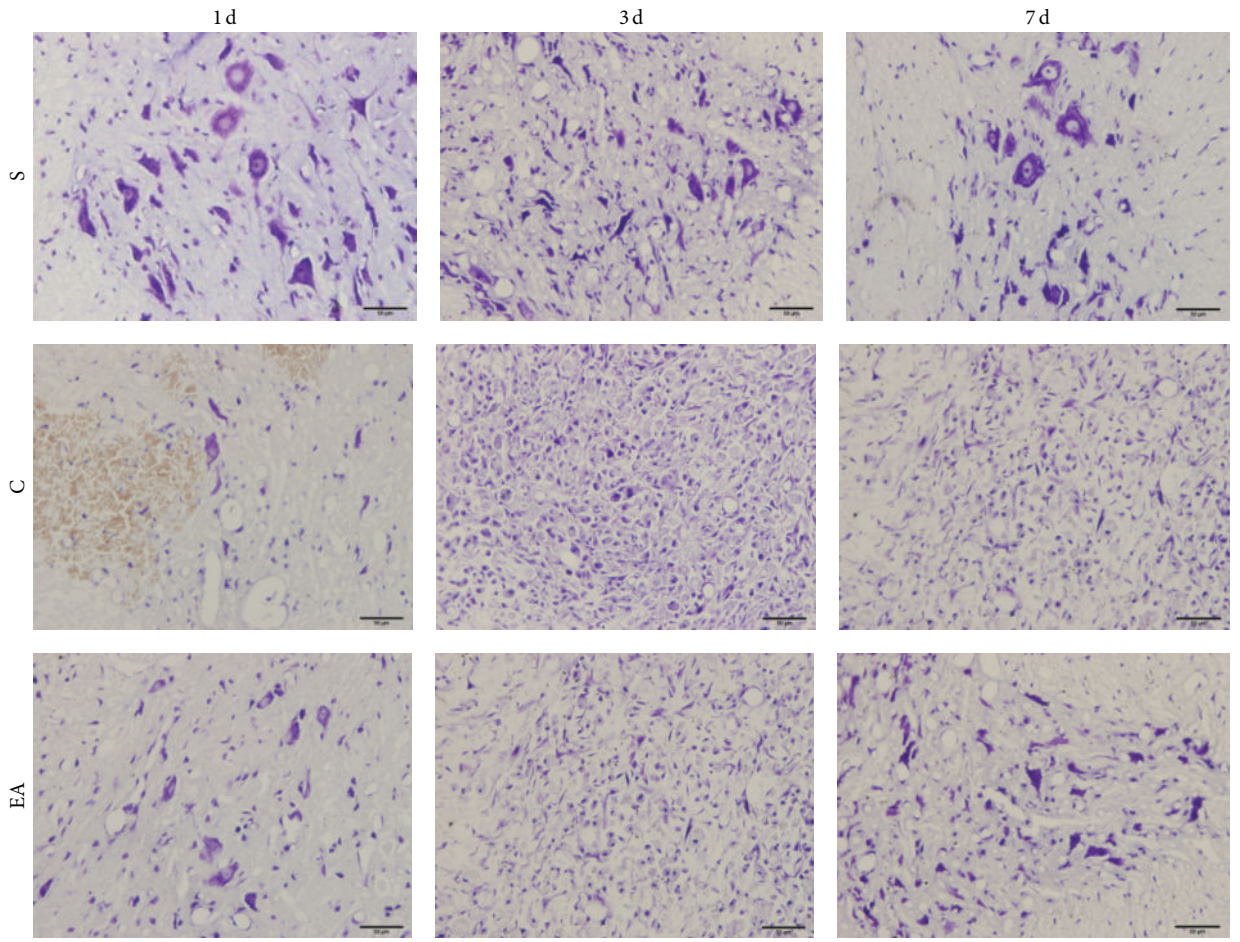

Figure 2: Neuronal conditions were evaluated using Nissl staining (original magnification ×400, 1 : 50) in the following groups: sham, control, and EA group at 1 d, 3 d, and 7 d (S: sham group; C: control group; EA: electroacupuncture group).

Table 2: Number of surviving neurons after SCI in the following groups ($n = 6$ per group): sham, control, and EA. $^{**}p < 0.01$, as compared with sham group; $^{\#}p < 0.05$; $^{\#\#}p < 0.01$, as compared with control group (S: sham group; C: control group; EA: electroacupuncture group).

Group	Number of survival neurons		
	1 d	3 d	7 d
S	39.67 ± 1.54	38.50 ± 1.34	37.33 ± 1.15
C	9.33 ± 1.12**	16.50 ± 1.12**	19.00 ± 0.97**
EA	19.33 ± 1.52$^{**\#\#}$	21.00 ± 1.07$^{**\#}$	27.50 ± 1.38$^{**\#\#}$

Table 3: The effects of EA on the inhibition of apoptotic cell death after SCI in the following groups ($n = 6$ per group): sham, control, and EA. $^{**}p < 0.01$, as compared with sham group; $^{\#\#}p < 0.01$, as compared with control group (S: sham group; C: control group; EA: electroacupuncture group).

Group	Apoptotic index		
	1 d	3 d	7 d
S	4.00 ± 1.87	5.00 ± 1.73	4.30 ± 1.15
C	27.40 ± 3.9**	29.00 ± 4.58**	20.00 ± 1.00**
EA	14.00 ± 1.58$^{**\#\#}$	14.00 ± 1.00$^{**\#\#}$	12.60 ± 2.08$^{**\#\#}$

[24]. At 7 d, the positive cells were less than before in the control group. In the control group, neurons shrank and exhibited abnormal morphology with condensed chromatin, introverted nuclear membranes, and increased apoptotic bodies [24]. Neurons in the EA group, however, showed less condensed chromatin and clear nuclear membranes [24]. EA group, however, showed significantly decreased brown-positive cells compared with that of the control group at 1 d, 3 d, and 7 d after SCI (Figure 3; Table 3) (data are presented as mean ± SD, $^{**}p < 0.01$, versus sham group; $^{\#\#}p < 0.01$, versus control group; $n = 6$ animals per group). This suggested that EA can reduce apoptosis, promote the survival of neurons, and has a certain protective effect.

3.4. EA Regulate Protein Expression of NT-3 after SCI. We used Western blotting analyses to determine the expression of NT-3 semiquantitatively for assessing the progression of SCI and the protective effects of EA. In the sham group, NT-3 demonstrated expression. In the control group, the expression of NT-3 decreased at 1 d and 3 d without statistical

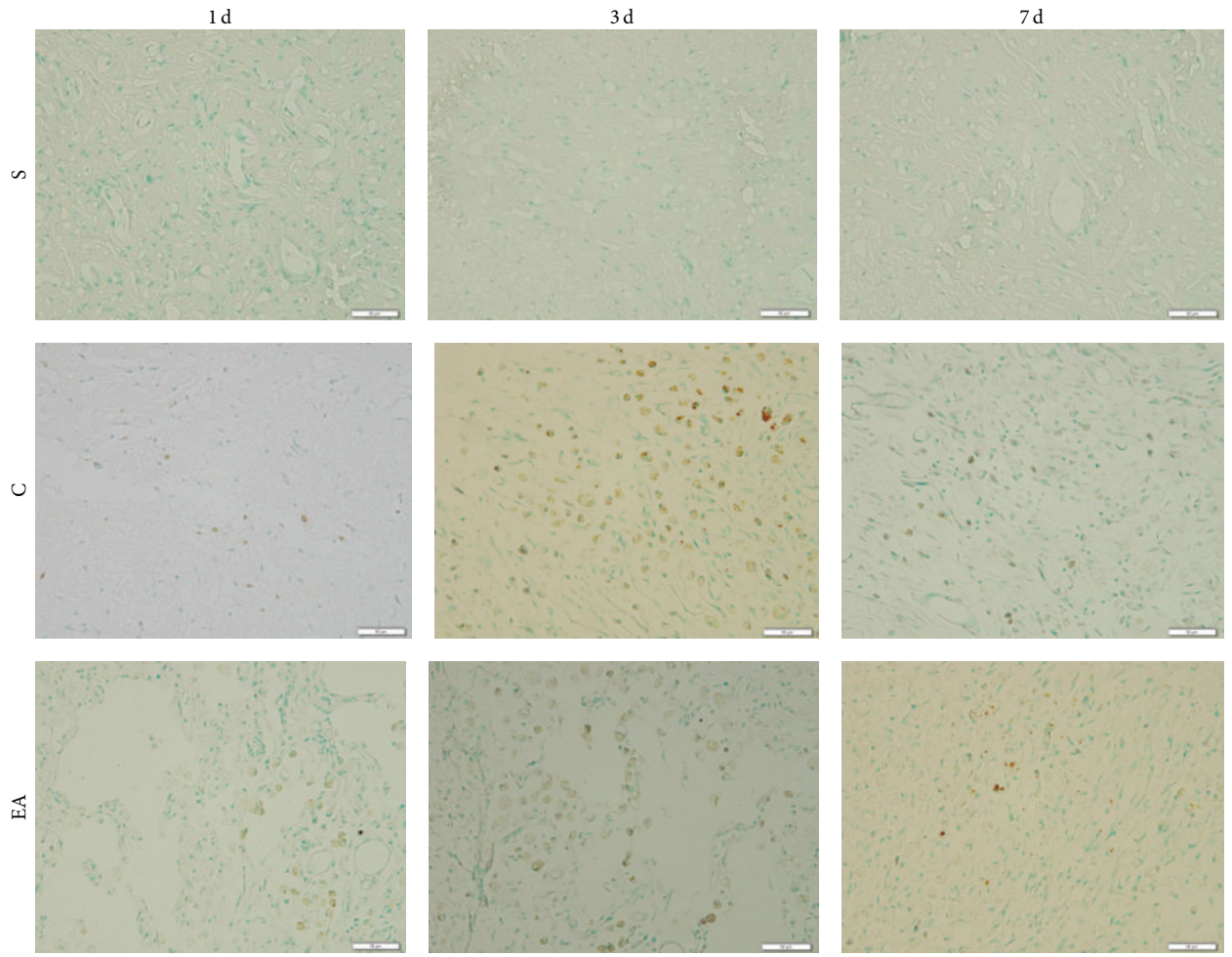

Figure 3: TUNEL staining (original magnification ×400, 1 : 50) identified apoptotic neurons in the following groups: sham, control, and EA group at 1 d, 3 d, and 7 d (S: sham group; C: control group; EA: electroacupuncture group).

Table 4: The effects of EA on the expression of NT-3 after SCI in the following groups ($n = 5$ per group): sham, control, and EA. $^{*}p < 0.05$, as compared with sham group; $^{\#\#}p < 0.01$, as compared with control group (S: sham group; C: control group; EA: electroacupuncture group).

Group	Relative expression of NT-3		
	1 d	3 d	7 d
S	0.88 ± 0.21	1.09 ± 0.27	1.00 ± 0.08
C	0.67 ± 0.14	0.60 ± 0.02	0.64 ± 0.28*
EA	0.80 ± 0.21	0.98 ± 0.05$^{\#\#}$	1.10 ± 0.25$^{\#\#}$

significance ($p > 0.05$, Figure 4; Table 4), but there was a tendency of reduction, and the expression of NT-3 still decreased at 7 d after SCI with statistical significance ($p < 0.05$, Figure 4; Table 4), and expressions were always lower than that of the sham group (Figure 4; Table 4). While NT-3 protein expression in spinal cord tissue of EA group was increased in comparison with those in the control group with statistical significance at 3 d and 7 d after SCI ($p < 0.01$, Table 4), there was no statistical significance at 1 d after SCI ($p > 0.05$, Table 4), but there still was an increasing trend. This indicated that EA increased the expression of NT-3 in spinal cord tissue.

4. Discussion

In this research, the BBB scores of control group and EA group which received SCI operation had statistical difference compared with that of sham group in 1 d, 3 d, and 7 d, which proved that the models of SCI were successfully established as the motor function of rats' hind limbs appeared paralyzed. At 7 d after SCI, the BBB scores began to show significant statistical difference between EA group and the control group, which indicated that the hind limbs' motor function of rats was gradually recovering, and the recovery of rats that received EA treatment was better than that of control rats without EA treatment. This signifies that EA treatment could promote motor function recovery after SCI, which was also shown by Nissl staining, TUNEL, and Western blotting.

In addition to the damage at the site of the spinal cord injury, secondary pathological changes occur in the following order: edema, ischemia, calcium overload, lipid

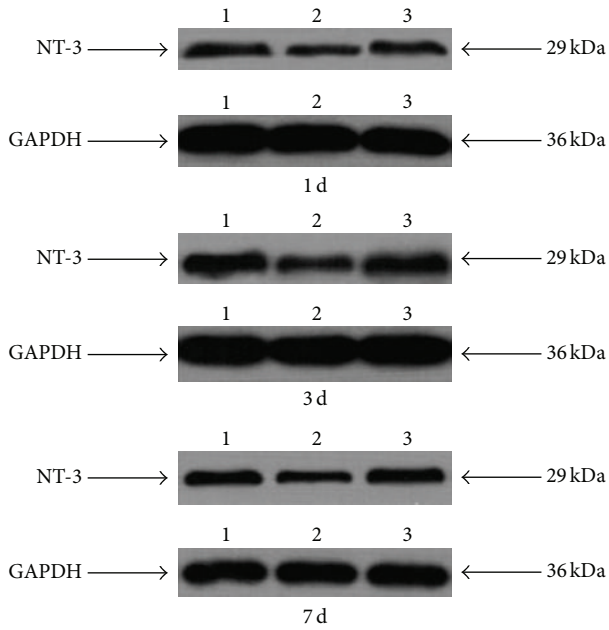

Figure 4: Western blotting identified the expression of NT-3 in the following groups: sham, control, and EA group at 1 d, 3 d, and 7 d (1: sham group; 2: control group; 3: electroacupuncture group).

peroxidation, microcirculation obstruction, and apoptosis [25, 26]. Unlike neurons of the peripheral nervous system (PNS), those of the central nervous system (CNS) do not spontaneously regenerate their axons following injury; hence, trauma to the brain or spinal cord frequently results in permanent neurological deficits [27]. SCI induced apoptotic cell death of neurons and oligodendrocytes has been known to cause progressive degeneration of the spinal cord, leading to permanent functional deficits [28]. The development of effective therapies that can restore lost neurological function is therefore critically dependent on strategies to promote robust axon regeneration [27]. Over the past several decades, a great body of work has chipped away at elucidating the biological mechanisms limiting the regeneration of injured CNS axons [27].

Our results showed that less postinjury neuronal death was occurring in the EA group compared with the control group, which was interpreted as neuroprotection. Furthermore our results still indicated that EA could maintain the cell morphology of neurons, which contributed to the functional recovery of the injured spinal cords of the rats.

Neurotrophic factors enter axons by way of its receptor mediated endocytosis at the end of axons, then reach neurons through plasma flow reverse transportation, which can cause different signaling pathway activation or inhibition in the cell, and regulate relative protein expression, to play its effect of supporting neuron development, survival, growth, and function integrity [16]. NT-3 is crucial to neuron survival, differentiation, and formation of neural circuits during neural development [17, 18].

NT-3 is widely distributed in peripheral and central nervous systems, mainly in the hippocampus, dorsal root ganglia, brainstem, and spinal cord et cetera [29]. Chen and Fang found that NT-3 like immunoreactive substance in the distribution of central nervous system involves both glial cells and neurons; the former is mainly distributed in the corpus callosum, substantia nigra, fimbria of hippocampus, subependymal zone, and cerebellum, while the latter is mainly distributed in the septum, diagonal band of Braco, granulosa cells of primitive olfactory cortex, amygdala, brainstem, and spinal motor neurons [29]. This could be understood as the gray matter of the spinal cord as the main expression site of NT-3, particularly expressed in motor neurons, so NT-3 for neurons in the gray matter of the spinal cord, especially in ventral horn motor neurons' survival and normal function, played an important role [29–31].

The present study found that the level of NT-3 in the injured spinal cords of the control group and EA group decreased in comparison with that in sham group rats' spinal cord cell where it was still synthesized and secreted. This might be injured spinal cord induced cell death or the decline of damaged cells' function in the damaged region and adjacent tissues which synthesize and secrete NT-3; therefore the NT-3 levels would be decreased [32]. We also found the level of NT-3 in the spinal cord injury region and adjacent tissues of EA group significantly increased compared to that of control group after receiving 7 days of Governor Vessel EA treatment. This might be induced by Governor Vessel EA treatment preventing the death of some damaged cells which synthesize and secrete NT-3 or possibly the regulation and restoration of the damaged cells' physiological function. No matter what the mechanism of increased NT-3 was, the increased level of NT-3 in the region of spinal cord injured and adjacent tissues created an appropriate microenvironment for spinal cord repair. It was shown in the following research results that Chen et al. [33] used immunohistochemical staining, in situ hybridization, and PCR technique to detect and observe the influence of EA for the expression of NT-3 in the spinal cord dorsal root. The study found that the expression of NT-3 in large or small neurons in cats' dorsal root ganglion of EA group was significantly higher than the other groups. Wang et al. [34] detected the treatment effect of EA through using a model of cats' spinal cord dorsal root partial resection and found that the positive neurons of NT-3 in the spinal cord lamina II increased and speculated that EA could accelerate the repair of a spinal cord injury through promoting the expression of NT-3.

In addition, NT-3 plays important roles in oligodendrocyte development [35, 36]. Huang et al.'s study indicated that EA treatment could promote NT-3 expression and increase the number and differentiation of endogenous oligodendrocyte precursor cells (OPCs) and remyelination in the demyelinated spinal cord [7]. Another study showed that EA treatment could increase NT-3 expression and promote oligodendrocyte-like cell differentiation from (NT-3) receptor (TrkC) gene modified mesenchymal stem cells (TrkC-MSCs), remyelination, and functional improvement of demyelinated spinal cord. However in our study, we did not observe EA effects on NT-3 and its action on oligodendrocytes and other glial cells [37].

According to TCM, GV 14 and GV 4 are points pertaining to the Governor Vessel. The spinal cord and Governor Vessel have direct contact on channels and collaterals. Based on the principle of "where meridians pass, indications for acupoints of this meridian could be considered," selecting the Governor Vessel to treat paraplegia related to spinal cord injury conforms to the TCM saying "searching for the primary cause of disease in treatment" [38, 39].

5. Conclusion

Governor Vessel EA on GV 14 and GV 4 could improve functional recovery by reducing apoptotic cell death after SCI. Meanwhile, the neuroprotective effects of EA treatment might be mediated by the level of NT-3 in the microenvironment around the spinal cord after injury. In addition, the present study suggested that stimulating GV 14 and GV 4, especially with electroacupuncture, might be an effective therapeutic strategy in spinal cord injury.

Additional Points

Limitations. This study has a small sample size. And the interaction among NT-3 and its receptor (such as TrkC) and the effect of EA on them at different times should be explored in the future. Furthermore, the EA-NT-3 effects on oligodendrocytes and other glial cells should be considered rather than neurons only. Lastly, quantitative analysis is also necessary, such as ELISA.

Competing Interests

The authors declare that there are no competing interests.

Authors' Contributions

Yu-ping Mo and Hai-jiang Yao contributed equally to this paper. This paper was written by Yu-ping Mo and revised by Hai-jiang Yao. Yu-ping Mo performed EA treatment and wrote the completed paper. Hai-jiang Yao, Wei Lv, and Hong-tao Song were in charge of model establishment and sample collection. The Nissl staining, TUNEL, and Western blotting were performed by Ying-qiu Mao and Xiao-chen Yuan, respectively. Liang-yu Song and Quan-kai Jing completed behavioral assessment and data extraction. Su-hua Shi performed data analysis and Zhi-gang Li arbitrated any disagreement and ensured that no errors occurred during the study. All authors contributed to the conception of the study and approved the publication of this paper.

Acknowledgments

This scientific work was supported by the National Natural Science Foundation (no. 81373728). Thanks were due to Mr. John M. Alsobrooks and Dr. Yu-tong Fei, from Beijing University of Chinese Medicine, who offered the authors some help in revising the English expression of this paper.

References

[1] B. B. Lee, R. A. Cripps, M. Fitzharris, and P. C. Wing, "The global map for traumatic spinal cord injury epidemiology: update 2011, global incidence rate," *Spinal Cord*, vol. 52, no. 2, pp. 110–116, 2014.

[2] C. H. Tator and M. G. Fehlings, "Review of the secondary injury theory of acute spinal cord trauma with emphasis on vascular mechanisms," *Journal of Neurosurgery*, vol. 75, no. 1, pp. 15–26, 1991.

[3] R. Carlos do Vale Ramos and N. Alegrete, "The role of pharmacotherapy in modifying the neurological status of patients with spinal and spinal cord injuries," *Revista Brasileira de Ortopedia*, vol. 50, no. 6, pp. 617–624, 2015.

[4] Q. Zhang, H. Yang, J. An, R. Zhang, B. Chen, and D. Hao, "Therapeutic effects of traditional chinese medicine on spinal cord injury: a promising supplementary treatment in future," *Evidence-Based Complementary and Alternative Medicine*, vol. 2016, Article ID 8958721, 18 pages, 2016.

[5] S. Furukawa, "Basic research on neurotrophic factors and its application to medical uses," *Yakugaku Zasshi*, vol. 135, no. 11, pp. 1213–1226, 2015.

[6] A. M. K. Wong, C.-P. Leong, T.-Y. Su, S.-W. Yu, W.-C. Tsai, and C. P. C. Chen, "Clinical trial of acupuncture for patients with spinal cord injuries," *American Journal of Physical Medicine and Rehabilitation*, vol. 82, no. 1, pp. 21–27, 2003.

[7] S.-F. Huang, Y. Ding, J.-W. Ruan et al., "An experimental electro-acupuncture study in treatment of the rat demyelinated spinal cord injury induced by ethidium bromide," *Neuroscience Research*, vol. 70, no. 3, pp. 294–304, 2011.

[8] Y. Ding, Q. Yan, J.-W. Ruan et al., "Bone marrow mesenchymal stem cells and electroacupuncture downregulate the inhibitor molecules and promote the axonal regeneration in the transected spinal cord of rats," *Cell Transplantation*, vol. 20, no. 4, pp. 475–491, 2011.

[9] W.-J. Li, S.-Q. Pan, Y.-S. Zeng et al., "Identification of acupuncture-specific proteins in the process of electroacupuncture after spinal cord injury," *Neuroscience Research*, vol. 67, no. 4, pp. 307–316, 2010.

[10] J. Xie, J. Fang, X. Feng, and Q. Liu, "Effect of electroacupuncture at acupoints of the Governor Vessel on aquaporin-4 in rat with experimental spinal cord injury," *Journal of Traditional Chinese Medicine*, vol. 26, no. 2, pp. 148–152, 2006.

[11] Q.-M. Han, J. Xie, S.-T. Chai, J. Fang, and Q. Liu, "Effect of Governer Meridian electro-acupuncture on water channel aquaporin-4 in experimental spinal cord injured rats," *Chinese Journal of Integrated Traditional and Western Medicine*, vol. 25, no. 7, pp. 637–639, 2005.

[12] B.-C. Shin, M. S. Lee, J. C. Kong, I. Jang, and J. J. Park, "Acupuncture for spinal cord injury survivors in Chinese literature: a systematic review," *Complementary Therapies in Medicine*, vol. 17, no. 5-6, pp. 316–327, 2009.

[13] P. T. Dorsher and P. M. McIntosh, "Acupuncture's effects in treating the sequelae of acute and chronic spinal cord injuries: a review of allopathic and traditional Chinese medicine literature," *Evidence-Based Complementary and Alternative Medicine*, vol. 2011, Article ID 428108, 8 pages, 2011.

[14] B. K. Li, B. Zeng, W. Chang et al., "Effects of Du Meridian electroacupuncture on neurological function of rats after spinal cord injury," *Chinese Journal of Rehabilitation Theory and Practice*, vol. 18, no. 7, pp. 619–622, 2012.

[15] I. Heo, B.-C. Shin, Y.-D. Kim, E.-H. Hwang, C. W. Han, and K.-H. Heo, "Acupuncture for spinal cord injury and its complications: a systematic review and meta-analysis of randomized controlled trials," *Evidence-Based Complementary and Alternative Medicine*, vol. 2013, Article ID 364216, 18 pages, 2013.

[16] L. F. Reichardt, "Neurotrophin-regulated signalling pathways," *Philosophical Transactions of the Royal Society B: Biological Sciences*, vol. 361, no. 1473, pp. 1545–1564, 2006.

[17] D. A. Duricki, T. H. Hutson, C. Kathe et al., "Delayed intramuscular human neurotrophin-3 improves recovery in adult and elderly rats after stroke," *Brain*, vol. 139, no. 1, pp. 259–275, 2016.

[18] Z. Y. Yang, A. F. Zhang, H. M. Duan et al., "NT3-chitosan elicits robust endogenous neurogenesis to enable functional recovery after spinal cord injury," *Proceedings of the National Academy of Sciences of the United States of America*, vol. 112, no. 43, pp. 13354–13359, 2015.

[19] P. J. Johnson, A. Tatara, A. Shiu, and S. E. Sakiyama-Elbert, "Controlled release of neurotrophin-3 and platelet-derived growth factor from fibrin scaffolds containing neural progenitor cells enhances survival and differentiation into neurons in a subacute model of SCI," *Cell Transplantation*, vol. 19, no. 1, pp. 89–101, 2010.

[20] Y. Ding, Q. Yan, J.-W. Ruan et al., "Electro-acupuncture promotes survival, differentiation of the bone marrow mesenchymal stem cells as well as functional recovery in the spinal cord-transected rats," *BMC Neuroscience*, vol. 10, article 35, 2009.

[21] Y. Q. Xu, S. Q. Feng, P. Wang et al., "Axonal regeneration promotion by chondroitinase ABC after spinal cord injury in rats," *Orthopedic Journal of China*, vol. 18, no. 7, pp. 573–578, 2010.

[22] J. Nicholas, "The bradford method for protein quantitation," in *The Protein Protocols Handbook*, pp. 15–21, Humana Press, 2nd edition, 2002.

[23] S. Zong, G. Zeng, Y. Fang et al., "The role of il-17 promotes spinal cord neuroinflammation via activation of the transcription factor stat3 after spinal cord injury in the rat," *Mediators of Inflammation*, vol. 2014, Article ID 786947, 10 pages, 2014.

[24] S.-H. Jiang, W.-Z. Tu, E.-M. Zou et al., "Neuroprotective effects of different modalities of acupuncture on traumatic spinal cord injury in rats," *Evidence-Based Complementary and Alternative Medicine*, vol. 2014, Article ID 431580, 9 pages, 2014.

[25] S. David, R. López-Vales, and V. Wee Yong, "Harmful and beneficial effects of inflammation after spinal cord injury: potential therapeutic implications," *Handbook of Clinical Neurology*, vol. 109, pp. 485–502, 2012.

[26] R. B. Borgens and P. Liu-Snyder, "Understanding secondary injury," *The Quarterly Review of Biology*, vol. 87, no. 2, pp. 89–127, 2012.

[27] J. N. Dulin, A. Antunes-Martins, V. Chandran et al., "Transcriptomic approaches to neural repair," *The Journal of Neuroscience*, vol. 35, no. 41, pp. 13860–13867, 2015.

[28] Y. J. Moon, J. Y. Lee, M. S. Oh et al., "Inhibition of inflammation and oxidative stress by *Angelica dahuricae radix* extract decreases apoptotic cell death and improves functional recovery after spinal cord injury," *Journal of Neuroscience Research*, vol. 90, no. 1, pp. 243–256, 2012.

[29] X. C. Chen and X. B. Fang, "Advances in basic and applied research on the 3 of neurotrophic factors," *Progress of Anatomical Sciences*, vol. 7, no. 3, pp. 257–260, 2001.

[30] C. F. Dreyfus, X. Dai, L. D. Lercher, B. R. Racey, W. J. Friedman, and I. B. Black, "Expression of neurotrophins in the adult spinal cord in vivo," *Journal of Neuroscience Research*, vol. 56, no. 1, pp. 1–7, 1999.

[31] A. Goto and S. Furukawa, "Experimental changes in BDNF- and NT-3-like immunoreactivities in the spinal cord following its transection," *Journal of the Japanese Orthopaedic Association*, vol. 69, no. 7, pp. 506–516, 1995.

[32] K. Zhang, Y. S. Zeng, L. N. Qin et al., "Effects of Governor Vessel electro-acupuncture on expression of neurotrophin-3 in rat spinal cord injured early," *Anatomy Research*, vol. 34, no. 6, pp. 411–414, 2012.

[33] J. Chen, J.-G. Qi, W. Zhang et al., "Electro-acupuncture induced NGF, BDNF and NT-3 expression in spared L6 dorsal root ganglion in cats subjected to removal of adjacent ganglia," *Neuroscience Research*, vol. 59, no. 4, pp. 399–405, 2007.

[34] T.-H. Wang, X.-Y. Wang, X.-L. Li, H.-M. Chen, and L.-F. Wu, "Effect of electroacupuncture on neurotrophin expression in cat spinal cord after partial dorsal rhizotomy," *Neurochemical Research*, vol. 32, no. 8, pp. 1415–1422, 2007.

[35] B. A. Barres, M. C. Raff, F. Gaese, I. Bartke, G. Dechant, and Y.-A. Barde, "A crucial role for neurotrophin-3 in oligodendrocyte development," *Nature*, vol. 367, no. 6461, pp. 371–375, 1994.

[36] E. J. Huang and L. F. Reichardt, "Neurotrophins: roles in neuronal development and function," *Annual Review of Neuroscience*, vol. 24, pp. 677–736, 2001.

[37] Y. Ding, R.-Y. Zhang, B. He et al., "Combination of electroacupuncture and grafted mesenchymal stem cells overexpressing trkc improves remyelination and function in demyelinated spinal cord of rats," *Scientific Reports*, vol. 5, article 9133, 2015.

[38] T. Guo, Z. Guo, X. Yang et al., "The alterations of IL-1beta, IL-6, and TGF-beta levels in hippocampal CA3 region of chronic restraint stress rats after Electroacupuncture (EA) pretreatment," *Evidence-Based Complementary and Alternative Medicine*, vol. 2014, Article ID 369158, 7 pages, 2014.

[39] Y. P. Mo, H. J. Yao, H. T. Song et al., "Alteration of behavioral changes and hippocampus galanin expression in chronic unpredictable mild stress-induced depression rats and effect of electroacupuncture treatment," *Evidence-Based Complementary and Alternative Medicine*, vol. 2014, Article ID 179796, 8 pages, 2014.